ZIRCONIA-BASED ELECTROCERAMIC MATERIALS FOR SOFC APPLICATIONS

Alan John Feighery

A Thesis Submitted for the Degree of PhD
at the
University of St Andrews

1999

Full metadata for this item is available in
St Andrews Research Repository
at:
http://research-repository.st-andrews.ac.uk/

Please use this identifier to cite or link to this item:
http://hdl.handle.net/10023/13601

Optical fibres in pre-detector signal processing

A thesis presented by

A R Flinn BSc AUS

to the

University of St Andrews

in application for the degree of

Doctor of Philosophy

November 1988

ProQuest Number: 10166557

ProQuest 10166557

TL
A932

Certificate

I certify that A R Flinn BSc AUS has spent nine terms at research work in the Physical Sciences Laboratory of St Salvador's college, in the University of St Andrews, under my direction, that he has fulfilled the conditions of Ordinance No 16 (St Andrews) and that he is qualified to submit the thesis in application for the degree of Doctor of Philosophy.

A Maitland

Research supervisor

Declaration

I hereby certify that this thesis has been composed by me, and is a record of work done by me, and has not previously been presented for a higher degree.

This research was carried out in the Physical sciences laboratory of St Salvador's college, in the University of St Andrews, under the supervision of Dr A Maitland.

A R Flinn

Acknowledgements

I would like to thank Dr. Arthur Maitland for his guidance and encouragement throughout this work. I am grateful to Admiralty Research Establishment for financial support and to my industrial supervisors Prof. Herbert French and Dr. Phil Sutton for their help, interest and not least, enthusiasm for the project.

Thanks also to all Physics postgrads, past and present, for making life enjoyable inside and outside the department, above and below 3000ft, especially; the merry band of Laser 1, Callum, Miles, Graham, Liz, and everone named Andy!

I would like to thank Denise, my wife, for her patience particularly during the later stages of the work.

Finally, my love to my parents for their ever present love, strength, and encouragement.

Author's career

The author was born in Redruth, Cornwall in 1962. He received his secondary education at Teignmouth Comprehensive school, Teignmouth, Devon. Between 1981 and 1985, he attended the University of Surrey, Guildford, where he obtained a BSc degree in Physics. The degree included a year spent at the Admiralty Research Establishment, Funtington, for which the Associateship of the University of Surrey was awarded. Since October 1985, the author has been working in the Physics department of St Andrews University on optical fibres in pre-detector signal processing under the supervision of Dr A Maitland. The research was funded by a MOD research grant from Admiralty Research Establishment, Funtington.

Contents

Abstract

The basic form of conventional electro-optic sensors is described. The main drawback of these sensors is their inability to deal with the background radiation which usually accompanies the signal. This 'clutter' limits the sensors performance long before other noise such as 'shot' noise. Pre-detector signal processing using the complex amplitude of the light is introduced as a means to discriminate between the signal and 'clutter'. Further improvements to pre-detector signal processors can be made by the inclusion of optical fibres allowing radiation to be used with greater efficiency and enabling certain signal processing tasks to be carried out with an ease unequalled by any other method.

The theory of optical waveguides and their application in sensors, interferometers, and signal processors is reviewed. Geometrical aspects of the formation of linear and circular interference fringes are described along with temporal and spatial coherence theory and their relationship to Michelson's visibility function.

The requirements for efficient coupling of a source into singlemode and multimode fibres are given. We describe interference experiments between beams of light emitted from a few metres of two or more, singlemode or multimode, optical fibres.

Fresnel's equation is used to obtain expressions for Fresnel and Fraunhofer diffraction patterns which enable electro-optic (E-O) sensors to be analysed by Fourier optics. Image formation is considered when the aperture plane of an E-O sensor is illuminated with partially coherent light. This allows sensors to be designed

using optical transfer functions which are sensitive to the spatial coherence of the illuminating light. Spatial coherence sensors which use gratings as aperture plane reticles are discussed.

By using fibre arrays, spatial coherence processing enables E-O sensors to discriminate between a spatially coherent source and an incoherent background. The sensors enable the position and wavelength of the source to be determined. Experiments are described which use optical fibre arrays as masks for correlation with spatial distributions of light in image planes of E-O sensors.

Correlations between laser light from different points in a scene is investigated by interfering the light emitted from an array of fibres, placed in the image plane of a sensor, with each other. Temporal signal processing experiments show that the visibility of interference fringes gives information about path differences in a scene or through an optical system.

Most E-O sensors employ wavelength filtering of the detected radiation to improve their discrimination and this is shown to be less selective than temporal coherence filtering which is sensitive to spectral bandwidth. Experiments using fibre interferometers to discriminate between red and blue laser light by their bandwidths are described. In most cases the path difference need only be a few tens of centimetres.

We consider spatial and temporal coherence in fibres. We show that high visibility interference fringes can be produced by red and blue laser light transmitted through over 100 metres of singlemode or multimode fibre. The effect of detector size, relative to speckle size, is considered for fringes produced by multimode fibres. The effect of

dispersion on the coherence of the light emitted from fibres is considered in terms of correlation and interference between modes.

We describe experiments using a spatial light modulator called SIGHT-MOD. The device is used in various systems as a fibre optic switch and as a programmable aperture plane reticle. The contrast of the device is measured using red and green, HeNe, sources. Fourier transform images of patterns on the SIGHT-MOD are obtained and used to demonstrate the geometrical manipulation of images using 2D fibre arrays. Correlation of Fourier transform images of the SIGHT-MOD with 2D fibre arrays is demonstrated.

1 Introduction

1.1 Electro-optic sensors.

Remote sensing may be defined as the detection of electromagnetic (EM) radiation emitted, reflected, or scattered from an object. The EM radiation from an object together with the EM radiation from the background is detected by an electro-optic (EO) sensor. The EO sensor converts the optical signal into an electrical signal. The task of the EO sensor is to measure the radiation from the object, i.e. the signal, in the presence of background radiation.

With the exception of heterodyne systems nearly all EO sensors have the general form shown in figure 1.1. They collect light from a scene using some combination of reflecting or refracting optics and then bandlimit the light by means of a spectral filter. The filter is chosen so as to maximise the ratio of signal to background radiation. The sensor can be imaging in which case the intensity is measured by a 2D detector array, figure 1.2a, or the scene is scanned over a small number of detectors. Alternatively, the sensor may be non-imaging, in which case it can only detect power in a determined waveband, figure 1.2b. Both the signal and background radiation can be modulated by a rotating reticle in the detector plane in order to aid the post-detector electronic processing. Signal processing aims to improve the discrimination between the signal and the unwanted background in a scene.

Image processing can be based on linear (space invariant) or non-linear (space variant) processing. Linear processing means that the output image is linearly related to the input so, as in electrical

circuits, we can study the image quality of an optical system by applying frequency response techniques, usually with the aid of transfer functions. Examples of linear processes are bandpass filtering, subtraction, convolution and correlation. In an optical system the detected output is always an intensity. With incoherent light, the input and output intensities have a linear relationship. With coherent light, the input and output are based on amplitude and intensity, respectively, so their relationship is no longer linear.

1.2 Pre-detector signal processing.

Signal processing may be carried out before or after square-law detection so we have the option of pre-detector or post-detector processing. The discrimination of E-O sensors which use post-detector processing is often poor because they have to discriminate between signal and background on the basis of intensity as all phase information is lost in the square-law detection process. Problems arise when the intensity of the background radiation approaches that of the signal. Pre-detector processing can take advantage of this phase and amplitude information which can give information about the spectrum, coherence, and polarisation of the light by selective modulation of these parameters prior to electronic detection [1.1].

The simplest form of spectral processing is a bandpass filter. If the signal is known to be centred at a certain wavelength then this approach may be sufficient to obtain a strong signal. If the background radiation has a similar power to the signal over that region of the spectrum then optical processing which takes into account the narrower spectrum of the signal must be used, for example, temporal coherence processing. Sources are usually small

5

and so exhibit a high degree of spatial coherence compared with normally diffuse background radiation. Optical pre-detector processing may be employed to take advantage of these differences in spatial coherence.

Pre-detector signal processing techniques can take advantage of polarisation differences between a source and background radiation. Laser sources are often highly linearly polarised but thermal sources are usually unpolarised. Features such as clouds reflect light which is elliptically polarised so a form of polarisation modulation may discriminate between differently polarised radiations.

Pre-detector optical signal processing techniques often make use of the Fourier transform. This branch of signal processing is known as Fourier Optics and is described in detail by Goodman [1.2], Steward [1.3], and Bracewell [1.4]. Other transforms may be performed optically, for example, the Hartley transform [1.5], and the Sine and Cosine transforms [1.6].

1.3 Optical fibres.

Optical fibres are waveguides made of transparent materials such as silica glasses which can transmit visible and infra-red light over long distances with low loss (> 0.2 dB/km at 1500nm). An optical fibre consists of an inner core which guides the light and an outer layer, called the cladding, of lower refractive index than the core. The fibre is usually covered with a protective sheath. The refractive indices of the core and cladding, n_1 and n_2 respectively, can be uniform with a sharp boundary between the two, or there can be a gradual transition in which n_1 decreases to n_2. The two types of fibre are called step-index and graded-index, respectively, figure 1.3.

For a wave to be guided by the fibre it is necessary for it to be totally internally reflected at the core-cladding boundary. Consequently, the light must enter the fibre core within a range of angles forming a solid cone. The solid half angle of the cone is known as the acceptance angle of the fibre and is related to the refractive indices of the core, cladding, and surrounding medium (usually air for which n=1). We define the numerical aperture of a fibre as the sine of the acceptance angle for the fibre.

The geometry of the guide together with Maxwell's equations define a series of modes which may be supported by the optical fibre. For a core diameter of greater than around ten wavelengths a large number of modes can propagate and so the fibre is known as a multimode fibre. When light is launched into a multimode fibre at an angle less than or equal to the acceptance angle it can only propagate in a finite number of paths. The transmitted wave undergoes total internal reflection at the core-cladding boundary, and after two reflections the wave is traveling parallel to its previous direction. If these two waves are in phase then constructive interference occurs and the wave will propagate. If these two waves are out of phase then destructive interference occurs and the wave will not propagate. Typical multimode fibres have diameters of 30-1000 microns and numerical apertures between 0.1 and 0.3. A fibre with a 1% difference in refractive indices has a numerical aperture of about 0.2. The number of modes which can propagate in a step-index fibre is proportional to the square of the product of the core diameter and the numerical aperture. A graded-index fibre supports about half as many modes as does a step-index fibre of similar diameter.

Each mode of a step-index multimode fibre propagates at a slightly different velocity along the axis of the fibre and this causes dispersion and modal noise. If the core diameter is decreased the number of modes decreases until, at wavelengths below a certain critical value, only one mode will propagate. A fibre in which only one mode propagates is called singlemode and has a core diameter, typically, in the range 3-5 microns.

1.4 Fibre optics

Fibre optics encompasses all the optics necessary to a system based around optical fibres. A fibre optic signal processing system consists of light from a source coupled into an optical fibre or optical fibre array. The fibres either transmit the light to a signal processing system with a predetermined geometry or carry out the signal processing by splitting or combining the light with predetermined delays between the beams. The intensity of the processed optical signal is detected at the output of the system.

We consider the sources, coupling of radiation from the sources into the fibre, and the splicing of two fibres together. We then consider optical fibre directional couplers or splitters and detectors for optical fibre systems.

The source wavelengths typically used in optical fibres are determined by the wavelength dependent losses of the fibre itself, figure 1.4. These losses include ultraviolet and infra-red absorption, and Rayleigh scattering which is caused by density and compositional variation within the fibre. Another source of losses is

due to absorption by dopant and impurity ions such as transition elements and the hydroxyl ion from water. For high bandwidth communications the wavelength dependent dispersion of the fibre determines the maximum permissible linewidth of the source.

Factors which affect the coupling of a source into an optical fibre include unintercepted illumination. This includes light which is not incident on the entrance to the core of the optical fibre due to an incorrect source spot size. Also, there may be numerical aperture loss. This is caused by that part of the source profile that falls outside of the fibre acceptance cone. To avoid this, many integrated optical components have a fibre 'pigtail' permanently mounted and properly aligned which may then be spliced to another cable. As the core of a monomode fibre is only a few microns in diameter, a slight inaccuracy in alignment at a joint can severely increase the losses, so most joints must be spliced.

Two basic methods are used to permanently join two fibres together. The most widely used is fusion splicing or welding in which the two ends of the fibres are heated, possibly by an electric arc, causing them to soften and fuse together. By this method, losses of less than 0.1dB have been obtained. A second method of permanently joining two fibres is to use an adhesive. This generally involves using some additional element to enable the fibres to be accurately aligned for bonding.

Directional couplers are devices which enable light to be coupled from one fibre into two or more fibres or conversely combine light from several fibres into one fibre. They play the same role in fibre

optics that beamsplitters play in conventional optics. Most singlemode couplers use evanescent or field coupling. In evanescent coupling energy is transferred from one optical fibre to another by virtue of the electric field overlap between the two cores.

1.5 Pre-detector signal processing with optical fibres.

The introduction of optical fibres into pre-detector signal processing systems allows particular signal processing tasks to be performed which cannot be easily achieved using free space paths, whilst retaining the ability to discriminate between signal and background radiation on the basis of phase and amplitude. One of the simplest tasks which may be considered is that of using a few optical fibres to sample the radiation at different points in the image of a scene. The radiation emitted by each fibre may be introduced to the same or different signal processing systems. Using fibre couplers, the radiation from each point may be processed in several ways.

Optical fibres can perform a spatial transformation. Radiation in an image plane may be guided through an array of fibres and by altering the relative positions of each fibre a new encoded image is produced.

The fibres can perform signal processing by delaying one beam with respect to another as in a fibre interferometer. The use of optical fibres as delay lines allows the temporal correlation of radiation in two or more fibres to be carried out with any required time delay. An advantage of fibre paths is that correlations may be sought between closely or widely separated points in an image with equal ease.

1.6 Optical Signal Processing with Optical Fibres.

Optical fibres are used in optical signal processing and some of the applications are discussed below.

In 1966 Leith [1.7] described holographic imagery through a diffusing media. By obtaining the phase conjugate of the diffusing media the object may be reconstructed. In 1976 Leith and Chang [1.8] applied the same process to a fibre bundle. The phase conjugate of the bundle is obtained so that when an image is transmitted through the bundle and incident on the hologram it will reconstruct the wavefront incident on the bundle and reproduce the image. Coherent bundles are often used for image transfer but the fibres in these bundles are arranged randomly. In order to be able to process an image the fibres need to be arranged in regular arrays. For example, the packing density of an array of photodetectors at high frequency is limited by the need for separate coaxial connectors to each detector. An array of optical fibres placed in the image plane allows a high packing density in the image plane to be realised and by fanning out the fibres we may have a low packing density in the detector plane. Two dimensional arrays of optical fibres were fabricated by Koepf and Market [1.9]. It is also possible to produce holographic optical elements (HOEs). which will allow arrays of coupling lenses and other elements such as beamsplitters to be included in a single hologram. High coupling efficiency can be obtained and the two dimensional fibre array can act as the object in the formation of the hologram so numerical aperture or spot size mismatch will not occur.

A paper by Youngquist, et al. [1.10] demonstrated coherence synthesis using an acousto-optic (AO) cell. The visibility curve or coherence function of a source is given by the modulus of the Fourier transform of the spectrum. So if the laser frequency is doppler shifted by the AO cell and then mixed with itself in an optical fibre a new spectrum exists and the coherence function is modified. An array of interferometers, which have the same source, may be constructed from optical fibre. If each interferometer has a different path difference then one interferometer may be selected and the others turned off by generating a coherence function which is unity for the path difference of the desired interferometer and zero for the others.

Optical fibres can be used as an alternative to metallic waveguides in many microwave systems by modulating an optical source. Most radar systems have a bandwidth of around 10Mhz and a singlemode optical fibre with a source near the dispersion minimum can carry a signal with a 20Mhz bandwidth 50km. Fibres can be used in optical signal processing systems such as optical delay lines [1.11]. Even allowing for dispersion time-bandwidth products of greater than 10^5 have been achieved compared with 10^3-10^4 for acoustic wave delay lines. The delay lines may be used for storing received radar pulses for re-transmission or with a non-coherent radar moving target indicator a returned signal is stored for subtraction from the next return [1.12]. Tapped delay lines with partially reflecting splices have been demonstrated by Jackson, et al. [1.13]. These can be used as a bandpass or matched filter or for pulse compression in high resolution radars. Unfortunately, these taps are not yet programmable.

Notch filters and bandpass filters for interferometric sensors can be made using a length of singlemode optical fibre and a directional coupler to form a recirculating loop. The frequency response of these filters is tunable by altering the length of the resonating fibre loop and the finesse may be adjusted by changing the coupling ratio and hence the proportion of light that is allowed to recirculate [1.14].

| Input optics | → | Spectral filtering | → | Square-law or optical power detection | → | Post-detector processing electronics |

Telescope

Reflecting or refracting optics

Band-limiter

Single element, linear, or 2D detector arrays

Respond to optical intensity changes at frequencies below 10GHz

Analogue signal processing. Matched filters, correlators, etc.

Digital signal processing. Contrast enhancement, fast Fourier transforms etc.

Figure 1.1 **Block diagram and features of conventional E-O sensor**
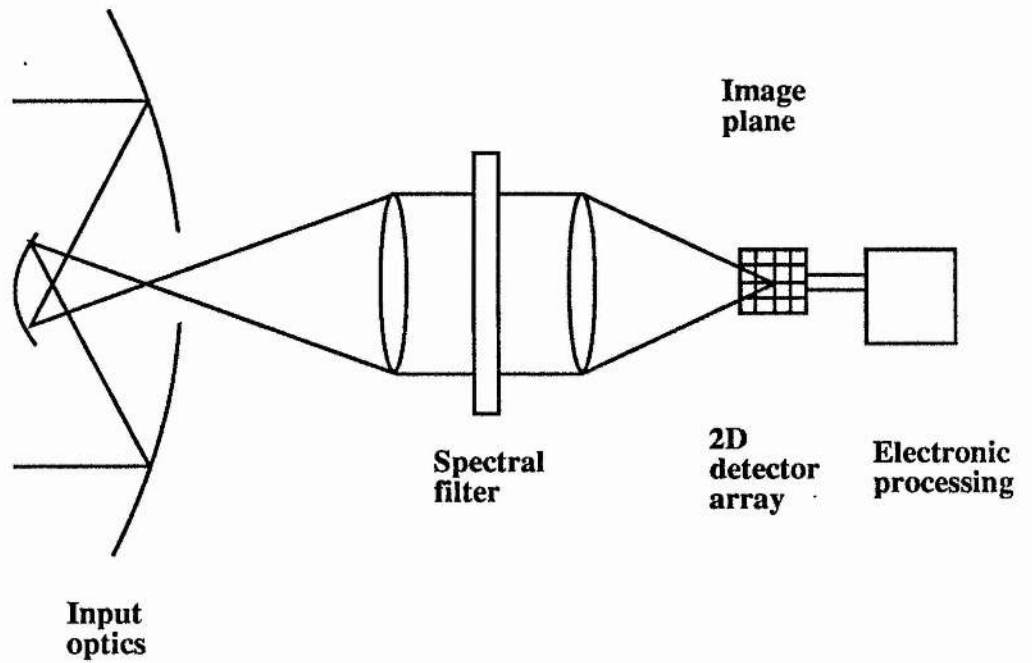
Figure 1.2a Conventional E-O sensor using reflecting input optics and a 2D detector array in image plane
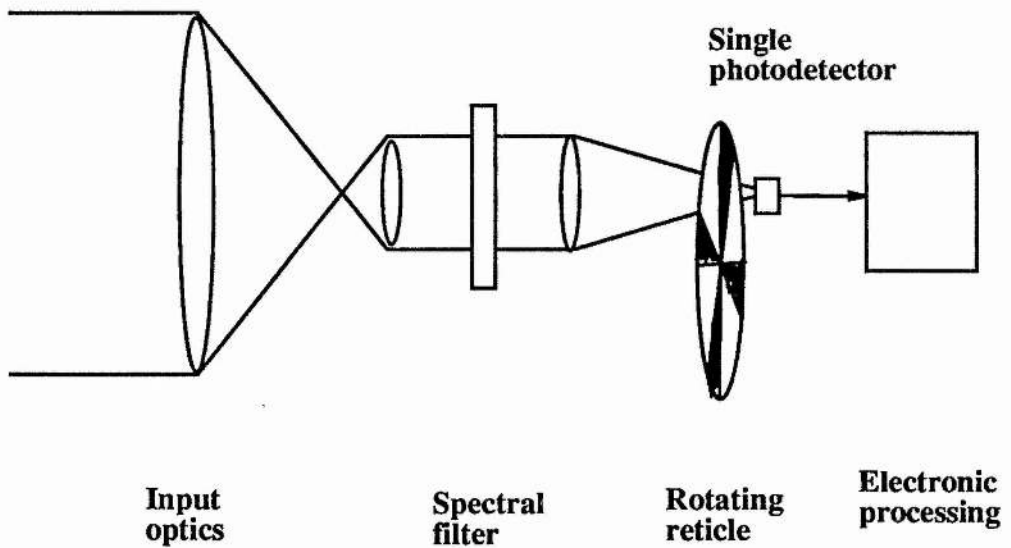
Figure 1.2b Conventional E-O sensor using refracting input optics, an image plane reticle, and a large area detector

Refractive index n_1 n_2 r — Singlemode Fibre

Refractive index n_1 n_2 r — Step-index Multimode Fibre

Refractive index n_1 n_2 r — Graded-index Multimode Fibre
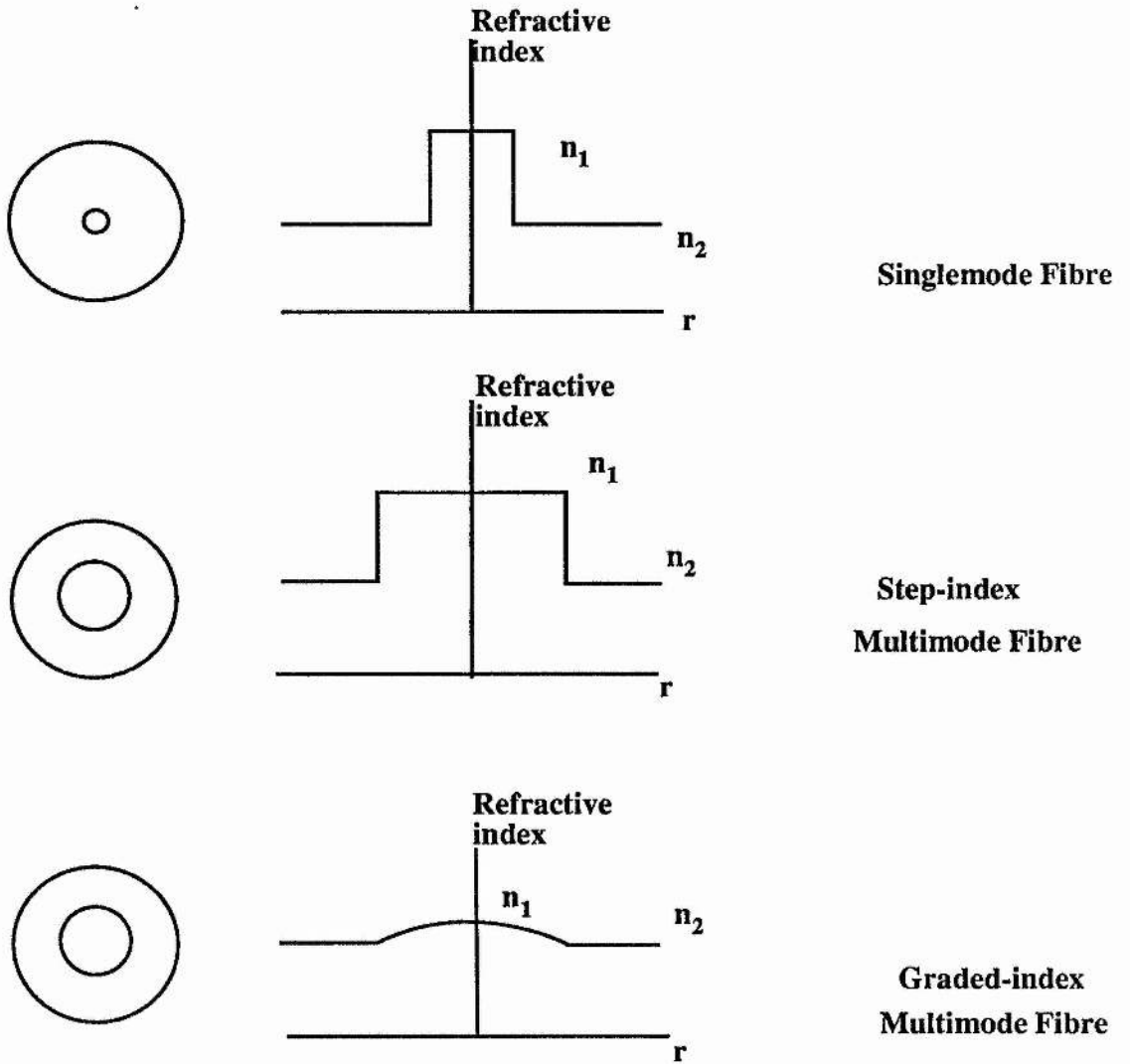
Figure 1.3 Refractive index profile of single and multimode optical fibres

Attenuation against wavelength for Silica
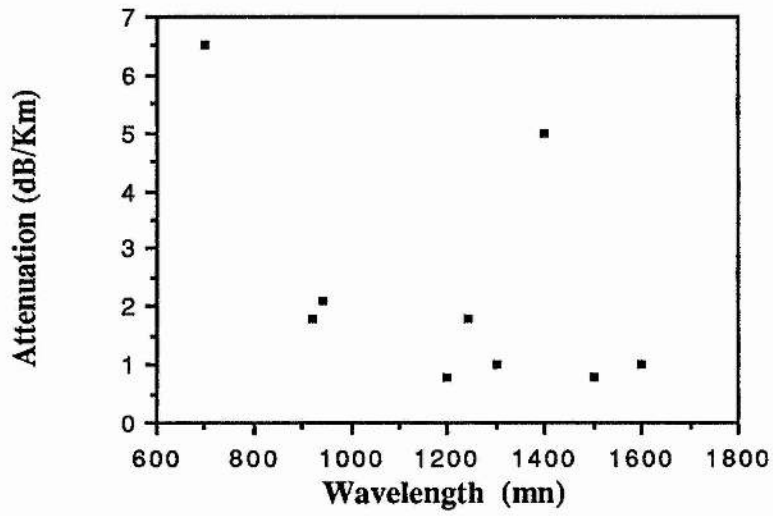
Figure 1.4

2 Theory

2.1 Waveguide theory

Guiding of light was first demonstrated by Lord Rayleigh in 1895 [2.1] using white light in a jet of water. Waveguiding in cylindrical dielectric rods was studied by Snitzer in 1961 [2.2]. With the arrival of the laser, interest in optical waveguides increased, but losses were still greater than 1000 dB/km. In 1966 Kao and Hockham [2.3] suggested that dielectric waveguides for communication could be made with losses of less than 20 dB/Km and this was achieved by workers at Corning Glass Works in 1970. Currently, losses are around 0.2 dB/Km at 1500nm which approaches the Rayleigh scattering limit of the fibre material.

The theory of weakly guiding optical fibres was discussed by Gloge in the early 1970's. Expressions for guided modes, their propagation constant and delay distortion were obtained [2.4,5,6]. Optical power flow is discussed in reference [2.7]. The theory of optical waveguides as given in this thesis follows the notation used by Gloge. Other useful references for theory are by Marcuse [2.8], Adams [2.9], and Cherin [2.10].

Dispersion limits the available bandwidth of an optical fibre and so the choice of source and fibre can be important if a high bandwidth is required. Time dispersion is discussed by Love [2.11] in terms of intermodal and chromatic dispersion and the effect of a broadband source on fibre bandwidth is discussed by Ohlhaber and Ulyasz [2.12]. Dispersion in singlemode fibres is wavelength dependant and has a

minimum value at about 1300nm but, recently, fibres have been produced with the minimum dispersion shifted to 1550nm in order to take advantage of the lower attenuation.

The polarisation properties of optical fibres have become more important as a greater number of systems are developed with singlemode fibre. These fibres propagate two orthogonal modes which normally do not preserve the polarisation state of the light as it propagates along the fibre. The preservation of polarisation in singlemode optical fibres is discussed by Rashleigh [2.13]. The polarisation optics of light in singlemode fibre depend on fibre imperfections such as bending or twisting stress which introduce birefringence. The birefringence may be introduced in a controlled manner in order to control the output polarisation by bending the fibre into a loop. A device described by Lefevre [2.14] consists of two coils of calculated radius which act as 1/4 wave plates to control the ellipticity of the polarisation and a single coil of different radius which acts as a 1/2 wave plate to control the orientation of the output polarisation. Using this device the output polarisation of two beams of a fibre interferometer can be made parallel for maximum interference to occur.

In optical fibres, the light propagates in a finite number of modes. If the losses in a fibre system are mode dependant, for example at a splice, then unwanted amplitude modulation of the transmitted signal can occur. This in known as modal noise and is discussed by Epworth [2.15].

A review article by White [2.16] discusses methods of characterising optical fibres in terms of their losses, bandwidth, refractive index profile etc.

In order to be able to use optical fibres for pre-detector signal processing it is necessary to understand the effects that waveguiding has upon the light. Firstly, as many optical sources are broadband an important parameter for signal processing is the bandwidth over which a fibre propagates one mode. Secondly, it is important to know the time delay experienced by radiation in a given length of fibre. Finally, a monochromatic source will experience dispersion effects in a multimode fibre and a broadband source will be dispersed even in a singlemode fibre. In the following sections we will derive the basic equations used in fibre optics. The step-index fibre will be considered as the simplest case of an optical fibre. We shall show that the full set of TE, HE, and EH modes may be approximated by a single set called linearly polarised modes. An expression for the approximate number of modes in an optical fibre is found. Group and phase velocity dispersion are considered.

2.1.1 The step-index optical fibre - ray model

For many purposes a ray model is sufficient to derive basic parameters of an optical waveguide. Consider a fibre of spherical symmetry with a core of diameter 2a. The refractive indices of the core and cladding are n_1 and n_2, respectively, with $n_1 > n_2$, figure 2.1. The angle between the wall of the guide and the ray which just undergoes total internal reflection is defined as the critical angle not the angle between the ray and normal to the surface as would be expected. The angle between the axis of the guide and an incident ray which just undergos total internal reflection at the core-cladding

17

boundary defines the numerical aperture of the fibre. From Snell's law, we have

$$\text{Sin} (90 - \theta_c) = \frac{n_1}{n_2} . \qquad (2.1.1.1)$$

Then, the critical angle is given by

$$\text{Cos } \theta_c = \frac{n_1}{n_2} . \qquad (2.1.1.2)$$

To meet this condition it is necessary for the light to enter the fibre within a cone defined by the numerical aperture, sin θ_m, given by

$$\text{Sin } \theta_m = \sqrt{n_1^2 - n_2^2} . \qquad (2.1.1.3)$$

The angle θ_m defines the maximum acceptance angle of the fibre and the sine of that angle defines the numerical aperture. We define a parameter Δ which is the relative difference between core and cladding refractive indices and is expressed

$$\Delta = 1 - \frac{n_2}{n_1} . \qquad (2.1.1.4)$$

By making the approximation

$$\Delta \cong \frac{n_1^2 - n_2^2}{2n_1^2} . \qquad (2.1.1.5)$$

we can relate the parameter to the critical angle and numerical aperture. By substitution we have

$$\text{Sin } \theta_m = n_1 \text{ Sin } \theta_c = n_1 \sqrt{2\Delta} . \qquad (2.1.1.6)$$

18

For most fibres $0.1 < \mathrm{Sin}\,\theta_m < 0.2$ which gives $5.7° < \theta_m < 11.5°$.

The ray model tells us about the acceptance angle of the fibre and the propagation of wavefronts through the fibre but does not give a complete picture of the individual modes within a fibre. To learn more about the modes we need a wave theory.

2.2 The step-index optical fibre - wave model

The basic equations that apply to any waveguide in terms of the electric and magnetic fields of a propagating wave are derived from Maxwell's equations in cartesian coordinates in appendix A. For wavelength dependant effects a scalar wave theory is sufficient. For polarisation effects a vector wave theory must be used. The theory given is a scalar theory.

2.2.1 The step-index optical fibre

Optical fibres have some features in common with metallic waveguides. Both can support a finite number of modes at any given frequency. Both suffer from mode coupling if the guide departs from perfect geometry. However, metallic guides support only guided modes but optical fibres support both a finite number of guided modes and a continuum of unguided radiation modes. These radiation modes are due to the boundary conditions at the core-cladding interface. Coupling can occur between the guided modes of an optical fibre and the radiation modes.

We now consider a step-index fibre with a core of uniform permittivity ε_1 and circular cross section extending to radius r=a.

19

The cladding has a lower permittivity ε_2. The permeability of both materials is taken as μ_0.

Any rectangular component of field such as E_z satisfies the Helmholtz equation which for a wave propagating as $e^{j\beta z}$ in cylindrical coordinates is

$$\frac{\partial^2 E_z}{\partial r^2} + \frac{1}{r}\frac{\partial E_z}{\partial r} + \frac{1}{r^2}\frac{\partial^2 E_z}{\partial \phi^2} + (k_1^2 - \beta^2)E_z = 0 . \qquad (2.2.1.1)$$

The propagation constant β of any mode is limited within the interval $n_2 k < \beta < n_1 k$ where k is the free space wave number. We can define parameters u and w in the core and cladding respectively. These parameters are given by

$$u^2 = a^2 k_c^2 = a^2(k_1^2 - \beta^2) , \qquad (2.2.1.2)$$

and

$$w^2 = a^2 \gamma^2 = a^2(\beta^2 - k_2^2) . \qquad (2.2.1.3)$$

For guided modes, u is real so from equation 2.2.1.2 we have $k_1^2 - \beta^2 > 0$ in the core so the modes may be described by ordinary Bessel functions. Only the first kind is used to maintain finite results on axis. For the cladding, w is real so from equation 2.2.1.3 we have $\beta^2 - k_2^2 > 0$ for guided modes and modified Bessel functions are used. The axial field H_z satisfies similar conditions. For $r < a$, we have

$$E_{z1} = AJ_l(ur/a) \, e^{jl\phi} , \qquad (2.2.1.4)$$

and

$$H_{z1} = BJ_1(ur/a) \, e^{jl\phi}. \qquad (2.2.1.5)$$

For r > a we have

$$E_{z2} = CK_1(wr/a) \, e^{jl\phi}, \qquad (2.2.1.6)$$

and

$$H_{z2} = DK_1(wr/a) \, e^{jl\phi}. \qquad (2.2.1.7)$$

The transverse field components E_x, E_y, H_x and H_y of equations (A.23) to (A.26) can now be obtained in cylindrical coordinates for both the core and cladding regions. The results for E_ϕ and H_ϕ are, for the core,

$$E_{\phi 1} = \left(-+\frac{j\beta a^2 l}{ru^2} AJ_1(ur/a) + \frac{j\omega\mu a}{u}BJ_1'(ur/a) \right) e^{jl\phi}, \qquad (2.2.1.8)$$

and

$$H_{\phi 1} = \left(-+\frac{j\omega\varepsilon_1 a}{u}AJ_1'(ur/a) -+\frac{j\beta a^2 l}{u^2 r}BJ_1(ur/a) \right) e^{jl\phi}, \qquad (2.2.1.9)$$

and for the cladding

$$E_{\phi 2} = \left(-+\frac{j\beta a^2 l}{rw^2}CK_1(wr/a) - \frac{j\omega\mu a}{w}DK(wr/a) \right) e^{jl\phi}, \qquad (2.2.1.10)$$

and

$$H_{\phi 2} = \left(\frac{j\omega\varepsilon_2 a}{rw^2}CK_1'(wr/a) -+\frac{j\beta a^2 l}{rw^2}DK_1(wr/a) \right) e^{jl\phi}. \qquad (2.2.1.11)$$

21

For the symmetrical case with l=0, we have separable transverse magnetic (TM) and transverse electric (TE) solutions. The continuity equations at the core-cladding boundary (r=a) $E_{z1} = E_{z2}$ and $H_{\phi 1} = H_{\phi 2}$ gives for the TM set of solutions

$$\frac{J_1(u)}{J_0(u)} = \frac{-\varepsilon_2 u K_1(w)}{\varepsilon_1 w K_0(w)} . \qquad (2.2.1.12)$$

Applying the continuity equations $E_{\phi 1} = E_{\phi 2}$ and $H_{z1} = H_{z2}$ at r = a gives for the TE set of solutions

$$\frac{J_1(u)}{J_0(u)} = \frac{-u K_1(w)}{w K_0(w)} . \qquad (2.2.1.13)$$

The longest wavelength which will propagate in a given mode is determined by the cut-off condition. Cut-off for the fibre may be considered to be the condition for which the fields in the cladding extend to infinity. This happens if w = 0. Then, from equation (2.2.1.13), we have $J_0(u_c) = 0$ and u at cut-off is given by

$$u_c = a\, (k_1^2 - k_2^2)^{1/2} = 2.405 , 5.52... \qquad (2.2.1.14)$$

The TE and TM modes correspond to rays which are meridional. That is, they propagate directly along the z axis. If $l \neq 0$ then the fields do not separate into TM and TE but become coupled through the continuity equations for E_ϕ, E_z, H_ϕ and H_z. Applying these at r=a gives us the characteristic equation for the fibre modes.

$$\left(\frac{k_1 J_1'(u)}{u J_1(u)}\right)^2 + \left(\frac{k_2 K_1'(w)}{w K_1(w)}\right)^2 + \frac{(k_1^2 + k_2^2)}{uw}\left(\frac{J_1'(u) K_1'(w)}{J_1(u) K_1(w)}\right) = \frac{\beta^2 l^2\, v^4}{u^4 w^4} , \qquad (2.2.1.15)$$

22

where

$$v^2 = u^2 + w^2. \qquad (2.2.1.16)$$

This quadratic summation gives us the so-called v number of the fibre which is the normalized frequency. Note that, at cut-off, we have $w = 0$ and then $u_c = v_c$. From equations (2.2.1.2) and (2.2.1.3) we have

$$v = a \, (k_1^2 - k_2^2)^{1/2} \, , \qquad (2.2.1.17)$$

or

$$v = k \, a \, (n_1^2 - n_2^2)^{1/2} \, . \qquad (2.2.1.18)$$

Solution of the characteristic equation for $l \neq 0$ leads to hybrid modes. These are modes that have six field components. If H_z dominates over E_z in the mode then it is described as an HE_{lp} mode. If E_z dominates over H_z then the mode is described as an EH_{lp} mode. The HE_{11} mode has no cut-off frequency although the energy is only retained within the core for wavelengths less than or equal to the core dimensions. The number of modes that will propagate for a given v number is plotted in figure 2.2.

2.2.2 Linearly polarised modes

In most optical fibres the core and cladding refractive indices differ by only 1 or 2 percent. So if we let $\varepsilon_1 = \varepsilon_2$ then all the field components at the core-cladding boundary satisfy the single equation

$$\frac{J_l(u)}{J_{l-1}(u)} = \frac{uK_l(w)}{wK_{l-1}(w)}$$

This is the characteristic equation for the linearly polarised modes. As before, at cut-off, $w = 0$. So the cut-off wavelengths are obtained from the roots of the equation $J_{l-1}(u) = 0$. The modes are designated LP_{lm} where $l-1$ is the order of the Bessel function and m is the mth root of the equation. Hence the HE_{11} mode, which is the first root of $J_1(u) = J_{-1}(u) = 0$, becomes the LP_{01} mode. The usefulness of this approximation is apparent from the hybrid modes where it is found that LP_{lm} modes are approximately superpositions of the $HE_{l+1,m}$ and $EH_{l-1,m}$ modes. Hence the HE_{31} and EH_{11} modes will produce an LP_{21} mode that has only four field components. As they are not exact solutions of the fibre the HE and EH modes have slightly different propagation constants, so their superposition changes with z.

2.2.3 Number of modes in a step-index fibre

Most problems of interest in fibres such as coupling, scattering, loss, and delay require only the transverse wavenumber, u, for a satisfactory description of each mode, figure 2.3. The propagation angle of a mode within the guide can be related to u. The field distribution of the mth mode is nearly sinusoidal and its transverse wave number is given by

$$u = \frac{\pi m}{2a} \cdot \qquad (2.2.3.1)$$

The longitudinal wavenumber is given by $n_1 k$. Each mode can be represented by a plane wave propagating at an angle θ given by

$$\theta = \frac{u}{n_1 k} = \frac{m\lambda}{4an_1} , \qquad (2.2.3.2)$$

where m is the mode group number. When the wave is emitted from the guide the angle becomes

$$\theta = \frac{m\lambda}{4a} \cdot \qquad (2.2.3.3)$$

All the waves with the same u travel at the same angle through the fibre so the far field diffraction pattern of the light emitted by the fibre consists of a number of spots located on the circumference of a circle whose radius is defined by u. When m is a maximum, θ is the critical angle. The number of modes with group number m is m/2. Taking two polarisations into account we have that the total number of modes ,N, is given by

$$N = 2mm/2 . \qquad (2.2.3.4)$$

Substituting for m into (2.2.3.4) from (2.2.3.2) and we have

$$N = (\frac{4an_1\theta_c}{\lambda})^2 . \qquad (2.2.3.5)$$

We can also write the total number of modes as

$$N = (\frac{4an_1}{\lambda})^2 2\Delta. \qquad (2.2.3.6)$$

Using the expression

$$v = k \, a \, n_1 \sqrt{2\Delta},$$

in equation (2.2.3.6) gives the expression for the total number of modes in a step-index fibre which is

$$N = \frac{4v^2}{\pi^2}.$$ \hfill (2.2.3.7)

2.3 Group dispersion in a step-index fibre

In the field of communications optical fibres are being developed for their large bandwidths. A figure of merit for an optical fibre is usually given as a length-bandwidth product and is measured in megahertz or gigahertz per kilometer. The bandwidth of an optical fibre is related to the dispersion effects in the fibre. From bandwidth theory the bandwidth δv is approximately $1/\delta t$ where δt is the pulse width of the signal. Any broadening of a pulse by an optical fibre decreases the available bandwidth. Pulse broadening by an optical fibre is principally due to two processes, namely intermodal and material dispersion. Intermodal dispersion arises from different modes having different propagation constants and hence traveling different optical paths, for example, the wavefront of a hybrid mode such as an EH mode follows a helical path about the optical axis as it propagates down the fibre. Material dispersion arises from the wavelength dependence of refractive index in silica. A graph of refractive index against wavelength is given in figure 2.4.

The combined effect of intermodal and material dispersion on the bandwidth of a fibre is given by

$$BW_{total}^{-2} = BW_{intermodal}^{-2} + BW_{material}^{-2}. \quad (2.3.1)$$

Bandwidths greater than 3Ghz/Km are achievable for a singlemode fibre at 1300nm but even a multimode step-index fibre has a bandwidth of around 200Mhz/Km which is far greater than is achievable electrically without significant attenuation losses. For example, for coaxial cable the attenuation losses start to rise quickly above a few megahertz. Large bandwidths allow optical signals to be modulated at high frequencies. This is desirable in optical signal processing for several reasons. The higher the modulation frequency the faster data can be transfered. Many optical sources are pulsed so processing must be carried out within the pulse duration. Many radar systems operate at gigahertz frequencies so fibre optical processing of radar signals requires gigahertz bandwidths. Integrated optical devices such as acousto-optic spectrum analysers doppler shift light which can be heterodyned giving frequencies of the order of 100 MHz.

Pulse dispersion in a step-index optical fibre is group delay dispersion. Group delay may be written

$$\tau_G = L \frac{d\beta}{d\omega} = \frac{L}{c} \frac{d\beta}{dk} . \quad (2.3.2)$$

When the difference in the core and cladding refractive indices are small, the v number of the fibre may be written

$$v = k \, a \, n_1 \sqrt{2\Delta} \, . \qquad (2.3.3)$$

Differentiating we have

$$\frac{dv}{dk} = \frac{v}{k} \, . \qquad (2.3.4)$$

Then we may write for τ_G

$$\tau_G = \frac{L}{c} \frac{d\beta}{dv} \frac{v}{k} \, . \qquad (2.3.5)$$

We have an expression for β, from equation (2.2.1.3), which is

$$\beta^2 = n_2^2 k^2 + \gamma^2 . \qquad (2.3.6)$$

We want to eliminate γ so we define a normalised propagation constant b such that

$$b = \frac{w^2}{v^2} = \frac{a^2(\beta^2 - k_2^2)}{v^2} = \frac{a^2 \gamma^2}{v^2} \, . \qquad (2.3.7)$$

Substituting for γ^2 and v we have

$$\beta^2 = n_2^2 k^2 \, (1 + 2\Delta b) \, , \qquad (2.3.8)$$

which may be approximated to

$$\beta = n_2 k \, (1 + \Delta b) , \qquad (2.3.9)$$

We now obtain an expression for the group delay dispersion which is

$$\tau_G = \frac{L}{c} \frac{d(n_2 k)}{dk} + \frac{L}{c} \frac{v}{k} \frac{d(n_2 k \, \Delta b)}{dv} \, . \qquad (2.3.10)$$

28

The group delay dispersion can be seen to separate into two components,

$$\tau_G = \tau_C + \tau_M , \qquad (2.3.11)$$

where τ_C is the group delay due to chromatic or material dispersion and depends on the linewidth of the source and τ_M is the group delay due to the difference in optical path length for each mode of the fibre.

2.3.1 Material Dispersion

We shall now consider the material dispersion in a step-index optical fibre. From equations (2.3.10) and (2.3.11) the group delay τ_c of a mode due to material dispersion is given by

$$\tau_c = \frac{L}{c} \frac{d(n_2 k)}{dk} . \qquad (2.3.1.1)$$

As $k = \omega (\mu \varepsilon)^{1/2}$ we have

$$\tau_c = \frac{L}{c} \frac{d(n_2 \omega)}{d\omega} , \qquad (2.3.1.2)$$

expanded this becomes

$$\tau_c = \frac{L}{c} (n + \omega \frac{dn}{d\omega}) . \qquad (2.3.1.3)$$

We define a group refractive index N_G given by

$$N_G = n + \omega \frac{dn}{d\omega} . \qquad (2.3.1.4)$$

In terms of wavelength this becomes

29

$$N_G = n - \lambda_0 \frac{dn}{d\lambda_0} \quad . \qquad\qquad (2.3.1.5)$$

The relative bandwidth of a source is $\delta\lambda/\lambda_0$ where $\delta\lambda$ is a spread of wavelengths λ_2-λ_1 around λ_0. If the energy propagates through a fibre of length L, then the spread of arrival times due to the different wavelengths is

$$d\tau_c = \frac{L}{c} N_G(\lambda_1) - \frac{L}{c} N_G(\lambda_2) \quad , \qquad (2.3.1.6)$$

or

$$d\tau_c = \frac{L}{c} \frac{dN_G}{d\lambda} \partial\lambda \quad . \qquad\qquad (2.3.1.7)$$

Now we can substitute for N_G to obtain the delay corresponding to the material dispersion in a step-index optical fibre. This is given by

$$d\tau_c = \frac{L}{c} \frac{\lambda_0 d^2 n_1}{d\lambda^2} \partial\lambda, \qquad\qquad (2.3.1.8)$$

or, if we include the relative bandwidth of the source, we get

$$d\tau_c = \frac{L}{c} (\frac{\partial\lambda}{\lambda_0}) D \quad \text{where} \quad D = \lambda_0^2 \frac{d^2 n_1}{d\lambda^2} \quad . \qquad (2.3.1.9)$$

A graph of D against wavelength is given in figure 2.5.

2.3.2 Intermodal Dispersion

We now want to consider the intermodal dispersion in a step-index multimode optical fibre. From equations (2.3.10) and (2.3.11) we have

$$\tau_M = \frac{L}{c} \cdot \frac{v}{k} \cdot \frac{d(n_2 k \Delta b)}{dv} \ . \qquad (2.3.2.1)$$

We also have an expression for v, equation (2.3.3), which is approximately

$$v = k\, a\, n_1 \sqrt{2\Delta} \cong k\, a\, n_2 \sqrt{2\Delta} \ . \qquad (2.3.2.2)$$

Substituting v into (2.3.2.1) allows the intermodal dispersion to be expressed as

$$\tau_M = \frac{L}{c}\, n_2 \Delta\, \frac{d(vb)}{dv} \ . \qquad (2.3.2.3)$$

The derivative may be shown to be given approximately by 1-π/v [2.10]. Thus, the following useful form for the intermodal dispersion is

$$\tau_M = \frac{L}{c}\, (n_1 - n_2)(1 - \frac{\pi}{v}). \qquad (2.3.2.4)$$

For highly multimode fibres with large v, this expression becomes approximately equal to the geometric result obtained by considering the optical path difference between the axial and critical ray, figure 2.6. By considering the path difference between the axial and critical ray we have

$$\tau_m = \frac{n_1}{c}\, [\, Lmax - L\,] \ . \qquad (2.3.2.5)$$

We now write Lmax in terms of L and the critical angle. Thus we have

31

$$\tau_m = \frac{n_1}{c} \left[L \left(\frac{1}{\cos \theta_c} - 1 \right) \right]. \qquad (2.3.2.6)$$

When the critical angle is expressed in terms of refractive indices we have

$$\tau_M = \frac{L}{c} n_1 \left(\frac{n_1 - n_2}{n_2} \right) \sim \frac{L}{c} (n_1 - n_2). \qquad (2.3.2.7)$$

2.4 Phase Dispersion in a step-index fibre.

An amplitude splitting optical fibre interferometer allows the correlation of an EM wave with a delayed version of itself. In free space the delay between the two waves is simply L/c where L is the path difference. However, in a dispersive medium the delay between the two waves becomes L / v_p, where v_p is the phase velocity of the wave in the medium. Phase velocity is given by

$$v_p = \frac{\omega}{\beta} , \qquad\qquad (2.4.1)$$

where β is the wavenumber of the light in the medium and ω the angular frequency which is fixed. The wavenumber of the light in the medium depends on the boundary conditions imposed on it. In a step-index multimode fibre illuminated by a monochromatic source each mode has a different wavenumber.

From equation (2.2.1.2) we have

$$\beta^2 = k_1^2 - k_c^2 , \qquad\qquad (2.4.2)$$

where $k_1 = n_1 k$ (n_1 is the refractive index of the medium and k is the free space wavenumber) and k_c is the wavenumber at cut-off. From section 2.2.2, the cut-off wavelength for a step-index fibre may be determined by the root of the equation

$$J_0(u_c) = 0 , \qquad\qquad (2.4.3)$$

or, since the parameter w is zero at cut-off we may write

33

$$J_0(v_c) = 0 . \qquad (2.4.4)$$

The phase velocity of a given mode may then be written as

$$v_p = \frac{\omega}{\beta} = \frac{\omega}{\sqrt{k_1^2 - k_c^2}} . \qquad (2.4.5)$$

The expression for the v number of a mode at cut-off is

$$v_c = k_c a (n_1^2 - n_2^2) , \qquad (2.4.6)$$

where k_c is the cut-off wavenumber. By substituting (2.4.6) into (2.4.5) we have for the phase velocity

$$v_p = \frac{\omega}{\sqrt{k_1^2 - (\frac{v_c}{a (n_1^2 - n_2^2)})^2}} . \qquad (2.4..7)$$

For a mode whose v number at cut-off is $v_{c,mn}$ the phase delay in a fibre of length L is

$$\partial t = \frac{L}{\omega} \sqrt{(n_1 k)^2 - (\frac{v_{c,mn}}{a (n_1^2 - n_2^2)})^2} . \qquad (2.4.8)$$

From equation (2.4.8) we see that, for a multimode optical fibre, the phase delay decreases as $v_{c,mn}$ increases. Now , substituting for ω (=ck) and with equation (2.2.1.18), which is

$$v = ka(n_1^2 - n_2^2)^{1/2}, \qquad (2.2.1.18)$$

we have

$$\partial t = \frac{L}{c} \sqrt{n_1^2 - (\frac{v_{c,mn}}{v})^2} \quad , \qquad (2.4.9)$$

or

$$\partial t = \frac{L}{c} \sqrt{n_1^2 - (\frac{k_{c,mn}}{k})^2} \quad . \qquad (2.4.10)$$

We know that the wavenumber β in the fibre lies between two values as follows

$$n_2 k \overset{<}{=} \beta \overset{<}{=} n_1 k. \qquad (2.4.11)$$

Rearranging equation (2.4.2) we see that

$$k_c^2 = k_1^2 - \beta^2. \qquad (2.4.12)$$

The maximum value of k_c occurs for $\beta = n_2 k$ and the minimum value of k_c occurs for $\beta = n_1 k$. The minimum value of the phase delay using (2.4.10) is therefore $n_2 k$ and the maximum value of phase delay is $n_1 k$. The maximum difference in the phase delay between the modes of a fibre, Δt, may be written

$$\Delta t \cong \frac{L}{c}(n_1 - n_2) . \qquad (2.4.13)$$

This expression is seen to be the same as the expression for intermodal dispersion but, this time, the higher order modes have the shorter delays.

2.4.1 Optical Path Length.

When considering the optical path length (OPL) of a fibre for inclusion in an interferometer, or any situation where the OPL is important, then it is the phase dispersion which must be taken into account. Phase velocity has been discussed in section 2.4 and has been defined as

$$v_p = \frac{\omega}{\beta_{mn}} \,,$$

(2.4.1)

where β_{mn} is the wavenumber of the wave propagating in the mn^{th} mode. The OPL between two points A and B is defined as the velocity of light in a vacuum, c, multiplied by the time taken to travel from A to B, δT. Thus, we can write

$$OPL = c\delta T \,.$$

(2.4.1.1)

We may also write that the time taken for light to travel from A to B, in the mn^{th} mode, is the distance, L, divided by the velocity in the medium. We have

$$\delta T = \frac{L}{v_p} = \frac{L\beta_{mn}}{\omega} \,,$$

(2.4.1.2)

The OPL of the mn^{th} mode is, therefore,

$$OPL_{mn} = \frac{cL\beta_{mn}}{\omega} \,.$$

(2.4.1.3)

In free space, we have $c = \omega / k$, so equation (2.4.1.3) becomes

$$OPL_{mn} = \frac{L\beta_{mn}}{k} \,. \qquad (2.4.1.4)$$

In a dispersive medium of refractive index n, we have

$$v_p = \frac{c}{n(\lambda)} \qquad . \qquad (2.4.1.5)$$

Thus, a different expression for the OPL is

$$OPL = c \; \frac{Ln(\lambda)}{c} \; = \; Ln(\lambda) \,. \qquad (2.4.1.6)$$

Comparing (2.4.1.4) with (2.4.1.6) we see that a mode of wavenumber β_{mn} has an effective refractive index, n_{eff}, given by

$$n_{eff} = \frac{\beta_{mn}}{k} \,. \qquad (2.4.1.7)$$

Following the working of section (2.4) on phase velocity we have that the optical path length of the mnth mode is given by

$$OPL_{mn} = L\sqrt{n_1^2 - (\frac{v_{c,mn}}{v})^2} \,, \qquad (2.4.1.8)$$

and the maximum optical path difference between the modes, for a fibre of length L, is given by

$$\Delta(OPL) \cong L(n_1 - n_2) \,. \qquad (2.4.1.9)$$

From equations (2.4.1.8) and (2.4.1.9) we see that a multimode optical fibre in which all of the modes are excited will emit light which has travelled a range of optical paths, the longest being travelled by the lowest order mode.

2.5 Interference

Many pre-detector signal processing techniques produce interference patterns. The apparent positions of two sources and their wavelength determines the fringe geometry, that is, whether the fringes are linear or circular and the fringe separation.

When two or more waves overlap they interfere in accordance with the principle of superposition to produce a series of bright and dark regions where the waves reinforce or cancel each other. By the principle of superposition the electric field at a given point, P, is the vector sum of the separate electric fields at that point. We can write

$$E_p = E_1 + E_2 + \ldots \qquad (2.5.1)$$

As the phase of an optical wave is repeated at about 10^{14} Hz, a detector measures the time average value of power or intensity.

$$I = <|E_p|^2> = <|E_1 + E_2|^2> . \quad (2.5.2)$$

If we consider E_1 and E_2 to be two linearly polarised plane waves propagating in directions r_1 and r_2 with wavenumbers k_1 and k_2 and frequency ω, then the two waves may be represented by

$$E_1 = E_{01} Cos (\omega t - k_1.r_1 + \phi_1) , \qquad (2.5.3)$$

and

$$E_2 = E_{02} Cos (\omega t - k_2.r_2 + \phi_2) . \qquad (2.5.4)$$

Expanding equation (2.5.2), we have

38

$$I = \langle |E_1|^2 \rangle + \langle |E_2|^2 \rangle + 2\langle |E_1 E_2| \rangle . \quad (2.5.5)$$

The third term on the right hand side is the interference term. Substituting for E_1 and E_2 , we have for the third term

$$E_1.E_2 = E_{01}.E_{02} \text{Cos} (\omega t - k_1.r_1 + \phi_1) \text{Cos}(\omega t - k_2.r_2 + \phi_2) , \quad (2.5.6)$$

or

$$E_1.E_2 = 1/2\, E_{01}.E_{02} \text{Cos} (\delta), \quad (2.5.7)$$

where

$$\delta = k_1.r_1 + \phi_1 - k_2.r_2 - \phi_2. \quad (2.5.8)$$

The intensity at P will be a maximum when Cos $\delta = 1$, that is, when the phase difference between the beams is $2m\pi$, where m is a positive or negative integer. This corresponds to the condition for constructive interference. The intensity at P will be a minimum when Cos $\delta = -1$. That is, when the phase difference between the beams is $(2m+1)\pi$, where m is a positive or negative integer. This corresponds to the condition for destructive interference.

If E_1 and E_2 are parallel then we may write

$$I = I_1 + I_2 + 2\sqrt{I_1 I_2}\, \text{Cos} (\delta). \quad (2.5.9)$$

If I_1 and I_2 are of equal intensity we have

$$I = 4I_0 \text{Cos}^2(\frac{\delta}{2}) , \quad (2.5.10)$$

where I_0 is the maximum intensity. The many ways of producing interference can be divided into three groups, polarisation splitting, wavefront splitting and amplitude splitting. Polarisation splitting will not be considered. Wavefront splitting implies that different portions of a single wavefront are used to produce two or more sources which then interfere. Amplitude splitting implies that a single wavefront is divided into several identical wavefronts which travel different paths before they overlap.

2.5.1 Wavefront splitting interferometers

An example of a wavefront splitting interferometer is that used in the Young's interference experiment, figure 2.7.

Light is incident on a single pinhole Q and then on a pair of pinholes Q_1 and Q_2. The two spherical waves emerging from Q_1 and Q_2 fall onto a screen and interfere in the region where the waves overlap. If the amplitudes of the waves are the same and the two slits are of equal width and very close together, then the intensity at a point P on the screen is given by equation (2.5.10), which is

$$I = 4I_0 Cos^2(\frac{\delta}{2}) . \qquad (2.5.10)$$

At P, the waves from Q_1 and Q_2 have traveled distances Q_1P and Q_2P. The phase difference between them at P is δ where

$$\delta = \frac{2\pi}{\lambda} (Q_2P - Q_1P) . \qquad (2.5.1.1)$$

It is assumed that the waves have the same phase at the two pinholes. The path difference $Q_2P - Q_1P$ is the distance Q_2R in figure

40

2.8. When the distance between the pinholes is small compared with the distance from the pinholes to the screen we can make the approximation

$$\text{Sin } \theta = \frac{Q_2 R}{d} \; . \qquad\qquad (2.5.1.2)$$

In this case, the phase difference between beams is given by

$$\delta = \frac{2\pi}{\lambda} \, (\, d \, \text{Sin } \theta \,) \; . \qquad\qquad (2.5.1.3)$$

For I to be a maximum, that is, for a bright interference fringe, $\delta = 2m\pi$ as before. Thus, for the mth bright fringe, we have

$$2m\pi = \frac{2\pi}{\lambda} \, d \, \text{Sin } \theta \; , \qquad\qquad (2.5.1.4)$$

or

$$m\lambda = d \, \text{Sin } \theta \; . \qquad\qquad (2.5.1.5)$$

We then make the further approximation that the angle between the optical axis and the light which travels to the mth fringe is given by

$$\text{Sin } \theta = \frac{r_m}{D} \; , \qquad\qquad (2.5.1.6)$$

where r_m is the position of the mth bright fringe. From equations (2.5.1.5) and (2.5.1.6) , we have that the position of the mth bright fringe is given by

$$r_m = \frac{m\lambda D}{d} \; . \qquad\qquad (2.5.1.7)$$

41

For I to be a minimum, or a dark fringe we require $\delta = (2m+1)\pi$. Thus, for the mth dark fringe we have

$$(2m+1)\pi = \frac{2\pi}{\lambda} d \sin \theta , \qquad (2.5.1.8)$$

or

$$(m + 1/2)\lambda = d \sin \theta . \qquad (2.5.1.9)$$

Using equation (2.5.1.6) as before we have

$$(m+1/2)\lambda = \frac{d\, r_m}{D} . \qquad (2.5.1.10)$$

This may be rearranged to give, for the position of the mth dark fringe, that

$$r_m = \frac{(m+1/2)\,\lambda D}{d} . \qquad (2.5.1.11)$$

2.5.2 Amplitude splitting interferometers

As an example of an amplitude splitting interferometer we consider the Michelson interferometer, figure 2.9. A wave from a source, S, is incident on the beamsplitter, B. The wave is split into two waves of equal amplitude. The first part travels to mirror m_1 where it is reflected and the second part travels to mirror m_2 where it is also reflected. The waves are recombined at B and propagate to a screen where circular interference fringes may be observed.

The two mirrors produce two apparent sources a distance 2d apart where d is the path difference in the arms of the interferometer, figure 2.10. The distance the waves appear to have traveled to a point

42

P on the screen is S_1P and S_2P. The phase difference between the beams at P is δ where

$$\delta = \frac{2\pi}{\lambda}(S_1P - S_2P).$$
(2.5.2.1)

This distance can be seen to be S_1R, so we can write

$$\delta = \frac{2\pi}{\lambda}(2\,d\,\text{Cos}\,\theta).$$
(2.5.2.2)

The intensity distribution across the rings is given by equation (2.5.10), written

$$I = 4I_0\text{Cos}^2(\frac{\delta}{2}).$$
(2.5.10)

For the waves to interfere constructively we require $\delta = 2m\pi$ where m is an integer. So, for a bright ring, we have

$$m\lambda = 2\,d\,\text{Cos}\,\theta.$$
(2.5.2.3)

For the waves to interfere destructively we require $\delta = (2m+1)\pi$. So, for a dark ring, we have

$$(m+1/2)\lambda = d\,\text{Cos}\,\theta.$$
(2.5.2.4)

The radius of the rings depends on the separation of the mirrors M_1 and M_2. For a ring of order m the angle of the ring from S_1 is given by

$$\text{Cos}\,\theta = \frac{m\lambda}{2d}.$$
(2.5.2.5)

As the path difference, d, is increased the radius of the mth fringe decreases. As d becomes smaller, the two sources S_1 and S_2 become coincident and the central fringe expands to fill the entire field of view.

2.6 Coherence Theory

Coherence is a measure of the degree of correlation of the phases of different waves at different times or locations. The degree of correlation may be investigated using an interferometer. If the correlation is between two waves separated in time we measure the temporal coherence of the light. If the correlation is between two waves originating from different points in space measure the spatial coherence of the light.

A source has a characteristic frequency spread or bandwidth dv. From the bandwidth theorem we have

$$dt \cong \frac{1}{dv} , \qquad (2.6.1)$$

where dt is the coherence time of the source. This corresponds to the time over which a wave packet from the source has a predictable phase and since a wave travels a distance cdt in this coherence time, cdt is the coherence length, L_c. We have

$$L_c = c\, dt = \frac{c}{dv} . \qquad (2.6.2)$$

The bandwidth δv is related to the linewidth $\delta \lambda$. Differentiating $v = c / \lambda$ we obtain

$$dv = \frac{-c}{\lambda^2}\, d\lambda . \qquad (2.6.3)$$

By substituting (2.6.3) into (2.6.2) we may express the coherence length in terms of the central wavelength and linewidth of a source. Thus, we have

$$L_c = \frac{\lambda^2}{d\lambda} . \qquad (2.6.4)$$

When a spatially incoherent source illuminates a plane, we may define a coherence width which is equal to the maximum separation of two points which will produce interference fringes.

Consider the geometry of figure 2.11. Two sources S_1 and S_2 each illuminate a plane containing two slits as with a Young's slits experiment. Both sources produce interference patterns in a second plane. The interference patterns are mutually incoherent. As S_2 is in a different position to S_1 the phases of the interference patterns are slightly different. If the separation of the slits, P_1 and P_2, is sufficient so that

$$QP_2 = S_2P_2 - S_2P_1 = \frac{1}{2}\lambda, \qquad (2.6.5)$$

then the bright fringes due to S_1 will be superimposed on the dark fringes due to S_2, and visa versa, so no fringes will be seen. The minimum separation of P_1 and P_2, before this occurs, defines the coherence width. The path difference QP_2 is given by

$$QP_2 = d_c \, \mathrm{Sin}\, \theta, \qquad (2.6.6)$$

where dc is the separation of the slits, or the coherence width. The angle θ may be expressed as

$$\mathrm{Sin}\, \theta = \frac{d_c/2}{D_2} = \frac{d_s}{D_1}. \qquad (2.6.7)$$

As D = D1 + D2 we have

$$\mathrm{Sin}\, \theta = \frac{1}{D}\left(d_s + \frac{d_c}{2}\right). \qquad (2.6.8)$$

46

From equations (2.6.6) and (2.6.8), the path difference QP_2 is given approximately by

$$QP_2 \cong \frac{d_c d_s}{D} . \qquad (2.6.9)$$

Thus, no interference will be seen when the two sources are separated by a distance d_s, where

$$d_s \cong \frac{\lambda D}{2 d_c} . \qquad (2.6.10)$$

If the two point sources a distance d_s apart, are replaced by an extended source of size d_s then no interference fringes will be seen. The area of the extended source, A_s, may be related to a coherence area, A_c. We can write

$$A_s \cong \frac{\lambda^2 D^2}{4 A_c} . \qquad (2.6.11)$$

2.6.1 The Analytic Signal

The analytic signal is of use in discussing a linear optical system and will be used in the following sections to define the coherence of two waves which are allowed to interfere. A linear system is one in which several impulses cause a response which is the sum of the individual responses.

The electromagnetic field for many practical optical sources covers a frequency range which is small compared with the centre frequency. The radiation is then said to be be quasi-monochromatic and may be

represented by the real function $E^{(r)}(t)$ which is a real disturbance and may be expressed in the form

$$E^{(r)}(t) = \int_{-\infty}^{\infty} A(\nu) \, Cos \, [\, \phi(\nu) - 2\pi\nu t \,] \, d\nu, \qquad (2.6.1.1)$$

where $A(\nu)$ is the amplitude and $\phi(\nu)$ the phase. A second real function $E^{(i)}(t)$ may be defined by replacing $\phi(\nu)$ by $\phi(\nu) - \pi/2$. We then have

$$E^{(i)}(t) = \int_{-\infty}^{\infty} A(\nu) \, Sin \, [\, \phi(\nu) - 2\pi\nu t \,] \, d\nu. \qquad (2.6.1.2)$$

These two functions may be combined in a single exponential function $E(t)$ which is written

$$E(t) = E^{(r)}(t) + i \, E^{(i)}(t) = \int_{-\infty}^{\infty} A(\nu) \, e^{i \, (\phi(\nu) - 2\pi\nu t)} \, d\nu. \qquad (2.6.1.3)$$

If $A(\nu)$ is the Fourier transform of $E^{(r)}(t)$, then since $E^{(r)}(t)$ is real we have

$$A(-\nu) = A^{*}(\nu) . \qquad (2.6.1.4)$$

This is because all the information about $E^{(r)}(t)$ is contained in the positive frequency region of the spectrum. Equation (2.6.1.3) can be written

$$E(t) = 2 \int_{0}^{\infty} A(\nu) \, e^{i2\pi\nu t} d\nu. \qquad (2.6.1.5)$$

The function E(t) is known as the analytic signal. If the operations carried out upon $E^{(r)}(t)$ are linear, then the more convenient function E(t) can be used in the analysis and $E^{(r)}(t)$ obtained at the end. If the amplitude of the components of the spectrum is significant only over a region δv which is small compared with the mean frequency v, then we write the analytic signal in the form

$$E(t) = E_0(t)\, e^{i\,(\,\phi(t)\,-\,2\pi vt)}. \qquad (2.6.1.6)$$

The real part is then given by

$$E^{(r)}(t) = E_0(t)\, \text{Cos}\, [\, \phi(t)\, -\, 2\pi vt\,]\,. \qquad (2.6.1.7)$$

2.6.2 Coherence as defined by correlation integrals.

We can use the analytic signal to define the coherence of an electromagnetic field in terms of a correlation over the field. If E(r,t) is the field at a given point in space and time and if the field is observed for a time τ which is large compared with its mean period $1/v$ then the auto-correlation, $\Gamma_{11}(r,t)$, or the self coherence function of the field may be expressed as

$$\Gamma_{11}(r,t) = \lim \tau \to \infty \frac{1}{2\tau} \int_{-\tau}^{+\tau} E(r,t)\, E^*(r,t)\, dt\,. \qquad (2.6.2.1)$$

The temporal coherence of the field may be expressed as

$$\Gamma_{11}(r,t+\tau) = \frac{1}{2\tau} \int_{-\tau}^{+\tau} E(r,t)\, E^*(r,t+\tau)\, dt\,, \qquad (2.6.2.2)$$

and the spatial coherence of the field may be written

$$\Gamma_{12}(r+dr,t) = \frac{1}{2\tau} \int_{-\tau}^{+\tau} E(r,t) \, E^*(r+dr,t) \, dt \,. \qquad (2.6.2.3)$$

These definitions will be used in the following sections.

2.6.3 Temporal coherence

The device most commonly used to measure temporal coherence is the Michelson interferometer. This interferometer has two air paths, one of which is used to alter the delay between the two waves. Light from a scene is introduced to the interferometer. The light is divided into two waves of equal amplitude by the beamsplitter, B. One wave is reflected from mirror m1 and other is reflected from mirror m2. The two waves are recombined at B and the resulting interference measured at the output plane P, as was shown in figure 2.9.

The light introduced to the interferometer is represented by $E(x,y;t)$ where x and y are the normal space coordinates and t is time. If $E_1(x,y;t_1)$ represents the amplitude of the wave which has been reflected from m_1 and $E_2(x,y;t_2)$ represents the amplitude of the wave reflected from m_2 then the complex field at P is

$$E_p(x,y;t_1,t_2) = E_1(x,y;t_1) + E_2(x,y;t_2). \qquad (2.6.3.1)$$

The intensity measured by a detector at P is the time averaged square modulus of the amplitude. We have

$$I_p(x,y;t_1,t_2) = <|E_p(x,y;t_1,t_2)|^2>, \qquad (2.6.3.2)$$

where $<>$ implies a time average and $|\,|$ means modulus. Expanding the right hand side of this equation gives us four terms , which are

$$I(x,y,t_1,t_2) = < |E_1(x,y,t_1)|^2 + |E_2(x,y,t_2)|^2 + E_1^*(x,y,t_1)E_2(x,y,t_2) +$$
$$E_1(x,y,t_1)E_2^*(x,y,t_2) > . \qquad (2.6.3.3)$$

An asterisk denotes complex the conjugate. If the statistics of the radiation are assumed to be stationary, we can write $t_1 = t$, and $t_2 = t + \tau$. Then we have

$$I(x,y,\tau) = < |E_1(x,y,t)|^2 + |E_2(x,y,t+\tau)|^2 + E_1^*(x,y,t)E_2(x,y,t+\tau) +$$

$$E_1(x,y,t)E_2^*(x,y,t+\tau) > . \qquad (2.6.3.4)$$

The first and second terms on the right hand side of equation (2.6.3.4) represent the intensities measured by the detector if either mirror were the only one present. They provide a constant background level and may be written as

$$| E_1(x,y,t) |^2 = I_1(x,y,t) , \qquad (2.6.3.5)$$

and

$$| E_2(x,y,t+\tau) |^2 = I_2(x,y,t+\tau) . \qquad (2.6.3.6)$$

The third and fourth terms can be replaced by

$$< E_1(x,y,t) \, E_2^*(x,y,t+\tau) > \, = \Gamma_{12}(\tau) , \qquad (2.6.3.7)$$

and

$$< E_1^*(x,y,t) \, E_2(x,y,t+\tau) > \, = \Gamma_{12}^*(\tau) , \qquad (2.6.3.8)$$

where $\Gamma(\tau)$ is the temporal mutual coherence function. The function represents the cross correlation of fields E_1 and E_2 at the same point but with time delay τ between them. Substituting equations (2.6.3.5), to (2.6.3.8) into (2.6.3.4) we have

$$I(x,y,\tau) = I_1(x,y,t) + I_2(x,y,t+\tau) + \Gamma_{12}(\tau) + \Gamma_{12}^*(\tau) . \qquad (2.6.3.9)$$

As $\Gamma_{12}(\tau)$ represents an auto-correlation of a wave with a delayed version of itself we may apply the auto-correlation, or Wiener-Khinchin, theorem. This states that the Fourier transform of the auto-correlation of function $\Gamma_{12}(\tau)$ is the power spectrum, $\Gamma_{12}(\nu)$, of that function. We also note that the position coordinates are the same and so we drop the position dependence. We can write

$$\Gamma_{12}(\tau) = \int_0^\infty \Gamma_{12}(\nu)\, e^{-2\pi i\nu\tau} d\nu\,, \qquad (2.6.3.10)$$

and

$$\Gamma_{12}^*(\tau) = \int_0^\infty \Gamma_{12}^*(\nu)\, e^{2\pi i\nu\tau}\, d\nu\,. \qquad (2.6.3.11)$$

Since the power spectrum must be real, we have

$$\Gamma_{12}(\nu) = \Gamma_{12}^*(\nu). \qquad (2.6.3.12)$$

The source is considered to be quasi-monochromatic, so $d\nu\,/\,\nu_0 << 1$ where $d\nu$ is the spectral width and ν_0 is the mean frequency. Then (2.6.3.9) becomes

$$I(\tau) = I_1(t) + I_2(t+\tau) + \int_0^\infty 2\,|\,\Gamma_{12}(\nu)\,|\,\mathrm{Cos}\,(2\pi\nu_0\tau + \phi(\tau)\,)\, d\nu\,. \qquad (2.6.3.13)$$

We can write

$$\Gamma_{12}(\tau) = |\,\Gamma_{12}(\tau)\,|\,\mathrm{Cos}\,(2\pi\nu_0 t + \phi_\Gamma(\tau))\,, \qquad (2.6.3.14)$$

so equation (2.6.3.13) becomes

$$I(\tau) = I_1(t) + I_2(t+\tau) + 2\,|\,\Gamma_{12}(\tau)\,|\,\mathrm{Cos}\,(2\pi\nu_0 t + \phi_\Gamma(\tau))\,, \qquad (2.6.3.15)$$

where $\Gamma_{12}(\tau)$ is the Fourier transform of the frequency distribution of the source. The cosine term can be seen to give information about the temporal mutual coherence function, $\Gamma(\tau)$ and through this $\Gamma(\nu)$.

We can define a normalised mutual coherence function which is

$$\gamma_{12}(\tau) = \frac{\Gamma_{12}(\tau)}{(\,I_1(t)\,I_2(t+\tau)\,)^{1/2}} \quad . \qquad (2.6.3.16)$$

written

Using equations (2.6.3.15) and (2.6.3.16), we have

$$I(\tau) = I_1(t) + I_2(t+\tau) + 2\,(I_1(t)I_2(t+\tau))^{1/2}\,|\,\gamma_{12}(\tau)\,|\,\text{Cos}\,(2\pi\nu_0 t+\phi_\Gamma(\tau)) \quad .$$

$$(2.6.3.17)$$

If the waves are of equal intensity, we have $I_1 = I_2 = I$ and (2.6.3.17) becomes

$$I(\tau) = 2I\,(\,1 + |\,\gamma_{12}(\tau)\,|\,\text{Cos}\,(2\pi\nu_0 t + \phi_\Gamma(\tau))\,) \quad . \qquad (2.6.3.18)$$

This is the relationship for the output of a Fourier transform spectrometer. As a measurable quantity we use Michelsons visibility v defined by

$$v = \frac{I_{max} - I_{min}}{I_{max} + I_{min}} \quad . \qquad (2.6.3.19)$$

The maximum value of $I(\tau)$ occurs when we have

$$\text{Cos}(2\pi\nu_0 t + \phi_\Gamma(\tau)) = 1 \, , \qquad (2.6.3.20)$$

and the minimum value when we have

$$\text{Cos}(2\pi\nu_0 t + \phi_\Gamma(\tau)) = -1 . \qquad (2.6.3.21)$$

Substituting these values into (2.6.3.19), we find

$$v = |\gamma_{12}(\tau)|. \qquad\qquad (2.6.3.22)$$

Thus, the visibility of the interference fringes is a measure of the absolute value of the degree of temporal coherence.

2.6.4 Spatial coherence

The coherence of a radiation field in terms of a correlation between two points in space, at the same time, is normally measured by a Young's slits experiment. Suppose an extended source, Σ, is placed a distance s from a screen containing two apertures P_1 and P_2 a distance d apart. Let s be large compared with d. The light from the source is sampled by the apertures. The resulting interference at a remote plane is measured by a detector at a point P. Let $E_1(x_1, y_1, t)$ and $E_2(x_2, y_2, t)$ be the complex fields at the points P_1 and P_2 due to an element, $d\sigma$, of the source, Σ. The complex field, E_p, at P is the vector sum of the fields at P_1 and P_2 after travelling a distance l_1 and l_2 respectively. So we have

$$E_P(x_1,x_2,y_1,y_2,t_1,t_2) = E_1(x_1,y_1,t-\frac{l_1}{c}) + E_2(x_2,y_2,t-\frac{l_2}{c}). \qquad (2.6.4.1)$$

The intensity measured by a detector at P due to $d\sigma$ is the square modulus of E_p. We write

$$dI_P = |(E_1 + E_2)|^2 d\sigma. \qquad\qquad (2.6.4.2)$$

Expanding equation (2.6.4.2) and assuming the equality

$$E_1^* E_2 + E_1 E_2^* = 2\,Re\,\{E_1^* E_2\}, \qquad (2.6.4.3)$$

we obtain

$$dI_P(x_1,y_1,x_2,y_2) = < |\, E_1(x_1,y_1,t - \frac{l_1}{c}) \,|^2 d\sigma + |\, E_2(x_2,y_2,t - \frac{l_2}{c}) \,|^2 d\sigma$$

$$+ 2\,\text{Re}\,\{\, E_1{}^*(x_1,y_1,t - \frac{l_1}{c})\,d\sigma \,\}. \qquad (2.6.4.4)$$

Now we may write

$$\frac{l_1}{c} = t_1 \; , \; \frac{l_2}{c} = t_2 \; , \qquad (2.6.4.5)$$

we then put

$$t_1 = t \; , \; t_2 = t + \tau. \qquad (2.6.4.6)$$

Equation (2.6.4.4) becomes

$$dI_P(x_1,y_1,x_2,y_2,\tau) = < |\, E_1(x_1,y_1,t) \,|^2 d\sigma + |\, E_2(x_2,y_2,t+\tau) \,|^2 d\sigma$$

$$2\,\text{Re}\,\{\, E_1{}^*(x_1,y_1,t)\,E_2(x_2,y_2,t+\tau)\,d\sigma \,\}. \qquad (2.6.4.7)$$

As each point in the source is assumed to be incoherent with all other points, the intensity at P due to the whole source is obtained by integrating (2.6.4.7) over the source. This is written

$$I_P(x_1,y_1,x_2,y_2,\tau) = \int_\Sigma dI_P. \qquad (2.6.4.8)$$

Equation (2.6.4.7) becomes

$$I_P(x_1,y_1,x_2,y_2) = \int_\Sigma |\, E_1(x_1,y_1,t) \,|^2 d\sigma + \int_\Sigma |\, E_2(x_2,y_2,t+\tau) \,|^2 d\sigma$$

$$+ 2\,\text{Re}\,\{\, \int_\Sigma E_1{}^*(x_1,y_1,t)\,E_2(x_2,y_2,t+\tau)\,d\sigma \,\}. \qquad (2.6.4.9)$$

The first and second terms on the right hand side of (2.7.4.9) represent the intensity measured at P if aperture P_1 or P_2 were the only one open. We can write

$$\int_\Sigma |E_1(x_1,y_1t)|^2 d\sigma = I_1, \qquad (2.6.4.10)$$

and

$$\int_\Sigma |E_2(x_2,y_2t+\tau)|^2 d\sigma = I_2. \qquad (2.6.4.11)$$

We now introduce the phase coherence factor, γ_{12}, between P_1 and P_2 defined by

$$\gamma_{12} = \frac{1}{\sqrt{I_1 I_2}} \int_\Sigma E_1{}^*(x_1,y_1,t) \, E_2(x_2,y_2,t+\tau) \, d\sigma. \qquad (2.6.4.12)$$

If the two waves have traveled equal distances, then $\tau = 0$ and we may drop the time dependence. However, we retain the x,y coordinates as the light is sampled at different points. Using (2.6.4.10) to (2.6.4.12) in (2.6.4.9) we have

$$I_P = I_1 + I_2 + 2\sqrt{I_1 I_2} \, \text{Re}\{\gamma_{12}\}. \qquad (2.6.4.13)$$

The phase coherence function may also be written in the form

$$\gamma_{12} = |\gamma_{12}| \, e^{i\beta_{12}}, \qquad (2.6.4.14)$$

where β_{12} is the phase coherence between the waves. Then (2.6.4.13) becomes

$$I_P = I_1 + I_2 + 2\sqrt{I_1 I_2} \, |\gamma_{12}| \cos\beta_{12}. \qquad (2.6.4.15)$$

So perfect coherence implies that $|\gamma_{12}|$ is unity. If the waves are of equal intensity then $I_1 = I_2 = I$ and we have

$$I_P = 2(1 + |\gamma_{12}| \cos\beta_{12}). \qquad (2.6.4.16)$$

56

Again, using Michelson's visibility, we find that

$$v = |\gamma_{12}(x_1,y_1,x_2,y_2)|. \qquad\qquad (2.6.4.17)$$

So, under the condition $I_1=I_2$, and with zero path difference, the visibility of the interference fringes is a measure of the absolute value of the degree of spatial coherence.
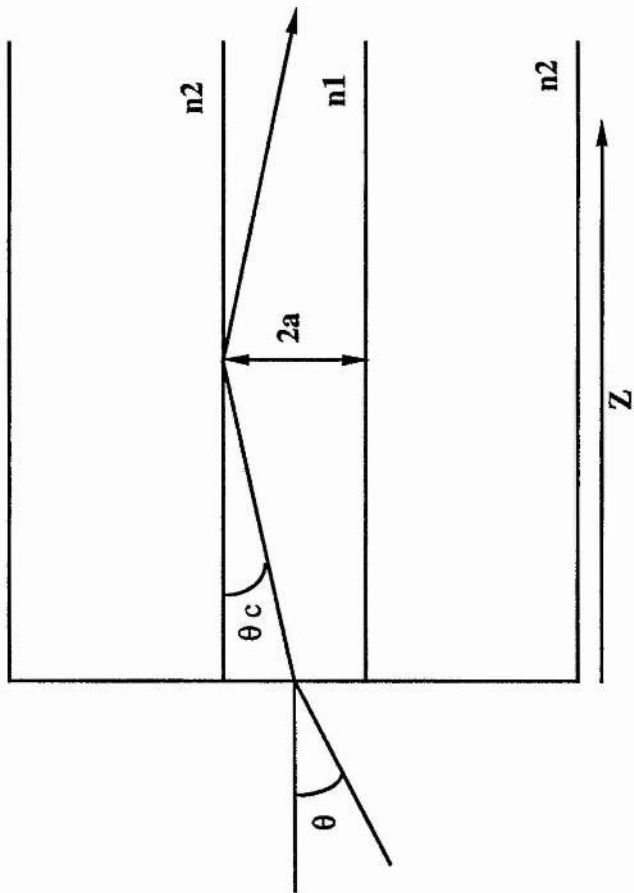
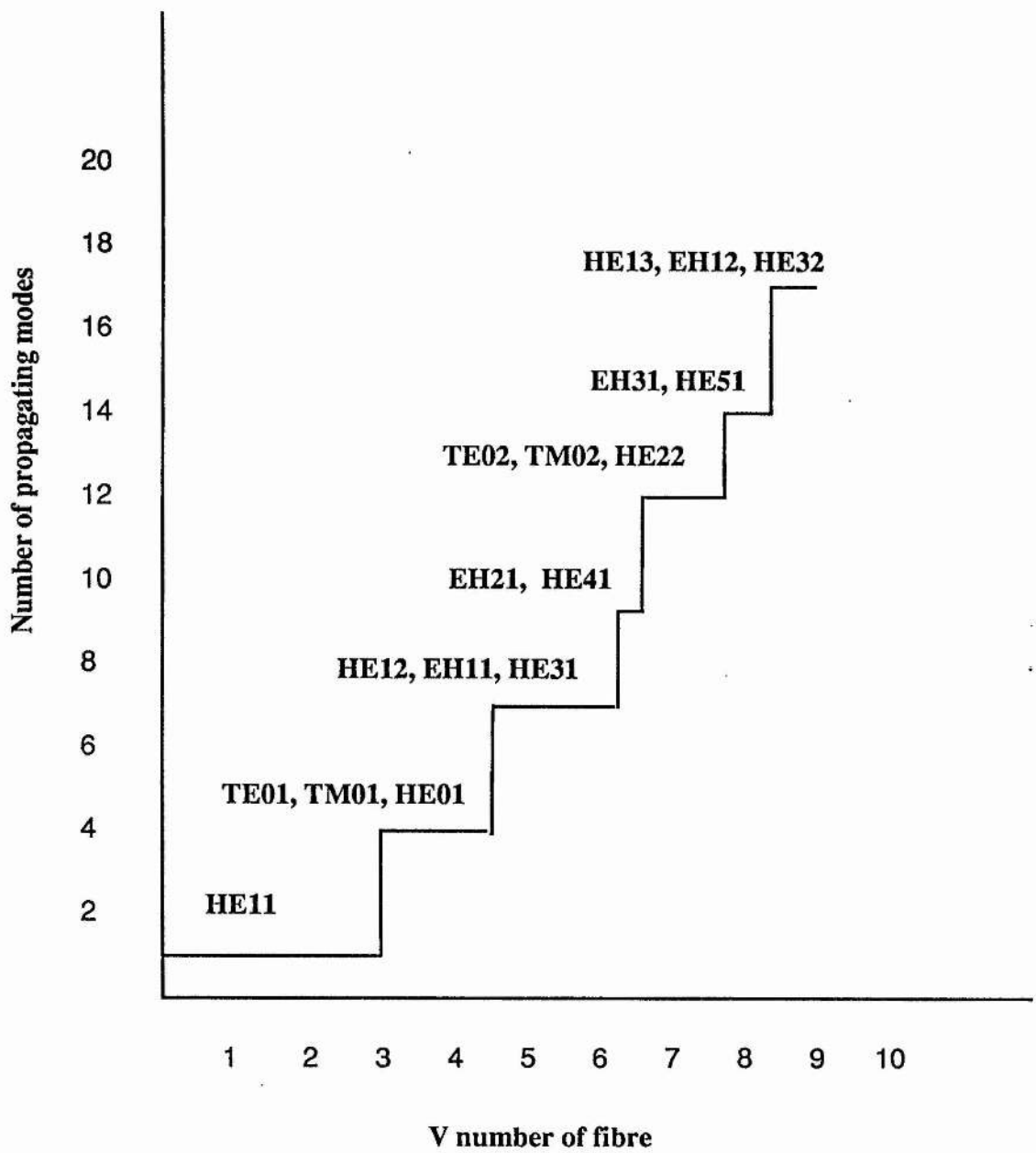Figure 2.1 Geometry for critical ray in optical fibre

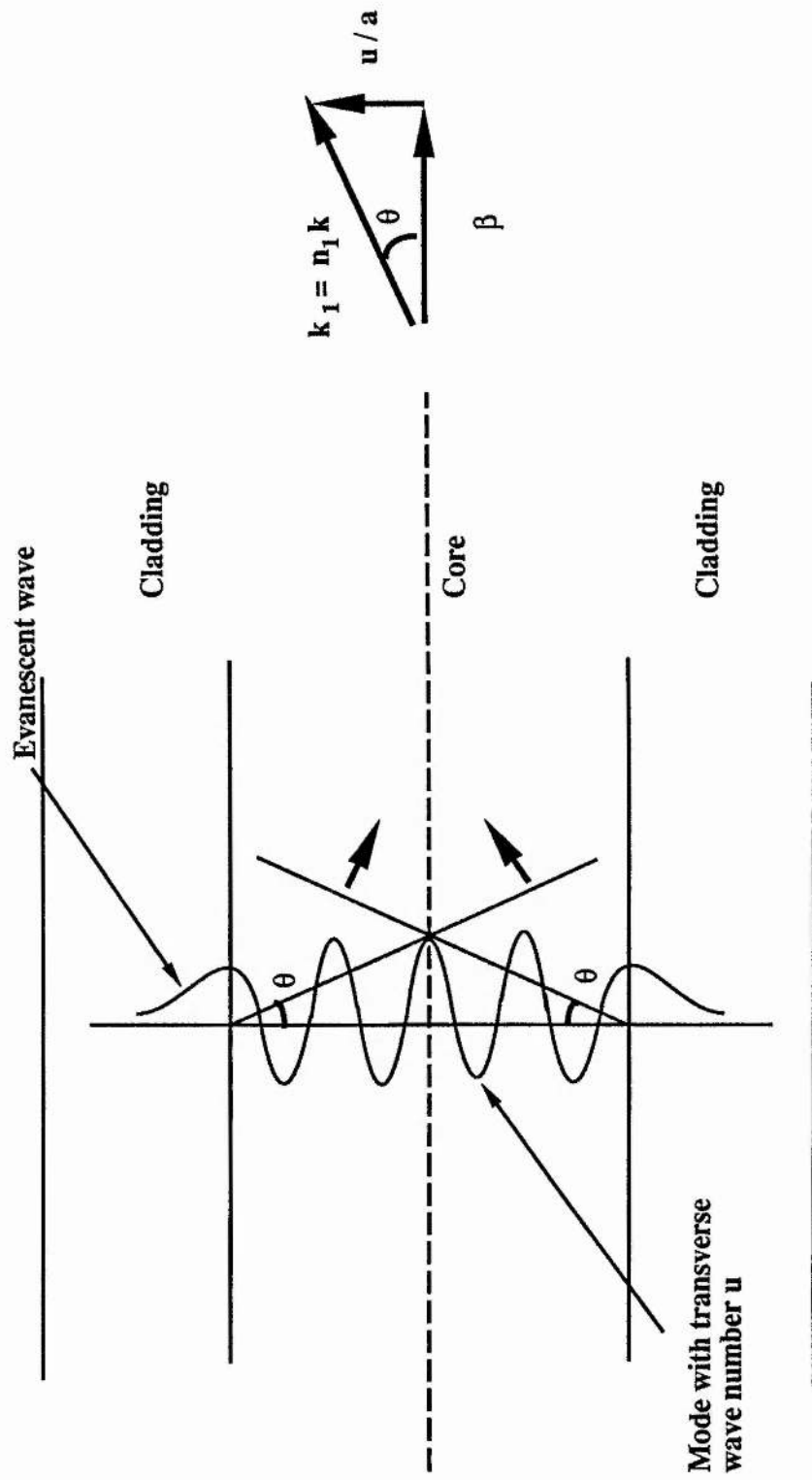Figure 2.2 Number of propagating modes against fibre V number.

Figure 2.3 Transverse wavenumber u.

Refractive index of Silica against wavelength
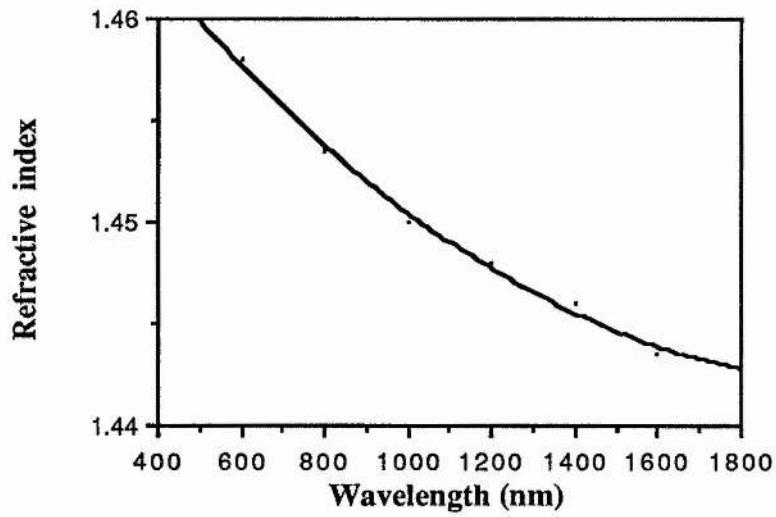
Figure 2.4

Material dispersion against wavelength
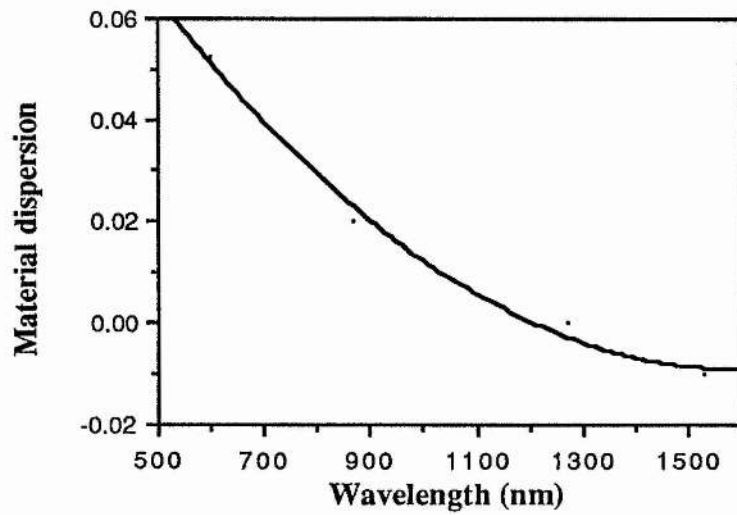
Figure 2.5
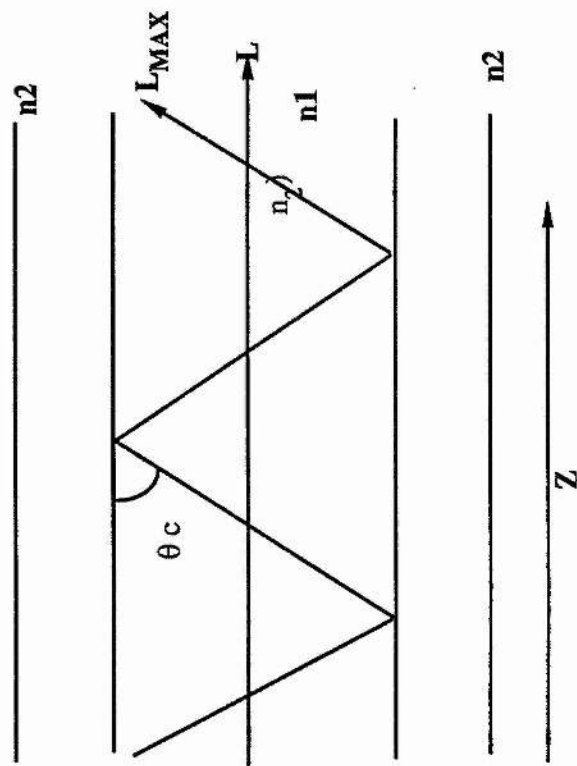
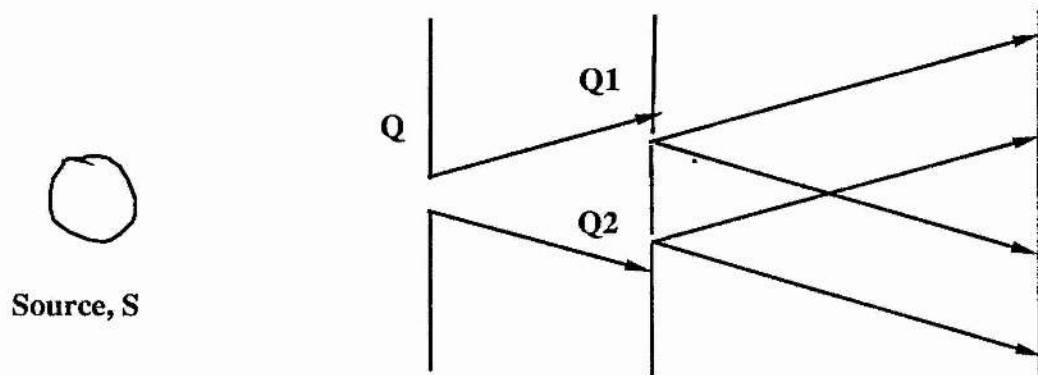Figure 2.6 Geometry for intermodal dispersion in an optical fibre.

Figure 2.7. Young's slits interferometer

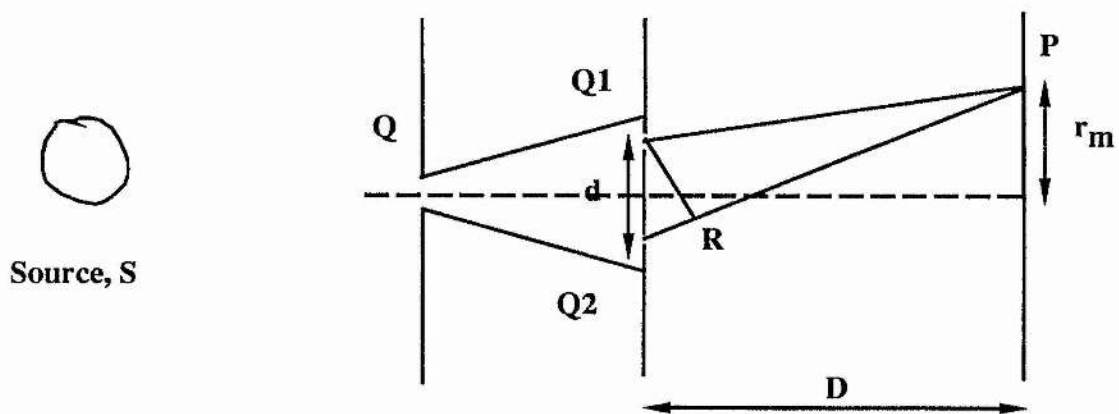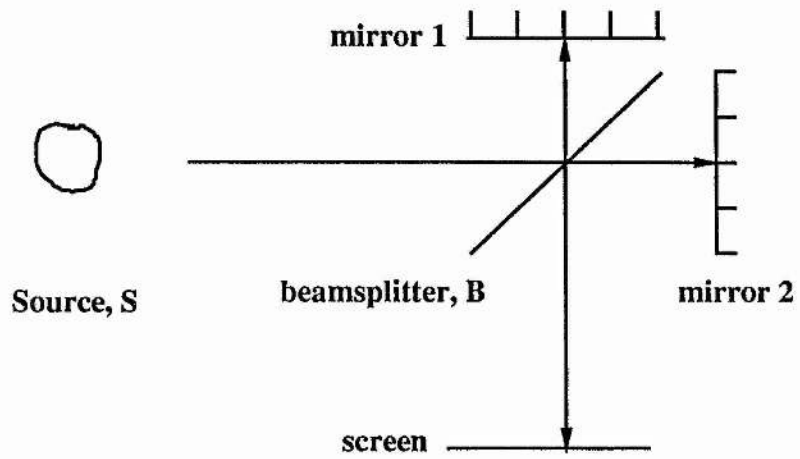**Figure 2.8. Geometry for fringes in Young's slits interferometer**
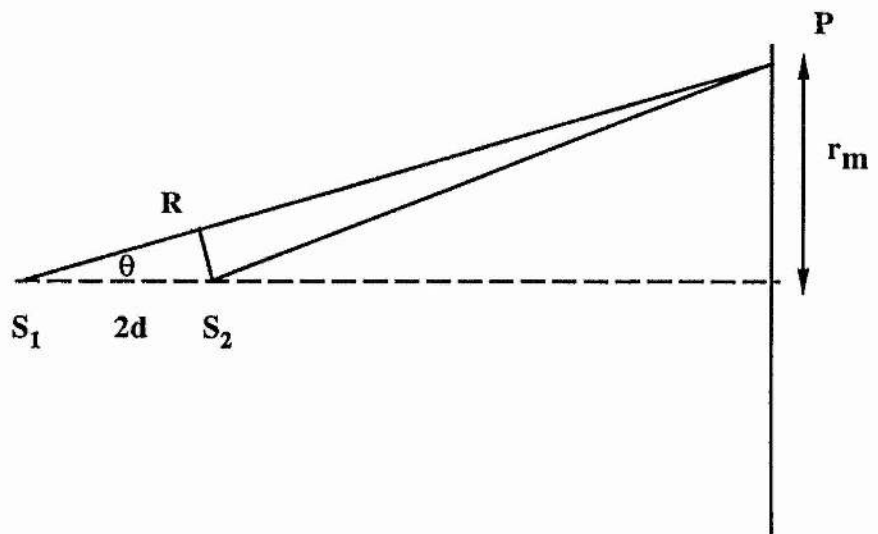
Figure 2.9   Michelson interferometer

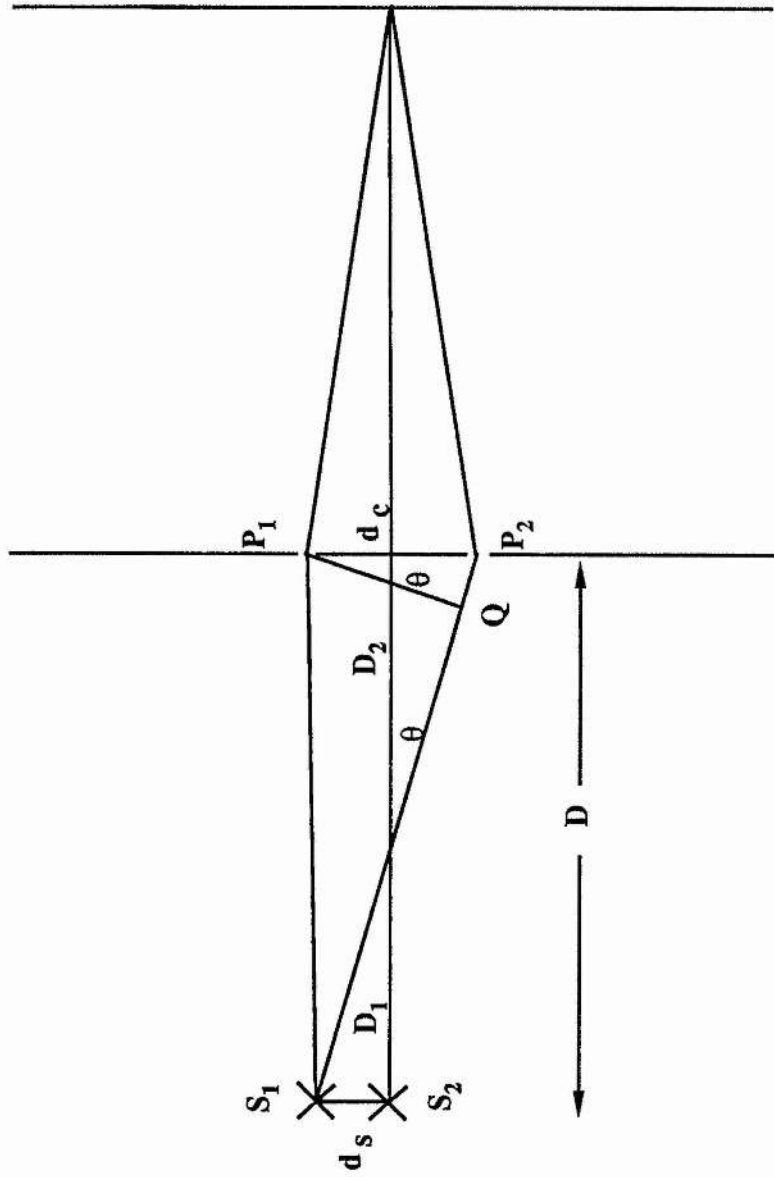**Figure 2.10   Geometry For fringes in Michelson interferometer**

Figure 2.11 Coherence area of a source.

3 Background and Review.

3.1 Fibre optic interferometric sensors

Much of the work contained in this thesis is concerned with measuring the visibility of interference fringes produced by a two beam fibre optic interferometer. The fringe visibility is important because it can be related to the spectrum of the light and because the visibility is a measure of the degree of correlation of the two beams.

The output of an interferometer depends on the superposition of two waves. A detector at the output measures intensity. This intensity, I, is given by

$$I = CE_1E_2 \left(1 - V \cos(\phi_1 - \phi_2) \right) , \qquad (3.1.1)$$

where C is a constant, E_1 and E_2 are the amplitudes of the two beams usually denoted as signal and reference, V is the fringe visibility, and ϕ_1 and ϕ_2 are the phases of the two beams. This equation reveals two of the problems associated with the use of an interferometer as a sensor. Firstly, the output is periodic, that is, if the phase change in the signal arm is greater than 2π radians, then the output becomes ambiguous. This problem can be overcome by the use of two wavelengths. By measuring the intensity due to each wavelength the unambiguous range is extended. Secondly, the sensitivity of the interferometer is also periodic. Differentiating (3.1.1) with respect to phase, we have

$$\frac{dI}{d\phi} = KE_1E_2 \sin(\phi_1 - \phi_2) , \qquad (3.1.2)$$

where K is a different constant. This second problem may be overcome by the use of feedback to maintain the output at quadrature.

The majority of fibre sensors employ singlemode fibre. Fibre optic interferometric sensors are designed to maximise the phase sensitivity of the singlemode fibre to the parameter of interest e.g. temperature, pressure, strain, magnetic field, etc. This may be expressed as

$$\frac{\delta\phi}{\delta x} = \frac{2\pi}{\lambda} \left(n_i \frac{\delta l}{\delta x} + l \frac{\delta n_i}{\delta x} \right) \qquad (3.1.3),$$

where ϕ is the phase of the signal arm and x is the parameter to be measured. The terms in the bracket correspond to a change in the length of the optical path of the signal arm. The first is due to a change in the fibre length and the second is due to a change in the refractive index. If the visibility of the interference fringes is required then the phase of one arm of the interferometer must be altered by at least 2π radians. This will allow the maximum and minimum of intensity to be measured and equation (3.1.1) solved for V.

Fully integrated fibre optic interferometric sensors have been around for about a decade, the main work being carried out using the Sagnac, Mach-Zehnder, and Michelson interferometers. A short review of fibre sensors is given by Davis [3.1].

A fibre ring or Sagnac interferometer for use as a gyroscope is described by Vali and Shorthill [3.2]. When the fibre ring is rotated the interference fringe shift is proportional to the change in angular

velocity. By measuring the total number of fringes seen by a detector the angle of rotation may be calculated.

Optical fibres are affected strongly by temperature and so a fibre interferometer will not normally remain in quadrature where it is most sensitive if homodyne detection is used. Jackson, et al. [3.3] used a piezoelectric (PZT) fibre stretcher in the form of a cylinder together with feedback from the two antiphase outputs of a Mach-Zehnder interferometer in order to eliminate the drift and maintain the interferometer in quadrature. An alternative is to use a heterodyne technique where the light in the reference arm is frequency shifted by a PZT cylinder. In this case, any periodic phase shift to the sensor arm appears as a frequency modulation with the carrier frequency being fixed by the modulation of the reference arm. Phase shifts of less than 10^{-5} radians were detected by Jackson, et al. [3.4] using the heterodyne technique.

An all-singlemode optical fibre Michelson interferometer was constructed by Kashyap and Nayar [3.5] for use as a hydrophone. They used a fibre directional coupler with silver mirrors deposited on the ends of the two fibre arms. The interferometer was operated remotely over a kilometre of fibre and a PZT cylinder was used to simulate acoustic signals in one arm.

A fibre Fabry-Perot sensor is described by Kersey, et al. [3.6]. An advantage of this detector is that the source and detector may be placed at the end of the same fibre whilst the sensor arm is remote. Other fibre Fabry-Perot interferometers have been constructed which use a series of partially reflecting splices to give multiple outputs. A Fabry-Perot interferometric-polarimetric fibre optic sensor is

described by Akhavan Leilabady, et al. [3.7]. Using polarisation maintaining singlemode fibre it was shown that a remote sensing Fabry-Perot cavity formed by a partially reflecting splice and a cleaved end could give both interferometric information seen as interference fringes and polarimetric information seen as a phase shift between the two orthogonal interference patterns. This can be used to extend the unambiguous range of the sensor.

3.2 Phase Modulation

As mentioned in section 3.1, phase modulation of light guided by an optical fibre may be achieved using the piezoelectric effect. The fibre is wrapped around a cylinder of piezoelectric material so that the fibre is stretched when the cylinder changes its dimensions. Electrodes were contacted on the inner and outer walls of the cylinder. When a voltage was applied the cylinder expanded radially by an amount proportional to the applied voltage. When n turns of fibre are wound around the cylinder and a source of free space wavelength λ is guided in a core of refractive index n_1, the number of wavelengths N corresponding to the extension of the fibre is

$$N = \frac{2\pi V d_{33} n \, n_1}{\lambda} \, . \qquad (3.2.1)$$

where V is the applied voltage and for our particular material d_{33} is $593 * 10^{-12}$ m/V at room temperature. For an applied voltage of 100 volts, 10 turns of fibre, and a core refractive index of 1.45 we have that N = 8.5. This value is only approximate as the strain produced in the fibre will cause a change in the fibre birefringence. This alters the value of n_1 and changes the output polarisation in a singlemode fibre.

3.3 Interferometric arrangements

All the classical interferometers can be made using optical fibres. The interferometers used in the experiments, and so described here, are Young's slits, the Mach-Zehnder and Michelson.

3.3.1 Young's Slits interferometers

The Young's slits experiment is usually carried out with two pinholes from which two spherical waves emerge and interfere. We can replace the two pinholes with the ends of two optical fibres. The light emitted by the fibres will produce two approximately spherical waves and interference fringes in the same manner.

The classical Young's slits experiment gives us information about spatial coherence. That is, it is a wavefront splitting interferometer. Light is sampled at two points on a phase front by two pinholes from which spherical waves emerge and are allowed to interfere. The visibility of the interference fringes formed is a measure of the spatial coherence of the two points on the wavefront. A problem with the classical Young's slits experiment is that the fringe spacing is inversely proportional to the separation of the two pinholes. So, in order to correlate two widely separated points, a correspondingly small detector is required. A fibre Young's slits interferometer can be made so that the fringe spacing is independent of sampling position.

3.3.2 Mach-Zehnder interferometer

The Mach-Zehnder interferometer is frequently used in fibre sensors. It is an amplitude splitting interferometer and is constructed from

two fibre couplers. The first coupler splits the light into two waves which travel a reference and signal path until being recombined by the second coupler. The reference arm is usually phase modulated. An advantage of this interferometer over the Michelson is that the two anti-phase outputs can be used in the post-detector signal processing. Interference fringes will be seen if the path difference between the reference and signal arm is less than the coherence length of the source.

3.3.3 Michelson interferometer

A Michelson interferometer, like the Mach-Zender, is frequently used in fibre sensors. It is constructed from a single fibre coupler which splits the light into signal and reference fibre arms and recombines the light when it is reflected from their ends. The reflection will occur from a cleaved fibre end but for high reflectivity a lens and mirror may be used or preferably the fibre end is silvered. An advantage of this interferometer is the few components required. Also the double pass of light in the signal arm makes its sensitivity twice that of the Mach-Zehnder. A disadvantage is that as 50% of the light is returned to the source the stability of the source can be affected. The same conditions apply for the production of fringes as for the Mach-Zehnder.

3.4 Multimode Optical Fibre Interferometry.

Singlemode optical fibre is used in the majority of fibre interferometers. Multimode optical fibre is more commonly used in devices which rely on intensity. A major advantage of multimode optical fibres is their collecting area which is typically 2 orders of magnitude greater that of a singlemode fibre. Two consequences of

this are relaxed tolerances for alignment of fibres with each other or with devices and greater coupled power. Note that the numerical aperture of the fibre relies only on the core and cladding refractive indices.

Singlemode fibre produces a beam with uniform amplitude and phase so interference fringes may be easily detected. Multimode fibres produce beams with distorted amplitude and phase but in many cases interference patterns can still be resolved. Roychoudhuri [3.8] suggested that a multimode fibre could be used in an interferometer and different optical path lengths obtained by exciting different modes of the fibre by changing the angle of illumination of the source. He obtained a graph which seems to indicate that optical path length increases as the angle of illumination increases although from equation 2.4.1.8, derived in section 2.4.1, one would expect the opposite to be the case.

Shajenko [3.9] considered multimode optical fibres for inclusion in optical hydrophones. High visibility fringes were obtained when light from a HeNe laser was guided to an air path Michelson interferometer through 1km of multimode fibre and the fringe pattern measured via a 25m long multimode optical fibre. In a second paper Shajenko [3.10] replaced the HeNe laser with a white light source and a 100nm interference filter. Despite the multimode nature of the fibre it was shown that a 0.05nm displacement of one mirror of the interferometer could be detected. A Mach-Zehnder interferometer made from multimode optical fibre and illuminated by a HeNe source was constructed by Shajenko [3.11]. When one arm was phase modulated by a PZT material at 400hz the minimum detectable optical path difference was 0.04nm.

Interference patterns in multimode optical fibre interferometers with path differences of up to 800m were obtained by Shajenko [3.12]. It was noted that the number of modes of a multimode laser detected over the output plane changed with position due to the wavelength dependence of each mode and the periodicity of the source visibility curve was reduced in amplitude.

When a monochromatic source illuminates an interferometer the relationship between the path difference and visibility of interference fringes becomes ambiguous after the phase in one arm has changed by 2π radians. A white light source has a very short coherence length and this can be used to transmit information about the path difference in an interferometer and overcome the ambiguity. The light emitted by a white light source can be considered to consist of a short wave packet. If this source illuminates the interferometer then the light emitted by the interferometer can be considered to consist of two short wave packets separated by the delay in the interferometer. If the light is guided to a second remote interferometer then scanning the second interferometer will produce interference fringes when the path difference is zero and also when the path difference is equal to the path difference in the first interferometer. Using this method Bosselmann and Ulrich [3.13] demonstrated remote detection of a 10 micron path difference to an accuracy of 0.15µm with white light coupled between two interferometers by a 75 micron core fibre. The two interferometers are being used as filters and this has relevance to optical fibre signal processing because light guided in a multimode fibre is emitted as a series of pulses which has a filtering effect on the spectrum.

Pavlath and Shaw [3.14] showed that a gyroscope could be made from multimode optical fibre which would allow more power to be coupled into the device and reduce alignment requirements.

3.4.1 Multimode Fibres in Astronomy.

Optical fibres are commonly used in Astronomy to couple light from a telescope to a spectrometer. As the intensity of the light is all that is required multimode optical fibres may be used. Core diameters from 50 to 1500 microns are available for this purpose.

A problem with the fibres is that their attenuation due to Rayleigh scattering increases rapidly as the wavelength decreases. So called 'wet' fibres, i.e. moderately OH^- doped, show the lowest losses in the blue and ultra-violet but fibre lengths are limited to a few meters. The main advantage of a fibre linked system over conventional free space coupling is the ability to carry out spectral measurements on many objects simultaneously using a two-dimensional optical fibre array. The multimode nature of the fibres used produces an output beam whose intensity is uniformly scrambled, and having the spectrometer remote from the telescope enables it to be mounted more stably than might otherwise be possible. The spectrometer can also be used by several telescopes as a common instrument.

The important criterion for coupling efficiency of a telescope to a fibre and of a fibre to a spectrometer is the product $A\Omega$ where A is the area of the fibre core and Ω the solid angle of light emerging from the fibre known as its numerical aperture. If the telescope and spectrometer were designed to give the product $A_t\Omega_s$ where A_t is the collecting area of the telescope and Ω_s is the solid angle accepted by the spectrometer then $A_t\Omega_s$ is a minimum for the system and a well

matched fibre will have a $A\Omega$ product equal to or only slightly larger than $A_t\Omega_s$. The angles of the cones of light emitted or accepted by a telescope and spectrometer are usually given in terms of an f-number. The relationship between f-number and numerical aperture is given in section 3.5.

Arrays of fibres used in the Anglo-Australian observatory are described by Gray [3.15]. Light from as many as 50 fibres placed in the image plane of the telescope is introduced to a spectrometer as a linear array and their spectra measured simultaneously. The maximum number of fibres is limited by the size of linear fibre array which can be accommodated by the spectrometer. It is interesting to note that so-called 'focal-length degradation' occurs in optical fibres and is a problem which may reduce resolution. If light is coupled into an optical fibre with an f-number larger than that of the fibre then, due to scattering and microbending in the fibre, the light can be emitted with an f-number greater than or equal to that of the fibre.

3.5 Coupling Light into Optical Fibres.

For highly multimode fibres, a geometric analysis is sufficient to ensure good coupling of light from a source into an optical fibre. The aim is to match the numerical aperture (NA) of the collecting optics to the numerical aperture of the fibre. The numerical aperture of the fibre is defined in section 2.1.1 as the sine of the angle of the cone of light accepted by the fibre. The square of the numerical aperture is a measure of the light gathering power of the system.

The f-number of a lens is defined as

$$f/\# = \frac{f}{d} \, ,$$
(3.5.1)

where d is the diameter of the lens and f is its focal length. For maximum coupling by a lens into a fibre the f-number of the lens should be matched to the numerical aperture of the fibre. So we need to know the relationship between the f-number of the lens and the numerical aperture of the fibre. We have for the half angle of the cone of light defined by the lens

$$\text{Tan } \theta = \frac{d}{2f} \cdot \qquad (3.5.2)$$

The numerical aperture of a fibre is typically less than 0.3 so we can say

$$\text{NA} \cong \text{ Tan } \theta = \frac{d}{2f} \cdot \qquad (3.5.3)$$

Then for maximum coupling by the lens to the fibre we have

$$f/\# = \frac{1}{2\,\text{NA}} \cdot \qquad (3.5.4)$$

For maximum coupling into singlemode optical fibres it is necessary to consider the problem in terms of gaussian beam optics. By determining the correct optics we can present the light at the entrance to the fibre with the same characteristics as the mode which is to be guided.

The diameter of the mode which propagates in a singlemode fibre is approximately 1.2 times the core diameter although this value increases as the wavelength of the source gets further above cut-off. In order for efficient coupling into a fibre a lens should focus the light to a beamwaist at the end of the fibre and the beamwaist should

68

have the same diameter as the mode. The Gaussian beam optics necessary for obtaining efficient coupling is given in appendix B.

3.6 Scalar Diffraction Theory.

Diffraction theory is necessary to fully explain the propagation of a wave through a linear optical system. It is also necessary to explain image formation by coherent and incoherent light. Diffraction theory is included here because although diffraction effects are not observed when light is guided in an optical fibre the light emitted from the fibre may be a source for a free space optical system or alternatively an optical fibre may be used to sample light from an image whose formation requires diffraction theory.

Kirchoff assumed that light could be treated as a scalar phenomena which obeyed the wave equation written

$$\nabla^2 E = \frac{1}{c^2} \frac{d^2 E}{dt^2} , \qquad (3.6.1)$$

where E is the electric field. If the wave is propagating along the z axis then it may be expressed as the real part of the exponential given by

$$E(z,t) = A\ e^{i(kz - \omega t + \phi)} . \qquad (3.6.2)$$

As a general case of diffraction consider a point P_0 in the plane (x_0, y_0) illuminating an aperture A in the plane (x_1, y_1) and then propagating to a point P_2 in a receiving plane (x_2, y_2), figure 3.1. The field at P_2 is given by the Fresnel-Kirchoff diffraction formula which is written

$$U_2(x_2,y_2) = \frac{-i}{2\lambda}\ A_0(x_0,y_0) \iint_A \frac{e^{ik(r+s)}}{rs} [\ Cos\,(n.r) - Cos\,(n.s)\ ]\ ds . \quad (3.6.3)$$

This integral is a superposition which may be considered to be a spherical wave described by e^{ikr}/r incident on the aperture A which produces new spherical waves at each point in the aperture. The integral sums all these waves over the aperture plane. The cosine terms define the directions of r and s relative to a unit vector n in the aperture plane. Equation (3.6.3) may be written as

$$U_2(P_2) = \iint U_1(P_1)\, h(P_1, P_2)\, ds\ , \quad (3.6.4)$$

where

$$U_1(P_1) = A_0(x_0, y_0)\, \frac{e^{ikr}}{r}\ , \quad (3.6.5)$$

and

$$h(P_1, P_2) = \frac{-i}{2\lambda}\, \frac{e^{iks}}{s}\, [\, Cos\,(n.r) - Cos\,(n.s)\,]\ . \quad (3.6.6)$$

The function $h(P_1, P_2)$ is known as the impulse response or point spread function of the system. In order to simplify equation (3.6.3) certain approximations can be made. For a small aperture $Cos\,(n.r)$ is close to 1 and $Cos\,(n.s)$ is close to -1 so the term in square brackets is approximately equal to 2. If r and s are much greater than the size of the aperture then we may replace them by z_0 and z except in the exponential term where the phase error may be a significant fraction of 2π radians. If we include these assumptions we may write the superposition integral (3.6.4) as

$$U_2(x_2, y_2) = \frac{-i}{\lambda z z_0} A_0(x_0, y_0) \iint e^{ik(r+s)} ds\ . \quad (3.6.7)$$

The wave incident on the aperture is given by

$$U_1(P_1) = A_0(x_0,y_0) \frac{e^{ikr}}{z_0} \quad , \qquad (3.6.8)$$

and the impulse response of (3.6.6) becomes

$$h(P_1,P_2) = \frac{-i}{\lambda z} e^{iks}. \qquad (3.6.9)$$

3.6.1 Region of Fresnel Diffraction.

The exact value of r from figure 3.1 is given by

$$r = \sqrt{z_0^2 + (x_0 - x_1)^2 + (y_0 - y_1)^2}. \qquad (3.6.1.1)$$

This may be approximated by

$$r \cong z_0 [1 + \frac{1}{2}(\frac{x_0 - x_1}{z_0})^2 + \frac{1}{2}(\frac{y_0 - y_1}{z_0})^2], \qquad (3.6.1.2)$$

and similarly for s we have

$$s \cong z [1 + \frac{1}{2}(\frac{x_2 - x_1}{z})^2 + \frac{1}{2}(\frac{y_2 - y_1}{z})^2]. \qquad (3.6.1.3)$$

When z_0 and z are sufficiently large for the approximation to be accurate the point P_2 is said to be in the region of Fresnel diffraction. The superposition integral (3.6.4) may be written as a convolution of the input $U_1(x_1,y_1)$ with the impulse response. Thus, we have

$$U_2(x_2,y_2) = \frac{-i}{\lambda z} e^{ikz} \iint U_1(x_1,y_1) e^{\frac{ik}{2z}((x_2 - x_1)^2 + (y_2 - y_1)^2)} dx_1 dy_1. \qquad (3.8.1.4)$$

Expanding the quadratic term we obtain

72

$$U_2(x_2,y_2) = \frac{-i}{\lambda z} e^{ikz} \iint U_1(x_1,y_1) e^{\frac{ik}{2z}((x_2-x_1)^2+(y_2-y_1)^2)} dx_1 dy_1. \quad (3.8.1.4)$$

Expanding the quadratic term we obtain

$$U_2(x_2,y_2) = \frac{-i}{\lambda z} e^{ikz} e^{\frac{ik}{2z}(x_2^2+y_2^2)} \iint U_1(x_1,y_1) e^{\frac{ik}{2z}(x_1^2+y_2^2)}$$

$$e^{(\frac{-i2\pi}{\lambda z}(x_2 x_1 + y_2 y_1))} dx_1 dy_1. \quad (3.6.1.5)$$

Apart from an amplitude term and constant phase factor the integral says that $U_2(x_2,y_2)$ is the Fourier transform of

$$U_1(x_1,y_1) \exp(ik(x_1^2+y_1^2)/2z), \quad (3.6.1.6)$$

with spatial frequencies u and v given by

$$u = \frac{x_2}{\lambda z}, \quad v = \frac{y_2}{\lambda z}. \quad (3.6.1.7)$$

3.6.2 Region of Fraunhofer Diffraction.

The Fraunhofer, or far field, approximation requires that the aperture must be small compared with the source and observation distances, figure 3.1. We write

$$z_0 \gg \frac{k(x_1^2+y_1^2)}{2} \text{ max}, \quad (3.6.2.1)$$

and

$$z \gg \frac{k(x_1^2+y_1^2)}{2} \text{max}, \quad (3.6.2.2)$$

where z_0 is the source distance and z the observation distance. The aperture size is given by x and y. The first condition may be met by a collimated beam illuminating the aperture. The second condition determines the minimum observation distance and may be satisfied by a lens, used to image the Fraunhofer pattern in its back focal plane. When these conditions are satisfied we may write equation (3.6.1.5) as

$$U_2(x_2,y_2) = \frac{-i}{\lambda z} e^{ikz} e^{\frac{ik}{2z}(x_2^2+y_2^2)} \iint U_1(x_1,y_1) e^{-\frac{2\pi i}{z\lambda}(x_2 x_1 + y_2 y_1)} dx_1 dy_1 .$$

$$(3.6.2.3)$$

If the aperture function is placed in the front focal plane then we have

$$z \gg \frac{k(x_2^2 + y_2^2)_{max}}{2} , \qquad (3.6.2.4)$$

This eliminates the quadratic terms in x_2 and y_2 and (3.6.2.3) becomes

$$U_2(x_2,y_2) = D \iint U_1(x_1,y_1) e^{-\frac{2\pi i}{f\lambda}(x_2 x_1 + y_2 y_1)} dx_1 dy_1 , \qquad (3.6.2.5)$$

where f is the focal length and D is a constant. Equation (3.6.2.5) shows that the Fraunhofer diffraction pattern is the Fourier transform of aperture distribution $U_1(x,y)$ evaluated at frequencies u and v where

$$u = \frac{x_2}{f\lambda} , \quad v = \frac{y_2}{f\lambda} . \qquad (3.6.2.6)$$

74

3.7 Fourier optics.

The Fourier transform (FT) occurs frequently in optical signal processing, for example, in the operations of correlation and convolution. It occurs as the Fraunhofer diffraction pattern of an aperture and it relates the optical power spectrum to the visibility envelope of interference fringes (FT spectroscopy). The branch of optics which makes use of the FT is known as Fourier optics.

3.7.1 The phase shifting properties of a lens.

If a wavefront is passed through a lens the lens will introduce a phase delay which is a function of the co-ordinates, (x,y), in the plane of the lens.

A point O, a distance d_1 from a lens will be imaged at a point I a distance d_2 from the lens, figure 3.2. The phase across a spherical wave radiating from O is given by

$$U_O(r) = e^{ikr}, \qquad (3.7.1.1)$$

where r is the distance from O. This may be written as

$$U_O(r) = e^{ik(x^2+y^2+d_1^2)^{1/2}}. \qquad (3.7.1.2)$$

If x and y are much smaller than d_1 then by the binomial theorem

$$U_O(x,y) = e^{ik(d_1 + \frac{x^2+y^2}{2d_1})}. \qquad (3.7.1.3)$$

The lens produces a spherical wave centred on I so the phase across the wave is given by

75

$$U_I(x,y) = e^{i k (d_2 + \frac{x^2 + y^2}{2d_2})} . \qquad (3.7.1.4)$$

The phase delay of the lens, $U_L(x,y)$, is the difference between (3.7.1.3) and (3.7.1.4). We have

$$U_L(x,y) = e^{-ik (d_1 + d_2)} e^{\frac{-i k}{2}(\frac{1}{d_1} + \frac{1}{d_2})(x^2 + y^2)} . \qquad (3.7.1.5)$$

Using the lens equation

$$\frac{1}{d_1} + \frac{1}{d_2} = \frac{1}{f} , \qquad (3.7.1.6)$$

and neglecting the constant phase term we have that the phase delay due to a lens of focal length f is given by

$$U_L(x,y) = e^{\frac{-i k}{2 f}(x^2 + y^2)} . \qquad (3.7.1.7)$$

3.7.2 The Fourier transforming properties of a lens.

We wish to determine the effect of a lens on light diffracted by an aperture. Consider the optical system of figure 3.3. The amplitude distribution of light in a plane P_1 a distance d_1 from a lens is $U_1(x_1,y_1)$, and the distribution at the lens in plane P_2 is $U_2(x_2,y_2)$. The light is transmitted, and propagates to plane P_3 with distribution $U_3(x_3,y_3)$.

From equation (3.6.1.5), section 3.6.1, the distribution of light at P_2 from an aperture at P_1, putting $z = d_1$, is given by

$$U_2(x_2,y_2) = \frac{-i}{\lambda d_1} \exp(ikd_1) \exp(\frac{ik}{2d_1}(x_2^2+y_2^2)) \iint U_1(x_1,y_1)$$

$$\exp(\frac{ik}{2d_1}(x_1^2+y_1^2)) \exp(\frac{-2\pi i}{\lambda d_1}(x_2x_1+y_2y_1)) \, dx_1 dy_1. \quad (3.7.2.1)$$

The distribution in plane P_2 is multiplied by the effect of the lens and propagated to plane P_3. We have for the effect of the lens

$$U_L(x_2,y_2) = P(x_2,y_2) \exp(\frac{-ik}{2f}(x_2^2+y_2^2)), \quad (3.7.2.2.)$$

where

$$P(x,y) = 1, \text{ inside the lens aperture}$$
$$= 0, \text{ otherwise.} \quad (3.7.2.3)$$

The light distribution, $U_3(x_3,y_3)$, a distance d_2 beyond the lens at plane P_3 is determined by putting the product $U_2(x_2,y_2)U_L(x_2,y_2)$ into equation (3.8.1.5).

In most remote sensing applications the source will produce waves which are effectively planar at the sensor. These waves will be focused at the back focal plane of a lens so we let $d_2 = f$. Then $U_3(x_3,y_3)$ may be shown to be given by

$$U_3(x_3,y_3) = A \exp(\frac{ik}{2f}(x_3^2+y_3^2)(1-\frac{d_1}{f}))$$

$$\iint U_1(x_1,y_1) \exp(-2\pi i(x_1(\frac{x_3}{\lambda f}) + y_1(\frac{y_3}{\lambda f}))) \, dx_1 dy_1, \quad (3.7.2.4)$$

where A is a constant. The equation shows that, but for a phase error, the amplitude distribution in plane P_3 is the FT of the aperture distribution in plane P_1. The phase error depends on the value of d_1. If $d_1 = f$ then the FT is exact and may be written

$$U_3(x_3, y_3) = A \iint U_1(x_1, y_1) \exp(-2\pi i (x_1 u + y_1 v)) \, dx_1 dy_1, \qquad (3.7.2.5)$$

where

$$u = \frac{x_3}{\lambda f} \quad \text{and} \quad v = \frac{y_3}{\lambda f}. \qquad (3.7.2.6)$$

3.8 Spatial coherence filtering.

Electro-optic (E-O) sensors which employ rotating reticles or choppers, chosen in order to modulate a signal image, may also modulate unwanted background features of similar spatial extent. We therefore have to consider and exploit the differences which exist between the signal and background, for example, differences in spatial coherence.

3.8.1 Convolution with incoherent and coherent illumination.

The process of multiplying each point of a function by the whole of another function and summing the results is called convolution. This may be written for two continuous functions as an integral. The convolution integral for two functions $f_1(x)$ and $f_2(x)$ yields a function $f_3(x')$ and is written

$$f_3(x') = \int_{-\infty}^{\infty} f_1(x)\, f_2(x'-x)\, dx \qquad (3.8.1.1)$$

3.8.2 Image formation with incoherent illumination.

Radiation processes at points separated by at least one wavelength in a conventional thermal light source are independent of each other, that is, they are spatially incoherent. The intensity distribution in the image plane due to a point source in the object plane is described by $|h(x,y)|^2$. This function is called the intensity point spread function. A scene illuminated by incoherent illumination will have an intensity distribution given by $I_O(x,y)$ where x and y are the co-ordinates in the plane. The intensity $I_I(x',y')$ at point x',y' in the image plane may be considered to be the summation of the images of

the individual object points so the image is the convolution of the object with the point spread function. Thus, we have

$$I_I(x',y') = \int\limits_{-\infty}^{\infty} I_O(x,y) \mid h\,(\,x'-x,y'-y\,)\mid^2 dx\,dy. \quad (3.8.2.1)$$

It may be shown that the product of the Fourier transforms (FTs) of the two functions involved in a convolution integral is the FT of the result. Thus, the FT of the object intensity function, $I_O(x,y)$, multiplied by the FT of the point spread function (PSF), $\mid h(x,y)\mid^2$, is the FT of the image intensity function, $I_I(x',y')$. The FT of the PSF is called the optical transfer function (OTF). The OTF consists of an amplitude and a phase term. The modulus of the OTF is the modulation transfer function, $T(x,y)$. Relationships between the various functions for incoherent illumination are given in figure 3.4.

Fresnel's diffraction integral shows that the PSF in incoherent illumination is the square modulus of the image of a point in the object plane. This is equal to the FT of the aperture function, $A(x,y)$. The transfer function is, therefore, the convolution of the aperture function with its own complex conjugate. We write

$$T\,(x,y) = \int\limits_{-\infty}^{\infty} A(x',y')A^*(x-x',y-y')dx'dy' \quad (3.8.2.2)$$

The convolution of a function with itself is referred to as an auto-correlation function, figure 3.5.

3.8.3 Image formation with coherent illumination.

There is a basic difference between imaging using coherent and incoherent light. Incoherent light as described in the previous section is linear in intensity. Thus, the image intensity is linearly related to the object intensity. Coherent light is linear in amplitude so the amplitude of the image is linearly related to the amplitude of the object. The convolution integral for image formation in coherent illumination is

$$E_I(x',y') = \int\limits_{-\infty}^{\infty} E_O(x,y) \, h\,(x'-x,y'-y) \, dx \, dy, \qquad (3.8.3.1)$$

where E_I and E_O are the image and object complex amplitudes and $h(x,y)$ is the amplitude PSF. The OTF for coherent illumination is the FT of the amplitude PSF. However, the FT of the amplitude PSF is itself the aperture function, figure 3.6.

3.8.4 Image formation with partially coherent illumination.

Incoherent and coherent illumination are the two extremes of partially coherent illumination. For a complete understanding of image formation the case of partial coherence must be considered [3.16].

We can use the phase-coherence factor introduced in section 2.6.4 to study the diffracted image of a reticle, illuminated by a source, in the aperture plane of an E-O sensor. An element dσ of the source produces a complex amplitude E(x,y) at a point (x,y) of the aperture plane. If the reticle has a transmission function A(x,y), then the transmitted complex amplitude of the radiation is E(x,y)A(x,y). The

81

diffracted image of (x,y) will be centred on (u,v) in the image plane, figure 3.7. Let h(u'-x,v'-y) be the complex point spread function of the optical system. The complex amplitude dE'_{s1} at (u',v'), produced by an area of the object ds_1, is given by

$$dE'_{s1}(u',v') = E(x_1,y_1)A(x_1,y_1)\, h(u'-x_1,v'-y_1)\, ds_1, \quad (3.8.4.1)$$

The total amplitude at (u',v') due to all elements of the object is given by

$$E'_{s1}(u',v') = \int_{s_1} E(x_1,y_1)A(x_1,y_1)\, h(u'-x_1,v'-y_1)\, ds_1. \quad (3.8.4.2)$$

An equivalent expression for a second point in the aperture plane $E(x_2,y_2)$ may be written

$$E'_{s2}(u',v') = \int_{s_2} E(x_2,y_2)A(x_1,y_1)\, h(u'-x_2,v'-y_2)\, ds_2. \quad (3.8.4.3)$$

The intensity dI at (u',v') due to the source element $d\sigma$ is given by

$$dI = E'_{s1}(u',v')\, E'_{s2}{}^*(u',v'). \quad (3.8.4.4)$$

The total intensity I(u',v') at (u',v') due to the whole source, Σ, is obtained by integrating over all the elements of the source. We have

$$I(u',v') = \int_{\Sigma} dI. \quad (3.8.4.5).$$

Equations (3.8.4.3) and (3.8.4.4) are substituted into (3.8.4.5) and, as all the variables are independent, the order of integration may be changed to give

$$I(u',v') = \iint_{s1\,s2} \left\{ \int_\Sigma E(x_1,y_1)\,E^*(x_2,y_2)\,d\sigma \right\} A(x_1,y_1)\ A^*(x_2,y_2)$$

$$h\,(u'-x_1,v'-y_1)\ h^*(u'-x_2,v'-y_2)\ ds_1 ds_2. \qquad (3.8.4.6)$$

From section 2.6.4, equation (2.6.4.12), we may make a substitution for the integral in brackets in equation (3.8.4.6). The phase-coherence term, γ_{12} , is defined as

$$\gamma_{12} = \frac{\displaystyle\int_\Sigma E(x_1,y_1)\,E^*(x_2,y_2)}{\sqrt{I_1 I_2}}, \qquad (2.6.4.12)$$

so we have

$$I(u',v') = \iint_{s1\,s2} \gamma_{12}(x_1 - x_2,\, y_1 - y_2)\,\sqrt{I_1 I_2}\ A(x_1,y)\,A^*(x_2,y_2)$$

$$h(u'-x_1,v'-y_1)\,h^*(u'-x_2,v'-y_2)\ ds_1 ds_2. \qquad (3.8.4.7)$$

If the source illuminates the reticle with coherent illumination, we have $\gamma_{12} = 1$ and $I(u',v')$ is given by

$$I(u',v') = \left| \int_s E(x,y)\ A(x,y)\ h(u'-x,v'-y)\ ds \right|^2. \qquad (3.8.4.8)$$

If the source illuminates the reticle with incoherent illumination, we have $\gamma_{12} = 1$ when $x_1 = x_2$ and $y_1 = y_2$ and is zero otherwise. The image intensity, $I(u',v')$, is then given by

$$I(u',v') = \int_s I(x,y)\ T\,|\,(x,y)|^2\ |\,h(u'-x,v'-y)\,|^2\ ds. \qquad (3.8.4.9)$$

83

3.8.5 Spatial coherence filtering with coherent and incoherent sources.

The imaging properties of a source depend upon the coherence of that source as discussed in sections 3.8.2 to 3.8.4. These imaging properties can be exploited to enable an E-O sensor to discriminate between a small spatially coherent source and spatially incoherent background radiation.

A remote source illuminating an object in the aperture plane of an E-O sensor forms an image in the back focal plane of a lens which is determined by the point spread function (PSF) of the optical system. For a spatially coherent, quasi-monochromatic, source, illuminating a 1D grating, the image consists of discrete points which are the Fourier transform image of the object centred on the image of the source. A spatially incoherent, narrowband, source illuminating the same 1D grating forms an image which is the convolution of the PSF with the intensity distribution of the source. The image consists of diffuse regions instead of discrete points due to the spatially coherent source. If the source is broadband, as would more normally be the case, the image is further blurred by the wavelength dependence of the Fourier transform which causes a continuum of images to form slightly offset from each other. The result of this technique is to form an image in which the only prominent features are those due to a spatially coherent, quasi-monochromatic, source.

A paper by French [3.17] describes the employment of this technique in order to take advantage of a small, spatially coherent source, s, in a spatially incoherent background, figure 3.8. A reticle consisting of a one-dimensional grating is placed in the aperture plane of the sensor. A lens is placed behind the reticle. A discrete diffraction

pattern of the grating occurs in the back focal plane of the lens only for the spatially coherent source, s, and not for the spatially incoherent background. As the aperture plane reticle is rotated, the diffraction pattern rotates and is modulated by a stationary reticle in the detector plane. By this means modulation of the source, s, has been achieved without modulating the background.

The single stage pre-detector signal processor which makes use of spatial coherence differences may be employed as a spectrum analyser to obtain information about the wavelength of a spatially coherent source in an incoherent background. This is achieved by selection of an appropriate stationary reticle. Youern has described such a sensor [3.18], figure 3.9. The sensor consists of a rotating aperture plane reticle divided into two halves. The two halves contain one dimensional gratings which are mutually perpendicular. The lens forms the Fourier transform image (FTI) of the two dimensional grating, but without the cross terms, in its back focal plane. As the aperture plane reticle rotates the FTI rotates. A stationary reticle consisting of clear and opaque regions placed in the image plane will transmit light when the FTI passes over the clear regions and block it when it passes over the opaque regions so the geometry of the reticle determines the modulation of the FTI. The points which comprise the FTI are wavelength dependant so modulation of the FTI which is spectrally dependant may be achieved by a reticle which has curved spokes. The curved spokes produce pulse width modulation. The pulse width being related to the signal wavelength.

French and Sutton [3.19] describe further applications of pre-detector signal processing which may be employed in several stages by

85

multiple transforms. A two stage sensor is described, figure 3.10. In the first stage, light from a spatially coherent signal and the incoherent background is introduced to the system. Only the signal is modulated by a rotating phase reticle and stationary reticle as described before. The FTI is not, however, compatible with conventional image processing techniques so it is retransformed by a second stage. The second lens and second phase reticle operate on the transformed image and reconstruct the original scene at the output plane of the second reticle. A final lens images the scene at the output plane of the sensor. The signal, however remains modulated by the first stage. This sensor, using multiple transforms can be regarded as employing an encoding and decoding process. The encoding is the formation of the rotating transformed image and decoding is achieved by the stationary reticle. The coded signal is the time modulated waveform.

3.8.6 Spatial coherence functions.

Several methods of processing optical scenes with interferometers have been proposed. In 1965 Mertz [3.20] discussed an interferometer which would record the two dimensional Fourier transform of an incoherently illuminated scene. The interferometer was similar to a Michelson and consisted of a beamsplitter and two roof mirrors arranged so that one roof mirror reflected the image in a horizontal axis and the other reflected the image in a vertical axis. This interferometer was used by Wessely and Bolstad [3.21] to measure the spatial coherence between two points in a scene and by Breckenridge [3.22, 3.23] to measure the angular subtense of stars. A similar interferometer was used by Bakut et al. [3.24] to obtain the

86

dependence of the spatial coherence function of a scene on the spatial coordinates.

3.9 Spectral filtering.

Most E-O sensors only process optical scenes by spectrally limiting the radiation using a bandpass filter. If the filter has a transmission function, $T_f(\nu)$, and the signal and background have spectral profiles $I_S(\nu)$, and $I_B(\nu)$, respectively, then the transmitted ratio of signal to background power $P_S(\nu)$ and $P_B(\nu)$, is given by

$$S_R = \frac{P_S(\nu)}{P_B(\nu)} = \frac{\int_0^\infty T_f(\nu) \, I_S(\nu) \, d\nu}{\int_0^\infty T_f(\nu) \, I_B(\nu) \, d\nu} \quad . \quad (3.9.1)$$

If the filter has $T_f(\nu) = 1$ within a bandwidth of $d\nu_f$, we may write

$$S_R = \frac{I_S(\nu) \, d\nu_f}{I_B(\nu) \, d\nu_f} . \quad (3.9.2)$$

If the signal has a bandwidth $d\nu_s$ which is less than that of the filter and the background has a bandwidth which is limited by the filter, we have

$$S_R = \frac{I_S(\nu) \, d\nu_s}{I_B(\nu) \, d\nu_f} . \quad (3.9.3)$$

Thus, by spectrally limiting the background, the rejection ratio is increased. The disadvantage of this approach is that it is still possible that high intensity broadband background radiation could appear as a signal because the processing still relies on the power

present at the detector. The sensor is now designed to respond to signals at one wavelength so signals outside the filter passband are always rejected. It would be much more useful if the sensor were designed to accept or reject signals by consideration of spectral bandwidth. This is the basis for temporal coherence filtering.

3.10 Temporal coherence filtering.

We have seen that the coherence length of a source is related to its bandwidth by equation 2.6.4. We want to consider a method which will enable us to design E-O sensors which are sensitive to temporal coherence.

A paper by Sutton [3.25] describes a pre-detector signal processing technique to take advantage of the difference in temporal coherence between a quasi-monochromatic source, s, and a broadband background in order to discriminate between them, figure 3.11. The sensor is based on a Mach-Zehnder interferometer with a path difference chosen to be shorter than the coherence length of the source, s, but longer than the coherence length of the background radiation. Interference fringes are formed only by the source, s. A loudspeaker vibrates a pellicle beamsplitter so modulation due to the signal only is detected at the two anti-phase outputs of the interferometer by two photodiodes. Post-detector signal processing is now possible. By subtracting one output from the other, the DC level due to the background is removed to leave only the modulated signal.

3.10.1 Temporal filtering with a Gaussian spectral profile.

A source with a Gaussian spectral profile may be described by

$$I_S(\nu) = I_p \, e^{-\frac{(\nu - \nu_0)^2}{2\nu_\alpha^2}} , \qquad (3.10.1.1)$$

where ν_0 is the centre frequency, I_P the maximum intensity and ν_α the half width frequency at 60.7% full height. From section 2.6.3, the spectrum of a source is obtained from the FT of its auto-correlation function. Conversely, the inverse FT of the spectrum is the auto-correlation function. We may write

$$\Gamma_{11}(\tau) = \int_{-\infty}^{\infty} U_1(\nu) \, U_1^*(\nu) \, e^{j2\pi\nu\tau} d\nu, \quad (3.10.1.2)$$

where $U_1(\nu)$ is the amplitude of the spectral profile and $\Gamma_{11}(\tau)$ is the auto-correlation function. Substituting (3.10.1.1) into (3.10.1.2) gives

$$\Gamma_{11}(\tau) = \int_{-\infty}^{\infty} |U_P|^2 \, e^{-\frac{(\nu - \nu_0)^2}{2\nu_\alpha^2}} \, e^{j2\pi\nu\tau} d\nu. \quad (3.10.1.3)$$

Using the identity

$$\int_{-\infty}^{\infty} e^{-(ax^2 + bx + c)} \, dx = \sqrt{\frac{\pi}{a}} \, e^{\frac{(b^2 - 4ac)}{4a}} , \quad (3.10.1.4)$$

it can be shown that

$$\Gamma_{11}(\tau) = |U_P|^2 \sqrt{2\pi\nu_a^2} \, e^{\frac{\nu_0}{2\nu_a^2}} \, e^{\frac{\nu_0^2}{\nu_a^2}} \, e^{-2\pi^2\tau^2\nu_a^2} \, e^{j2\pi\nu_0\tau} . \quad (3.10.1.5)$$

Equation (2.6.3.7), section 2.6.3, defined a mutual coherence function. The self coherence function may be written

$$\gamma_{11}(\tau) = \frac{\Gamma_{11}(\tau)}{\Gamma_{11}(0)} \ . \qquad (3.10.1.6)$$

Thus, we have

$$\gamma_{11}(\tau) = \exp(-2\pi^2\tau^2\nu_a^2) \exp(j2\pi\nu_0\tau) \ . \qquad (3.10.1.7)$$

The second term describes the interference fringes and the first term gives the envelope of the fringes. The ratio of the half width of the spectral distribution to the centre frequency may be given in terms of wavelength by

$$\frac{2\nu_\alpha}{\nu_0} = \frac{\partial\lambda}{\lambda_0} \ . \qquad (3.10.1.8)$$

Rearranging (3.10.1.8) and substituting for $c = \lambda_0\nu_0$ gives the equation

$$\nu_a = \frac{\partial\lambda\ \nu_0}{\lambda_0} = \frac{c\ \partial\lambda}{\lambda_0^2} \ . \qquad (3.10.1.9)$$

The ratio $\lambda_0^2 / \partial\lambda$ is referred to as the coherence length, Lc, of the source so we may write

$$\nu_a = \frac{c}{L_C}. \qquad (3.10.1.10)$$

The temporal delay, t, may be expressed as a spatial path difference by

$$L = c\,\tau \ . \qquad (3.10.1.11)$$

90

Finally, equation (3.10.1.7) may be expressed as

$$\gamma_{11}(\tau) = \exp\left(-\frac{\pi^2}{2}\left(\frac{L}{L_C}\right)^2\right) \exp\left(\frac{j2\pi L}{\lambda_0}\right). \qquad (3.10.1.12)$$

So we see that the fringe visibility falls off with path difference as given by the first exponential term of (3.10.1.12).Using this expression we can design EO sensors with path differences that make use of this processing. The visibility curve obtained with a Lorentzian spectral profile is determined in appendix C.
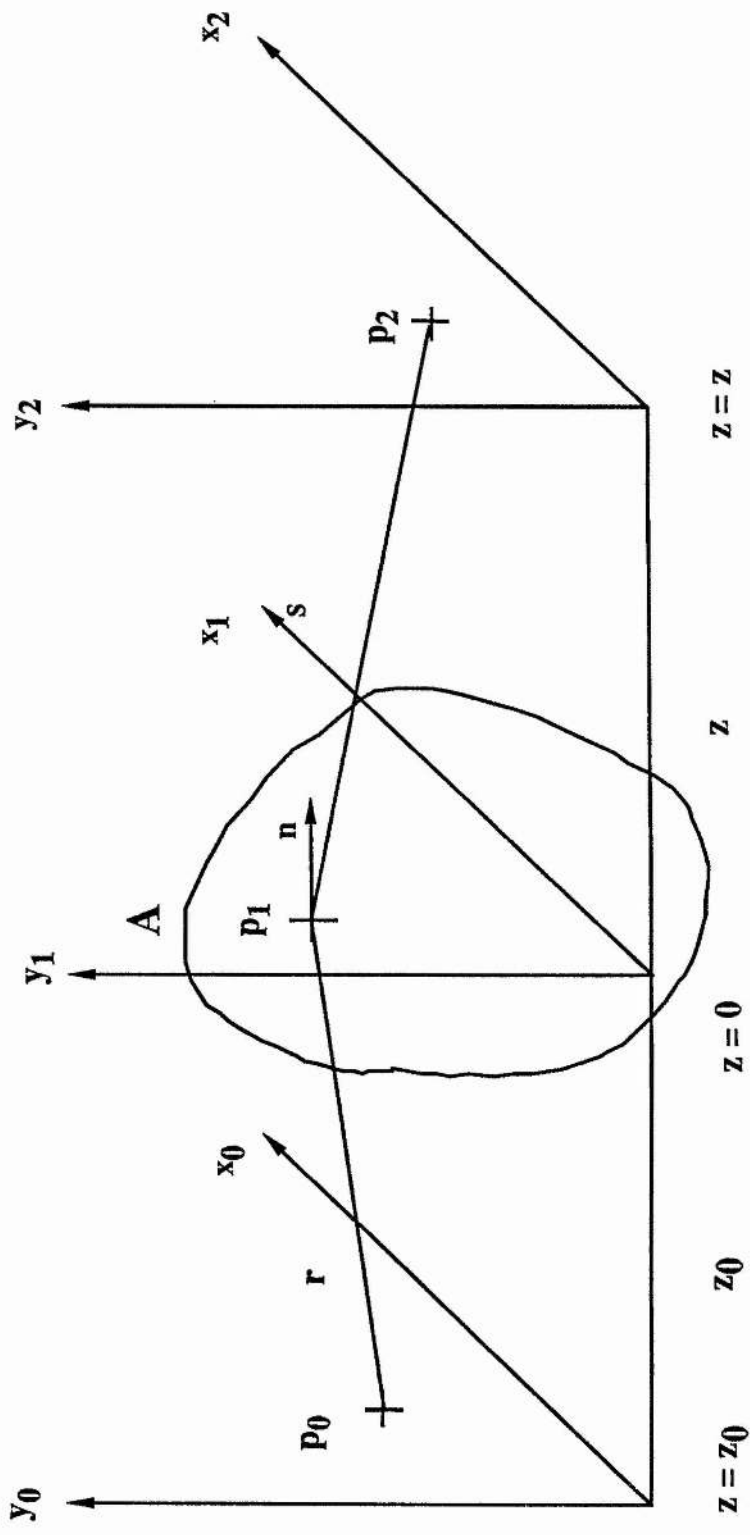
Figure 3.1 Coordinates For diffraction of light at aperture A.
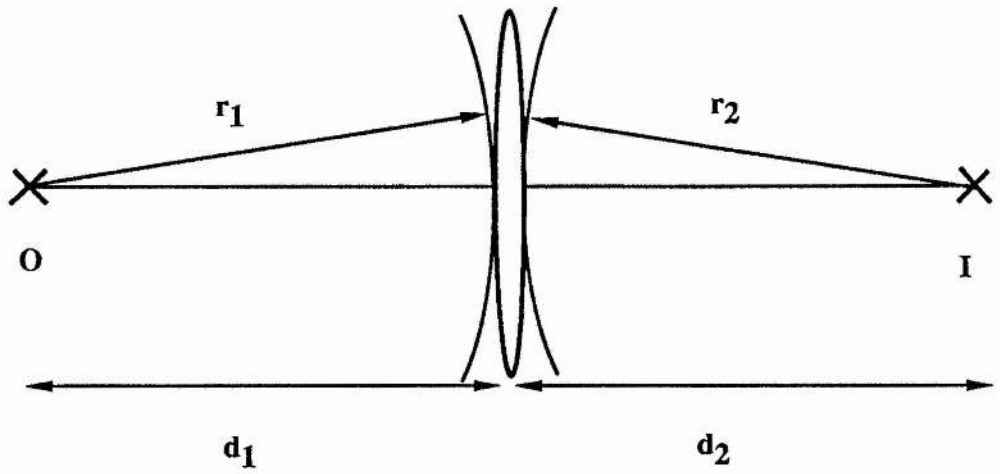
Figure 3.2 Phase delay due to a lens.
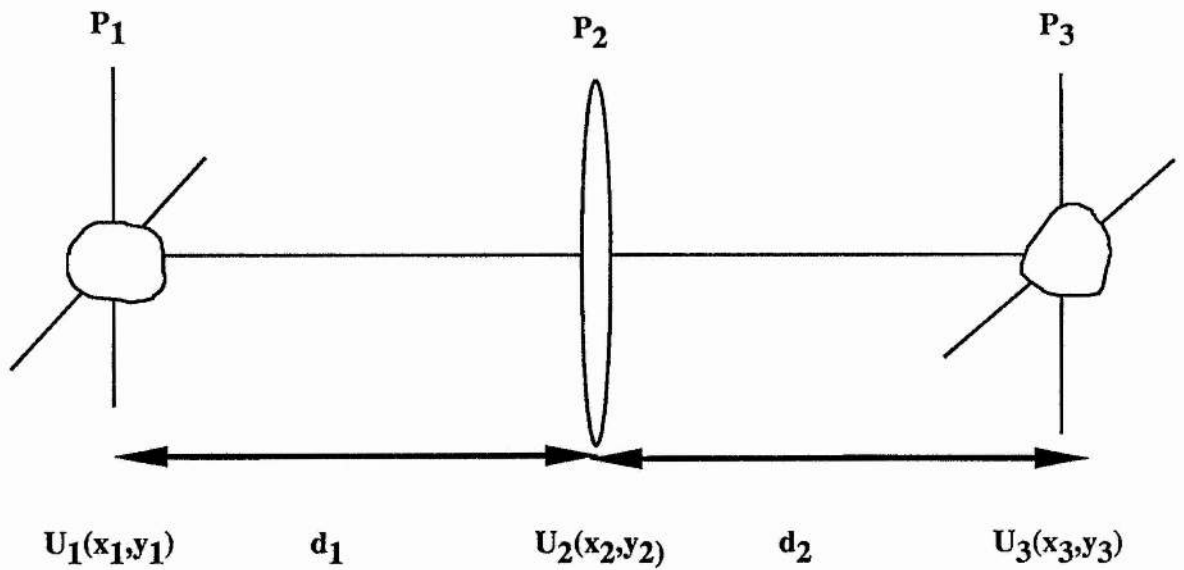
Figure 3.3 Fourier transform by a lens.

Object intensity function ⊛ Point spread function = Image intensity function

Object spectrum × Modulation transfer function = Image spectrum

Fourier transform
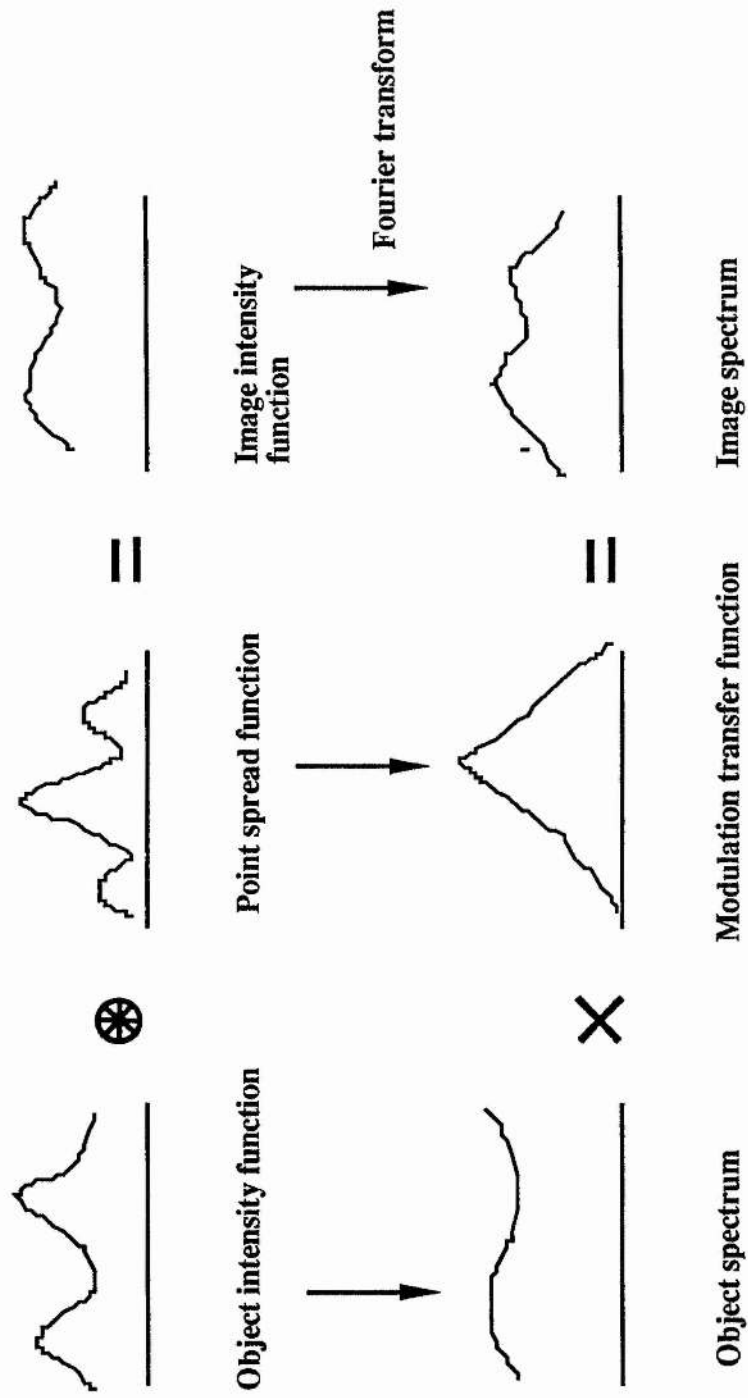
Figure 3.4 Functional relationships for incoherent illumination.

Aperture function

⊛ Complex
conjugate of
aperture function

=

Modulation transfer
function

→ Fourier transform

Point image function

× Complex
conjugate of point
image function

=

Point spread function
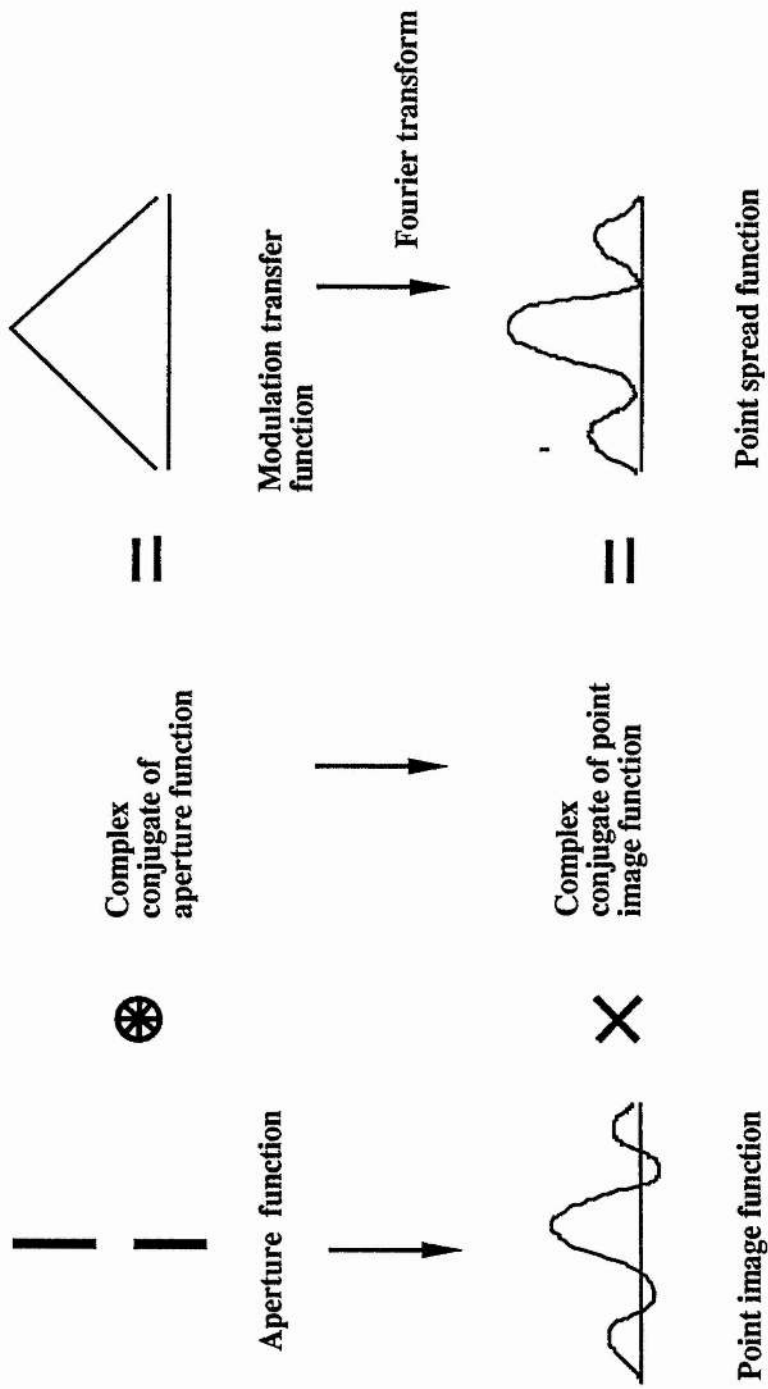
Figure 3.5   Functional relationships for incoherent illumination.
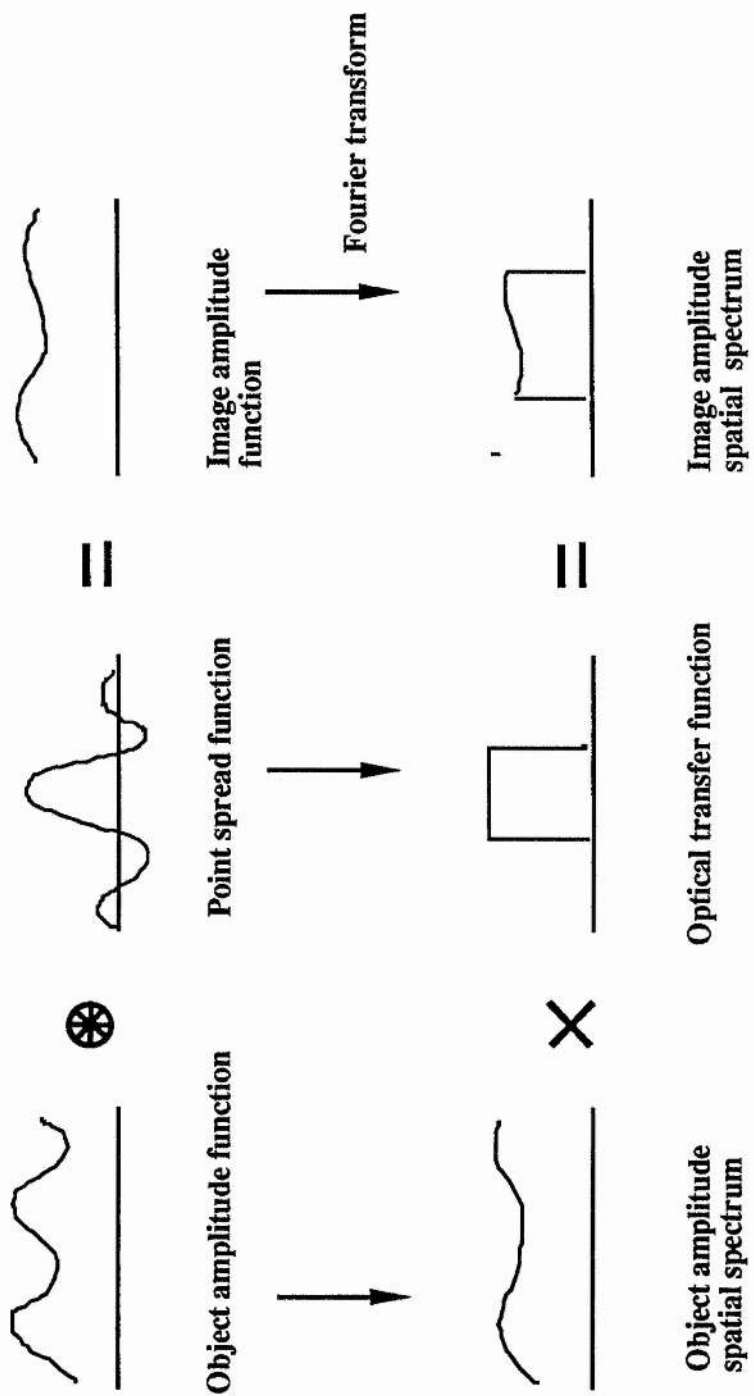
Figure3.6   Functional relationships for coherent illumination.
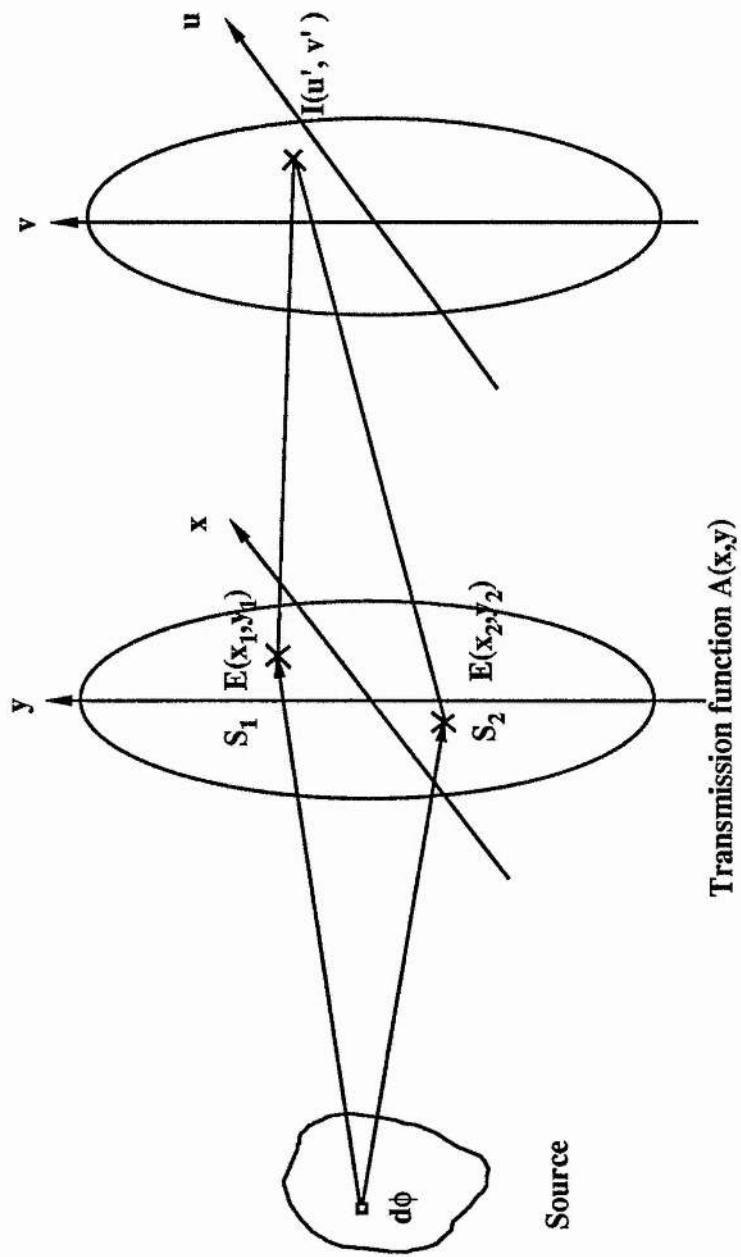
Figure 3.7 Image formation in partially coherent light.

Detector.

Stationary Modulating
Reticle.

Lens

Rotating Aperture Plane
Reticle

o s

Background and Spatially
Coherent Source s.
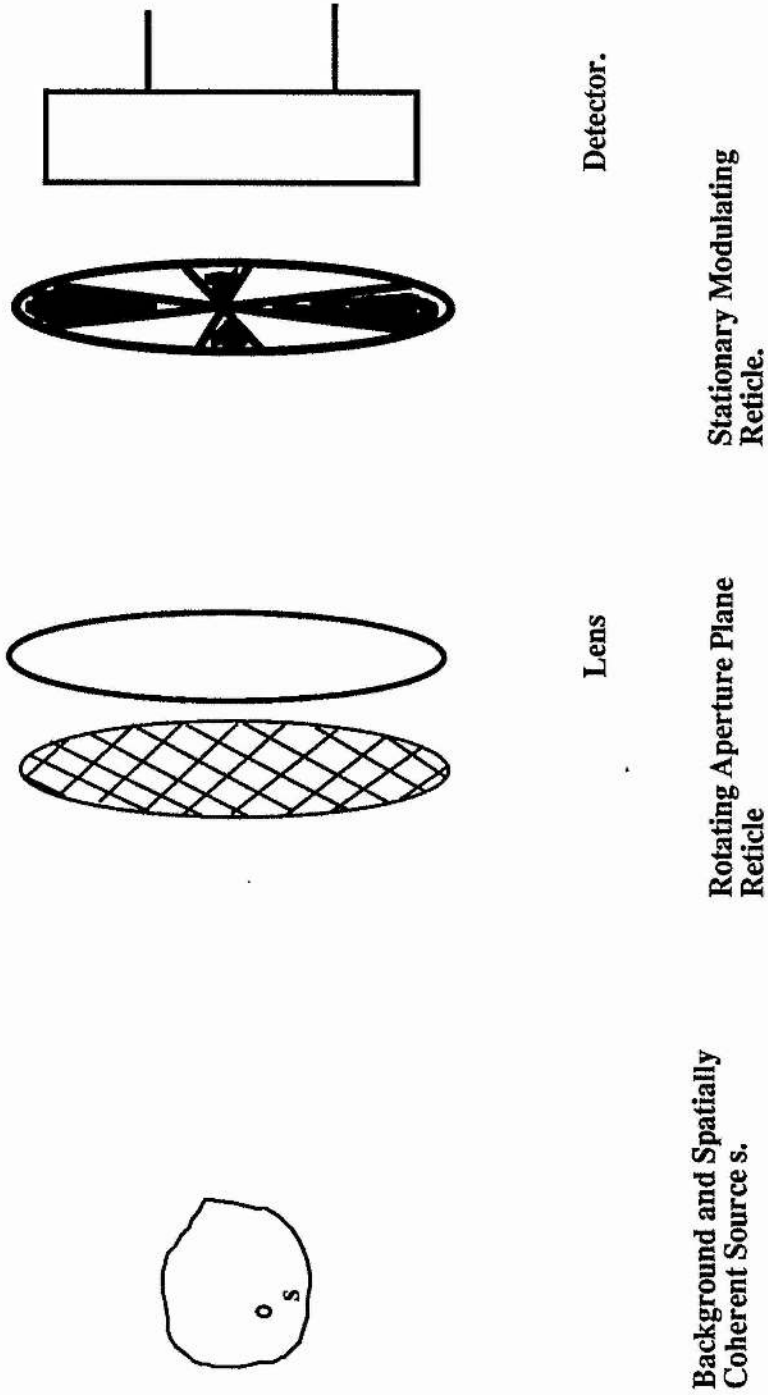
Figure 3.8   Optical Transform Image Modulation.   A spatial coherence sensor.

Detector

Spectrally conscious
transform plane reticle.

Lens

Rotating aperture reticle with
two, one dimensional,
perpendicular gratings

Background and
spectrally narrow source.
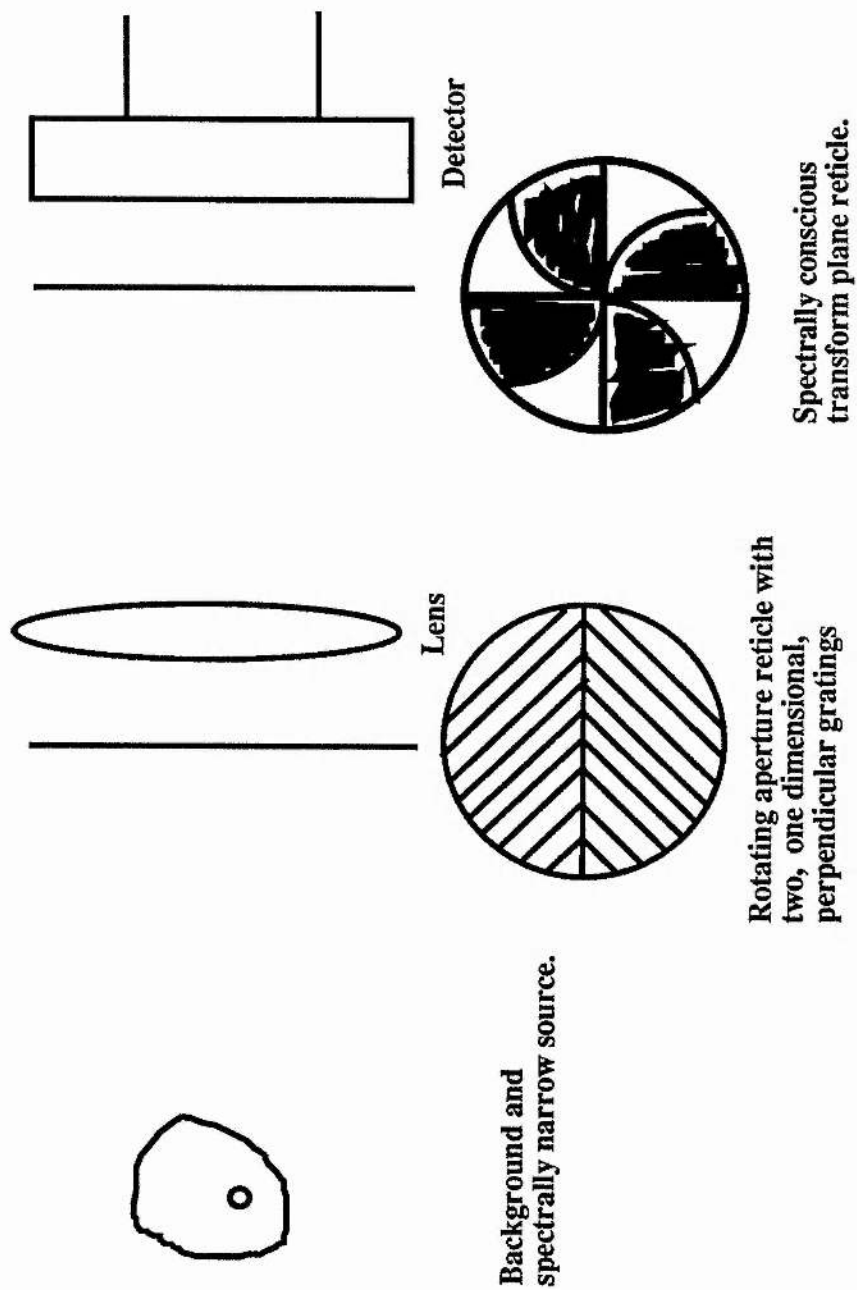
Figure 3.9   Optical Transform Image Modulation.   A spectrum analyser.
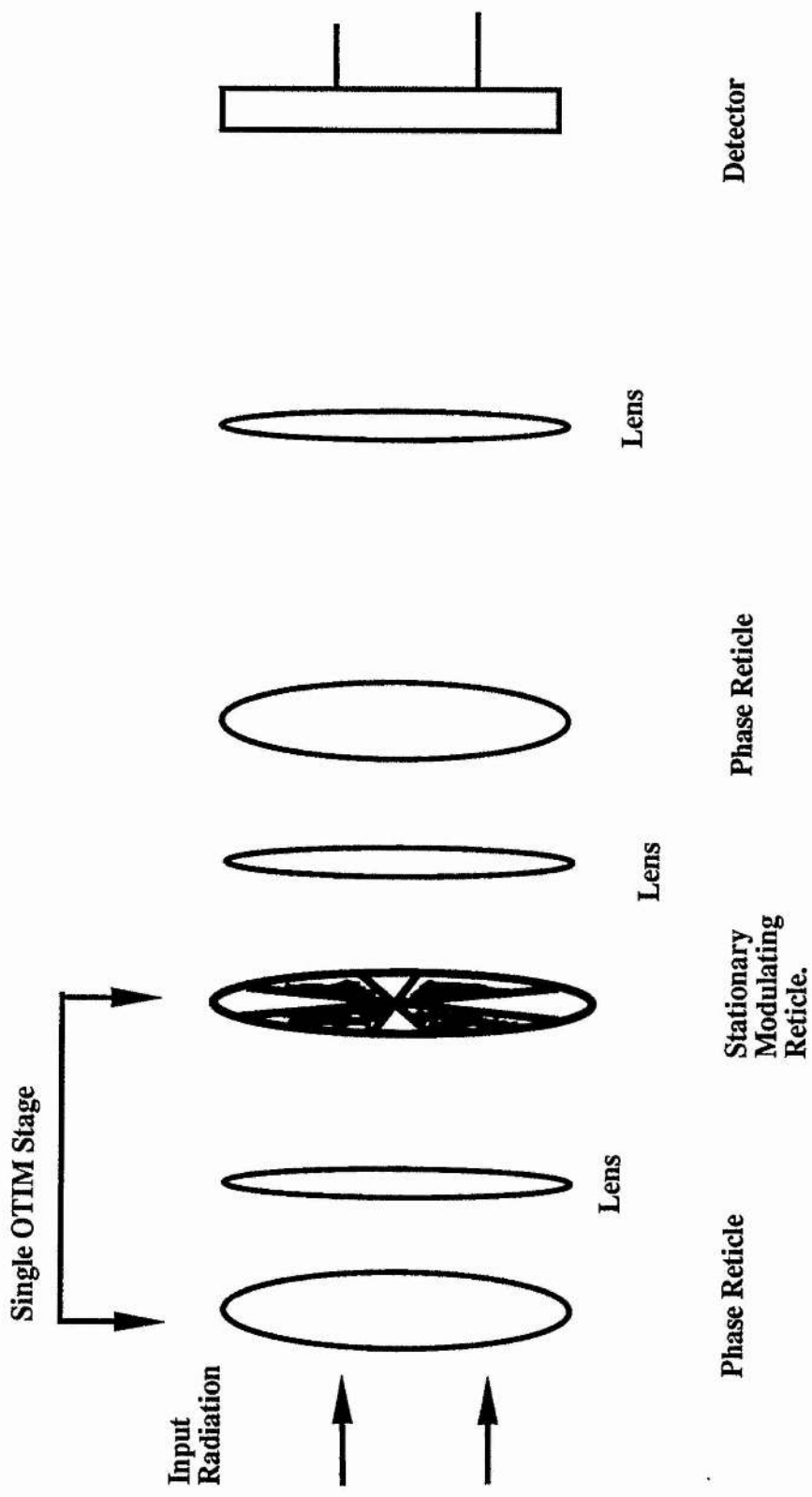
Figure 3.10 Optical Transform Image Modulation.

A two stage spatial coherence sensor.
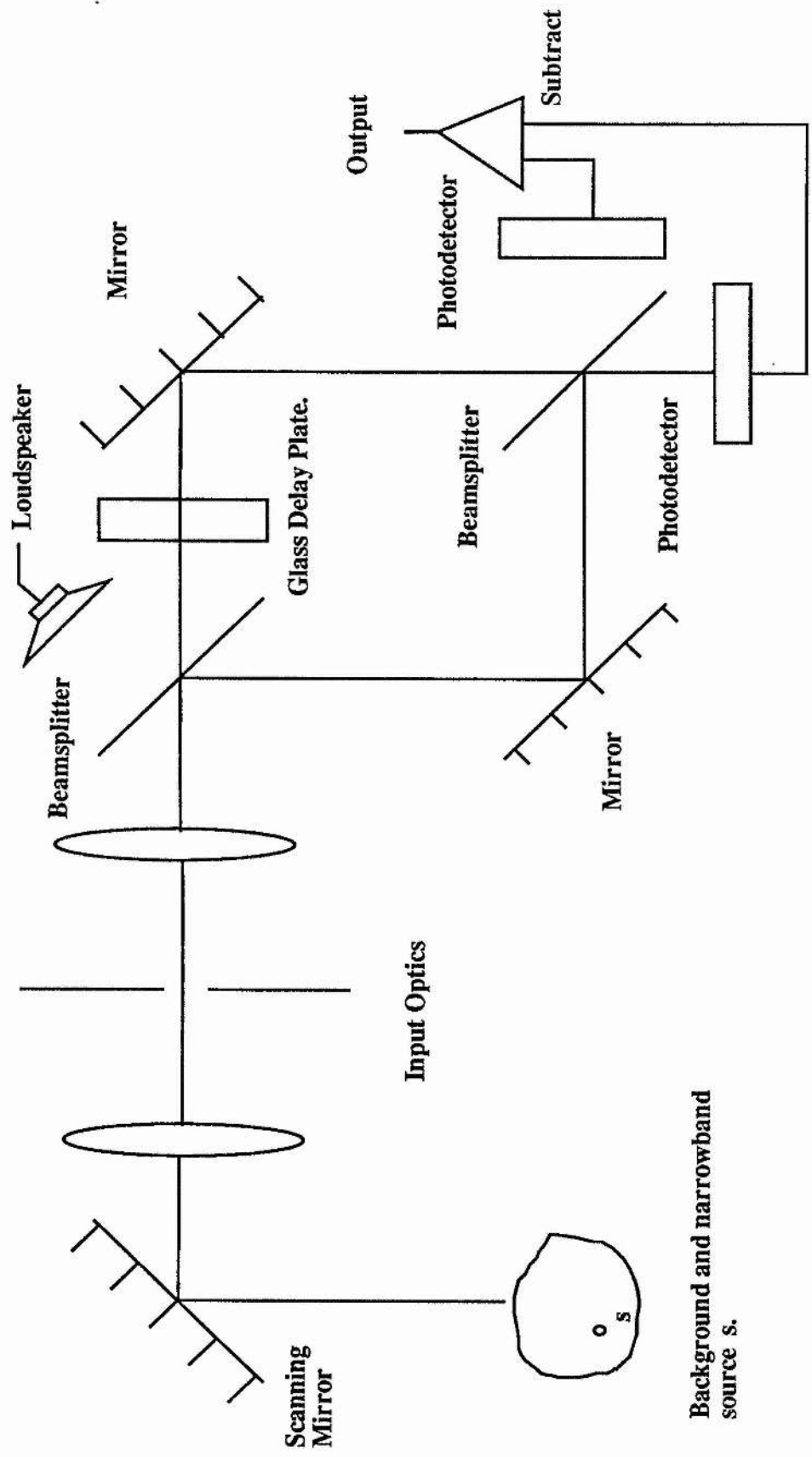
Figure 3.11 Optical Transform Image Modulation. A temporal coherence sensor.

4 Experimental.

4.1 Young's slits interference patterns.

Interference patterns can be obtained very simply by allowing the light emitted by two optical fibres to overlap. If the light from each fibre is coherent then interference patterns will be produced.

Interference patterns were produced by two sources placed side by side in the manner of Young's slits. Light was coupled into two singlemode optical fibres, each 1m in length, by amplitude splitting the light from a HeNe laser using a pellicle beamsplitter. The ends of the optical fibres were placed side by side and the light emitted from each fibre was allowed to overlap on a screen placed a few tens of centimetres beyond the fibre ends, figure 4.1. The fringes are equally spaced because the two sources are side by side. The fringe spacing is inversely proportional to the separation of the two sources so the maximum fringe spacing is limited by the minimum separation of the fibre cores. This is limited by the size of the cladding and any other coatings which may surround the fibre. The fibres were measured to have an outer diameter of 200 microns. The wavefront emitted by each fibre was of uniform amplitude and phase and so the interference fringes produced are as would be expected for a Young's slits experiment except that the light was emitted from the fibre end in a cone defined by the numerical aperture. The electric field, E_P, at a point P on the screen for two singlemode optical fibres may be written

$$E_p = E_1 e^{i(\omega t + \phi_1)} + E_2 e^{i(\omega t + \phi_2)}. \qquad (4.1.1)$$

A second difference is that the the phase of the light emitted by each fibre, ϕ_1 and ϕ_2, need not be the same so that there need not be constructive interference at zero path difference beyond the fibres. When viewed on a monitor using a ccd camera equally spaced fringes with high contrast were seen. With equal intensities coupled into each fibre, the maximum and minimum fringe intensity could be measured on a linear ccd array placed at the screen. The fringes were found to have unity visibility.

The singlemode optical fibres were changed to 1m long 50/125 micron multimode fibres, that is, a 50 micron core surrounded by a 125 micron cladding plus any other coatings. The outer diameter was measured to be 200 microns. The wavefront emitted by a multimode fibre is a superposition of many modes and assuming dispersion effects are small the effect of the fibre is to produce many modes all with a different phase. Hence, the light emitted from one multimode fibre does not give the uniform illumination of the singlemode fibre but a speckle pattern consisting of bright and dark regions where the modes have interfered constructively or destructively with one another. Any interference fringes which are formed by the two fibres are superimposed on this background of speckle. For two multimode optical fibres, which support n_1 and n_2 modes respectively, the electric field, E_P, at a point P on the screen is given by

$$E_p = \sum_{n_1} E_{n_1} e^{i(\omega t + \phi_{n_1})} + \sum_{n_2} E_{n_2} e^{i(\omega t + \phi_{n_2})}. \qquad (4.1.2)$$

The numerical aperture of the 50/125 μm fibre is given as 0.2 so at a wavelength of 633 nm the fibre has a v number of about 50. From section 2.2.3, the number of guided modes is about 1000. When viewed

on a monitor interference fringes were seen with high contrast but they were not completely linear. Distortions and discontinuities of the fringe pattern could be seen. When equal intensities were coupled into each fibre, unity visibility fringes were measured by a linear ccd array.

Both the singlemode and 50/125 fibres were phase modulated using a piezoelectric cylinder. This phase delay in one arm caused the fringe pattern to appear to 'scan' across a single photo-detector placed at the screen. Provided the detector was much smaller than the fringe separation the fringe visibility could be measured. The fibre was wrapped 10-20 times around the cylinder and a linear voltage ramp of a few 100 volts was applied across the wall of the cylinder. The expansion of the cylinder stretched the fibre causing a phase delay. As the two fibres can be of different lengths linear interference fringe patterns can be produced from a single source with a time delay set by the difference in the path lengths of the two fibres.

A second multimode fibre was used. This was a plastic fibre with a core diameter of around 400 microns. This fibre guides many more modes than the 50/125 fibre i.e. n_1 and n_2 of equation (4.1.2) are about 64 times larger. Consequently, the wavefront emitted by each of the two 1m long, 400 micron, fibres shows much more distortion so the speckle pattern formed is much finer. Interference fringes were formed with equal intensities in each fibre and measured to have a visibility greater than 0.8. When the interference fringes were viewed on a monitor and compared with previous experiments they still could be seen to have high contrast but the fringe distortion was greatly increased. It was harder to distinguish the fringes from the background speckle. This is probably because the speckle from each

fibre is very fine and so the regions of overlap of one speckle from each fibre i.e. regions of constant spatial phase gradient are very small.

Two very large core multimode optical fibres were used to produce interference fringes. The fibres were 1m long plastic fibres with a core diameter of 970 microns so n_1 and n_2 of equation. (4.1.2) are increased to about 400 times the number of modes in a 50/125 μm fibre. The interference fringes formed were viewed on a monitor but it was almost impossible to distinguish the fringes from the speckle when they were stationary, though they could be distinguished dynamically. The easiest method was to warm one of the fibres using a finger which caused sufficient phase shift to move the fringes but not so much as to significantly alter the speckle pattern. The visibility of the interference fringes was measured, using a linear ccd array, to be greater than 0.7. The repeatability of the measurement is very low because of the difficulty of distinguishing fringes and speckle. Photographs of the interference patterns obtained with each of the multimode fibres are given in figures 4.2, 4.3, and 4.4.

4.1.1 Multiple beam interference patterns.

Light emitted from two optical fibres has been shown to produce an interference pattern whose similarity to a Young's slits pattern decreases as the number of guided modes increases. Light emitted from many optical fibres with their ends all placed side by side in a linear array will produce a fringe pattern which is related to a multiple slit experiment, figure 4.5. Light from a HeNe laser was coupled into four 50/125 μm optical fibres, each 2m in length. The ends of the fibres were placed side by side and a superposition of

several interference patterns was seen on a screen placed 20cm away, figure 4.6. For m singlemode fibres the electric field, E_P, at a point P on the screen is given by the sum of all the individual electric fields. We have

$$E_p = \sum_m E_m e^{i(\omega t + \phi_m)}. \qquad (4.1.3)$$

For m multimode fibres which each support n_m modes the electric field at a point P on the screen is given by

$$E_p = \sum_m \sum_{n_m} E_{n_m} e^{i(\omega t + \phi_{mn})}. \qquad (4.1.4)$$

Two of the fibres were phase modulated at different frequencies using piezoelectric cylinders. Some of the fringes were seen to scan with frequencies characteristic of both piezoelectric cylinders. The fringes were seen to drift due to thermal effects. With two fibres this occurs slowly so it is not much of a problem but with more fibres the combined phase effect can be large.

The interference pattern formed by multiple slits may be compared to a multiple fibre experiment. With multiple slits, the source illuminates the slits with the same phase and so the phase difference between the individual electric fields at a point P is fixed and depends only on the optical path length between the slit and P. As the phase of the light emitted by each fibre is unpredictable, another variable is added and the interference pattern is simply a superposition of all the possible interference patterns. It is only when all the beams are in phase that the interference pattern characteristic of multiple slits is seen.

4.2 Mach-Zehnder type interference patterns.

When interference patterns are formed from two sources which are on a line parallel to the interference plane then they are of a Young's slits type. When interference patterns are formed from two sources which are on a line perpendicular to the interference plane then they are of a Mach-Zehnder, or Michelson, type.

Light from a HeNe laser was divided by a beamsplitter and coupled into two singlemode optical fibres each 1m long. The light then travelled through the fibres and when emitted from the fibre ends it was collimated by a 50mm focal length f/1 lens and recombined using a second beamsplitter, figure 4.7. When the fibres were aligned correctly circular interference fringes were seen on a screen. The size of the central fringe and also the total number of fringes in the field of view could be altered by changing the relative positions of the ends of the two fibres or by adjusting either of the lenses to change the divergence of the beams. When viewed on a monitor using a ccd camera the fringes were symmetrical and of high contrast. One of the fibres was phase modulated using a piezoelectric cylinder. This caused the fringes to be modulated about the centre of the fringe pattern so that a photodetector placed at the centre of the pattern measured the maximum and minimum of the fringe intensity. The fringe visibility was found to be unity.

The fibres were replaced by two 1m long 50/125 micron fibres. Interference fringes were produced as before but this time they were superimposed on a background of speckle. When viewed on a monitor they were seen to be symmetrical and have high contrast. When one of the fibres was phase modulated, the fringe visibility at the centre of

the pattern was determined to be unity. If a single interference fringe filled the whole field of view then the speckle pattern appeared to be modulated but different regions had different phases.

The fibres were then replaced by two 1m long plastic optical fibres with a core diameter of 400 microns. The fringes were seen to have good contrast but were distorted. The circular fringes seen in previous experiments now showed discontinuities and were no longer circularly symmetric. The effect was even more marked when fibres with 970 micron cores were used. Fringes showing good contrast were present but the circular symmetry was almost completely distroyed. The centre fringes were very difficult to distinguish from the speckle. As it was not possible to phase modulate the two large core fibres using the piezoelectric cylinder, phase modulation was achieved by warming one fibre with a finger; then, the visibility could be measured as before. The visibility of the fringes formed by the 400 micron core fibre was measured to be 0.7 and, for the 970 micron core fibre, the visibility was measured to be 0.6. . The interference fringes present at the screen were recorded by a camera on black and white film. The lens of the camera was removed and the interference fringes allowed to fall directly onto the film. Photographs of the fringe patterns formed with 50/125 μm, 400 μm, and 970 μm fibre are given in figures 4.8, 4.9, and 4.10.

4.3 Phase front maps.

The phase front of a beam of light emitted by an optical fibre affects the uniformity of the interference fringes which the beam can produce. A map of the phase front of the beam can be obtained by allowing the light to interfere with a uniform reference beam. The

interference fringes obtained are a map of the phase difference between the phase front of the light emitted from the fibre and the phase front of the reference beam.

As the distortion of the wavefront of a beam emitted from a fibre must depend upon the number of guided modes, we looked at the phase front of a 970μm core fibre, figure 4.11. The experimental arrangement was as follows. Light from a HeNe laser was divided into two beams by a pellicle beamsplitter. One beam was coupled into the 970 micron core fibre and the other beam was spatially filtered, expanded and collimated to provide the reference. The beams were recombined by a second beamsplitter. Interference fringes were produced which fell onto a screen at the output of the interferometer. The radius of curvature and divergence of the two beams were matched by focusing the reference beam to a point the same distance from the interference plane as the fibre end. This was done using a lens with a focal length which produced a beam with the same divergence as the light from the fibre. A slight difference in the radii of curvature at the screen caused a number of circular fringes to be present. The distortion of the fibre wavefront was seen as distortion of the circular fringes, figure 4.12.

4.4 Measurement of visibility curves by fibre interferometer.

In order that experiments could be carried out with non-zero path differences it was necessary to determine the visibility curves for our sources. The two sources were a 5mW HeNe laser (633nm) and a 15mW HeCd laser (442nm).

The visibility curves were measured by introducing the light to an air path Michelson interferometer consisting of a pellicle beamsplitter,

which divided the light into two beams. The beams were each reflected off a mirror and recombined by the same beamsplitter. Circular interference fringes were obtained. One arm of the interferometer was phase modulated using a rotating glass slide and the maxima and minima of intensity were measured by a photodetector at the centre of the pattern. The path difference between the two arms of the interferometer was increased in steps from zero to around 160cms. A graph of visibility against path difference was plotted for each source (figures 4.13 and 4.14). The graph of visibility against path difference for the HeNe laser shows a periodicity of around 70cm. When radiation from the laser was measured by a spectrum analyser a frequency of 409MHz was detected which would beat over a distance of 73.3cm in space. The HeCd shows a visibility curve which has a coherence length of about 12cm.

Using the graph of visibility against path difference for each source as a reference the same experiment was carried out using a fibre Mach-Zehnder interferometer. Each source, in turn, was coupled into two fibres which were singlemode at 1300nm. The fibres were initially of equal length. One arm of the interferometer was phase modulated and the two beams emitted from the fibres were superimposed by a beamsplitter in order to obtain circular fringes. The fringe visibility was measured by a photodiode at the centre of the circular fringe pattern. A known length of fibre was cut from one arm and the visibility measured again. In this way a graph of visibility against path difference was plotted as before (figures 4.15 and 4.16). It was seen that the only difference between the results taken with air paths and those with fibre paths was that the geometrical path difference for a given change in visibility to occur

was about 1.5 times smaller in the later case due to the refractive index of the fibre.

4.5 Optical fibre bandpass coherence filtering.

When light of bandwidth $\delta\lambda$ and centre wavelength λ is introduced to an interferometer and one arm of the interferometer is phase modulated the light is modulated only if its coherence length, L_c, is greater than the optical path difference (OPD) in the interferometer. From section 2.6,

$$L_C = \frac{\lambda^2}{\delta\lambda}. \qquad (2.6.4)$$

If the light consists of a narrow band signal and broadband background radiation then the path difference may be chosen to cause modulation of the signal only. In the case where a laser source is the signal and the sun provides the background radiation the path difference need only be of the order of millimetres. This is an example of a high pass temporal coherence filter.

A bandpass temporal coherence filter may be realised by using two fibre interferometers with different OPDs sampling the same radiation. The path difference, L_A, in interferometer A is chosen to be less than the coherence length of the signal radiation, that is, it is a high pass filter. The path difference, L_B, in interferometer B is chosen to be greater than the coherence length of the signal radiation. Light which is modulated by interferometer A and not B has a coherence length which falls between the OPDs of the two interferometers, that is,

$$L_A < L_C < L_B. \qquad (4.5.1)$$

A bandpass temporal coherence filter was demonstrated using two PZT phase modulated optical fibre Mach-Zehnder interferometers, figure 4.17. Light from two laser sources was coupled into each interferometer. The two laser sources were a HeCd (442nm) with a coherence length of around 12cm and a HeNe (633nm) with a coherence length of 35cm (taken as the first minimum of the visibility curve). The light from the HeNe laser was chopped. Interferometers A and B had fibre path differences of 4cm and 13cm respectively. This corresponds to OPDs of 6cm and 19.5cm when the refractive index of the fibre core is taken into account. Modulation due to interferometer A is shown in figure 4.18. The OPD is less than the coherence length of both sources so both sources produce interference fringes which are modulated at frequencies proportional to their wavelength. Modulation due to interferometer B is shown in figure 4.19. As the OPD is greater than the coherence length of the HeCd source, only HeNe interference fringes are produced and modulated.

If the general shape of the spectral profile of a source is known the two interferometers may be used to measure its coherence length in the presence of background radiation. For example, a source with a Gaussian spectral profile may be expressed as, from section 3.10.1,

$$I_S(\nu) = I_P\, e^{-\frac{(\nu - \nu_0)^2}{2\nu_\alpha^2}}, \qquad (3.10.1.1)$$

where ν_0 is the centre frequency, I_P the maximum intensity and ν_α the half width frequency at 60.7% full height. Then the visibility of interference fringes produced by an interferometer with a path difference L is

$$v \cdot (L) = \exp\left(-\frac{\pi^2}{2}\left(\frac{L}{L_C}\right)^2\right). \qquad (4.5.2)$$

The maximum and minimum intensities measured will be $(I_{max}+I_{background})$ and $(I_{min}+I_{background})$ so the measured fringe visibility will be

$$v(L) = \frac{(I_{max}+I_{background}) - (I_{min}+I_{background})}{(I_{max}+I_{background}) + (I_{min}+I_{background})}. \qquad (4.5.3)$$

In order to determine the true visibility we need to eliminate the background intensity. If two interferometers have path differences L_A and L_B, respectively, the ratio of the two visibility measurements is

$$\frac{v(L_A)}{v(L_B)} = \frac{(I_{max} - I_{min})_{L_A}}{(I_{max} - I_{min})_{L_B}}, \qquad (4.5.4)$$

which is independent of the background intensity if it is the same in both cases. Equation (4.5.2) is applied to each interferometer, and one expression divided by the other, so we have

$$\ln\left[\frac{v(L_A)}{v(L_B)}\right] = \frac{1}{2}\left[\frac{\pi(L_A^2 - L_B^2)}{L_C^2}\right]. \qquad (4.5.5)$$

Thus, knowing L_A and L_B we can determine L_C.

4.6 Coherence spectrometer.

A spectrometer enables the wavelength content of a scene to be determined. Given a scene which contains several spectrally narrow sources of different wavelengths it would be useful to have a system which would give information about the spectrum of each source without the need for high quality and high resolution components.

Such a system may be realised by a combination of an interferometer and low resolution spectrometer. The experimental arrangement was as shown in figure 4.20. Light from a scene was coupled into a PZT phase modulated Mach-Zehnder fibre interferometer with a 4.5cm optical path difference between its arms. The light was then collimated and passed through a diffraction grating and the zero and plus one orders of the diffraction pattern focused onto a linear fibre array. The fibres of the array guided the light to a single photodetector. A rotating reticle consisting of a transmitting spiral the width of one fibre scanned across the array enabling the light coupled into each fibre to be measured separately so the spatial distribution was converted to a temporal signal. The signal measured by the photodetector when the scene contained red, green and blue laser sources is shown in figure 4.21. The first order of the diffraction pattern consists of separate signals due to the three sources. The zero order shows the signal due to an intensity sum of each modulated source. A closer look at the first order, figure 4.22, shows the modulation due to the interferometer. The red, green and blue sources show progressively lower visibility fringes and hence broader linewidths.

4.7 Optical fibre couplers.

Directional couplers are necessary to divide and combine light efficiently in an all optical fibre system. A singlemode optical fibre uses evanescent wave coupling. A wave propagating in the core of a fibre decays as an evanescent wave in the cladding. If this evanescent wave is allowed to overlap the core of a second fibre then coupling will occur and light will propagate in the second fibre. A multimode fibre coupler works by converting high order modes to cladding modes which are subsequently recaptured by a second fibre. Splitting ratios in multimode fibre couplers are therefore a function of the degree of mode filling.

The first all fibre couplers to be made had a variable coupling ratio and were described by Sheem and Giallorenzi [4.1]. Two optical fibres were twisted together and placed in a container filled with acid. The fibre cladding was removed by etching allowing the two fibre cores to come close enough for evanescent coupling to occur. The acid was removed and replaced with an index matching fluid. The coupling ratio was controlled by the tension in the two twisted fibres.

A second method of producing singlemode optical fibre couplers with variable splitting ratio was described by Bergh et al. [4.2]. This method is to embed an optical fibre in each of two glass blocks and remove the exposed cladding by polishing until very close to the core. The polished fibres are then placed together with some index matching fluid. Adjusting the relative positions of the fibres gives some control over the splitting ratio.

105

The most common couplers are directional couplers made by fusing together two optical fibres, first described by Villarruel and Moeller [4.3]. Two glass fibres are heated together at around $1500°C$, in order to soften and fuse them, and then stretched whilst hot. This decreases the core diameter and causes the evanescent wave to spread further from the core. This allows coupling to occur when the cores are further apart than would otherwise be possible. Heating and stretching the fibre is continued until the required splitting ratio has been achieved. Fused fibre couplers known as star couplers are now available with 3,4,8 or even 16 input and output ports. Most fibre couplers do not preserve the polarisation when the light is split or combined. A fused polarisation maintaining coupler is described by Nayar and Smith [4.4].

As the coupling ratio depends on the wave guided in the fibres the coupling ratio is wavelength dependant. A device which exploits this characteristic is said to be a wavelength division multiplexer/demultiplexer. A device which showed unity coupling at 1300nm but close to zero coupling at 1550nm is described by Lawson et al. [4.5].

Although for our purposes light can be coupled between fibres using lenses and beamsplitters it was decided to try and make 2 by 2 couplers (i.e. 2 input ports and 2 output ports) by fusion using single and multimode optical fibre.

The multimode fibre had 50/125 micron core / cladding diameters. The fibre is covered with a protective outer coating which brings the fibre to about 200 microns in diameter. This outer layer was removed from a 5cm length at the centre of each of two 1m long fibres by a loop

of cotton pulled along the fibre. The stripped regions of the fibres were then twisted together with one or two turns and fixed to two adjustable mounts, figure 4.23. Light from a chopped HeNe laser was coupled into one of the fibres. The output from both fibres was monitored using two photodiodes. The fibres were then softened using a propane flame and tapered by winding the mounts slowly apart. The twist in the fibres caused the two cores to be pulled together as the cladding softened. Care had to be taken not to try and taper the fibres too quickly as the fibres would snap. Overheating the fibres distorted them and caused large losses in the coupler.

The heating and tapering was continued until coupling occurred between the fibres with the required splitting ratio. If the tapering was continued then the splitting ratio was seen to oscillate. There is therefore a beatlength associated with the fabrication of these couplers. Coupling was easily achieved using the multimode fibre and 50/50 splitting ratios were obtained. The process was repeated with singlemode fibres. These have a core diameter of about 8 microns and a cladding of 125 microns. So the separation of the two singlemode cores is much greater than in the case of the multimode fibres. The couplers are therefore much more difficult to make. The fibres were prepared in the same manner and stretched and heated until coupling occurred. The losses for both multimode and singlemode couplers were typically greater than 6dBs. Commercially available couplers may have losses as low as 0.1dBs.

The optical fibre couplers then had to be packaged. The best solution available was found to be supporting the coupler on a glass slide and the covering it in epoxy. However, couplers packaged in this manner deteriorated within a few days. It was found that this was due to the

107

different temperature coefficients of expansion of the silica fibre and the epoxy. This problem was overcome by loading the epoxy with silica powder.

4.8 Coherence In Optical Fibres

In section 4.4 the visibilities of HeNe (633nm) and HeCd (442nm) laser sources were measured against path difference using an air path Michelson interferometer and a multimode optical fibre Mach-Zehnder interferometer. It was shown that the same curves were obtained if visibility was plotted against optical path length. Multimode optical fibres are of interest for inclusion in E-O sensors because of their larger core size which makes them easier to handle and more tolerant to misalignment. Multimode fibres also have a greater core / cladding ratio, so smaller 'dead zones' between fibres occur. However, multimode fibres must only be used for pre-detector signal processing when any effect on the complex amplitude of the light is unimportant. Hence, it is necessary to determine the effect of an optical fibre on the light guided by that fibre. In particular it is important to consider the coherence of the guided light.

Dispersion in a fibre is either group dispersion or phase dispersion. Group dispersion is further divided into intermodal and material dispersion. It was expected that dispersion in a fibre would affect the coherence of guided light. Coherence is a measure of the degree of correlation of one wave with a second wave. If the complex amplitude of a wave guided through a fibre is altered then the degree of correlation with a second wave and hence, their coherence must alter.

Consider first a singlemode fibre. This will only induce chromatic, or material, dispersion in the light. The material dispersion, from section 2.3.1, is given by

$$d\tau_c = \frac{L}{c}\left(\frac{\partial\lambda}{\lambda_0}\right)D \quad \text{where} \quad D = \lambda_0\frac{d^2 n_1}{d\lambda^2}. \quad (2.3.1.9)$$

For a source of wavelength 633 nm, linewidth 0.1 nm, and a value of $D = -0.050$ (from figure 2.5) the material dispersion in 10m of fibre is 0.2psec. This delay corresponds to about 0.18cm in space between the longest and shortest wavelengths. From this calculation it is seen that the length of a pulse is increased in time and space by dispersion.

If the waveguide is a multimode fibre with $n_1=1.45$, and $n_2=1.4465$ then the intermodal dispersion, from section 2.3.2, is given approximately by

$$d\tau_M = \frac{L}{c}(n_1-n_2), \quad (2.3.2.7)$$

so for 10m of fibre we have that $\delta T = 0.12$nsec. This delay corresponds to about 3.6 cm in space between the highest and lowest order modes.

Phase dispersion will have an effect on the coherence of the light because the optical path length of light is determined by the phase velocity. The limits of the phase delay for the highest and lowest order modes are such that dt_{mn} lies between Ln_2/c and Ln_1/c; so the maximum phase dispersion, from section 2.4, must be given by

$$dt_P = \frac{L}{c}(n_1-n_2). \quad (2.4.13)$$

This is the same expression as was derived for intermodal dispersion but the sign of the dispersion is reversed. The higher order modes have the lowest phase dispersion.

110

It may be possible to make use of the intermodal dispersion in certain cases. For example, if the light from the multimode fibre is interfered with a singlemode reference beam, and if the path difference of the reference is altered, a series of visibility maxima will occur corresponding to zero path difference between the reference and a particular mode of the multimode fibre. It should be possible to use a singlemode fibre together with a fibre supporting a few modes to produce a fibre interferometer which consists of several path differences which could be selected by exciting a particular mode of the multimode fibre.

4.8.1 Temporal Coherence In Fibres

In a multimode fibre the intermodal dispersion would be expected to have the dominant effect on the coherence of the light. Neglecting the effect of the material dispersion and assuming the illuminating source is spatially coherent we see that a single wavetrain input to the fibre becomes a series of wavetrains each corresponding to one guided mode of the fibre and each shifted in time and space with respect to each other. This shift is by an amount equal to the difference in optical path length between the modes. In a singlemode optical fibre the material dispersion would be expected to have an effect on the coherence of guided light. The small amount of dispersion suggests that it will often be negligible when compared with the length of a wavetrain but if we consider a source such as white light with a temporal coherence of only a few wavelengths then the material dispersion becomes significant. A wavetrain originally a few microns long may become a few thousand wavelengths long in a few tens of meters of fibre.

We can use a phase diagram to represent the amplitude and phase of each mode at a given point in the output plane of the fibre. If the modes have travelled a distance such that the difference in their optical paths is much less than the coherence length of the source then the resulting intensity at a point will be the vector sum squared of all the individual modes.

$$ I = \mid E_n e^{i\phi_n} \mid^2 = \mid \sum E_m e^{i\phi_m} \mid^2 . \qquad (4.8.1.1) $$

The angular frequency of the resultant will be the same as the individual components as no new frequencies have been introduced.

So it would appear that the temporal coherence of the source cannot have changed.

If the modes have travelled a distance such that the difference in their optical paths is much greater than the coherence length of the source then the modes will be uncorrelated and the resulting intensity at a point in the output plane will be an intensity summation of all the modes.

$$I = |E_n|^2 = \sum |E_m e^{i\phi_m}|^2 . \qquad (4.8.1.2)$$

4.8.2 Spatial Coherence In Optical Fibres

If a multimode optical fibre of length Z and refractive indices n_1 and n_2 is illuminated by a spatially coherent source then the resulting amplitude at a point in the fibre, for intermodal dispersion small compared with the coherence length, is as given above. We now want to consider the spatial distribution of the modes and see what happens to the spatial coherence of the light.

As only certain modes can be guided (solutions of the Helmholtz equation) the field can be written as

$$E(r,t) = \sum_{m=0}^{5} \sum_{n=0}^{5} (C_{mn}(\omega)\text{Cos}(n\theta) + S_{mn}(\omega)\text{Sin}(n\theta))$$
$$\times J_{mn}(\frac{u_{mn} r}{a}) \exp(i(\beta_{mn} z - \omega t)), \qquad (4.8.2.1)$$

where $\beta_{m\,n}$ is the wavenumber of the mn^{th} mode.

By including an expression for the linewidth of the source and substituting for $E(r,t)$ in an expression for the complex degree of coherence it has been shown by Crosognani and Di Porto [4.6] that the correlation function

$$< E_1(r_1,t)\, E_2{}^*(r_2,t+\tau) > ,\qquad (4.8.2.2)$$

is a periodic function of z. That is, the spatial distribution of the modes is periodic along the fibre as the modes beat due to their different group velocities.

Whatever the actual spatial distribution for the modes of a multimode fibre the phase front of the light emitted from the fibre will be very complicated. The more modes there are the more complicated the phase front will be.

In order to obtain high visibility interference fringes a high degree of spatial coherence is required. As the source was spatially coherent the modes will be correlated and the light emitted by the fibre will be spatially coherent but the rate of change of phase with position across the phase front will increase with increasing number of modes.

The effect of the modes is to cause discontinuities across an interference pattern. In particular, the single fringe associated with a singlemode fibre interferometer will not occur. Instead regions of constructive and destructive interference, or speckles, will be seen. There is a link between the number of modes guided in a fibre and the distortion of the phase front emitted by the fibre. The phase front will show discontinuities at the boundary between two speckles so the speckle size is a measure of the distortion.

The number of guided modes is approximately equal to the number of speckles so we can write

$$N_{modes} = N_{speckle} . \qquad (4.8.2.3)$$

The area of a speckle, A, is therefore the area illuminated by the fibre, πr^2, divided by the number of guided modes. We have

$$A = \frac{\pi r^2}{N_{modes}} . \qquad (4.8.2.4)$$

From equation (2.2.3.7) we know that the number of guided modes in a step-index fibre is given by

$$N = \frac{4v^2}{\pi^2} , \qquad (2.2.3.7)$$

The v number is equal to

$$v = ka\,(NA) , \qquad (4.8.2.5)$$

where NA is the numerical aperture of the fibre and a is its radius.

Using equations (4.8.2.3),(4.8.2.4), (2.2.3.7), and (4.8.2.5) it can be shown that the diameter, d, of a single speckle is approximately given by

$$d = \frac{\lambda}{2(NA)} \left(\frac{r}{a}\right) . \qquad (4.8.2.6)$$

For these experiments we used a 50 mm diameter lens to collimate the light, so the speckle size at the lens with 50μm, 400μm and 970μm core fibres is 1.6mm, 0.2mm, and 0.082 mm respectively.

115

4.8.3 Coherence In Optical Fibres - experimental.

In order to measure the visibility of light emitted from an optical fibre, the light was introduced to an air path Michelson interferometer with a variable path difference. Circular interference fringes were obtained and the maximum and minimum intensities of the fringes was measured at the centre of the interference pattern. The fringe visibility was then plotted against path difference.

The first experiment was carried out with 1m of 50/125 micron fibre. Light from both the HeNe and HeCd sources was coupled, in turn, into the fibre and the light emitted was collimated using a 50mm focal length lens and introduced into a Michelson interferometer, figure 4.24. Circular interference fringes were obtained. Phase modulation of the interferometer allowed a photomultiplier tube to measure the maximum and minimum intensities of of the fringe pattern via a large core (970 micron) fibre placed at the centre of the pattern. The visibility of the fringes was plotted against path difference. The graphs obtained for HeNe and HeCd sources, figures 4.25 and 4,26, showed no differences from the graphs of visibility against path difference for the input light, figures 4.13 and 4.14. The fibre length was increased to 10m and the experiment repeated. The results were the same as the graphs of visibility for the input light. The fibre length was increased to 20m and the experiment repeated again. The graphs obtained were of the same form as the graphs of the input light but the visibility was slightly lower, and the curve was not as smooth for large path differences in the interferometer, figures 4.27 and 4.28. So it appears that short lengths of multimode 50/125 μm fibre have little effect on the visibility as there is little

difference when visibility against path difference is measured before and after transmission through up to 20 m of fibre.

Another experiment was carried out with light from the HeNe laser guided through a 1m length of 400 μm core, plastic optical fibre. The light emitted from the fibre was introduced to a Michelson interferometer and the fringe visibility measured, for a known path difference. This fibre was then replaced by a 1m length of 970μm core, plastic fibre, and the fringe visibility against path difference measured again. The two sets of results were plotted in figure 4.29a and 4.29b.

The curves obtained using the 400 and 970 micron fibres appeared at first to show a decrease in the temporal coherence because the visibility fell rapidly, in each case, after only a few centimetres path difference. The reason for the decrease, however, was suspected to be due to the central fringe becoming smaller in size than the core of the detector fibre. The core size of the optical fibre is the size of the effective source. The minimum divergence angle must be given by the angle subtended by the source placed at the focal point of a lens from the lens. For larger core fibres the minimum divergence will be greater. The size of the central fringe of the interference pattern depends on the radii of curvature of the two interfering wavefronts. A small difference in the two radii of curvature will give a large central fringe. As the air path of one beam is increased its radius of curvature increases and the radius of the central fringe decreases to a limiting size where the delayed wavefront is effectively planar. To test this we decided to determine the effect on the measured visibility of different optical fibres in the detector plane.

Light from the HeNe source was coupled into a few meters of the 400 micron core fibre. The output from the fibre was collimated and input to a Michelson interferometer as before. Circular interference fringes were obtained and the visibility of the central fringe measured against path difference by a photomultiplier. Light was guided from the output plane of the interferometer to the detector by a fibre. Three optical fibres were used, in turn, in the detector plane. They had core diameters of 50, 400, and 970 μm respectively. The visibility against path difference was plotted for each fibre on the same graph as shown in figure 4.30.

It was seen from the graph that the visibility remained significantly higher when measured using a small detector fibre. When the visibility against path difference over the first 10 cm is compared with the source visibility before transmission through the fibre then the 400 micron fibre appears to have no effect on the temporal coherence of the source. This leads us to believe that short lengths of fibre have little effect, whatever their diameter, on the temporal coherence of light. A fibre is considered to be short if the dispersion is small compared with the coherence length.

A final experiment was to guide light from a HeNe laser through 100m of 50/125 μm multimode fibre. An air path Michelson interferometer was used to produce interference fringes and a graph of visibility against path difference was plotted, figure 4.31. The graph showed a marked change in the visibility of the source. The visibility curve still showed beats but they were of greater amplitude than before. The experiment was repeated and graph 4.32 was obtained. This showed a decrease in the visibility of the source. The conclusion was that exciting different groups of modes in each

118

experiment had caused two different effects to be seen. In figure 4.31, interference between well correlated modes caused a filtering of the transmitted spectrum to increase the visibility of the light. In figure 4.32, the fibre is sufficiently long for the modes excited to travel significantly different optical path lengths and be less well correlated at the end of the fibre giving a lower fringe visibility.

4.8.4 An Interferometer and an optical fibre as an Optical Filter.

It has already been mentioned in section 3.4 that an interferometer may be treated as an optical filter. The following discussion of this property will be shown to be applicable to a multimode optical fibre.

A Michelson Interferometer, when illuminated by a single wavelength, will either transmit or reflect that wavelength depending on whether the path difference in the interferometer causes constructive or destructive interference to occur. If the wavelength is scanned, the interferometer transmits or reflects the radiation periodically as the phase difference between the two arms changes through 2π radians and constructive or destructive interference occurs. Zero path difference implies that constructive interference always occurs and so the interferometer is transmitting over all wavelengths. The interferometer can be thought of as a filter whose filter function is periodic and depends upon its path difference. For a broadband source illuminating the interferometer, we may write

$$\Delta k \, \Delta x = 2\pi, \qquad (4.8.4.1)$$

119

where Δk is the change in wavenumber of the radiation and Δx is the path difference in the interferometer. So the periodicity of the filter in terms of wavelength, $\Delta \lambda$, is

$$\Delta \lambda = \Delta x. \qquad (4.8.4.2)$$

Now consider an interferometer with, for example, a path difference of 1 micron illuminated by a broadband, white light source. The transmission function of the interferometer will go from a maximum to a minimum and back to a maximum over 1 micron in bandwidth, so the filter function is so wide that its effect may not be seen. It would obviously be very difficult to set up an interferometer with, for example, a 50 nm path difference which would have a filtering effect visible on a spectrometer.

By Fourier analysis a white light source may be considered to emit a short wavetrain whose coherence length may be a few microns. A Michelson interferometer will split the single wavetrain into two wavetrains with a delay between them equal to the time taken to travel the path difference in the interferometer. If the path difference is Δx then the delay, τ, is given by

$$\tau = \frac{c}{\Delta x}. \qquad (4.8.4.3)$$

By the Weiner-Khintchine theorem, the power spectrum of the light emitted from the interferometer is given by the Fourier transform of the auto-correlation of the double pulse. This is written

$$|F(\nu)|^2 = \int_{-\infty}^{\infty} e^{i2\pi\nu t} \left(\int_{-\infty}^{\infty} f(t) \, f^*(t+\tau) \, dt \right) dt, \qquad (4.8.4.4)$$

120

where $F(v)$ is the spectrum of the light and $f(t)$ is the signal emitted from the interferometer. The signal $f(t)$ may be considered to be an even impulse pair which may be written

$$f(t) = 1/2 \, \delta(t+1/2) + 1/2 \, \delta(t-1/2). \qquad (4.8.4.5)$$

The auto-correlation of $f(t)$ becomes

$$\int_{-\infty}^{\infty} f(t) \, f^*(t + \tau) \, dt = 1/4 \, \delta(t+1) + 1/2 \, \delta(t) + 1/4 \, \delta(t-1). \quad (4.8.4.6)$$

So the power spectrum, obtained by Fourier transforming (4.8.4.6), is

$$| F(v) |^2 = 1/2 \; (1 + Cos \, 2\pi vt). \qquad (4.8.4.7)$$

Similarly, the spectrum emitted by a multimode optical fibre, at a point in the output plane, when illuminated by a source, is given by the Weiner-Khintchine theorem. The problem is to determine the signal $f(t)$. If a single wavetrain is input to the optical fibre then a number of wavetrains will be emitted corresponding to the number of guided modes. In the case of white light each wavetrain may be represented by an impulse, the sum of which, at appropriate intervals, make up the function $f(t)$ which may be compared to the impulse response.

Screen

Optical fibre

Beamsplitter
and coupling
lenses

Source
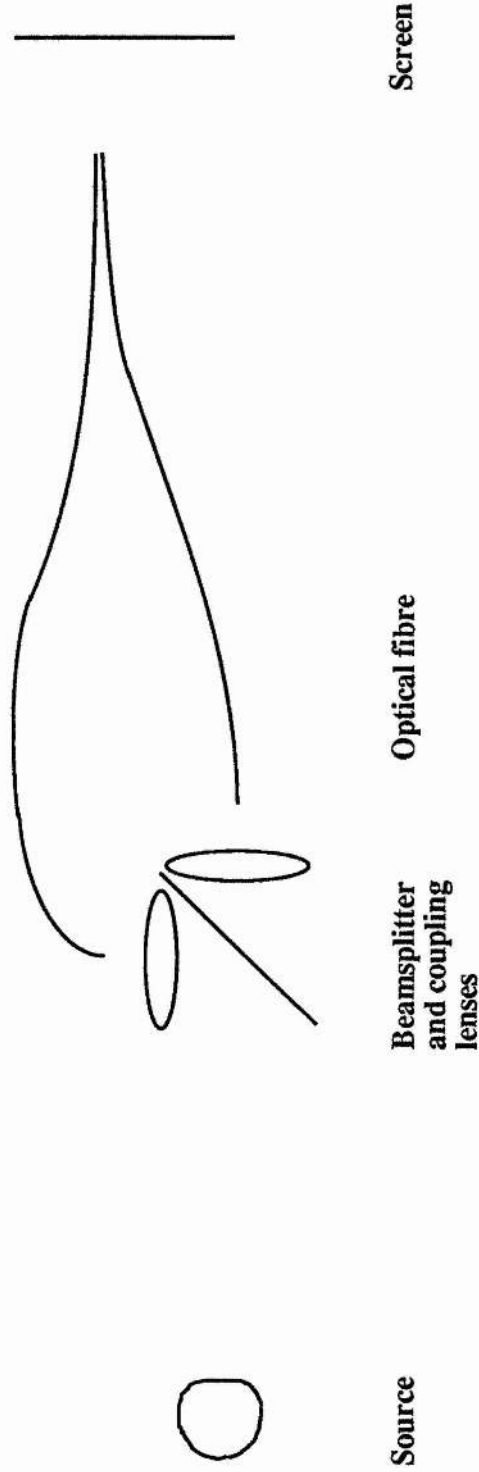
Figure 4.1. Two pinhole interferometer
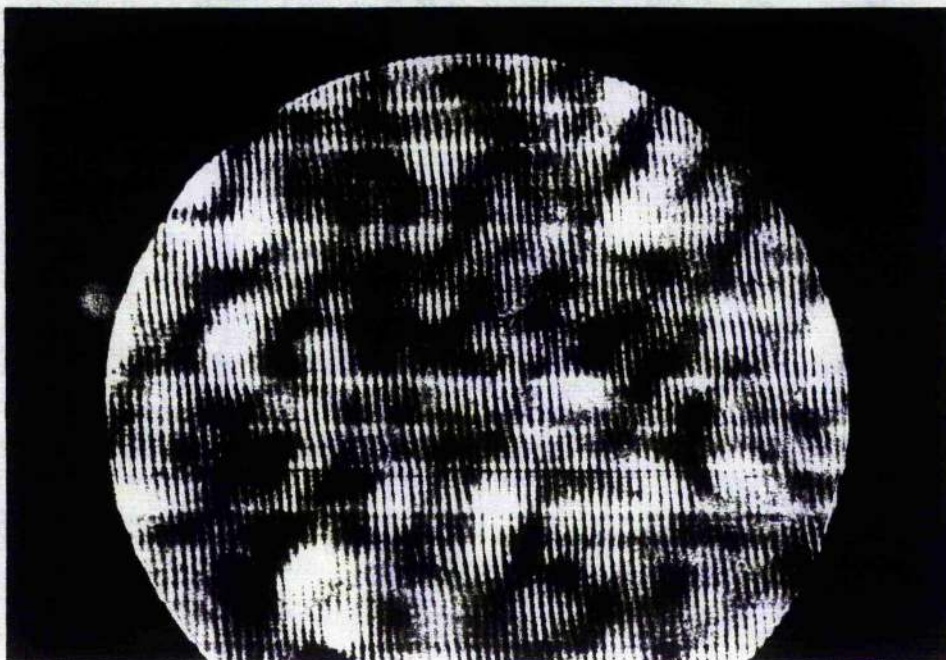
Figure 4.2 Photograph of linear interference fringes produced using two 50/125μm fibres

Figure 4.3 Photograph of linear interference fringes produced using two 400μm core fibres
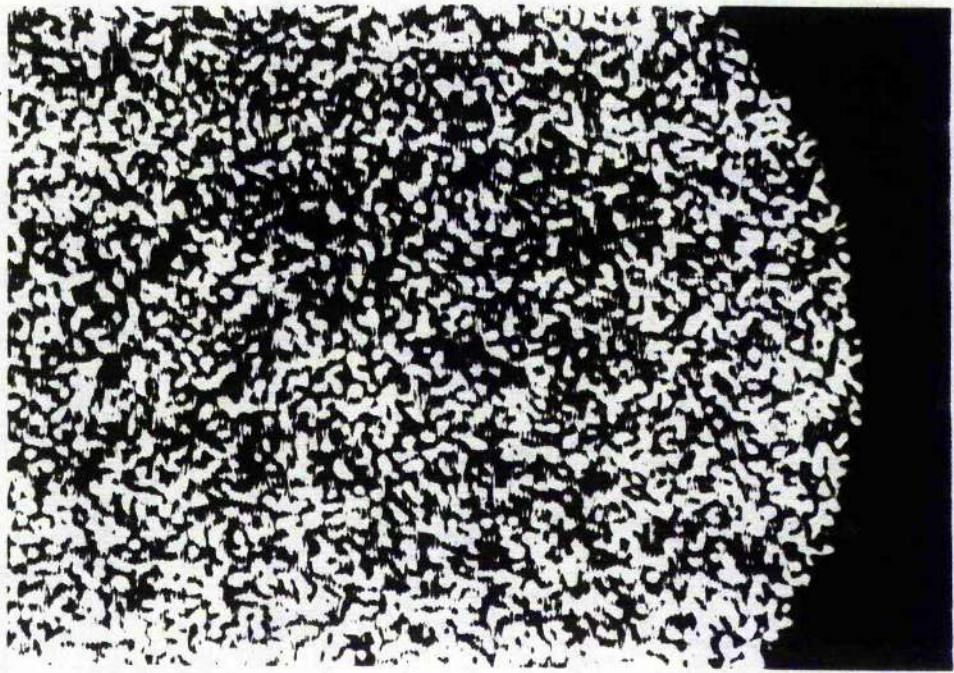
Figure 4.4   Photograph of linear interference fringes produced using two 970μm core fibres
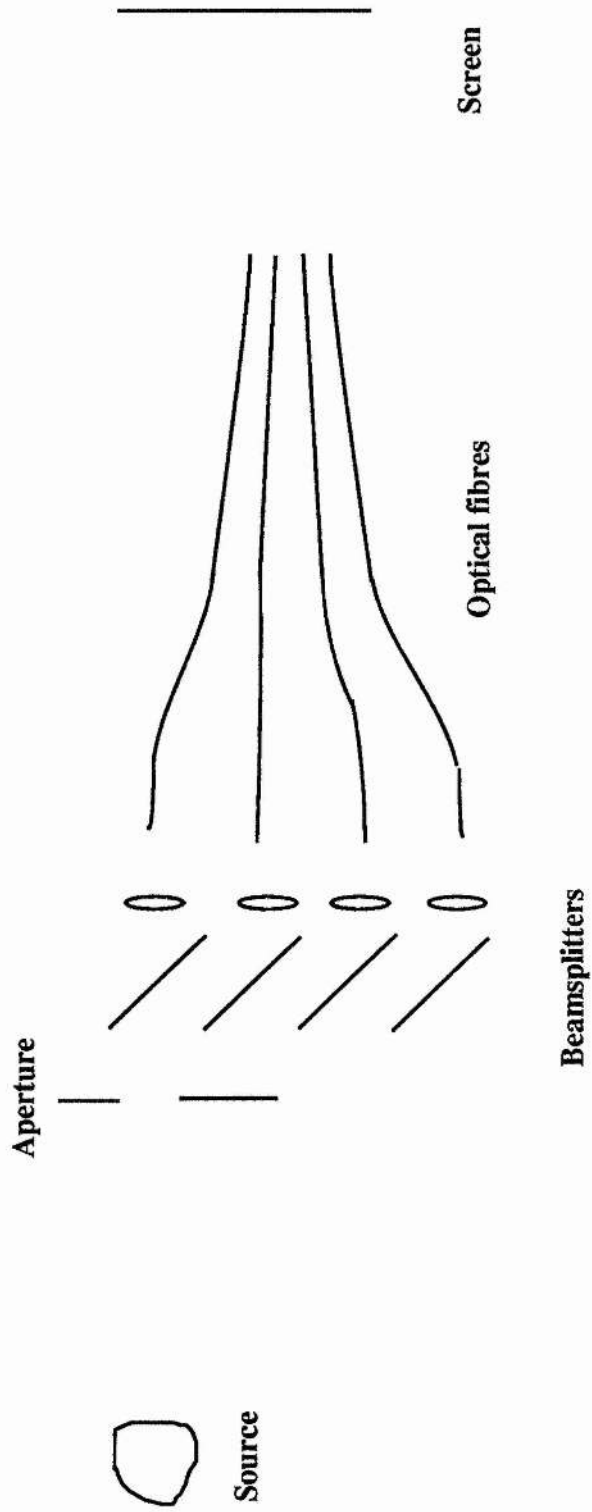
Figure 4.5 Multiple optical fibre interference pattern
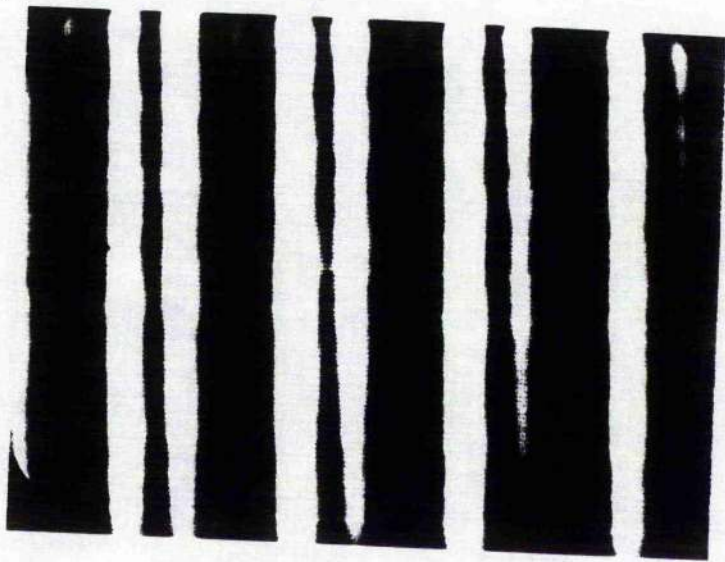
Figure 4.6   Photograph of linear interference fringes produced using four 50/125μm fibres

HeNe
Laser

Beamsplitter

Optical Fibre

Optical Fibre

Beamsplitter

Detector

Output
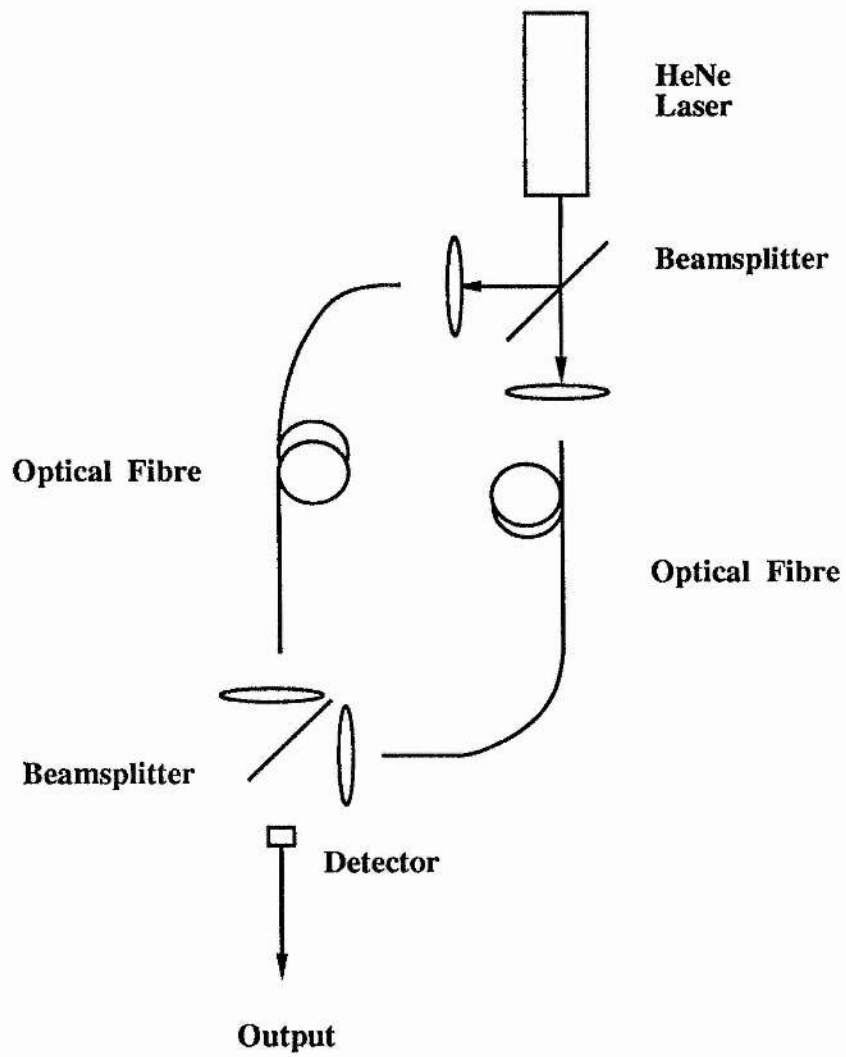
Figure 4.7   Mach - Zehnder interference patterns
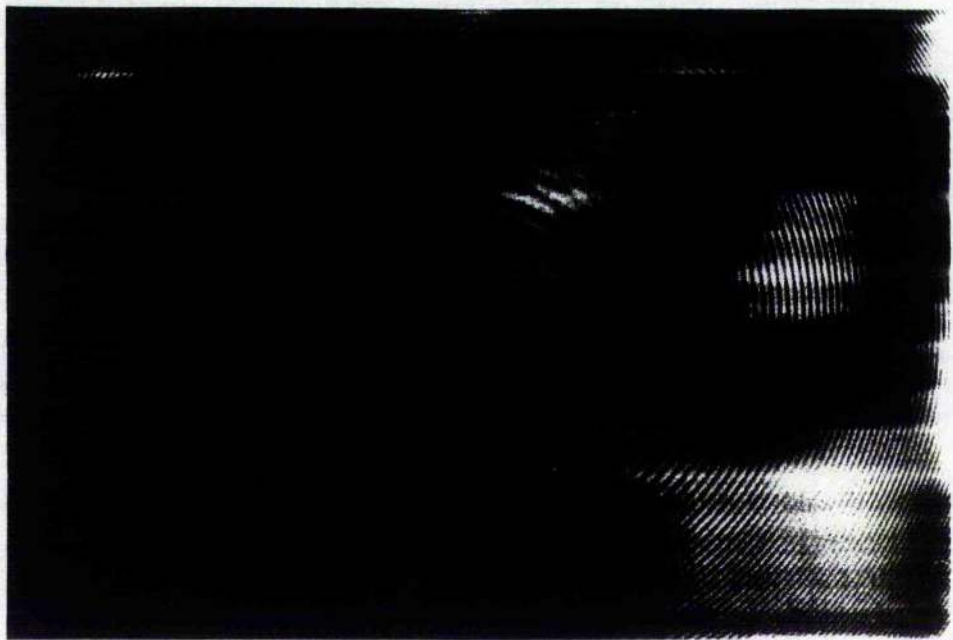
Figure 4.8   Photograph of circular interference fringes produced using
two 50/125μm fibres
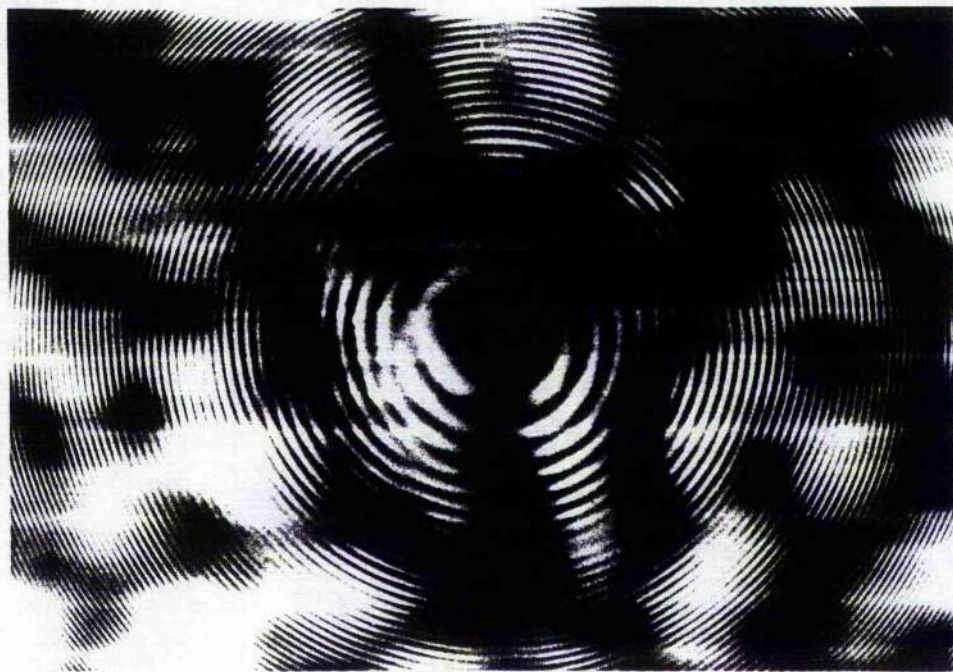
Figure 4.9   Photograph of circular interference fringes produced using
two 400μm core fibres
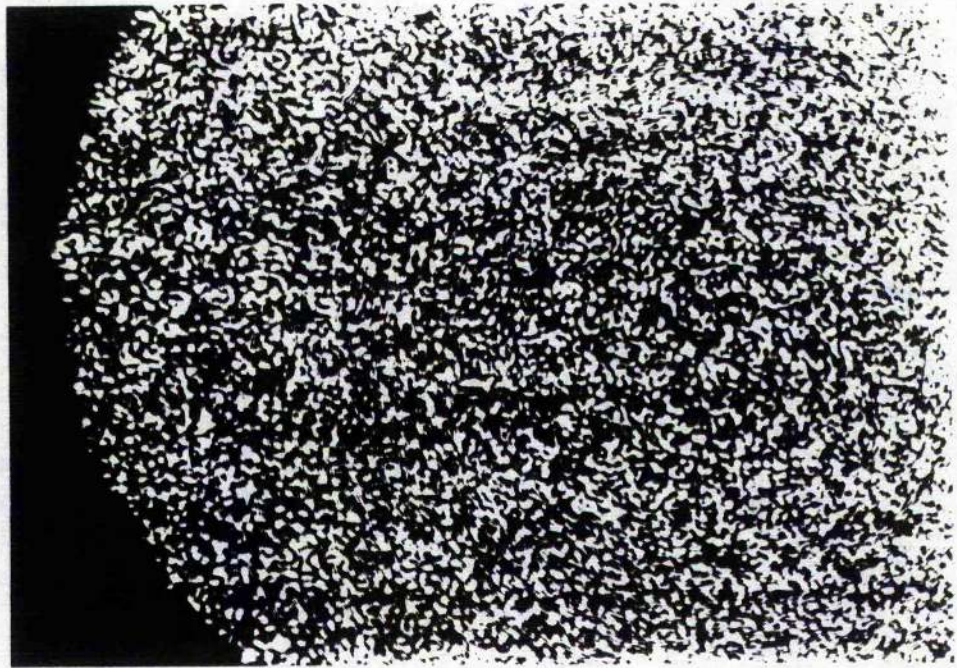
Figure 4.10 Photograph of circular interference fringes produced using two 970μm core fibres
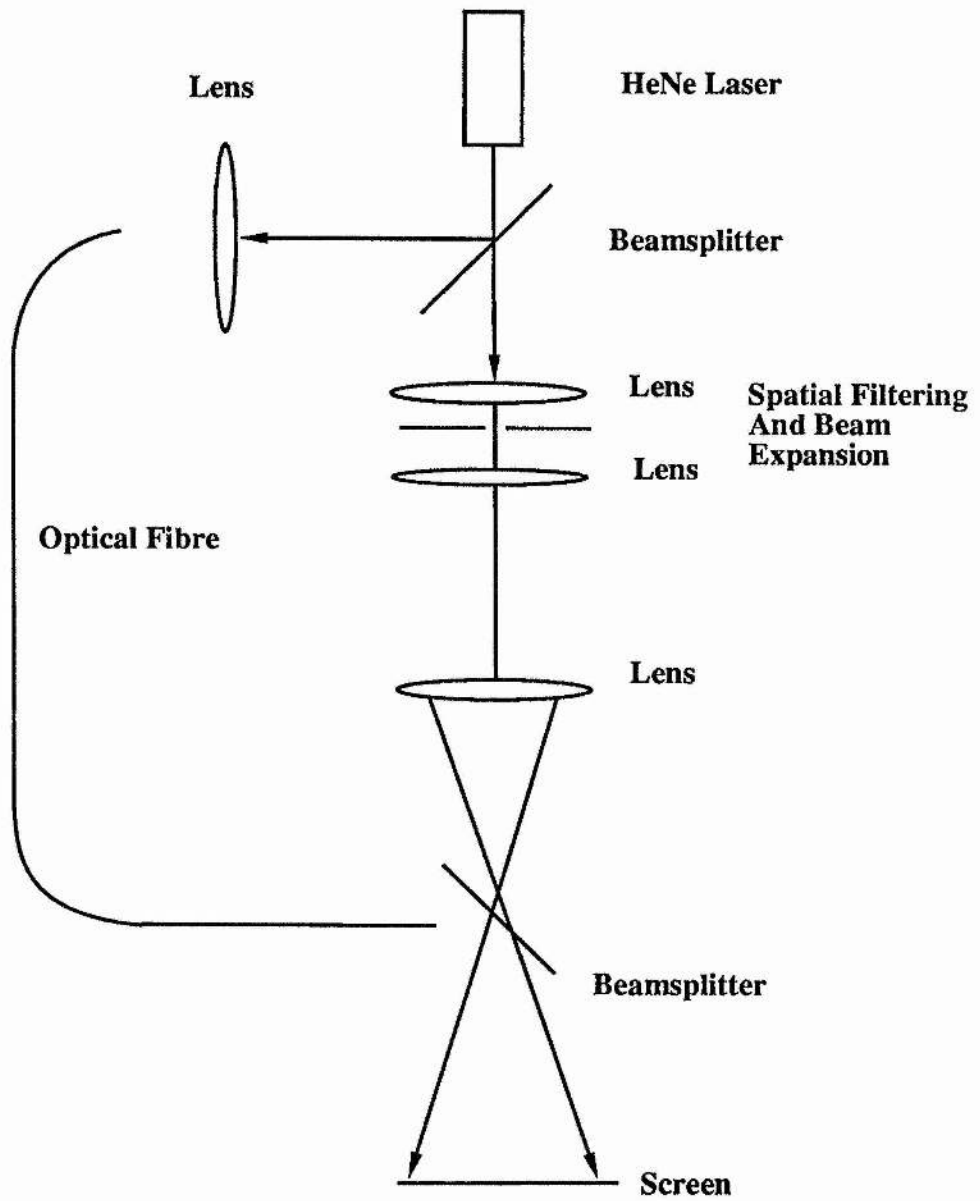
Figure 4.11   Arrangement to obtain map of phase front of light emitted from a fibre
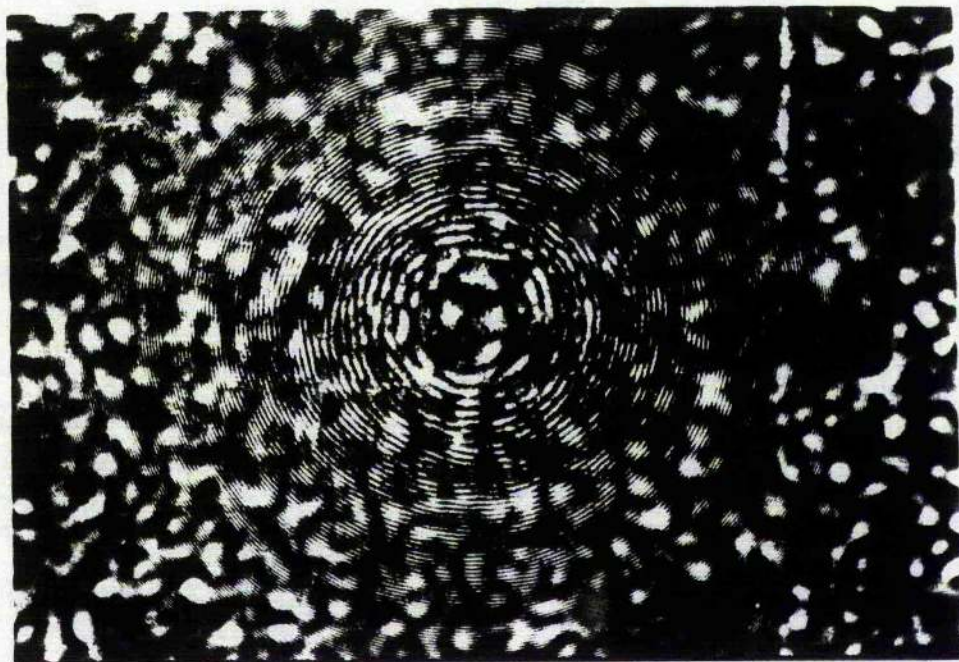
Figure 4.12   Photograph of phase front map of 970μm fibre

Visibility against path difference for HeNe
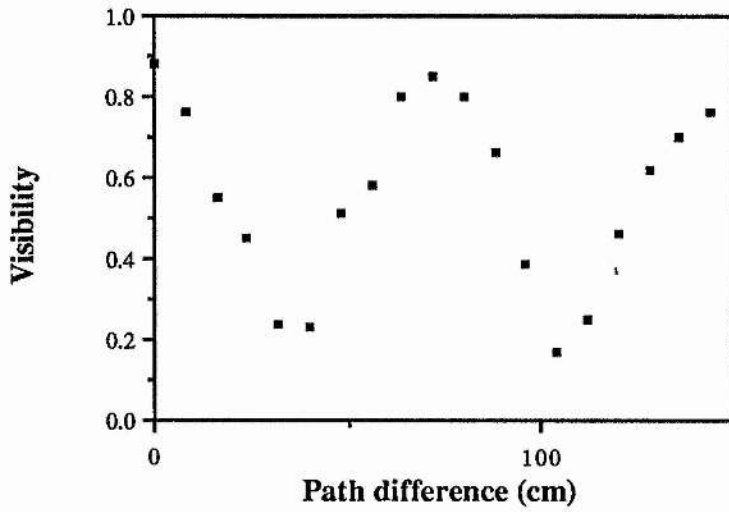
Figure 4.13

Visibility against path difference for HeCd.
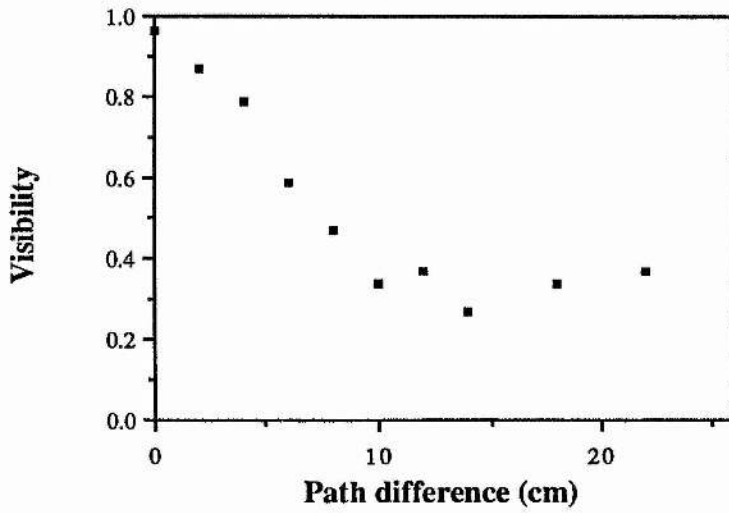
Figure 4.14

Visibility vs path difference for 50/125 fibre Mach-Zehnder
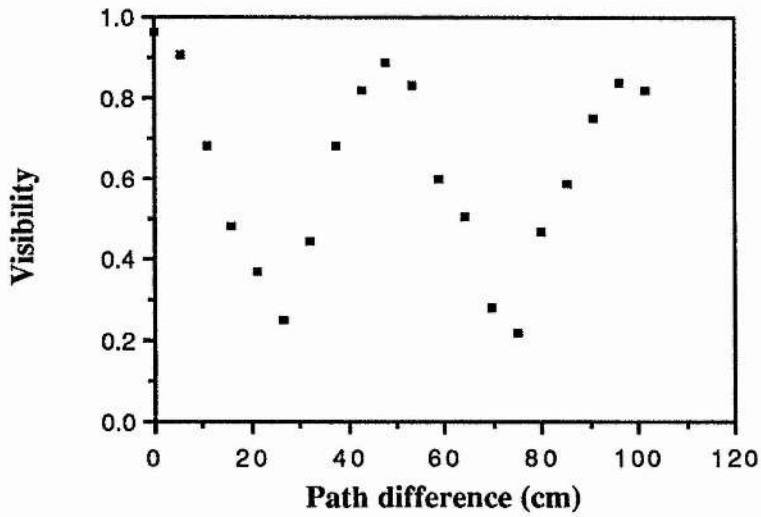
Figure 4.15

Visibility vs path difference for 50/125 fibre Mach-Zehnder

Figure 4.16

Sources

Collecting
lens

Collimating lens

Beamsplitter   Beamsplitter

Beamsplitter

Detector

Piezoelectric
cylinder

Fibre
Mach-Zehnder with
6cm OPD

Detector

Fibre
Mach-Zehnder with
19.5cm OPD
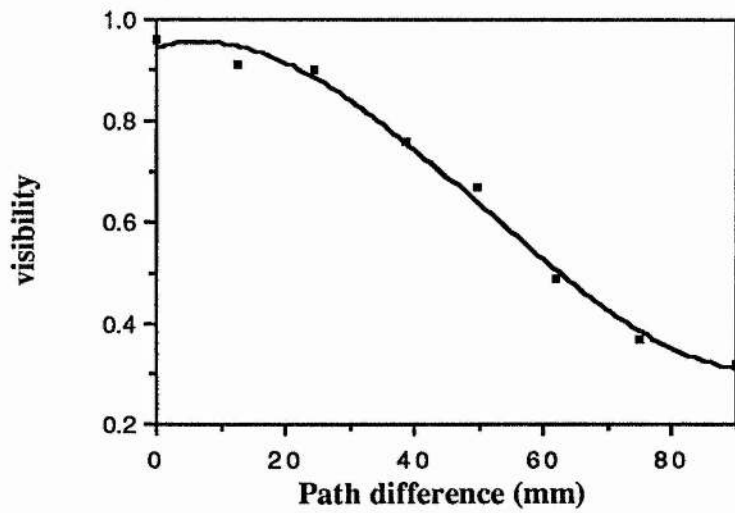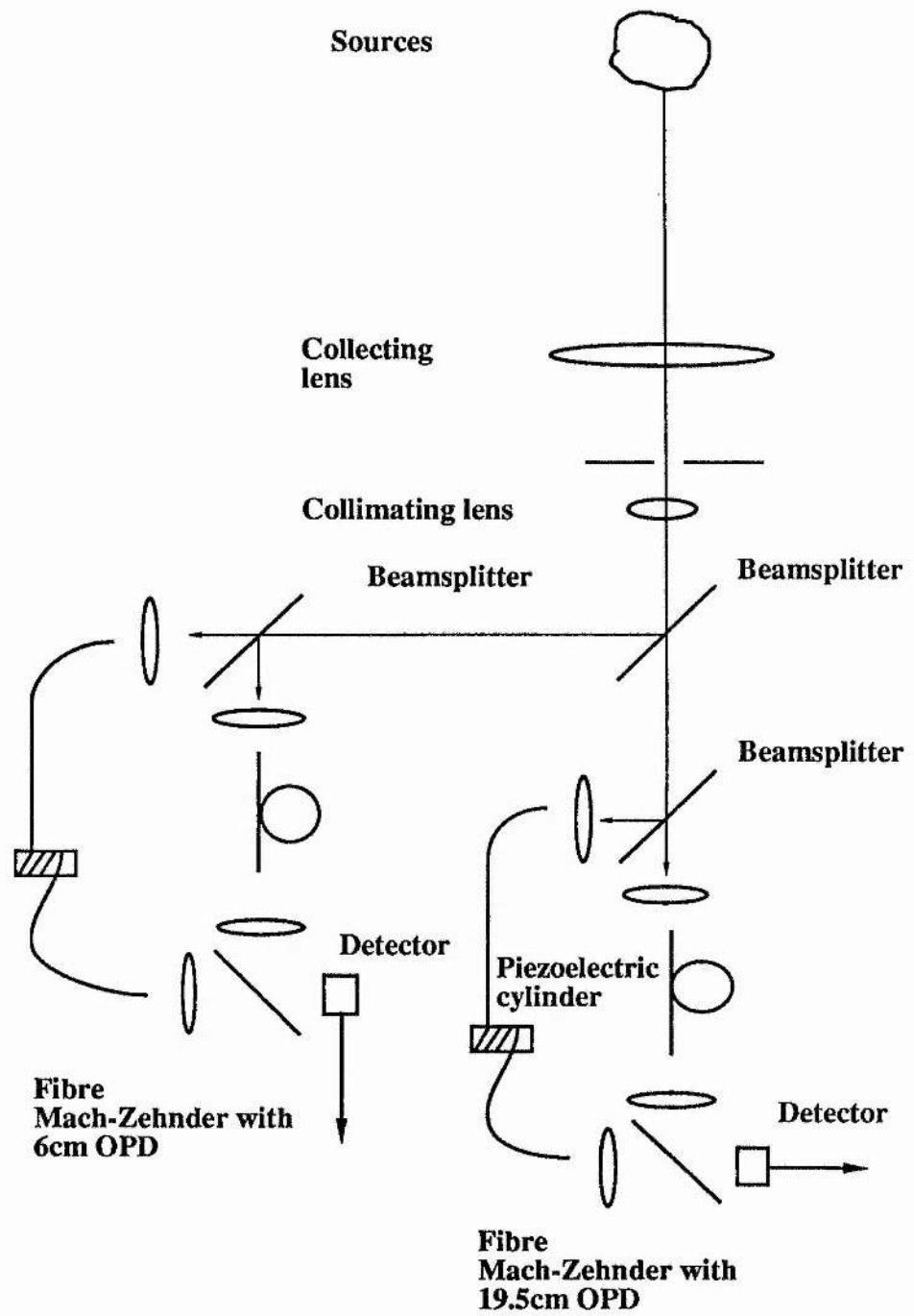
Figure 4.17   Temporal coherence bandpass filter
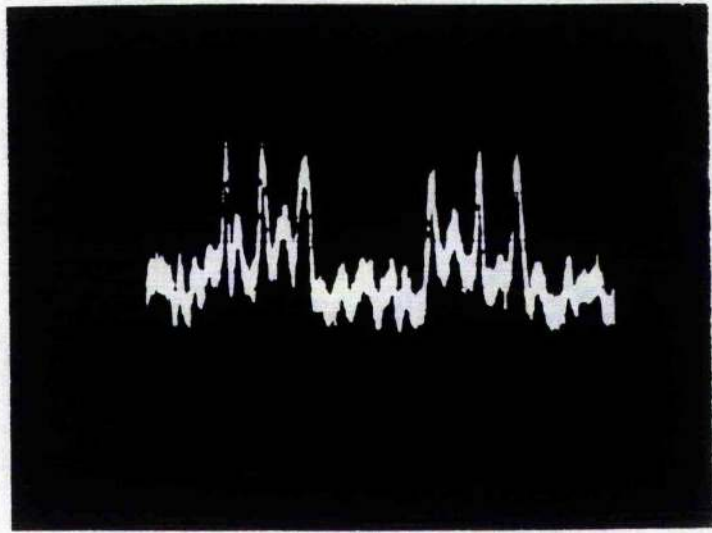
**Figure 4.18 Modulation due to two sources with a coherence length
greater than the path difference of the interferometer**
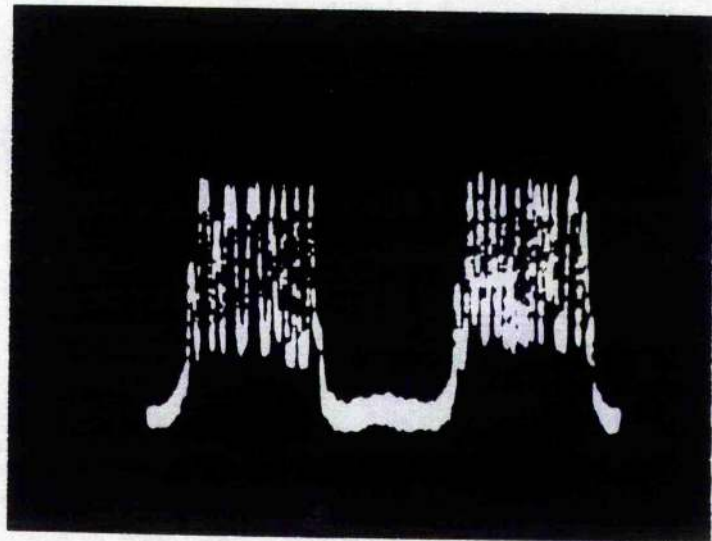
**Figure 4.19 Modulation due to one source with a coherence length
greater than the path difference of the interferometer**

Output

Sources
HeNe 633nm
HeNe 543nm
HeCd 442nm

Beamsplitter
s

Detector

**Large core (970
micron) fibres.**

**50/125 micron
optical fibre**

Beamsplitter

**Rotating
reticle**

**First order of
diffraction
pattern**

**50/125 micron
optical fibre**

**Piezoelectric
material**

**Diffraction
grating**

Beamsplitter

**50/125 micron
optical fibre**
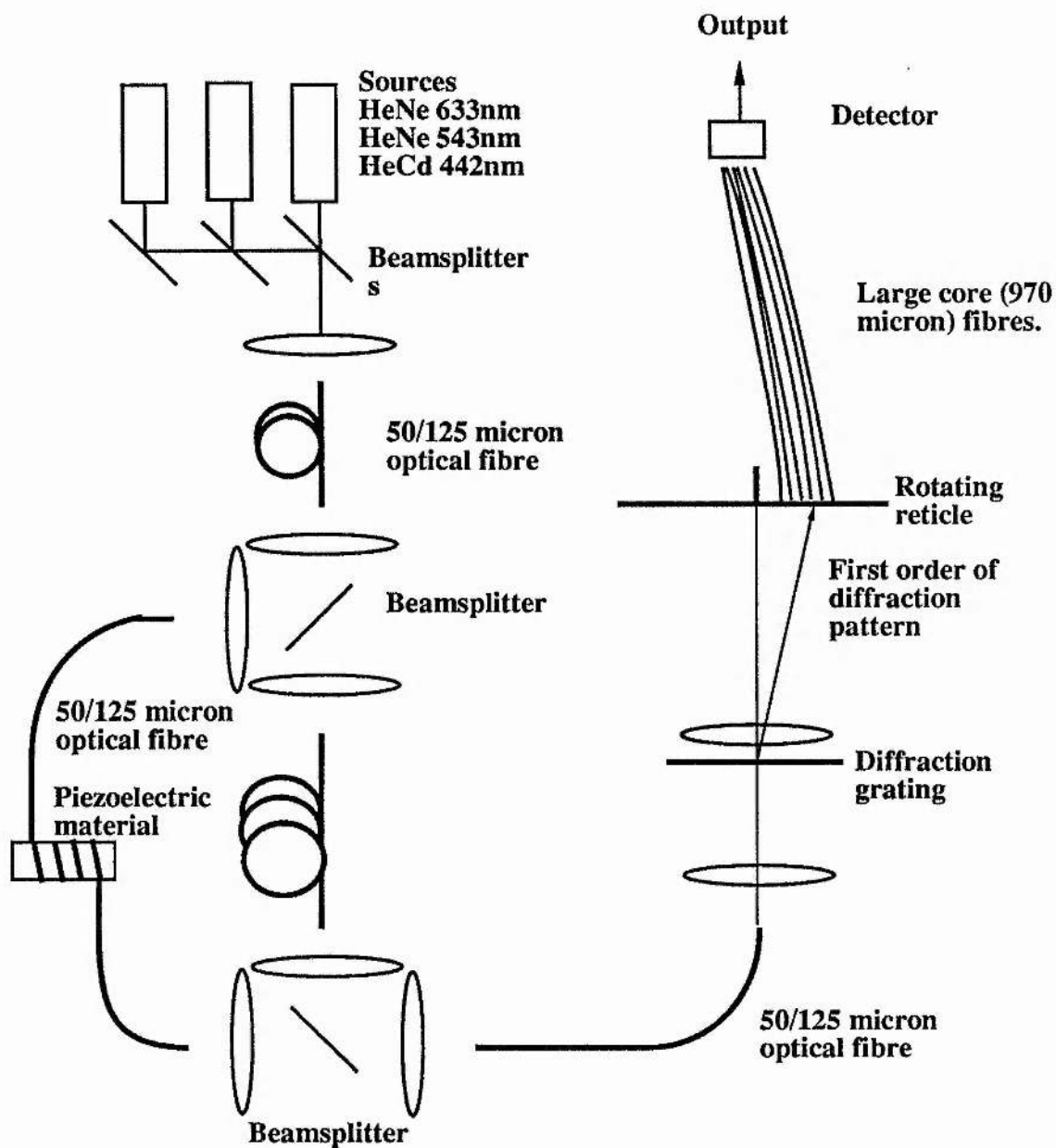
Figure 4.20 Measurement of visibility of several sources simultaneously.
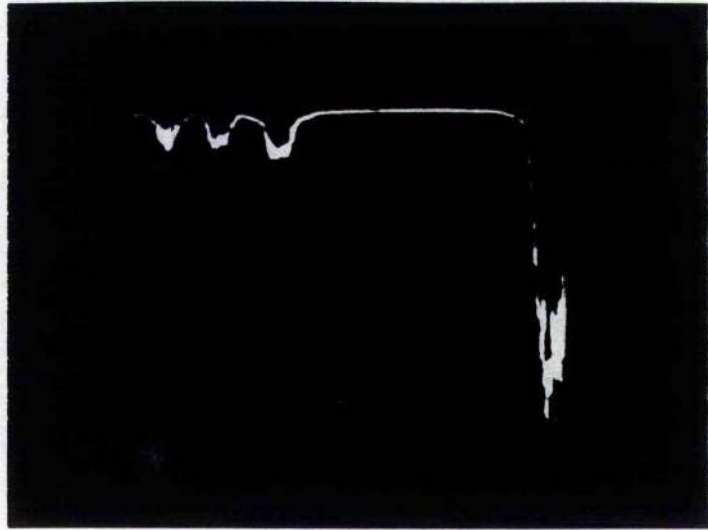
Figure 4.21 Spectrometer signal measured across fibre array
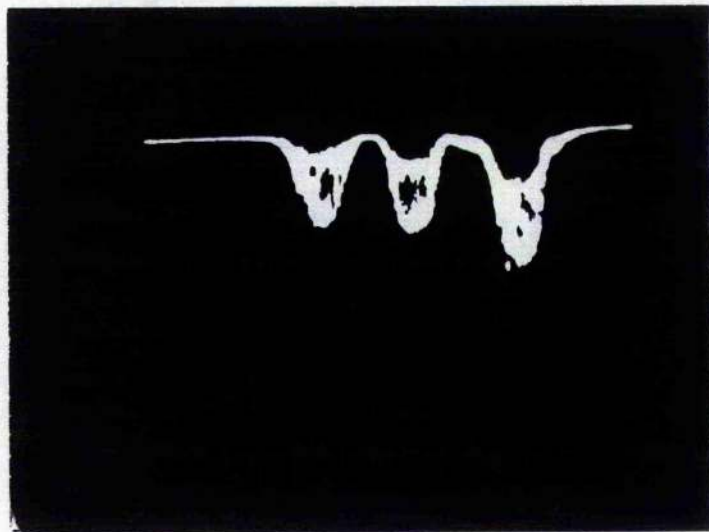
Figure 4.22 First order of spectrometer signal measured across

fibre array
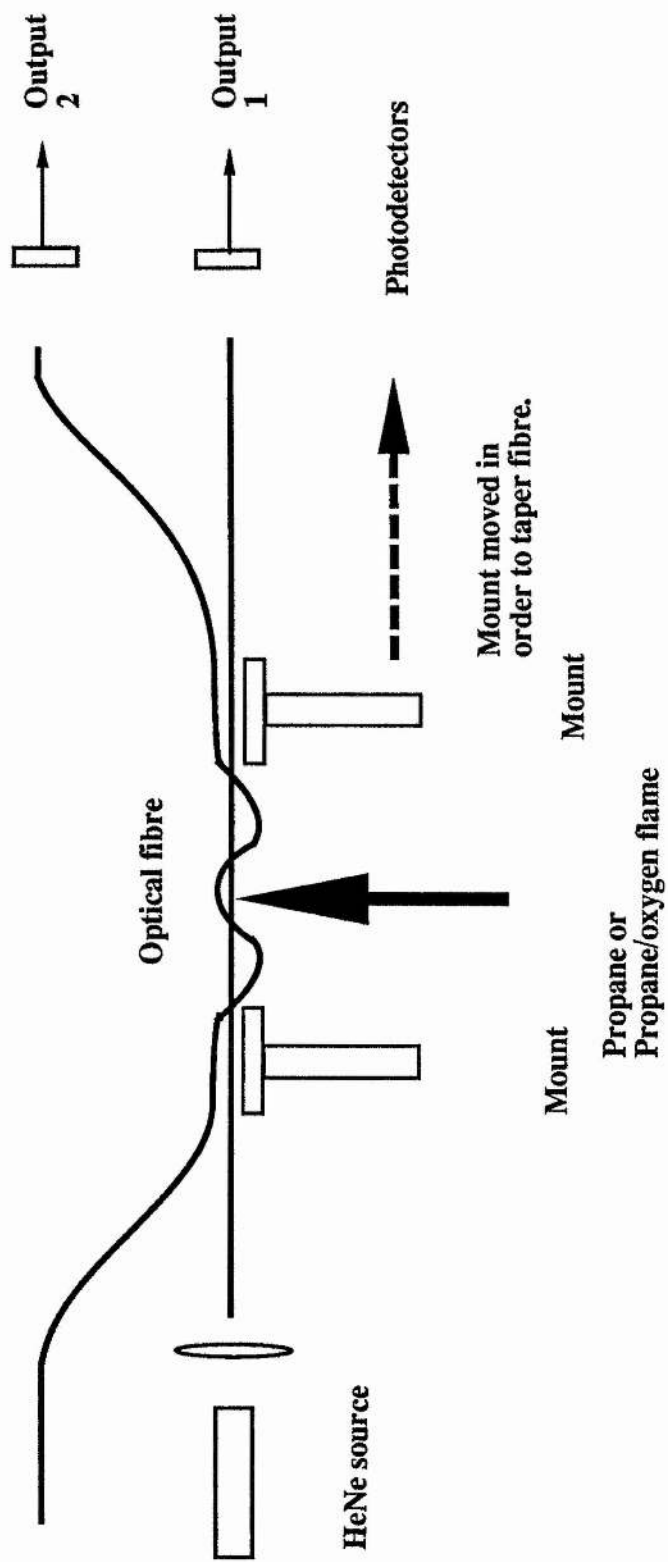
Figure 4.23 Making single and multimode optical fibre couplers

LED

Lens

Optical fibre

Lens

Beamsplitter

Detector fibre

Output

Detector

Mirror

Mirror
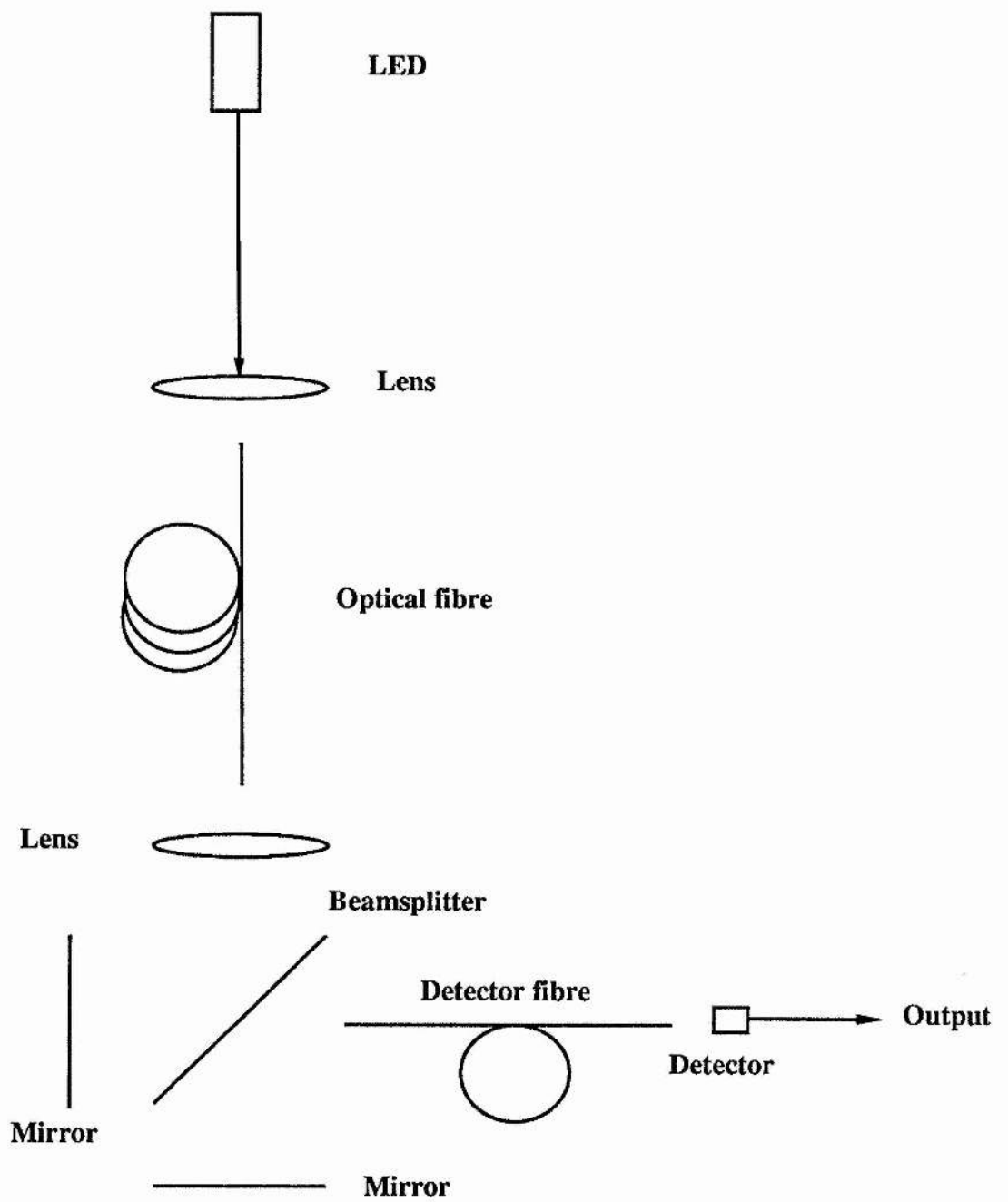
Figure 4.24 Measurement of the effect of dispersion on coherence.

HeNe source guided through 1m, 50/125μm fibre.
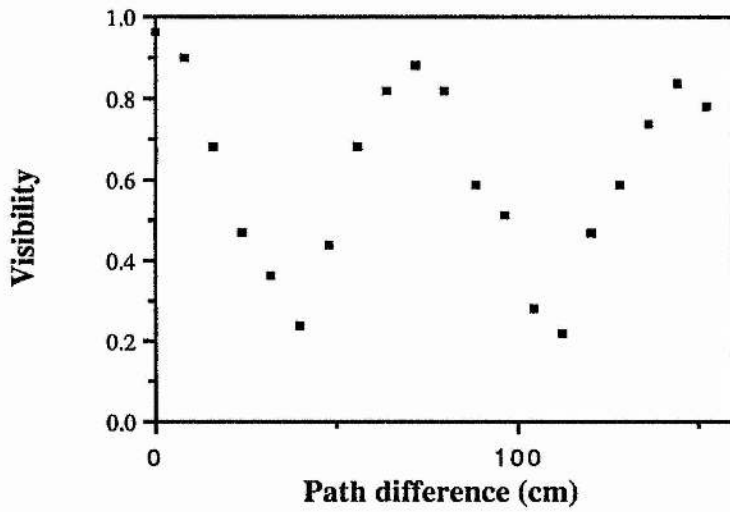
Figure 4.25

HeCd guided through 1m, 50/125μm fibre.
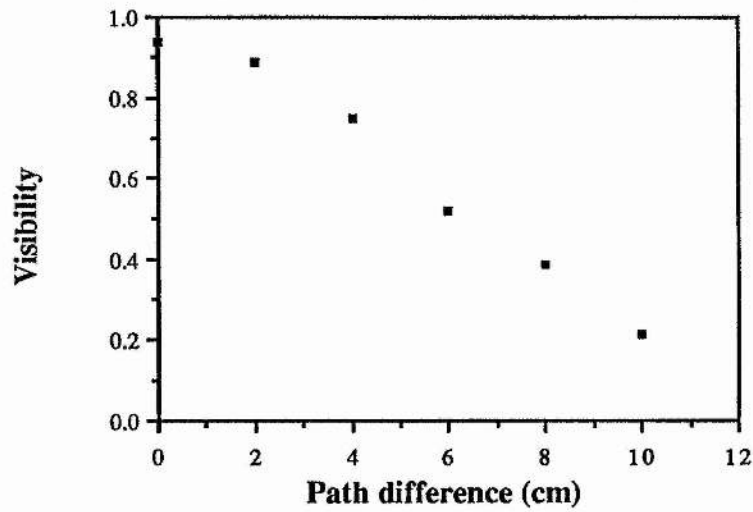
Figure 4.26

HeNe guided through 20m, 50/125μm fibre.
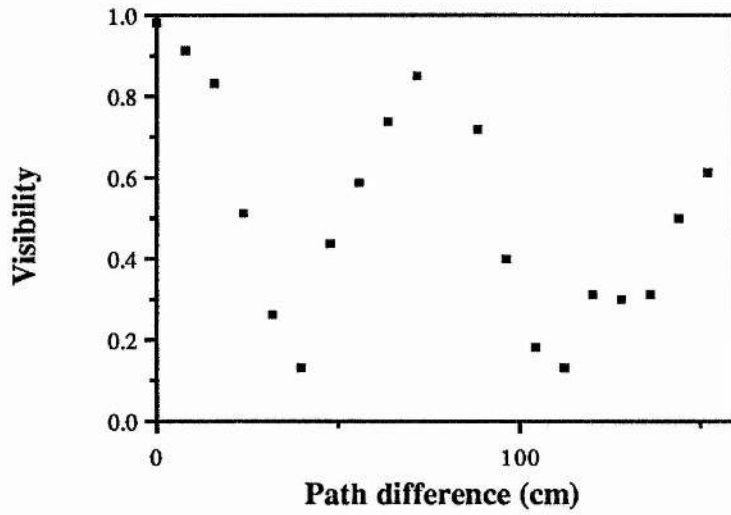
Figure 4.27

HeCd guided through 20m, 50/125μm fibre.
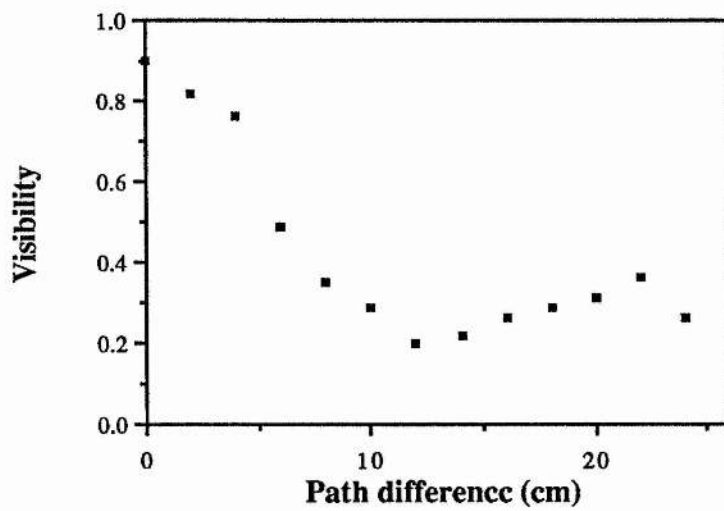
Figure 4.28

HeNe guided through 1m, 400 micron fibre.
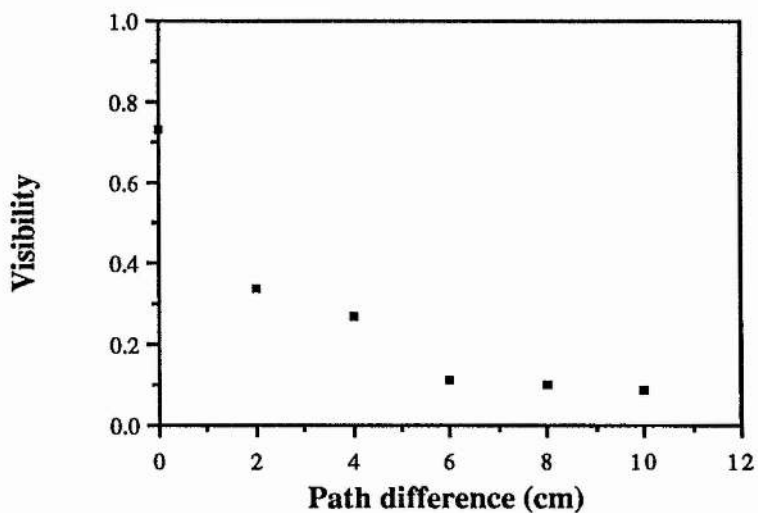
Figure 4.29a

HeNe guided through 1m, 970 micron fibre.
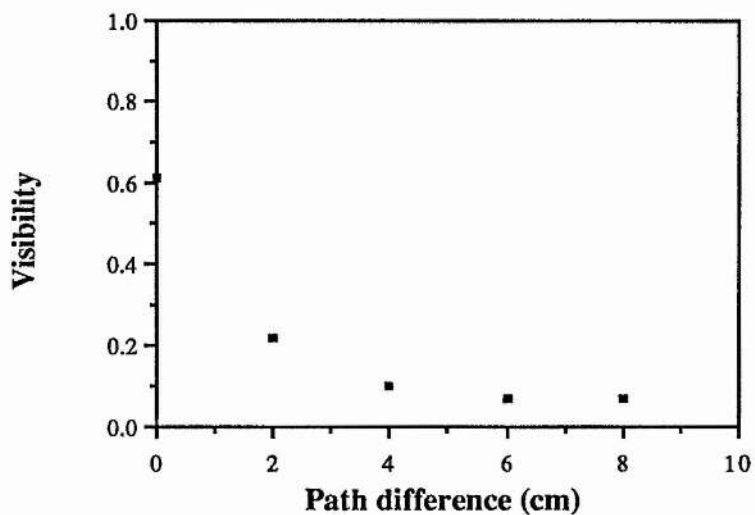
Figure 4.29b

Effect of detector size on Visibility.
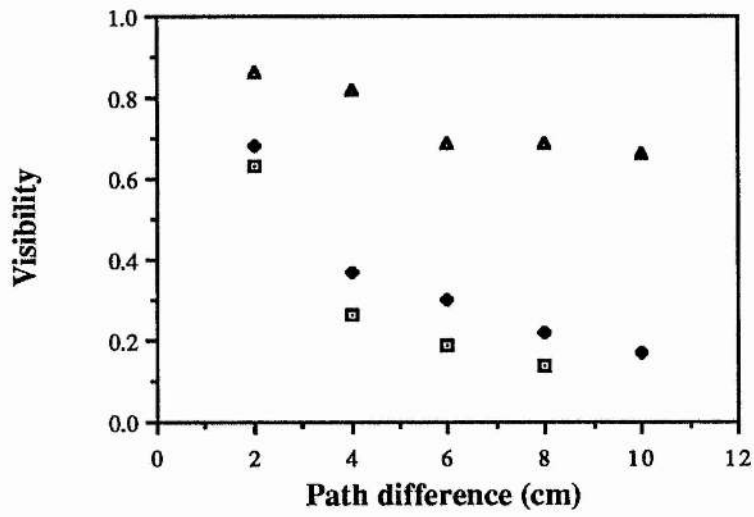
Figure 4.30

□ 1mm core
● 400micron
▲ 50micron

HeNe guided through 100m, 50/125μm Fibre.
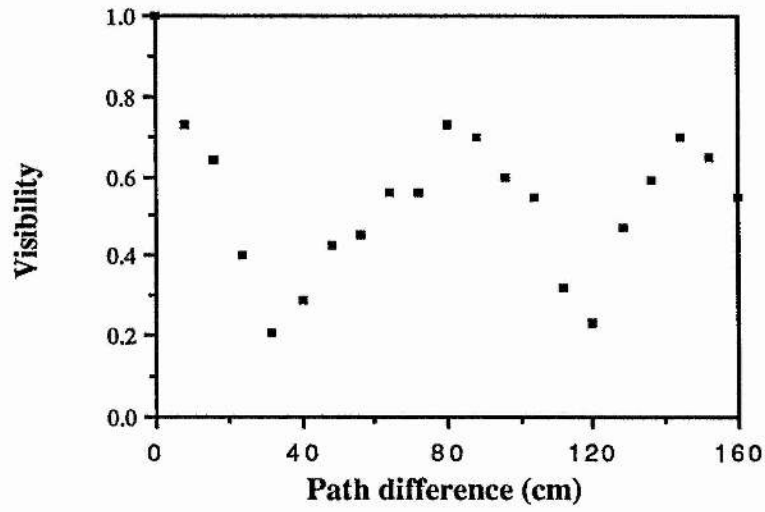
Figure 4.31

HeNe guided through 100m, 50/125μm Fibre
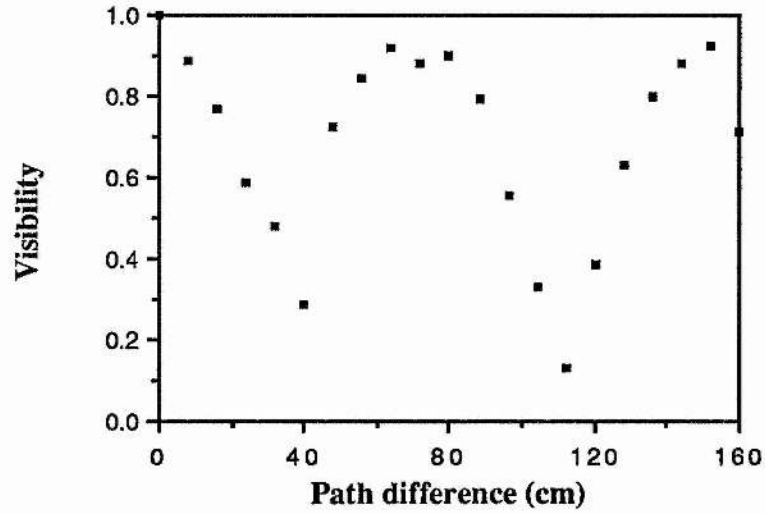
Figure 4.32

5 Experimental.

5.1 Fibre arrays.

Charge-coupled devices (ccds) and photodiode arrays are square-law detectors which can convert intensity information from the spatial to temporal domain.The output from a one-dimensional (1D) array, may be viewed on an oscilloscope and the output from a two-dimensional (2D) array, may be viewed on a video monitor. The elements of the image usually have the same spatial or temporal relationship as the elements of the object. If an image is to be reconstructed where the elements have a more complicated relationship then sophisticated electronic signal processing must be carried out. Optical fibres can sample images and encode them with comparative ease. For example, the conversion of a one-dimensional spatially varying signal to a temporal signal was carried out in section 4.6 by scanning a slit across an array and measuring the transmitted light using a single photodetector.

A scene, imaged onto a two dimensional fibre array, may be reconstructed at a second plane. This image may be magnified or reduced over the length of the fibre bundle by altering the separation of the fibres in the output plane, although the total number of resolvable points is fixed. Alternatively, the scene may be reconstructed in two different planes by the use of interleaved fibres which reduces the resolution or by the use of fibre couplers which reduces the intensity. Optical fibre detector arrays can be produced which convert one geometry in the image plane to a second geometry in another plane where square-law detection or further signal

processing can be carried out. An example of this is the transformation of a 2D image to a 1D image.

The above examples show the ease with which optical fibre arrays can manipulate information based on intensity, but optical fibre arrays can also be employed in signal processing using the complex amplitude of the light.

Light which is coupled into an optical fibre from a scene retains many of the characteristics of the light present at the entrance to the fibre. These characteristics are normally lost when square-law detection occurs. Most importantly, information about the spectrum and coherence of the light is retained. If 'polarisation maintaining' fibre is used then information about the polarisation of radiation in a scene may also be retained. The light in a 1D or 2D array of optical fibres may be used to process the light from a scene in many ways, for example, the spectrum at different points in the scene may be obtained from different fibres. Alternatively, the light in particular fibres and, therefore, at particular points in the scene, may be correlated with one another.

5.1.1 Correlation of interference fringes with a 1D fibre array.

An optical correlator is a system which correlates two 2D functions, say a signal and reference, by an optical method, figure 5.1. The system performs the correlation by Fourier transforming the functions, multiplying them together, and then taking the inverse Fourier transform of this product. The Fourier transform of the reference function is recorded as a function of phase and amplitude on photographic film or on a spatial light modulator and is placed in the back focal plane of the lens. The signal is introduced to the system as phase and amplitude variations across a spatially coherent source and its Fourier transform is obtained in the back focal plane of the lens. The product of the two Fourier transformed functions is itself Fourier transformed by a second lens and the correlation appears at its output. A maximum of intensity is obtained at the output when the mask is the exact complex conjugate of the Fourier transform of the input to the correlator.

We demonstrated the possibility of correlating an optical signal with a fibre array when an interference pattern was correlated with a linear fibre array. The experiment was set up as shown in figure 5.2. A linear interference pattern on a background of speckle was produced by a HeNe laser coupled into two, 1m long, 50/125μm, multimode optical fibres with their ends placed side by side. The fibres were positioned 0.26 mm apart. One of the fibres was phase modulated by a piezoelectric cylinder so that the interference pattern appeared to scan. The linear optical fibre array consisted of twelve, 970 μm, fibres. The transmission function of the array was determined by combining the outputs from given fibres onto a single

124

detector. In this case, the output from particular fibres was combined so that the transmission function of the array approximated to a square wave. When the interference pattern was scanned across the array, the detector measured a signal whose frequency was proportional to the frequency of phase modulation. The modulation depth was a measure of the degree of correlation of the linear interference fringes with the fibre array.

The maximum signal modulation was obtained with the fibre array at a distance of 81cm from the two sources. This distance corresponds to the fringes having a spatial frequency of 2mm which is approximately that of the array. Figure 5.3 shows the correlation signal and the triangle wave used to drive the phase modulator. A second correlation signal was obtained with the fibre array a distance of 160cm from the sources. This corresponds to fringes of half the spatial frequency of the array. The modulation depth was about half that obtained previously but of the same frequency.

5.1.2 Correlation of radiation across a scene.

If light from a scene is imaged onto a 2D fibre array then the mutual coherence of light coupled into any two fibres can be measured. This measurement is made by allowing the light emitted from those fibres to interfere, and measuring the visibility of the interference fringes produced.

An experiment was carried out to show the ability of optical fibres to correlate light from different points in a scene with each another. A scene, illuminated by light from red and green HeNe lasers, was imaged onto a 3 by 3 optical fibre array. The fibres in the array were 400µm diameter core, plastic fibre, 50 cm in length. The central fibre

of the array was taken as the reference fibre, and the light emitted from it was allowed to interfere with the light emitted from each of the other fibres in turn, including the auto-correlation of the reference fibre using a zero path difference Michelson interferometer, figure 5.4. Interference fringes, if formed, were viewed by a ccd camera and monitor. A photodetector placed at the centre of the interference pattern measured the fringe visibility. A graph of fringe visibility against fibre position was plotted, figure 5.5. Red or green filters placed in front of the array enabled the source responsible for the interference to be determined.

5.1.3 Measurement of path difference across a scene.

A spatially coherent plane wave, passing through an optical system, may not emerge planar but may be distorted by asymmetry. This can introduce coherent noise and cause degradation of any image the system may form. Optical correlations between different points in the image can be used to obtain information about path differences, and hence asymmetry, in the optical system. Alternatively, if a scene, illuminated by spatially coherent light, is imaged by an optical system, correlations between different points in the image can be used to obtain information about the path differences in the remote scene.

An experiment was performed which demonstrated the ability of an optical fibre array to help measure the path differences across an optical system illuminated by spatially coherent light. The experimental arrangement was as shown in figure 5.6. The optical system consisted of three beamsplitters and a mirror which, when illuminated by an expanded HeNe laser, produced four parallel

collimated beams. The beams were made to be of equal intensity using neutral density filters and the path difference between adjacent beams was around 8cm. The beams were coupled into a linear array of four optical fibres. The fibres were 50/125 micron multimode and 1m in length. One of the fibres was defined as the reference fibre and the light emitted by it was phase modulated and allowed to interfere with the light emitted from each of the other fibres in turn, including itself. The visibility of the interference fringes produced was determined and plotted against position, figure 5.7. When this graph is compared with a graph of visibility against path difference for the source, figure 4.13, a path difference can be assigned to the light in each fibre relative to that in the reference fibre.

In the ideal case, an optical system would form an image of a laser enhanced scene. The image plane would be filled with optical fibres so path differences compared to a reference could be determined over the entire plane.

5.2 Scanning light over fibres.

Many electo-optic sensors include some method for scanning an image across a detector or detector array, for example, a 2D image may be scanned over a 1D detector array. Optical fibre arrays may be used in image planes so it is of interest to consider the scanning of light across an optical fibre.

5.2.1 Scanning a Fourier transform image over a single fibre.

Light from a scene containing a tungsten lamp and a HeNe (633nm) laser was combined on a diffraction grating. The two sources were of similar intensity at the grating. A lens placed beyond the grating

formed the diffraction pattern in its back focal plane via a scanning mirror, figure 5.8. The size of the plane was restricted so as to receive only the zero and first orders of the diffraction pattern. The mirror scanned the diffraction pattern across an optical fibre placed in the back focal plane of the lens. It may be considered that the zero order of the diffraction pattern reveals the spatial coherence of the source from the image spot size and the first order gives information about the bandwidth of the source from the dispersion of the grating. Scanning the light across the fibre convolves the diffraction pattern with the aperture of the fibre. The intensity of the light emitted by the optical fibre was measured by a photodetector and displayed on an oscilloscope. The signals due to the zero, and plus and minus one, orders of the diffraction pattern, scanned across a 970 μm core fibre, are shown in figure 5.9. In both first orders the figure shows the broad band signal of the white light and narrow peaks of the laser. In the zero order it shows the spatial convolution of the white light and HeNe spots with the fibre.

When the large core fibre was replaced by a 50/125 micron fibre the signal obtained was as shown in figure 5.10. The signal due to the laser in the plus and minus first orders is similar to figure 5.9, but the signal due to the white light shows a significant decrease in intensity due to the greater resolution of the smaller fibre core diameter. The diffraction pattern due to the broadband source can be regarded as being smeared out by the many wavelengths present and by the fact that it is spatially incoherent.

5.2.2 Scanning light over two fibres.

If plane wave illumination from a laser beam is incident on two optical fibres placed side by side and light is coupled into each fibre then they can produce a linear interference pattern on a screen (see section 4.1). Light from a HeNe laser was incident upon two 50/125 μm fibres via a scanning mirror. A detector whose size was much smaller than one fringe was placed at the screen, figure 5.11. The scanning mirror rotated the angle of the incident wavefront which caused a change in the phase difference between the two beams emitted by the two fibres and so the fringe pattern appeared to scan across the detector, figure 5.12. Only for small angles, of the order of milliradians, is the intensity at the detector unambiguously a function of the angle of the incident wavefront.

5.3 Spatial coherence sensors.

Discriminating between spatially coherent and incoherent sources may be achieved in several ways. The Young's slits interferometer described in section 4.1 relies on spatial coherence across the incident wavefront to produce interference fringes. A spatially coherent source will form a diffraction limited spot in the image plane of a lens, a spatially incoherent source will not. The experiment described in section 5.1.3 to measure path difference across a scene relies on spatial coherence so that fringe visibility depends solely on path difference. A sensor has been constructed which uses fibre arrays in the detector plane in order to distinguish between a spatially coherent source and an incoherent background. The geometry of the arrays may permit additional information about the spatially coherent source to be determined.

129

The sensors to be described rely on the Fourier transforming properties of a lens. Radiation from a scene containing white light and a laser source of similar intensity is incident on a reticle containing a one-dimensional grating. A lens placed behind the grating is used to produce the Fourier transform image (FTI) of the grating, figure 5.13. The FTI consists of sharp points due to the laser content of the scene and a diffuse spectrum due to the white light. The FT of a 1D grating is given in appendix D. The size of the FT plane is restricted to receive only the zero and first orders of the diffraction pattern. Rotation of the grating causes the FTI to rotate at the same angular frequency about its centre. Figure 5.14 shows four arrays of optical fibres placed normally to the optical axis at 90 degree intervals like the spokes of a wheel. The optical axis of the sensor is aligned with the centre of the scene. Each array guides light to a single photodetector. As the FT image passes over an array, a pulse due to the laser source is detected by an array's photodetector. Spatially incoherent white light does not form a sharp FTI therefore the background radiation produces low frequency modulation at the detector. Using the linear arrays of figure 5.14, the pulses detected by two of the photodetectors are as shown in figure 5.15.

If the spatially coherent signal does not lie on the optical axis of the sensor, then the centre of the FTI, O(x,y), is not formed on the optical axis and rotation of the FTI will not be symmetrical about the optical axis of the sensor. The first order of the FTI will describe an arc between each of the fibre arrays. By measuring the proportion of time spent in each quadrant, the position of the centre of the FTI, and hence the position of the source in the scene, may be determined, figure 5.16. The grating rotates with angular frequency ω and the

first order of the diffraction pattern rotates about O(x,y) with the same angular frequency at a radius r. The first order traces out an arc of length a $_n$ in sector n in a time, t $_n$. The length of the arc is given by

$$a_n = \omega\, r\, t_n. \qquad (5.3.1)$$

The angle subtended by each arc, α_n, in radians, is given by

$$\alpha_n = \frac{a_n}{r} = \omega\, t_n. \qquad (5.3.2)$$

The radius of the first order of the diffraction pattern, r, is obtained by substituting the equation for the Fourier transforming lens given by

$$Sin\, \theta = \frac{r}{f}, \qquad (5.3.3)$$

where f is the focal length of the lens and θ the angle between the zero and first order rays, into the equation for the first order of the diffraction pattern given by

$$\lambda = d\, Sin\, \theta, \qquad (5.3.4)$$

where λ is the wavelength of the spatially coherent source and d the period of the grating. Thus, we have

$$r = \frac{f\lambda}{d}. \qquad (5.3.5)$$

From triangle ABO we find that

$$x = r\, Cos\left(\frac{a_3 + a_4}{2}\right), \qquad (5.3.6)$$

and from triangle CDO we find that

131

$$y = r \cos \left(\frac{a_2 + a_3}{2} \right). \qquad (5.3.7)$$

The difference between the times spent in each quadrant of the detector plane can be used to produce an error signal which can be used to re-align the sensor so that the signal lies on the optical axis.

An input scene consisting of a white light source and a HeNe laser (633nm) was allowed to fall onto a diffraction grating. A lens was placed behind the grating. The lens produced the two dimensional Fourier transform image (FTI) of the grating in its back focal plane. The two dimensional FTI due to the spatially incoherent white light consisted of diffuse polychromatic regions. The two dimensional FTI due to the spatially coherent laser source consisted of discrete points. Rotating the grating caused the FTI to rotate at the same frequency. The HeNe laser was positioned at 8 points around the optical axis and its position was calculated at each from the separation of the pulses from the four photodiodes, as described. The results are plotted in figure 5.17.

The optical fibre arrays in the Fourier transform plane need not be linear. That is, the spokes in the detector plane may be curved. By using four curved arrays, figure 5.18, the same sensor as before may be used to obtain spectral information about a spatially coherent signal aligned on the optical axis in the presence of incoherent background radiation. As the grating rotates, the first order of the diffraction pattern moves on a circle whose radius, from equation (5.4.5) depends on the signal wavelength. As the optical fibre arrays are curved, the time at which a particular detector receives a pulse depends on the wavelength of the signal. If we consider a scene

containing two spatially coherent sources, say one red and one green, then the radius of the first order of the diffraction pattern due to the red signal is greater than that due to the green signal. Therefore, as the FTI rotates, there is a phase difference between the pulses received at the detectors for the red and green signals, although the temporal separation of the four red pulses at the four photodetectors is the same as for the four green pulses. The signal received by two photodiodes from two of the curved arrays when red and green sources are present is shown in figure 5.19. The times for which pulses from red, green, and blue sources are received relative to the green source are plotted in figure 5.20.

By using four arrays, two curved and two linear, figure 5.21, the spectral information may be encoded so that the wavelength of the signal affects the pulse separation. Again, we considering a scene containing red and green spatially coherent sources aligned on the optical axis. As the FTI rotates, say anticlockwise, about the optical axis, both sources produce a pulse at the same time in the linear arrays. However, the longer the wavelength the greater the radius of the first order so the pulse emitted from the curved arrays due to the red source occurs later than the pulse due to the green source. The signal detected by two photodiodes from 1 curved and one linear array when red and green sources are present is shown in figure 5.22. The delay between the pulses from the curved and linear arrays for red, green and blue sources is plotted in figure 5.23.

If the spatially coherent source is not aligned on the optical axis then the centre of the FTI is not formed on the optical axis and, as before, rotation of the FTI will not be symmetrical about the optical axis. By considering the geometry of the arrays, and by using the time delay

133

between pulses from the four arrays, it is possible to determine both the wavelength and position of the source simultaneously.

5.4   The spatial light modulator known as SIGHT-MOD.

Some of the pre-detector signal processing techniques described rely on rotating aperture or image plane reticles to produce modulation. For example, the spatial coherence sensors described in section 5.3 rely on a rotating grating to modulate a spatially coherent source. In many applications a device which had no moving parts and which could be programmed by computer would be preferred.

Many pre-detector signal processing techniques employ optical correlations or convolutions with two-dimensional phase and amplitude masks. A different mask is required for each correlation or convolution. For example, in section 5.1.1, an interference pattern was correlated with an optical fibre array. This technique would be more attractive if a single device could easily be tailored for many applications. A device known as a SIGHT-MOD can be used as a spatial light modulator, that is, it can be used to write information onto an optical beam or to perform spatial filtering in either the image or Fourier planes.

The SIGHT-MOD is a magneto-optic device manufactured by Semetex. The device consists of a two-dimensional array of 48 by 48 pixels. The pixels are 109 µm square and the pixel spacing, horizontally and vertically, is 127 µm. The Faraday effect is used to determine whether a pixel will rotate incident linearly polarised light clockwise or anti-clockwise in phase. The direction of Faraday rotation depends on the magnetic state of the pixel. The Faraday rotation of the plane of polarisation of light transmitted through a pixel can be converted into an amplitude or a phase effect by plane polarisers placed on each side of the array. For maximum contrast

135

between opposite pixel states the polarisers are rotated with respect to one another so that light transmitted by the first polariser and rotated by a pixel will be completely transmitted or stopped by the second polariser, figure 5.24a. If the SIGHT-MOD is to be used as a phased array, then the second polariser should be orientated at the same angle as the first so that opposite pixel states have a pi phase difference, figure 5.24b.

The magnetic state of each pixel is controlled by computer and each pixel may be individually addressed. Computer control allows any pattern, or series of patterns, to be written onto the array at any time. For our experiments, the SIGHT-MOD was connected to an Amstrad 1512HD computer via an IBM interface card.

5.7.1 Control of the SIGHT-MOD.

Changing a pixel from one magnetic state is a two stage process. When a pixel at co-ordinates x,y is addressed, the computer sends a current pulse along the x and y drive lines of the array. This partially flips the magnetic state. Application of an external magnetic field is required to send the pixel into its highest contrast state. This field is applied by a coil placed around the outside of the array. When a pattern is to be written onto the device the device is cleared, i.e. all the pixels are put into the same state. Then, all the pixels which are to have their state changed are addressed. Finally, the external magnetic field is applied to complete the process.

Each pixel is addressed via the interface board with segment address &HA000 (hex). The pixels are divided into 6 rows of 8 pixels, called a byte row, and 48 columns. One byte sent to the device addresses a vertical group of 8 pixels with one bit addressing one

pixel. A 0 corresponds to one state and a 1 corresponds to the other. A byte can be sent to the device from a BASIC program by the command POKE address,byte. Any byte sent to address 2048 will ERASE all pixels and any byte sent to address 2049 will produce a PRINT pulse completing the writing process.

5.7.2 The SIGHT-MOD as a fibre optic switch.

The SIGHT-MOD was investigated for use as a fibre optic switch. In the first experiment, light from a HeNe (633nm) laser was coupled into a large core, 970 µm, fibre. Light emitted from the fibre was collimated and passed through the SIGHT-MOD. The transmitted light was focused into a second large core fibre and the intensity of the light emitted from the second fibre was measured by a photodetector, figure 5.25. The device was cleared of data and the linear polarisers were adjusted for minimum transmitted light, or maximum contrast. The pixels were then switched sequentially, in the manner of a raster scan. The detected intensity was seen to rise uniformly to a maximum value which jumped to its highest value when the PRINT command was received. The difference in intensity between the opaque and transmitting states was measured to be greater than 6dB, figure 5.26. The experiment was repeated sending a PRINT pulse after addressing each pixel. The result was a uniform increase in intensity without the jump to the maximum value achieved previously, figure 5.27.

A second experiment was carried out to examine the possibility of using the SIGHT-MOD as a switch for an array of optical fibres. Collimated light from the HeNe laser (633nm) was incident over the entire device. The device was cleared and the polarisers adjusted for

137

minimum transmission. A single large core, 970 μm, optical fibre was placed at the output with no coupling lenses, figure 5.28. The pixels were switched by a raster scan and the intensity of the light emitted from the fibre was measured by a photodetector. When viewed on an oscilloscope, the detector signal was seen to climb in a number of steps. This is as expected because the light collected by the fibre depends upon fewer pixels than when a lens was employed. When the PRINT pulse was received by the array, the intensity jumped to a maximum, figure 5.29. The large core fibre was replaced by a fibre with a core diameter of 50 μm. The device was switched as before and the transmitted intensity was measured. This time only two steps in intensity were seen before the PRINT pulse was received, figure 5.30.

5.7.3 Contrast of SIGHT-MOD.

When a SIGHT-MOD is used to write information onto a beam of light it is important to have high contrast between the transmitting and non-transmitting pixels. A graph of Faraday rotation and absorption against wavelength is given in figure 5.31. This shows that the device will be at its least efficient in the red region of the visible spectrum.

The SIGHT-MOD was illuminated by collimated light from a 5mW HeNe laser (633nm). A grating with a periodicity of 2 columns was written onto the device. An image of the grating was obtained on a ccd camera. A video line selector allowed any one line of the video signal to be displayed on an oscilloscope, figure 5.32. A photograph of the oscilloscope trace is given in figure 5.33. The contrast or

extinction ratio was around 6dB, the same as the value obtained for the fibre optic switch.

The SIGHT-MOD was then illuminated by collimated light from a 15mW HeCd laser operating at 442nm. According to figure 5.31 this wavelength is below the minimum useful wavelength for the device. Semetex give 480 nm as an assymptote for the absorption curve. It was found that practically no light was transmitted even when the polarisation state of the device was fully transmitting. Detection of the transmitted pattern was not possible using the ccd camera because its wavelength sensitivity peaks in the infra-red and falls off rapidly beyond the green. At wavelengths where the absorption is very high care must be taken not to overheat the SIGHT-MOD.

When comparing the effects of absorption and Faraday rotation, a compromise must be reached where the Faraday rotation is sufficient for good contrast between the on/off states of the pixels but the absorption does not require the use of several watts of incident power and extra cooling for the device. The ideal wavelength for the device is in the green region of the spectrum so we chose to use a 0.5mW HeNe laser operating at 543nm known as a GreNe.

The SIGHT-MOD was illuminated with collimated light from the GreNe and a grating with an 8 column periodicity was written on to it. An image of the grating was obtained on a ccd camera and a video line selector allowed a single line to be displayed on an oscilloscope. A photograph of the oscilloscope trace is shown in figure 5.34. The contrast between the on and off states is greater than 10dB. The trace shows it can be seen that the transmitted intensities are not quite

equal. This was probably due to structure in the illuminating GreNe beam.

5.7.4 Fourier transforms of gratings produced by the SIGHT-MOD.

The previous experiments showed that the SIGHT-MOD could achieve extinction ratios of greater than 10dB using a GreNe laser (543nm). It was decided to look at the diffraction patterns produced by these gratings. The experimental arrangement to detect the diffraction patterns was the same as in figure 5.32. The distances shown as u and v were both made equal to the focal length of the lens (30cm). The diffraction pattern is then equal to the spatial Fourier Transform (FT) of the grating function. The FT of the SIGHT-MOD when it was clear of data and fully transmitting was obtained. As the SIGHT-MOD consists of a 2 dimensional array of pixels, its FT is that of a 2 dimensional grating. A video line selector was built which allowed any video line from the ccd camera to be displayed on an oscilloscope. A video line was chosen which corresponds to the x axis of the optical system. Any point on the x axis corresponds only to a spatial frequency in the x direction. The spatial frequency is proportional to the distance from the origin. The spatial frequencies in the x direction of the device are shown in figure 5.35.

Gratings were the written onto the SIGHT-MOD. These gratings had a periodicity of 2, 4, 6 and 8 pixel columns. Their FT patterns were obtained and the spatial frequencies in the x direction for each grating are shown in figures 5.36 to 5.39. The spatial frequencies of the gratings are clearly seen but the 2D FT of any pattern written onto the SIGHT-MOD will also include the 2D FT of the array.

5.7.5 Manipulation of Fourier transform images using a fibre array.

A 2D optical fibre array was used to perform spatial transforms of Fourier Transform Images (FTIs). The FTIs were produced from a pattern on a Spatial Light Modulator (SLM). The SLM was the Semetex SIGHT-MOD.

A 2D to 1D fibre array was used to transform the 2D FTI to a 1D image and a 2D to a point array was correlated with the FTI of a pattern on the SIGHT-MOD. The SIGHT-MOD was illuminated by a collimated beam from a HeNe (633nm) laser. A 1m focal length lens placed beyond the SIGHT-MOD produced the FTI of the device in its back focal plane. An optical fibre array, consisting of 40, 1m long, large core fibres (970µm) arranged in a two dimensional 10 by 4 array, was constructed by mounting the ends of the fibres in epoxy resin. The other ends of the fibres were formed into a one dimensional array with a random relationship between the position in the 2D array and the position in the 1D array. Thus, any image on the face of the 2D array was converted to a 1D image. The 2D array was placed in the FT plane of the lens, figure 5.40. The intensity across the 1D array was measured using a linear ccd array connected to an oscilloscope. A sequence of patterns was written, in turn, onto the SIGHT-MOD. As the pattern changed the FTI changed and this was detected as a change in the 1D image detected by the ccd array. The intensity detected by the ccd array for two patterns is shown in figures 5.41 and 5.42. The position of each fibre in the 1D array could have been used to encode information about the spatial frequency content of the FTI, such as the spatial frequency in the FTI plane increasing from left to right in the 1D array.

The Fourier transform of one pattern was to be correlated with the 2D fibre array. Fibres from the 10 by 4 array, in positions corresponding to the FTI of the pattern, were selected and positioned in front of a single, large area, photodetector connected to an oscilloscope. This is similar to placing a mask in the FTI plane whose transmittance is either zero or unity and varies across the mask. A sequence of 10 patterns were written onto the SIGHT-MOD and the correlation of the FTI of each pattern with the chosen fibres in the 2D array measured by the intensity of light detected by the photodetector. Figure 5.43 shows the correlation of the FTI of each pattern with the fibres. A peak is seen corresponding to the pattern for which the fibre mask was designed. Smaller signals are present where partial correlations have occurred or where the resolution of the fibres in the array was not sufficient to discriminate against slightly different spatial frequencies.

5.7.6 Correlation of linear interference fringes with gratings on the SIGHT-MOD.

Linear interference fringes were produced by shearing a Mach-Zehnder interferometer illuminated by a collimated beam from a chopped 0.5mW GreNe (543nm). The interferometer had close to zero path difference. The SIGHT-MOD was placed at the output of the interferometer. One arm of the interferometer was phase modulated by a rotating glass slide. This caused the interference fringes to appear to scan across the SIGHT-MOD. Any light transmitted through the SIGHT-MOD was focused into a large core optical fibre placed on the optical axis and the intensity of the light was measured by a photomultiplier tube. Any correlation between the fringes and the SIGHT-MOD would be seen as modulation of the transmitted

142

light in the manner of Moire fringes, figure 5.44. The spacing of the interference fringes was calculated by expanding the second output from the interferometer. The SIGHT-MOD was cleared of data and made to be fully transmitting. The size of the interference fringes was adjusted until modulation was detected. Two correlations were obtained. The first corresponded to the spacing between pixels and the second to the pixel size. Gratings were now written onto the SIGHT-MOD. They had spatial periodicities of 2, 4, 6 and 8 columns. Correlations were obtained with linear interference fringes which were found to closely match the spatial periodicity of the gratings. The signal obtained when fringes were correlated with a grating which had a periodicity of 2 columns is shown in figure 5.45. The square wave is due to the chopped laser beam. The calculated sizes of the linear interference fringes when correlation occurred and the actual periodicity of the SIGHT-MOD are given in the following table.

Grating period (columns)	Grating period (micron)	Measured fringe period (micron)
0	0	56
0	0	260
2	254	246
4	508	504
4	509	162
6	762	738
8	1016	1054

A second method of producing linear interference fringes is to couple light into two optical fibres with their ends placed side by side as described previously in section 4.1. Fringes were produced with the centres of the two fibres 260µm apart and correlated with gratings on the SIGHT-MOD, figure 5.46. The source was a chopped GreNe as before. The fibres were 50/125 micron fibres and each 1m long. One fibre was phase modulated by a piezoelectric material which causes the fringes to appear to scan. The size of the fringes is proportional to the distance between the fibres and the SIGHT-MOD. The result of this is that as the fibres are moved closer to, or further from, the device correlation occurs with fringes of a different size. The light transmitted through the device was focused into an optical fibre placed on the optical axis and its intensity measured by a photomultiplier as before. A grating with a periodicity of 4 columns was written onto the SIGHT-MOD. The distance between the SIGHT-MOD and the fibre interferometer was adjusted until correlation occurred. This corresponded to fringes with a periodicity of 508µm, figure 5-47.

The distance between the SIGHT-MOD and the fibre interferometer was then kept constant and the periodicity of the grating written onto the SIGHT-MOD was increased. No correlation was seen until the grating periodicity was 12 columns, when a much reduced signal was detected. The grating size was further increased and when the grating periodicity was 20 columns a third correlation signal of very small amplitude was detected. These signals correspond to correlations of the grating with 3 and 5 times the fundamental spatial frequency of the interference fringes.
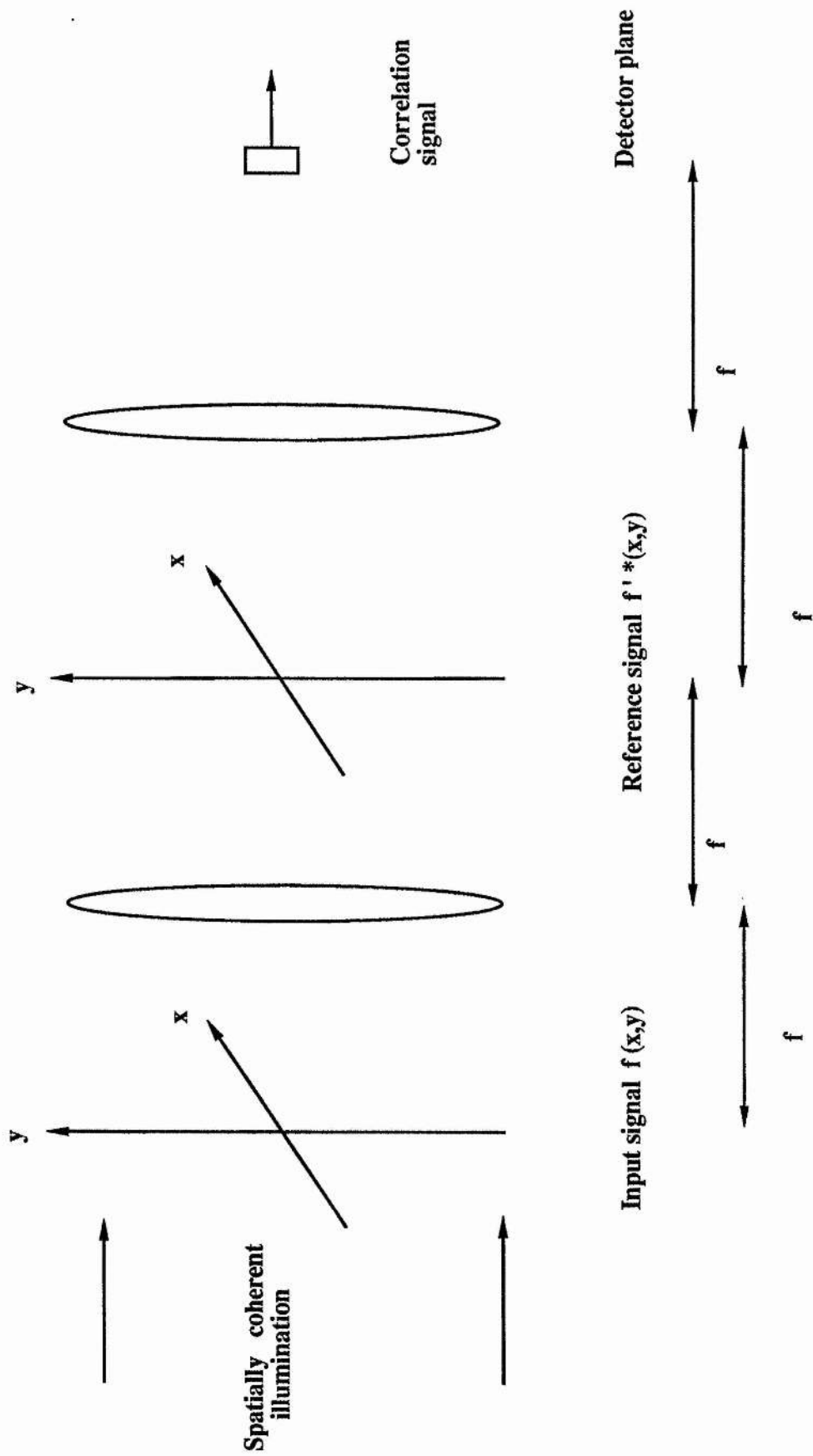
Figure 5.1 An optical correlator.

Source

Optical fibre

Piezoelectric cylinder

Optical fibre

Linear fibre array

Detector

Output to oscilloscope
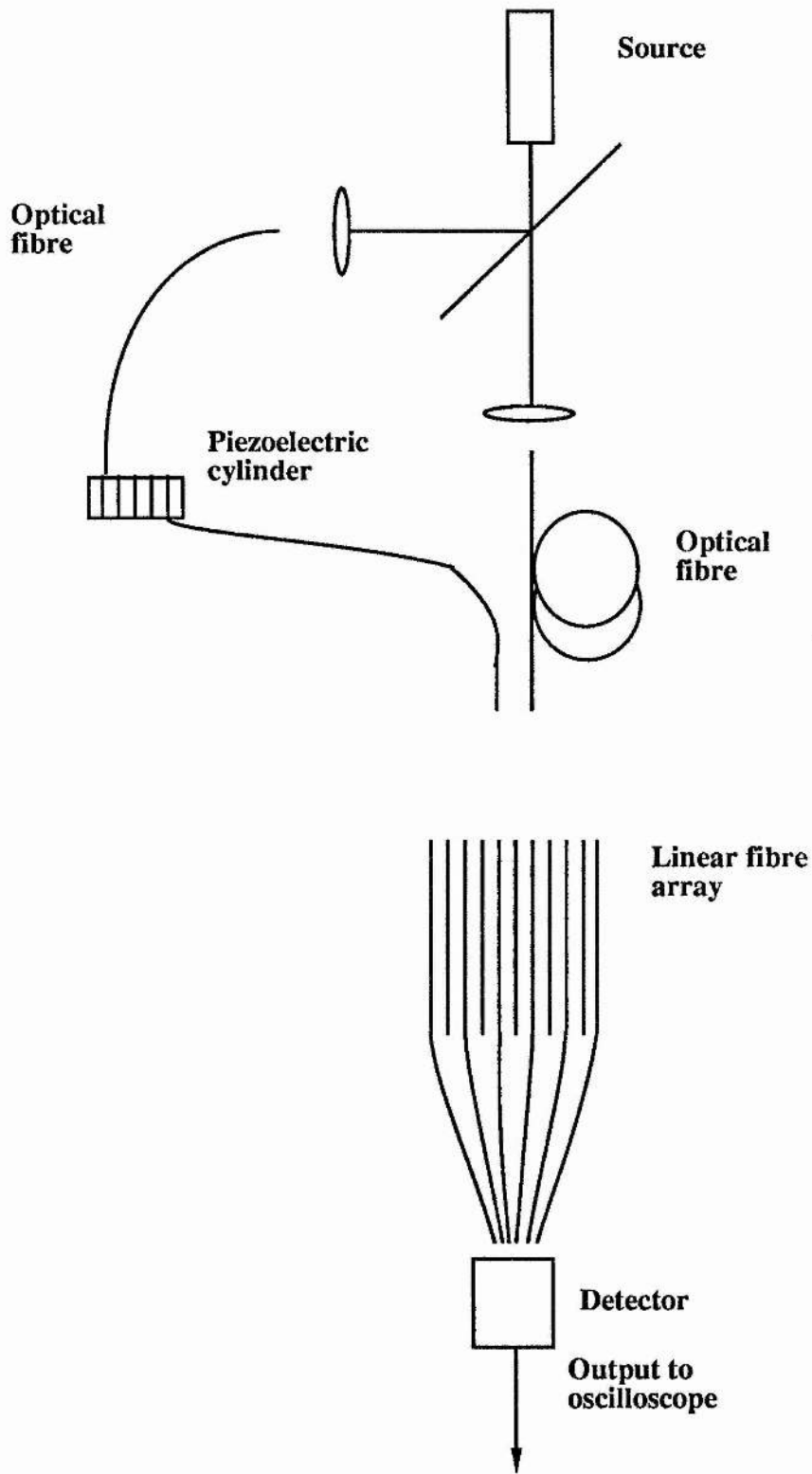
Figure 5.2 Correlation of fringe pattern with linear fibre array.
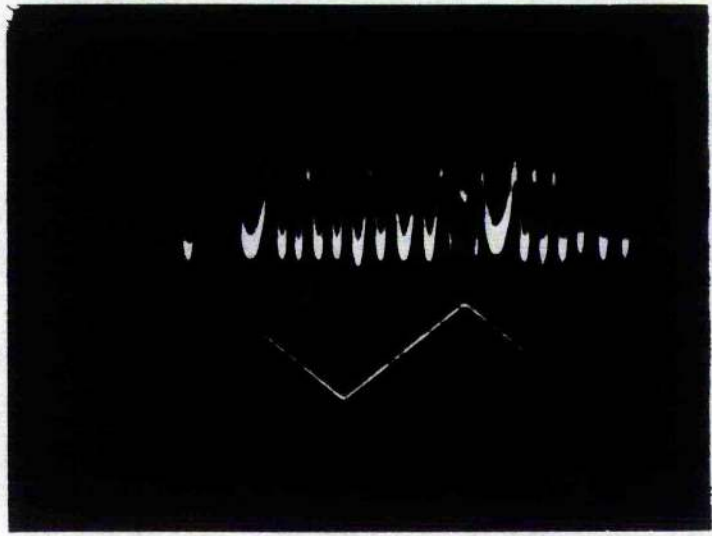
Figure 5.3 (a) Correlation signal between interference fringes and fibre array

(b) Piezoelectric driving signal

3 by 3 array of equal
length, multimode, fibres

Beamsplitter

Output

Image plane

Scene illuminated by
red and green lasers
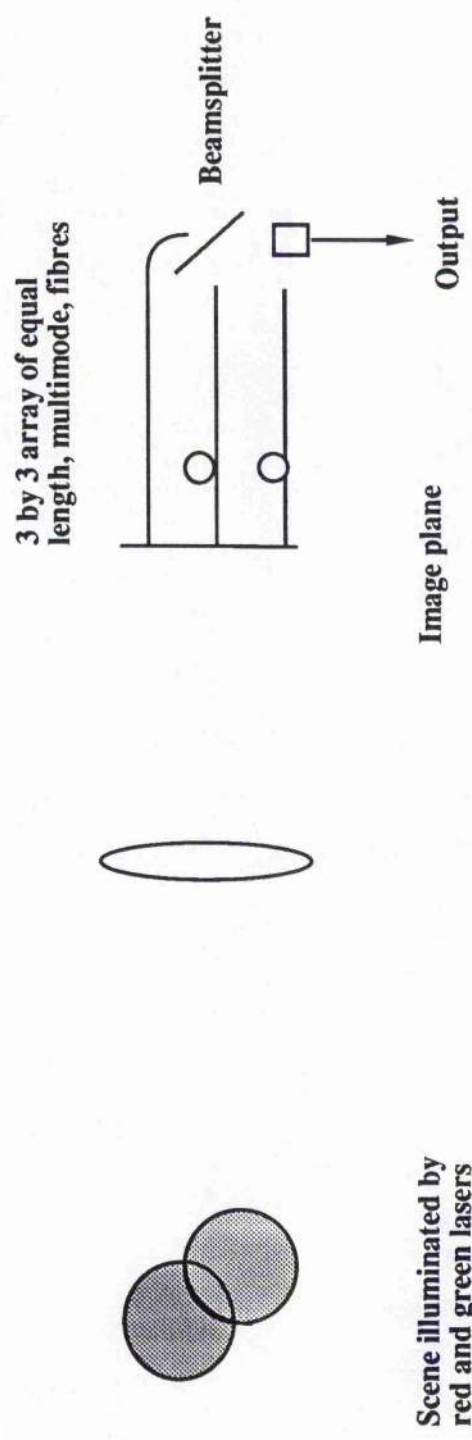
Figure 5.4   Correlation of radiation over a 2D scene.

Visibility across top row
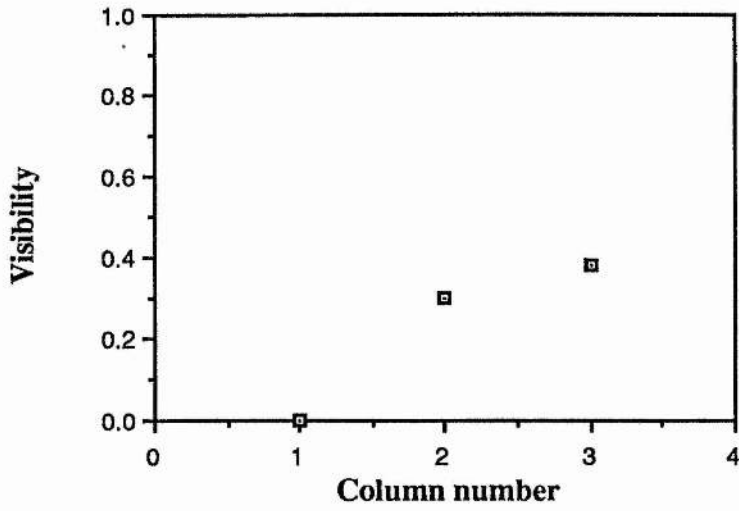
Figure 5.5a

Visibility across middle row
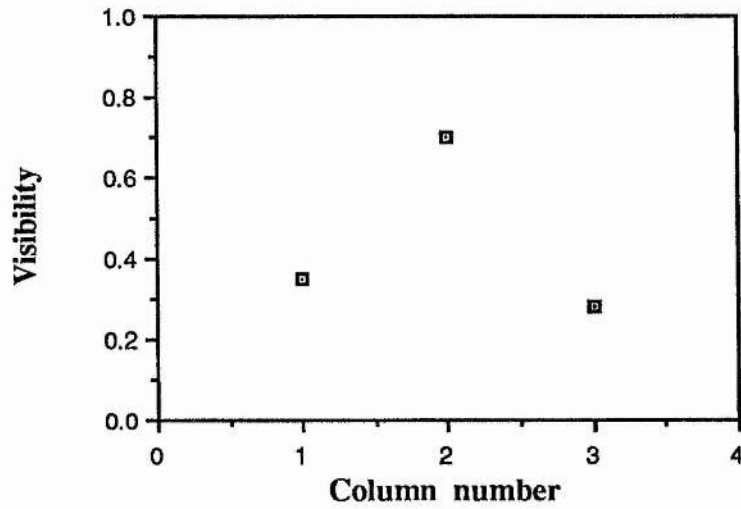
Figure 5.5b

Visibility across bottom row

Figure 5.5c

Source

Glass beamsplitters and mirror

Coupling lenses

1D array of equal length fibres

Beamspitter

Detector
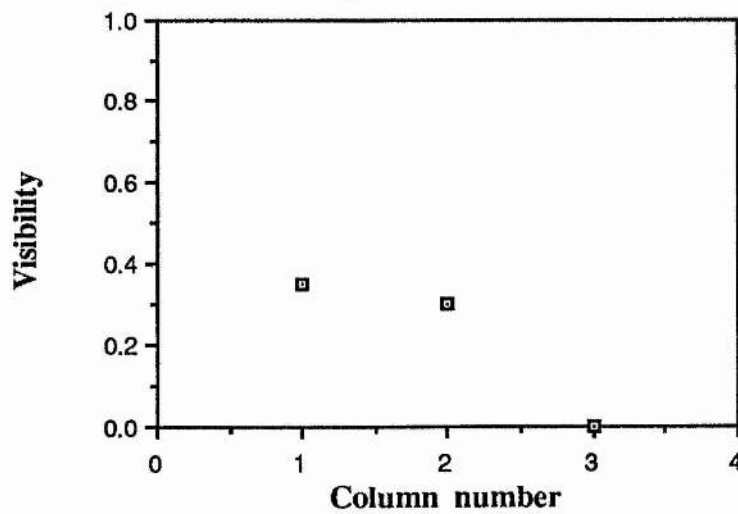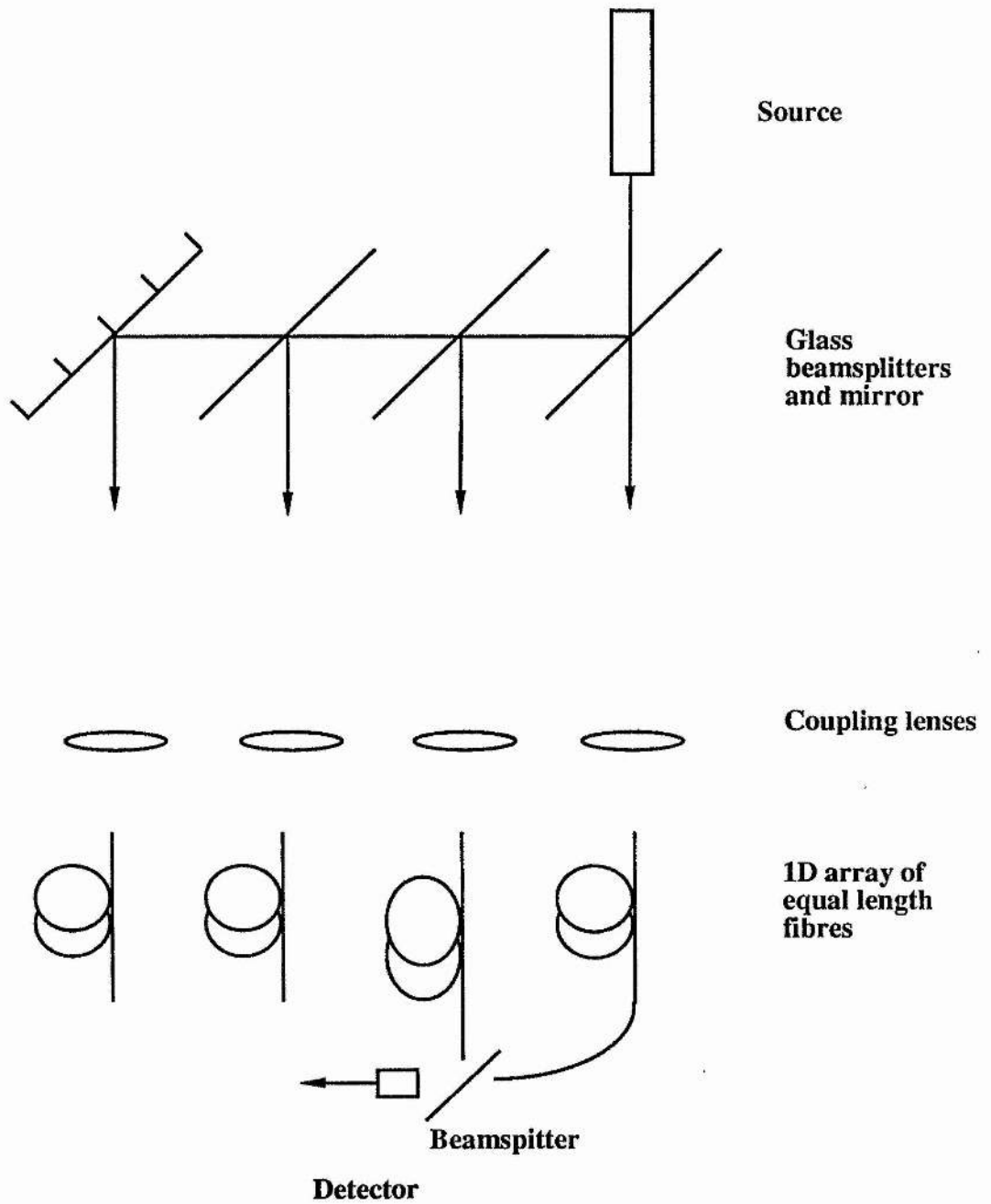
Figure 5.6   Measurement of visibility across a scene using a 1D fibre array

Visibility across 1D fibre array.

Visibility

Fibre position / path difference (cm)
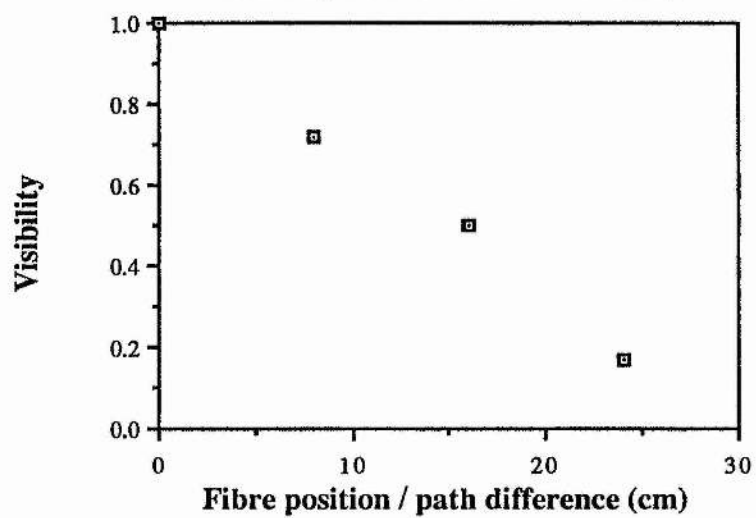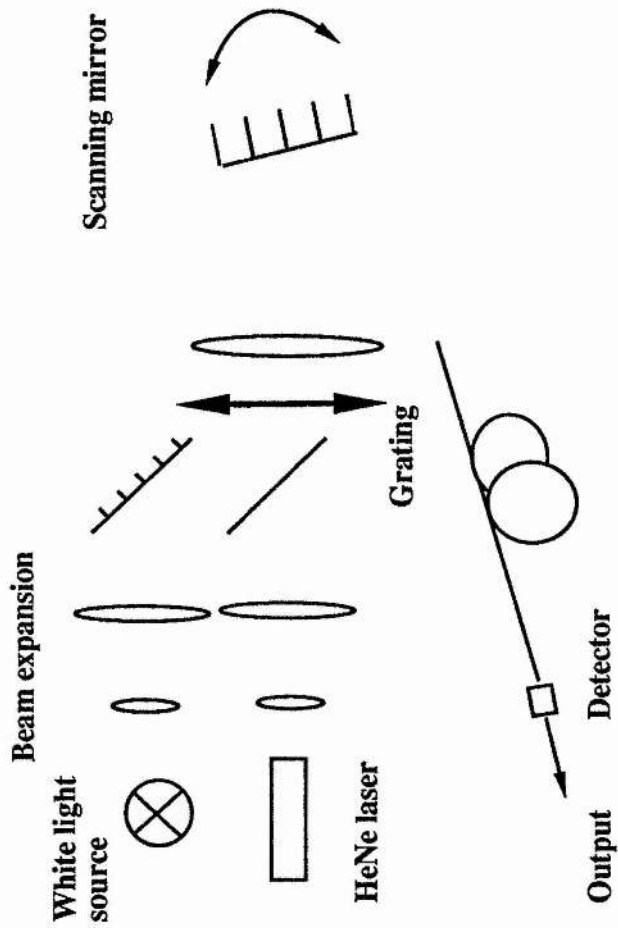
Figure 5.7

Figure 5.8 Scanning radiation across one optical fibre
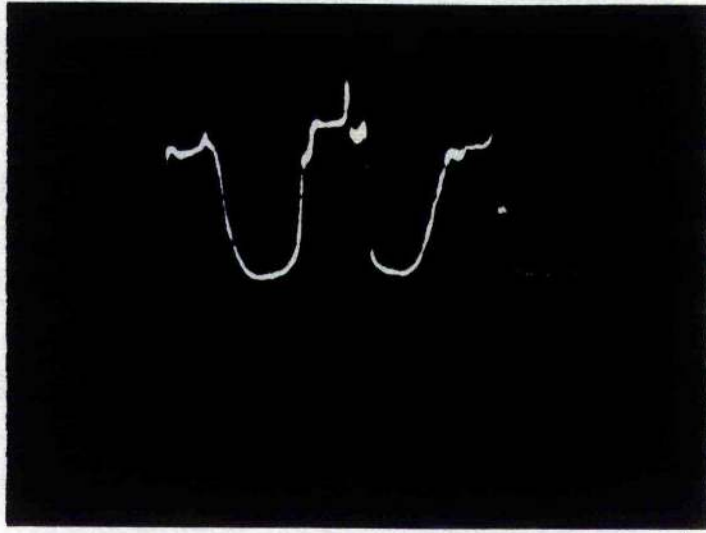
Figure 5.9 Signal due to Fourier transform image scanned across 970μm fibre
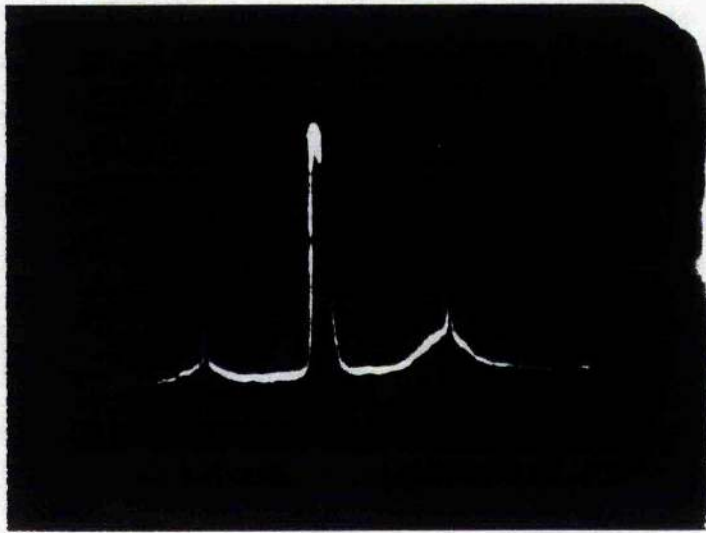
Figure 5.10 Signal due to Fourier transform image scanned across 50/125μm fibre

Scanning mirror

HeNe laser   Beam expansion

Two 50/125
optical fibres

Detector

Output
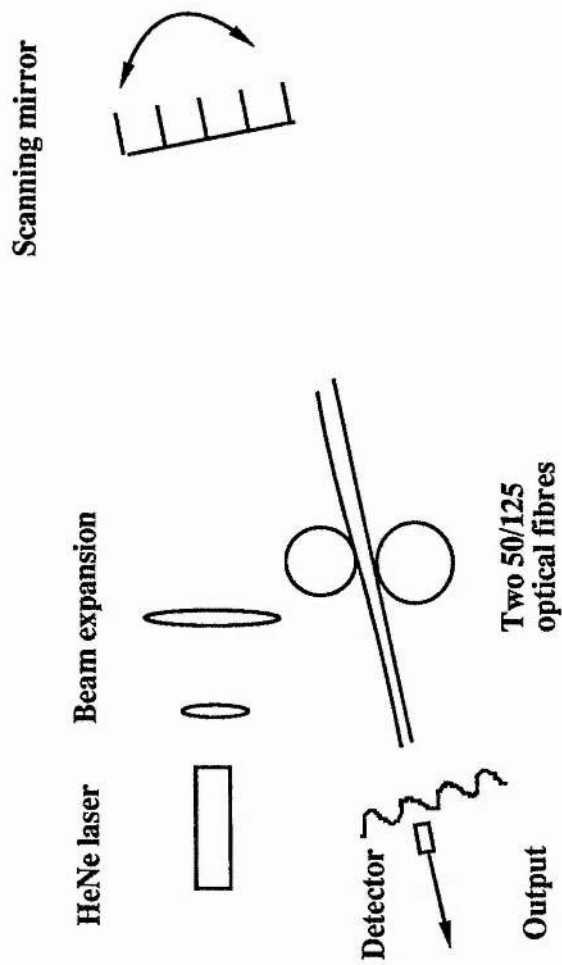
Figure 5.11 Scanning radiation across two optical fibres
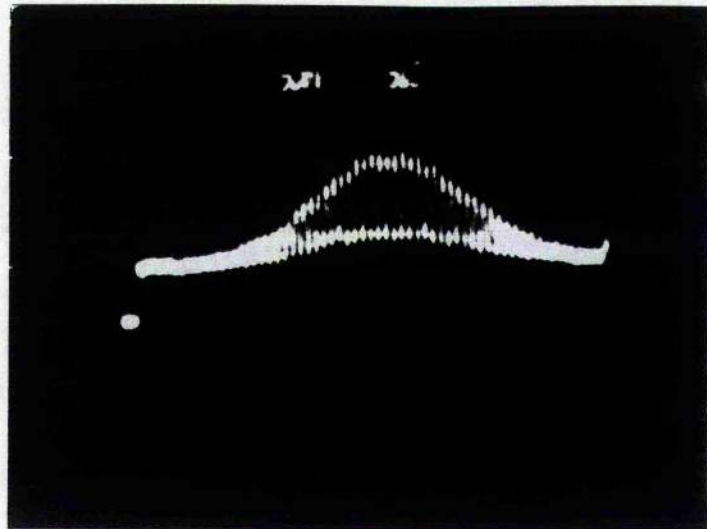
Figure 5.12 Interference obtained at a point on a screen when the angle
of incidence of a plane wave was rotated with respect to two
optical fibres used to produce fringes

Output 1
Output 2
Output 3
Output 4

Fourier transform
image plane
containing fibre
arrays

f

Diffraction
grating

Lens

Telescope
arrangement

Input scene consisting
of white light and
laser source.
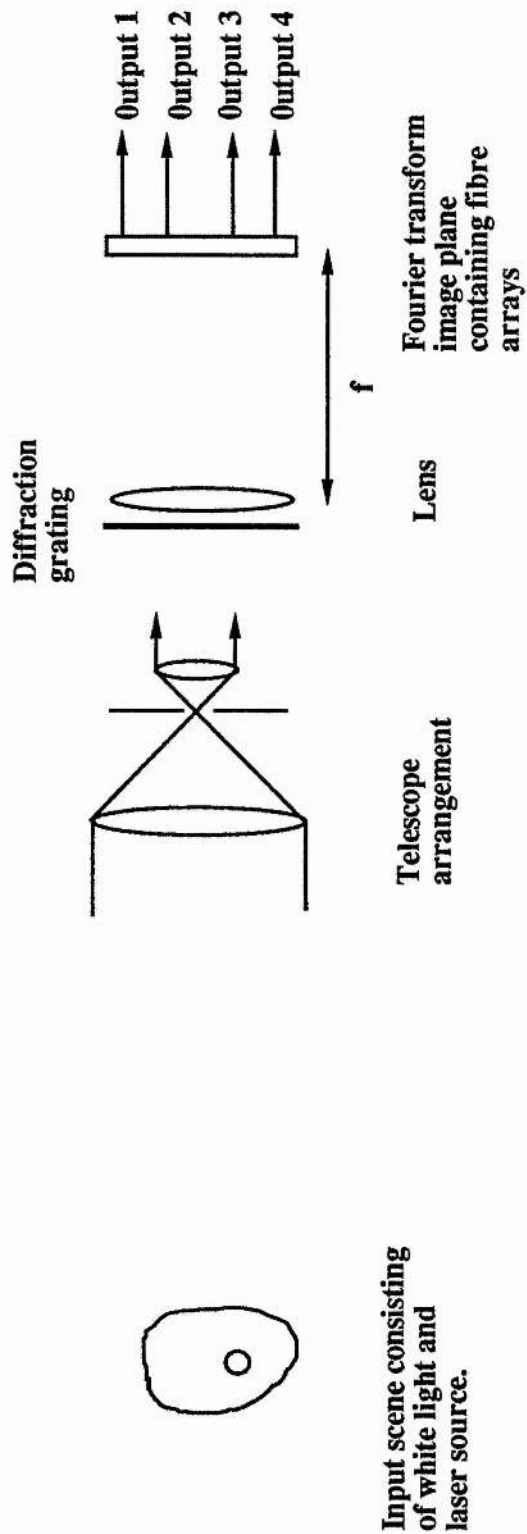
Figure 5.13. Optical Transform Image Modulation. Spatial coherence sensor.

Relative positions of the four fibre arrays placed in the Fourier plane.
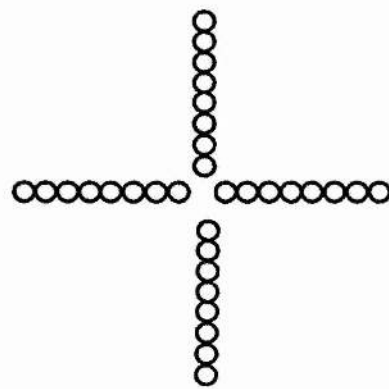
Figure 5.14 Four linear arrays
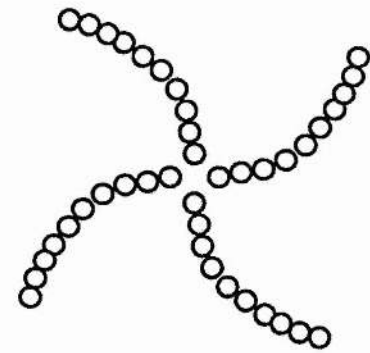
Figure 5.18. Four curved arrays
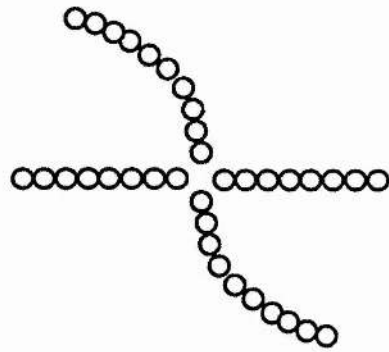
Figure 5.21. Two linear, two curved arrays
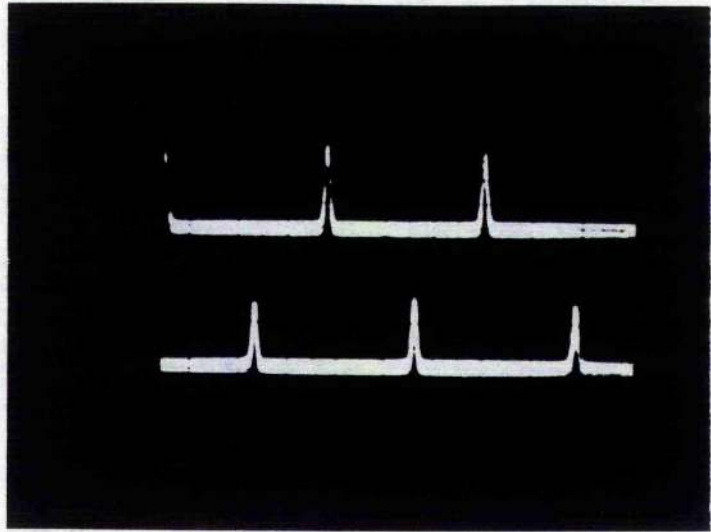
Figure 5.15 Pulses obtained from two linear arrays in the Fourier transform image plane of a spatial coherence sensor
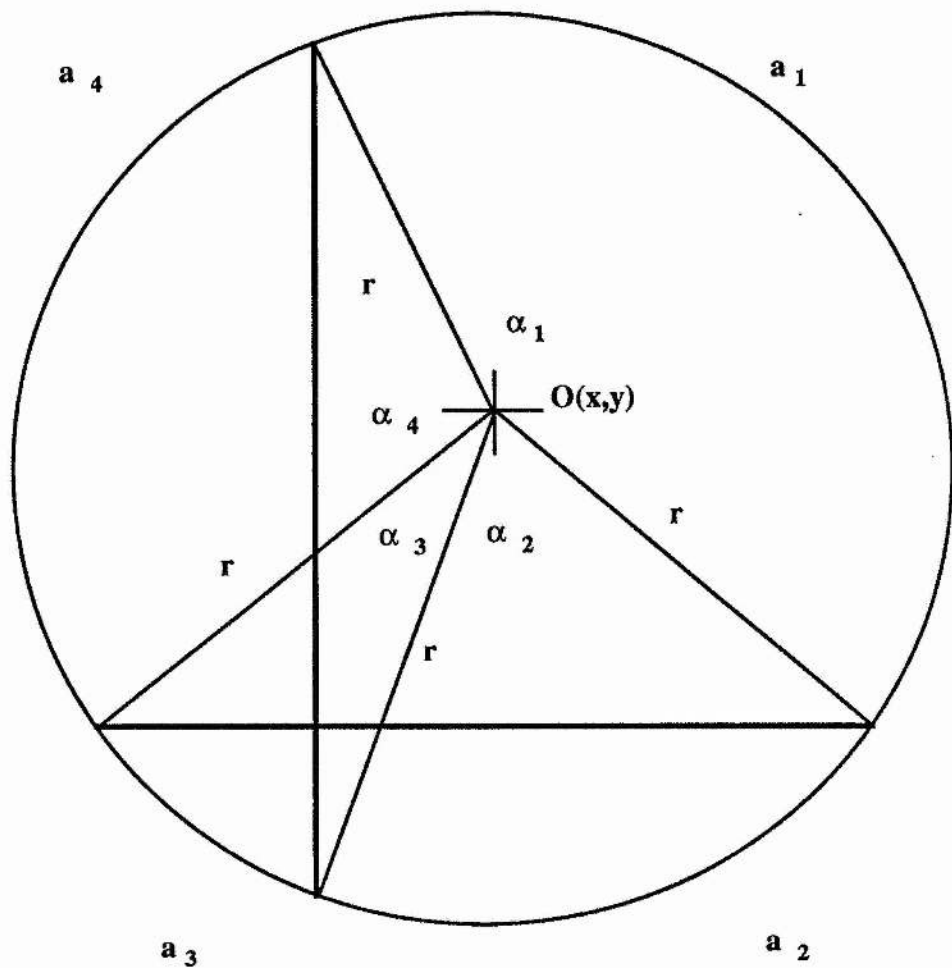
Figure 5.16 Geometry for position sensor

Position sensor with four linear arrays
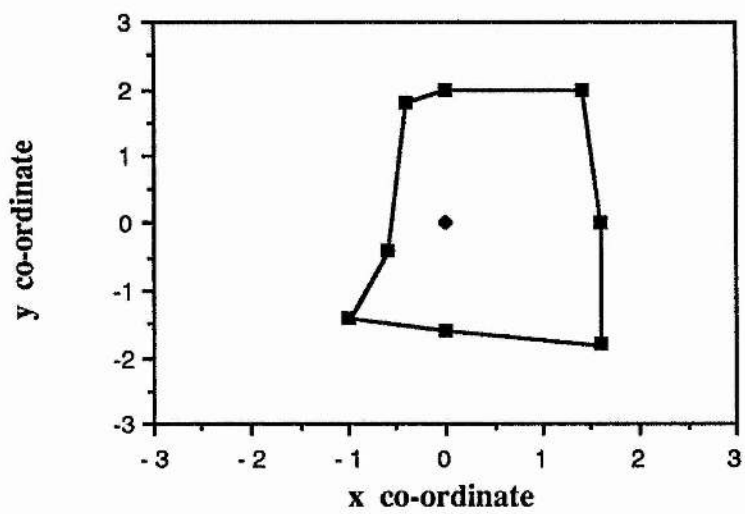
Figure 5.17
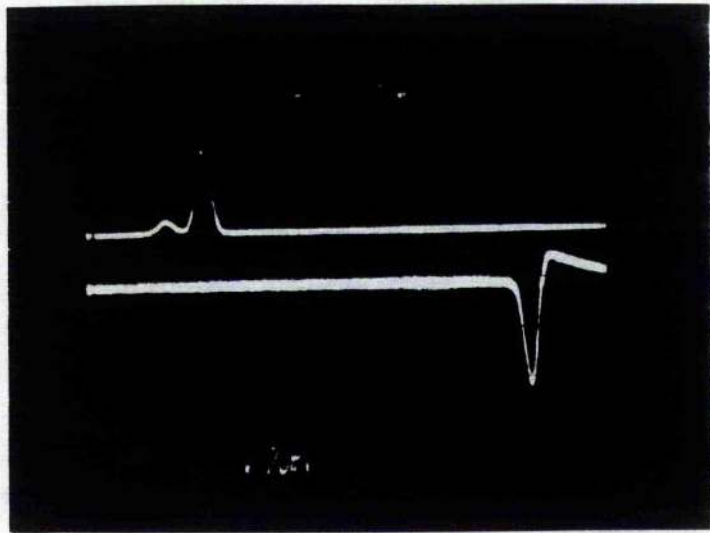
Figure 5.19 Pulses obtained from two curved arrays in the Fourier
transform image plane of a spatial coherence sensor (the
lower trace is inverted)

E-O sensor with 4 curved arrays
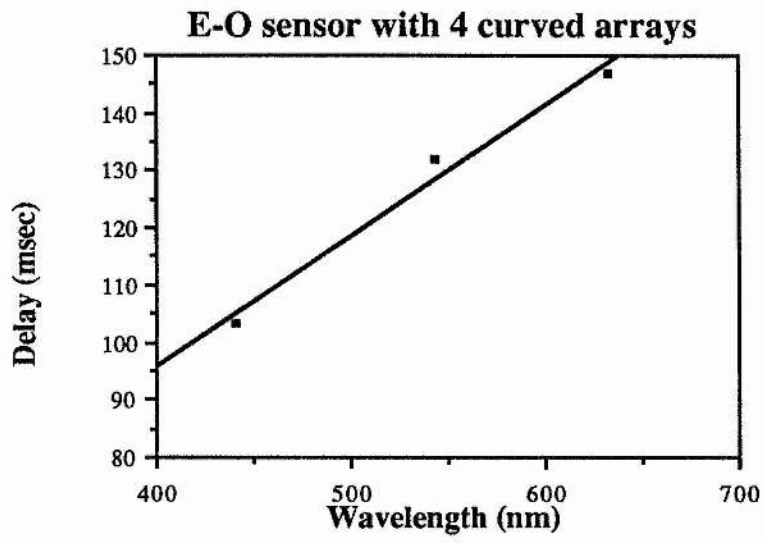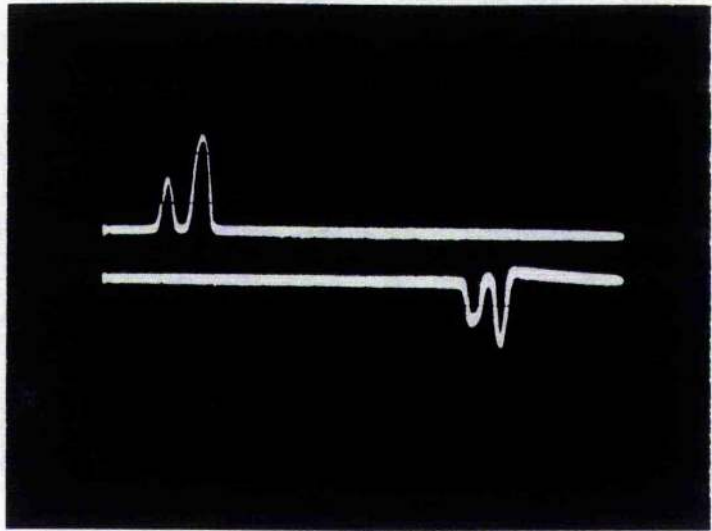
Figure 5.20

Figure 5.22 Pulses obtained from one linear and one curved array in the
Fourier transform image plane of a spatial coherence
sensor (the lower trace is inverted)

E-O sensor with 2 curved , 2 linear arrays

Delay (msec)

Wavelength (nm)

Figure 5.23

Input polariser

Pixels in opposite magnetic states

Output polariser

Polarisation vector
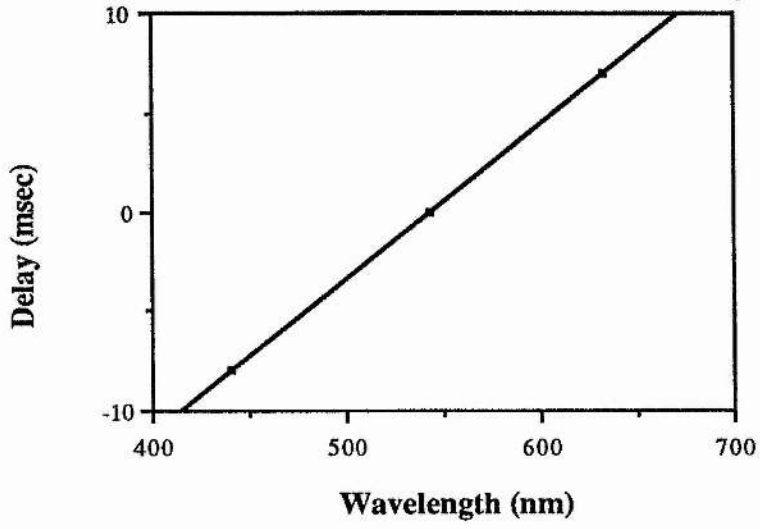
Transmitted intensities
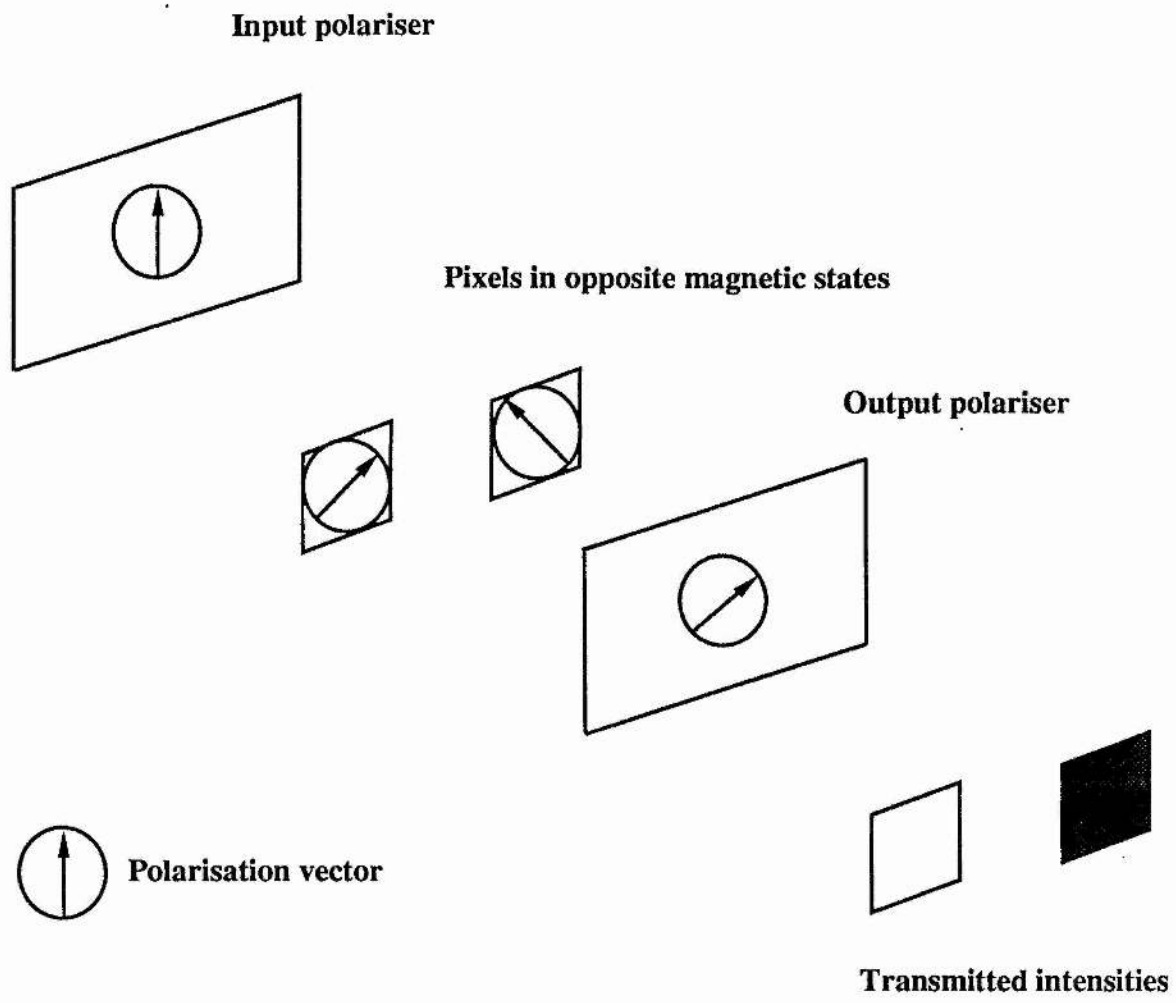
Figure 5.24 (a). Operation of magneto-optic device called SIGHT-MOD.

Input polariser

Pixels in opposite magnetic states

Output polariser

Polarisation vector

Transmitted
polarisations
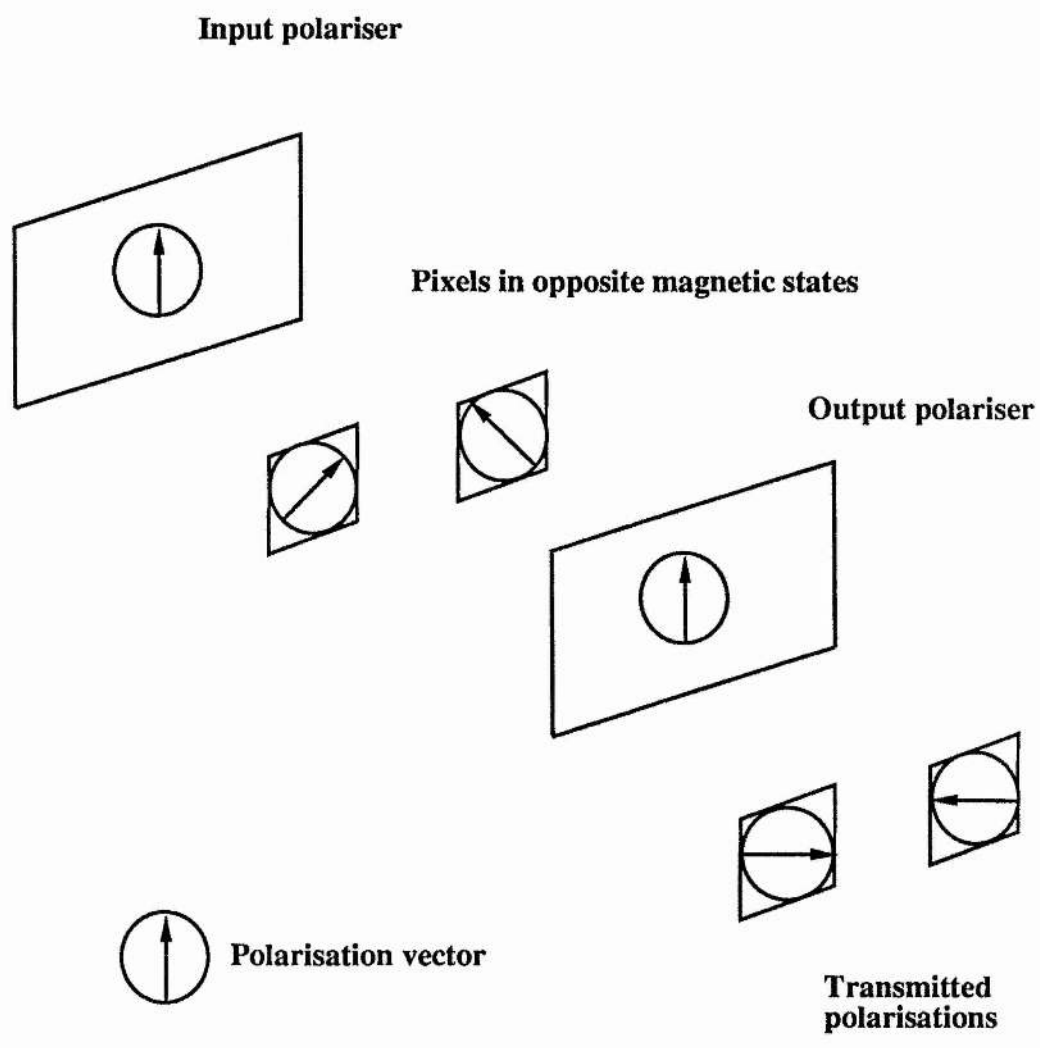
Figure 5.24 (b) Operation of magneto-optic device
called SIGHT-MOD.
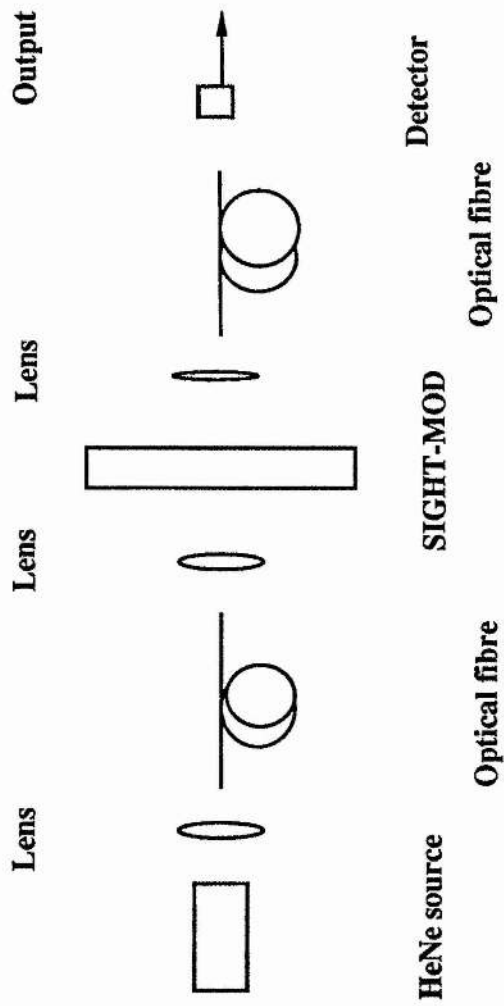
Figure 5.25 SIGHT-MOD as a fibre optic switch (lens coupled).
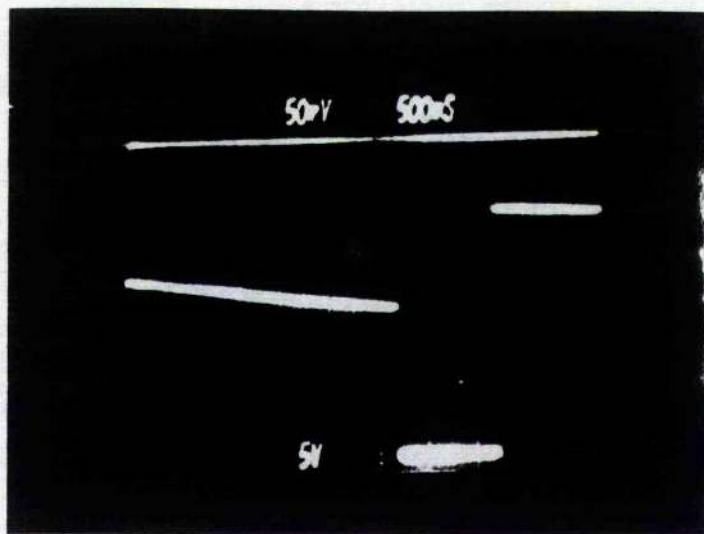
Figure 5.26 Intensity transmitted through SIGHT-MOD during raster scan, one write pulse (source 633 nm)
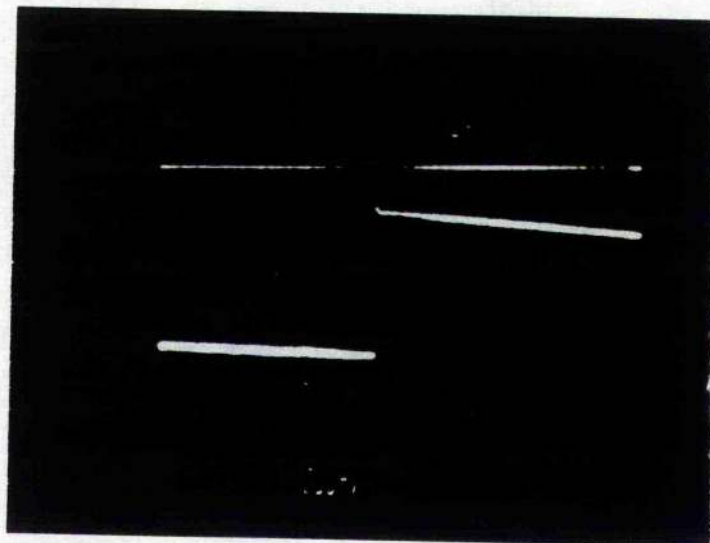
Figure 5.27 Intensity transmitted through SIGHT-MOD during raster scan, many write pulses (source 633 nm)

Output

Lens

Lens

Detector

Optical fibre

SIGHT-MOD

Lens

Beam expansion

HeNe source
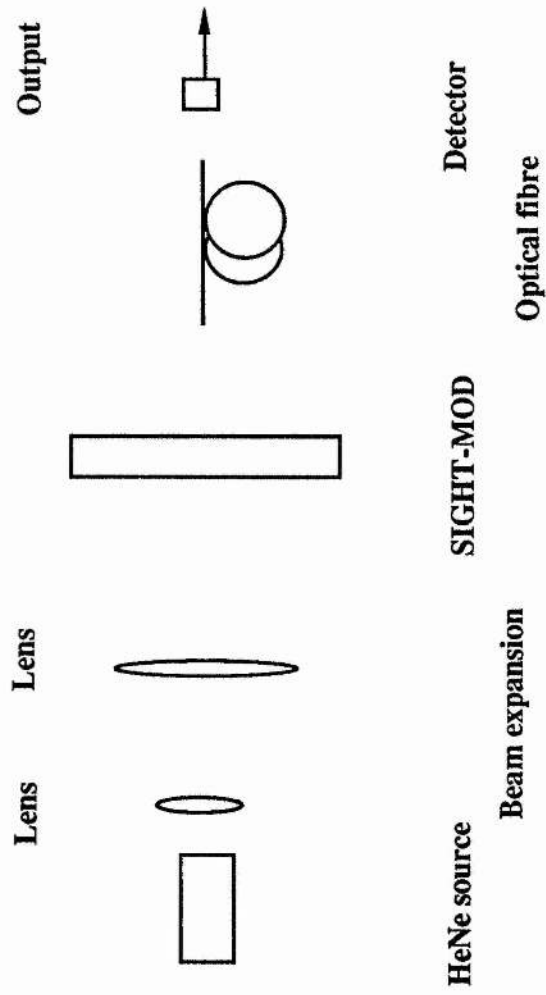
Figure 5.28 SIGHT-MOD as a fibre optic switch (not lens coupled).
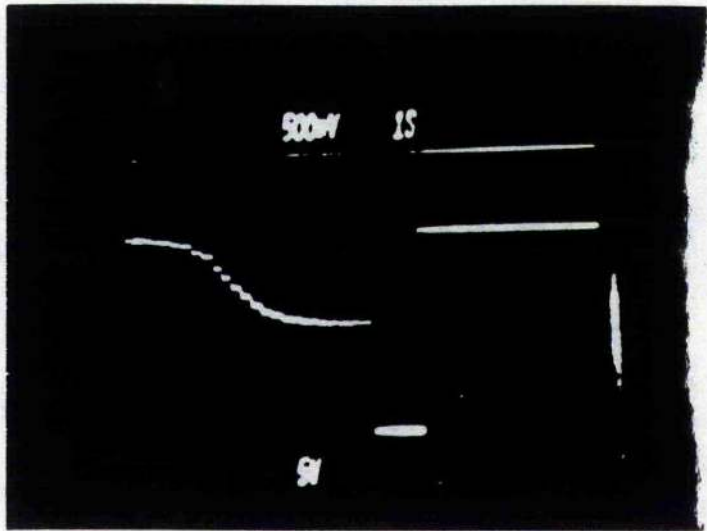
Figure 5.29 Intensity coupled into 970µm fibre at output of SIGHT-MOD

during raster scan (source 633 nm)
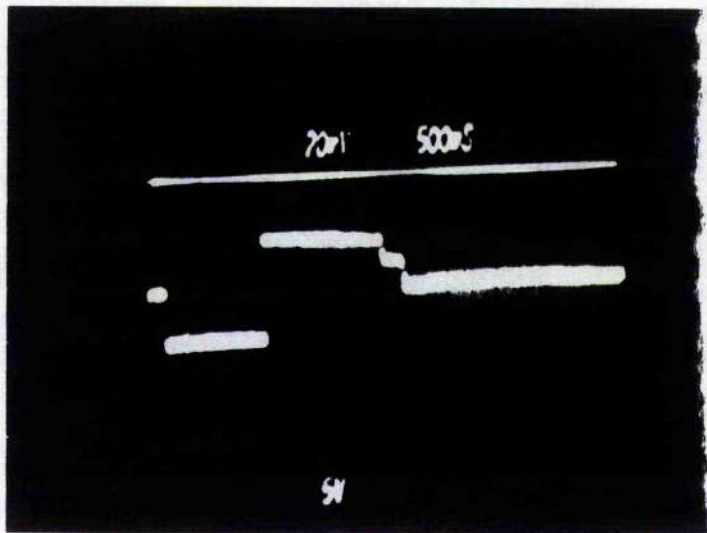
Figure 5.30 Intensity coupled into 50/125µm fibre at output of

SIGHT-MOD during raster scan (source 633 nm)
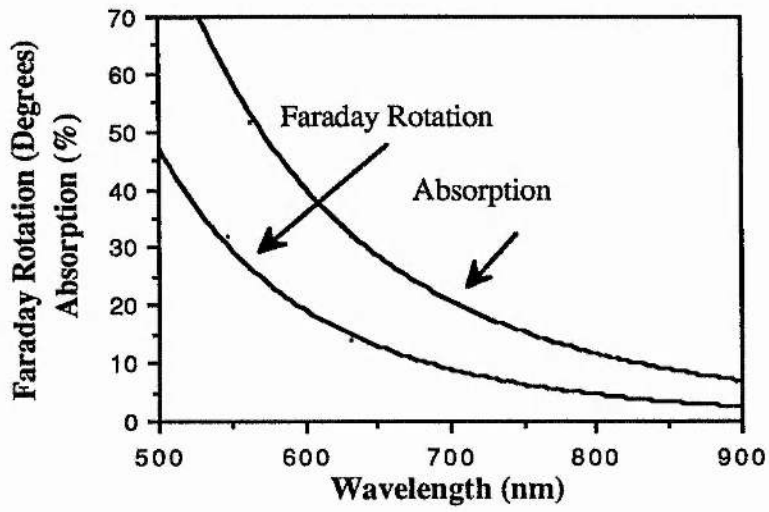
Absorption and Faraday Rotation of SIGHT-MOD
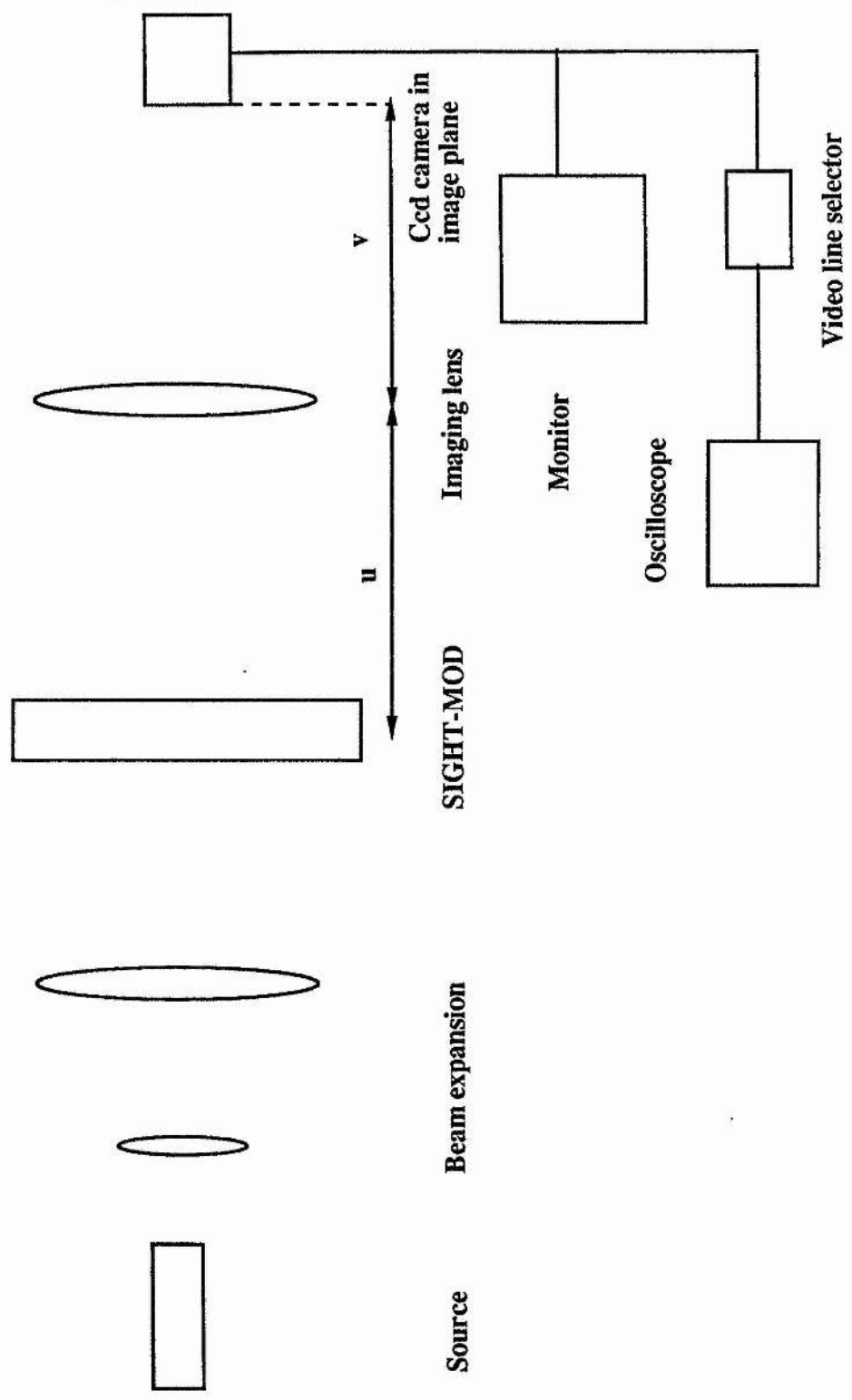

Figure 5.31

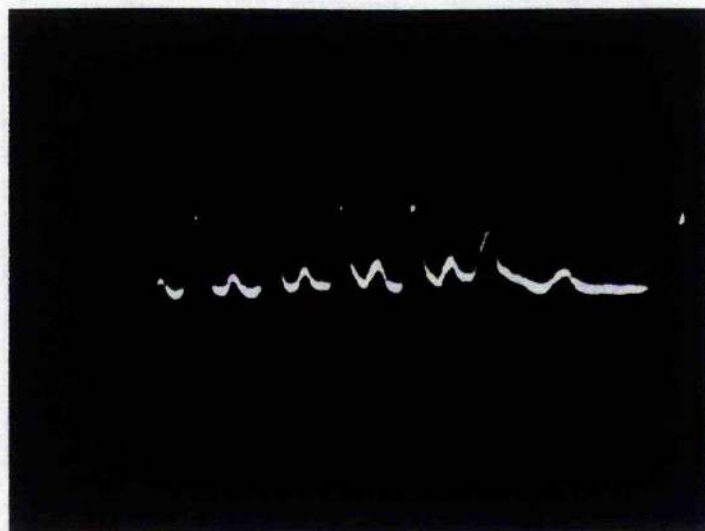Figure 5.32 Imaging patterns from SIGHT-MOD to ccd camera

Figure 5.33 Transmitted intensity across single line of ccd camera with grating written on SIGHT-MOD (source 633 nm)
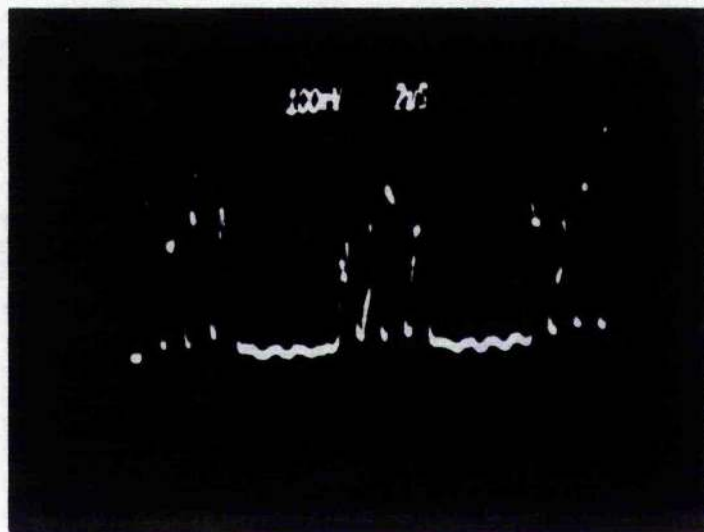

Figure 5.34 Transmitted intensity across single line of ccd camera with grating written on SIGHT-MOD (source 544 nm)
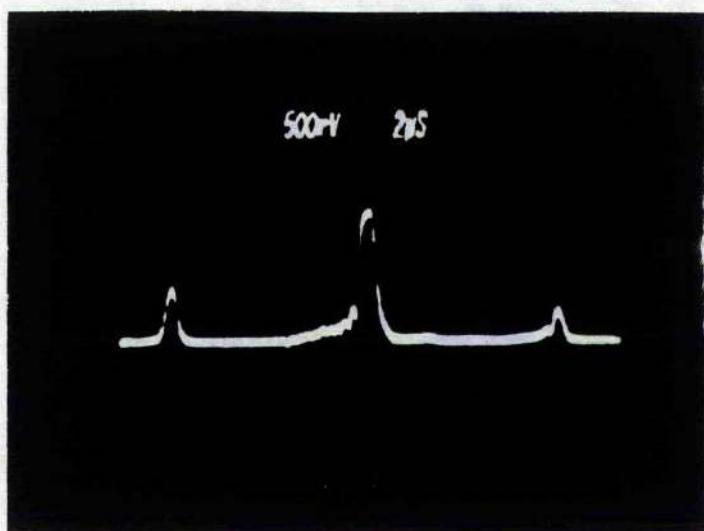
Figure 5.35 **Fourier transform image of SIGHT-MOD cleared of data**

(source 544 nm)

Figure 5.36 **Fourier transform image of SIGHT-MOD containing**
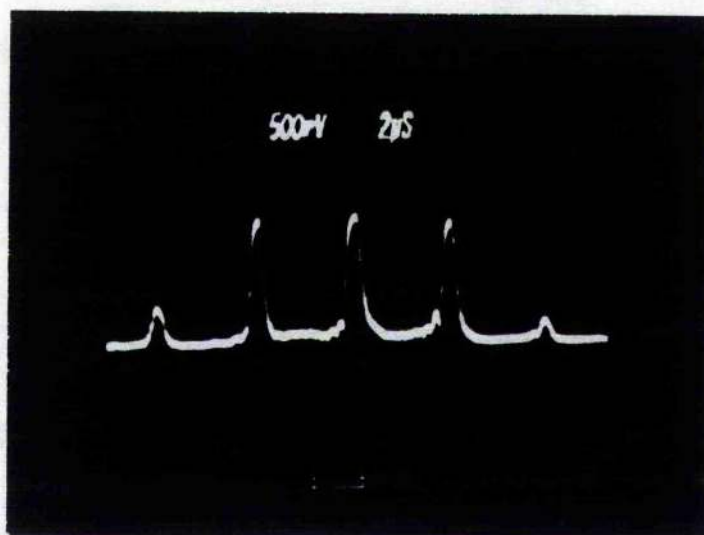**grating with periodicity of 2 columns (source 544 nm)**

Figure 5.37 Fourier transform image of SIGHT-MOD containing grating with periodicity of 4 columns (source 544 nm)
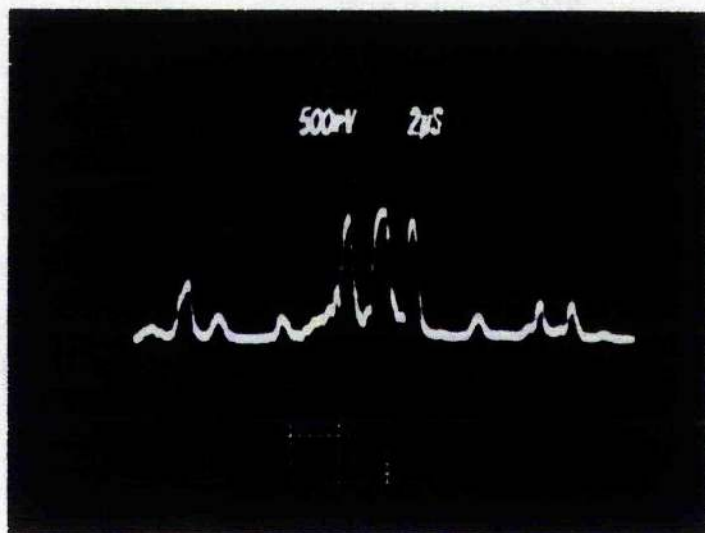

Figure 5.38 Fourier transform image of SIGHT-MOD containing grating with periodicity of 6 columns (source 544 nm)
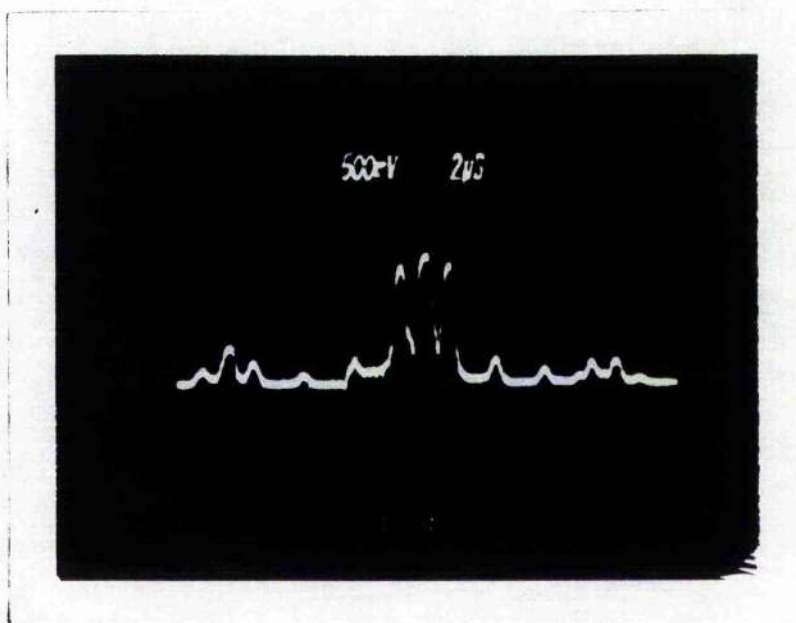
Figure 5.39 Fourier transform image of SIGHT-MOD containing
grating with periodicity of 8 columns (source 544 nm)

HeNe Laser
(633nm)

Beam
expansion

SIGHT-MOD

Fourier transform
image plane

2D to 1D fibre array

Linear ccd array

Oscilloscope

2D to point fibre array

Single
photodetector

Oscilloscope

Figure 5.40 2D fibre arrays in Fourier plane of SIGHT-MOD
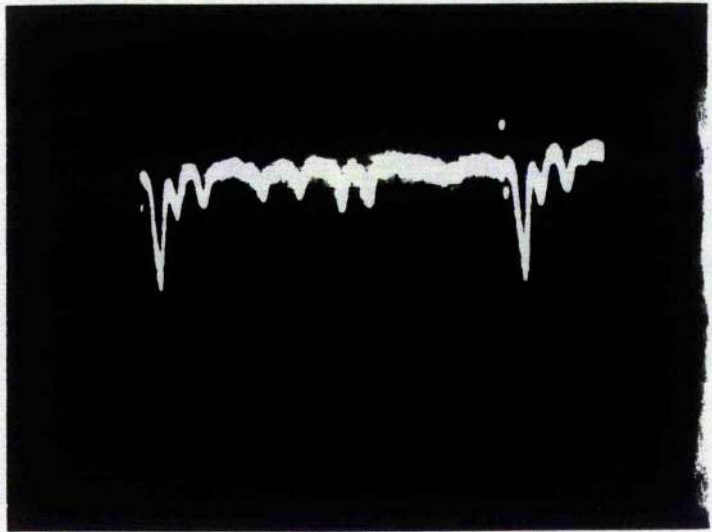
Figure 5.41 1D spatial signal transformed from 2D by a fibre array
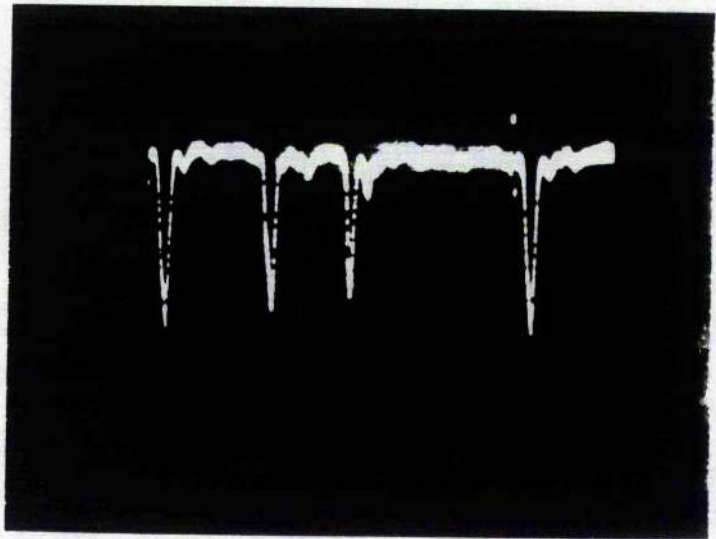
Figure 5.42 1D spatial signal transformed from 2D by a fibre array
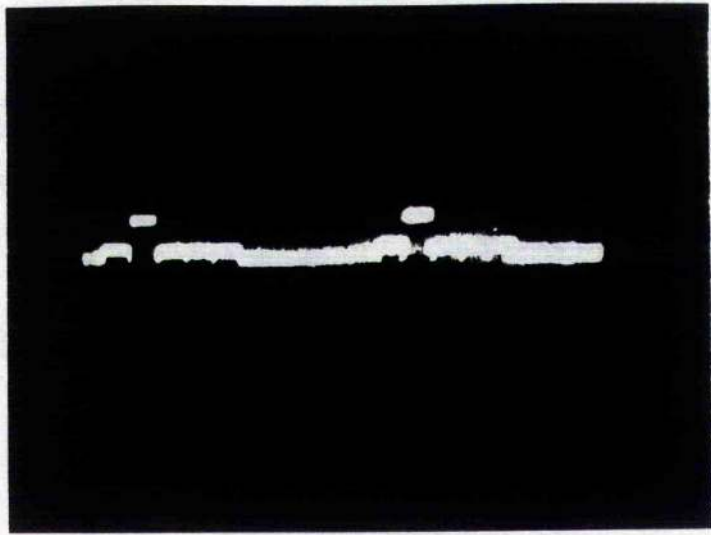
Figure 5.43 Correlation signal between 2D fibre array and 2D Fourier
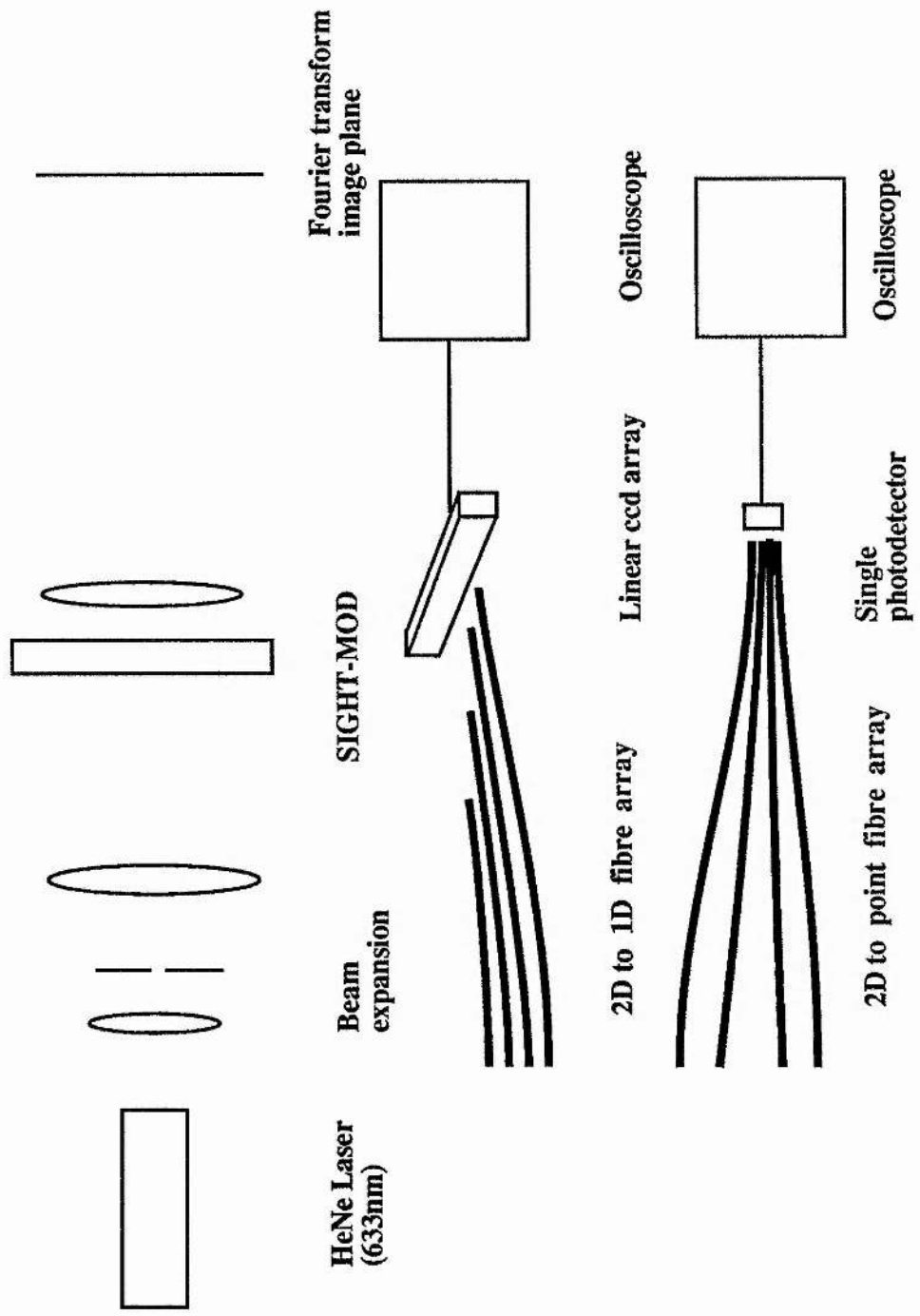transform image
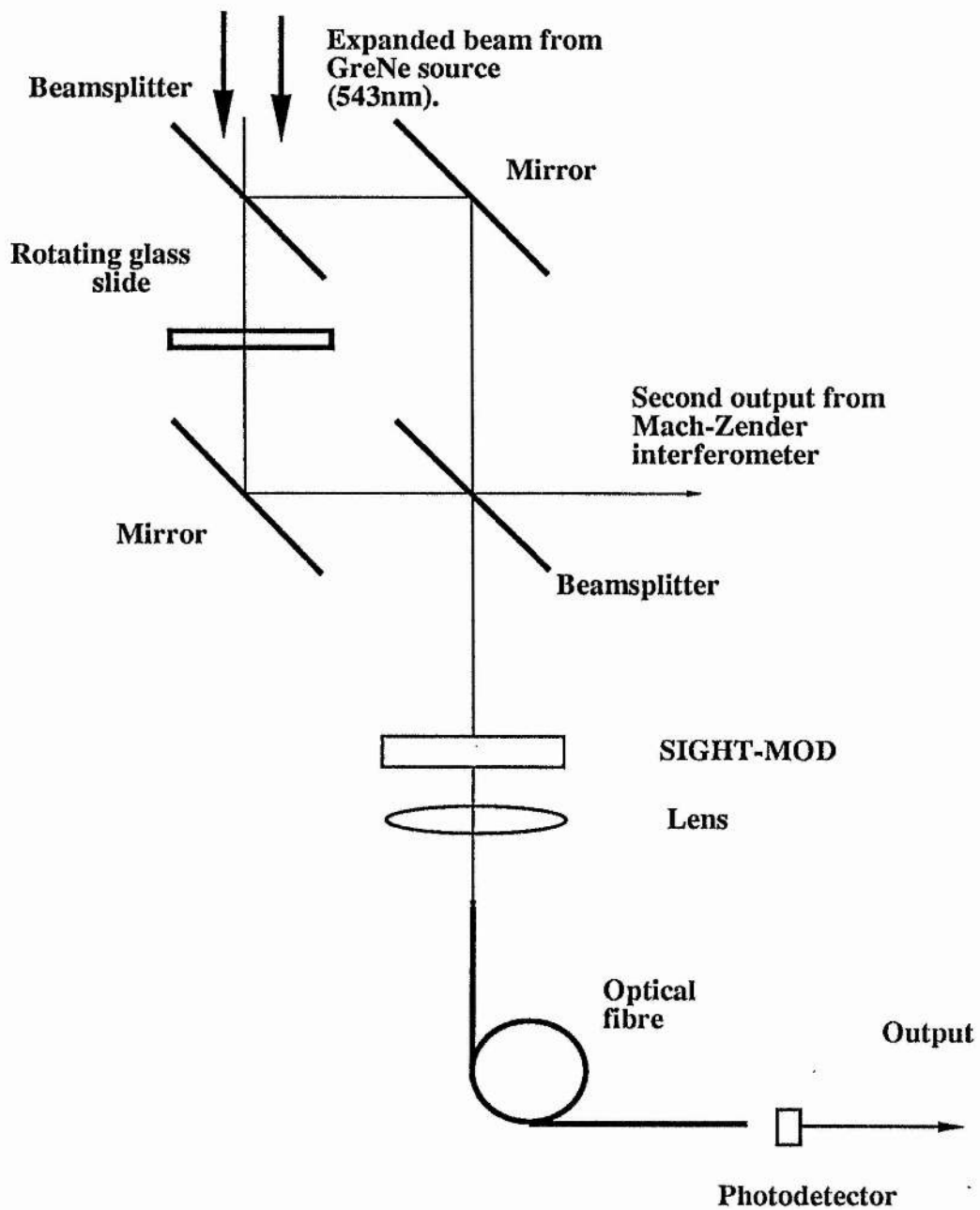
Figure 5.44 Correlation of linear interference fringes with SIGHT-MOD
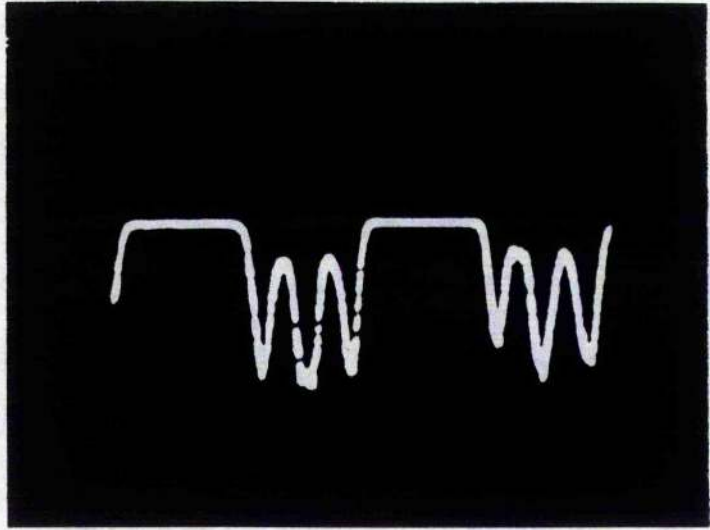
Figure 5.45 Correlation signal between linear interference fringes produced by a sheared Mac-Zehnder and a grating on the SIGHT-MOD
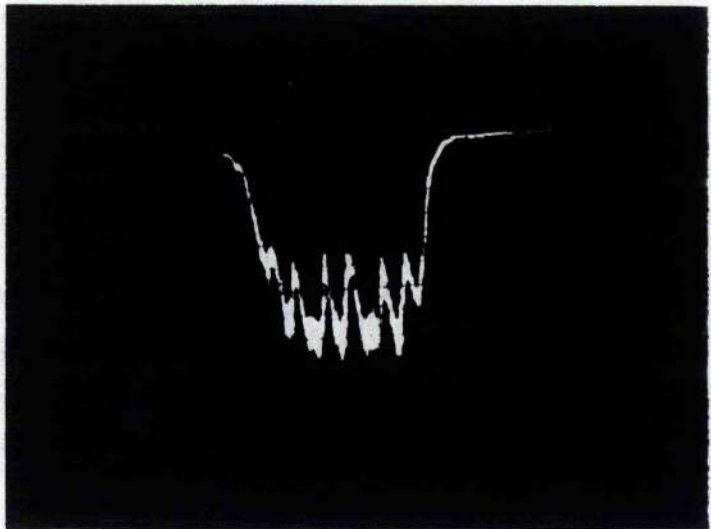
Figure 5.47 Correlation signal between linear interference fringes produced by a fibre 'Young's slits' interferometer and a grating on the SIGHT-MOD

Figure 5.46 Correlation of linear interference fringes with

SIGHT-MOD

6 Discussion : Pre-detector signal processing.

The philosophy behind pre-detector signal processing is, given a scene containing signal and background radiation, to impose modulation on the signal which depends on particular characteristics of the signal such as temporal and spatial coherence and polarisation in such a manner as to produce no modulation or different modulation of the background. This may be carried out in any waveband where suitable compo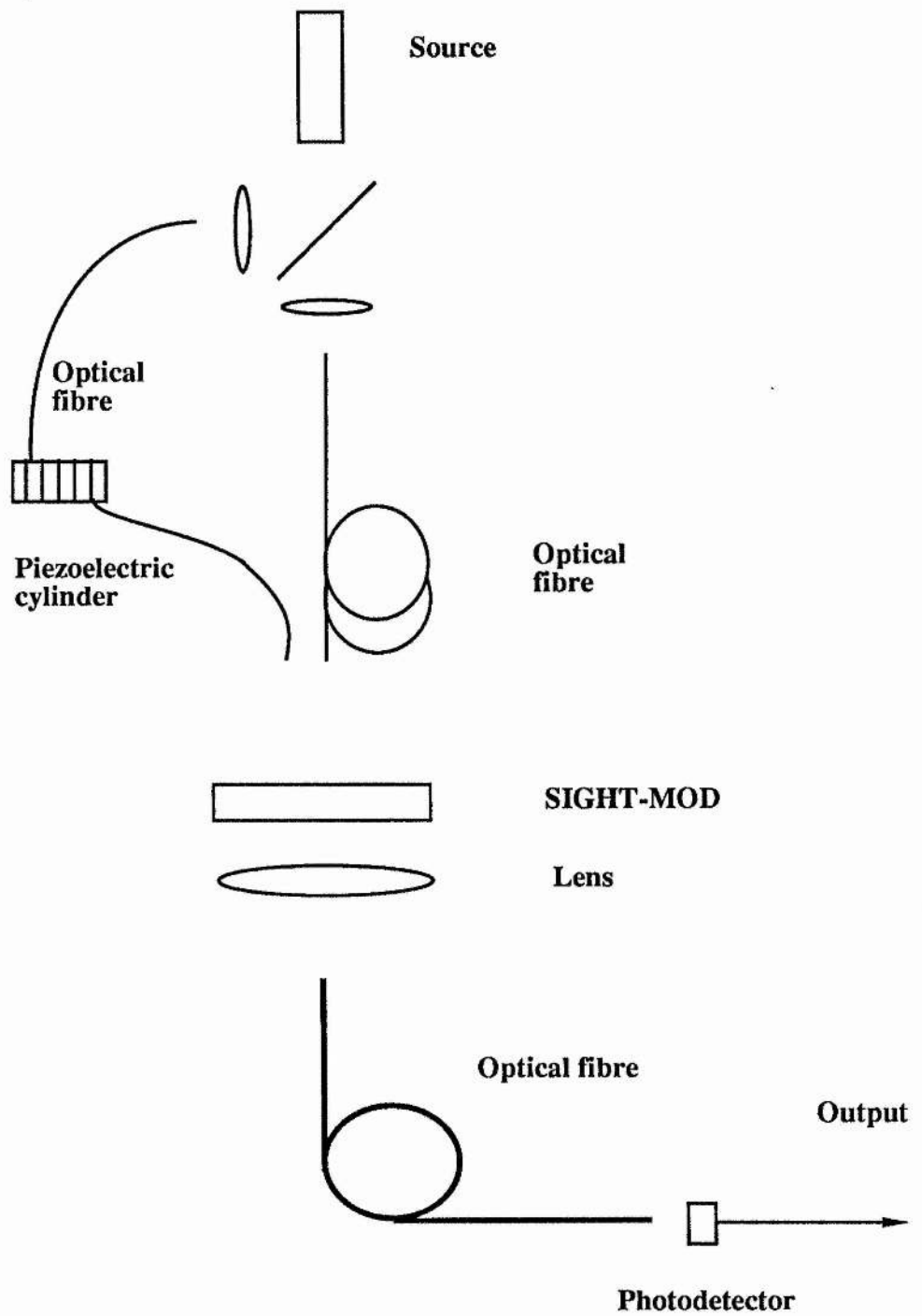nents are available, for example, lenses, mirrors and beamsplitters etc are available in both the infra-red and millimeter wavebands. Optical fibre waveguides are available throughout the visible and infra-red. For longer wavelengths metal waveguides are used.

Optical fibres add extra dimensions of manipulation to pre-detector signal processors and radiation coupled into a fibre can be used very efficiently. Optical fibres are useful for performing optical functions such as geometrical transformations and are ideal for special transforms such as correlations over a scene which are difficult to perform with bulk optics.

Radiation guided in optical fibres can be phase modulated by straining the fibre or by producing acoustic standing waves on the fibre, using a piezoelectric material, at frequencies which can be greater than 100 kHz. The Faraday and electro-optic effects enable the state of polarisation of light guided in polarisation maintaining fibres to be modulated.

Within this thesis it has been shown that optical fibres can be of use in many pre-detector signal processing systems. In particular

(i) multimode optical fibres can be used with much more freedom in coherent systems than would be expected;

(ii) temporal coherence bandpass filtering can be performed using optical fibre interferometers;

(iii) spatial coherence filtering can be performed using arrays of optical fibres in detector planes;

(iv) geometrical transformations from 2D to 1D have been achieved using fibre arrays;

(v) Correlations of fibre arrays with 2D intensity distributions have been achieved by fibres performing a transform from 2D to a point and the intensity at that point was measured by a photodetector;

(vi) a spatial light modulator has been shown to be of use in pre-detector signal processing to provide masks for correlation or as a programmable reticle.

6.1 Discussion of interference patterns produced by optical fibres.

In sections 4.1 and 4.2 it was seen that interference patterns can be produced using singlemode and multimode optical fibres. If light from a coherent source is coupled into a singlemode fibre interferometer, then the uniform beam of the singlemode fibre produces high visibility interference fringes which, for many purposes, are independent of effects due to the fibre. If light from a coherent source is coupled into a multimode optical fibre interferometer, interference fringes are present but are harder to detect. The many modes of the fibre produce a non-uniform phase

146

front which distorts any fringes present. The distortion occurs on the same scale as the speckle size so the detector must be reduced to a similar size. As the light is generally diverging from the end of the fibre, this may only mean increasing the distance between the fibre and detector.

If a multimode laser source is coupled into a singlemode fibre and a detector connected to a spectrum analyser is scanned over the output beam, the spectrum analyser will read the same over the whole beam. If the fibre is multimode, then a variation in the intensity of the laser modes with position is seen. This is explained by interference between the laser modes in the various modes of the fibre, section 4.8.4.

The periodicity of linear interference patterns produced by coupling light into two singlemode fibres, placing the ends side by side, and allowing the emitted beams to overlap depends on the wavelength of the source and the separation of the fibre ends. If the output ends of the fibres are fixed the input ends may be moved to any location in the input plane without affecting the fringe spacing.

As optical fibres are very sensitive to their environment, the phase of light emitted from a fibre cannot be predicted. This means that coherent radiation emitted from two fibres may interfere, at a given point, anywhere from constructively to destructively. A linear array of radio antennae produces a far field diffraction pattern which is the Fourier transform of the array. The diffraction pattern is steered by adjusting the phases of the antennae. Radiation emitted from an array of optical fibres, illuminated by a single source, also produces a far field diffraction pattern which is the Fourier transform of the

147

spatial distribution of the array. However, because of the unpredictable phases, the principle maxima may be located anywhere in the pattern.

A plane wave making an angle θ with a linear array will produce an intensity, by coherent addition, which is related to the angle θ. As the angle changes the intensity scans through the far field diffraction pattern, but the principle maxima need not be located on the optical axis when the angle between the wavefront and array is zero.

6.2 Discussion of coherence in fibres.

After radiation has been propagated through an optical fibre, its temporal coherence, $\gamma(\tau)$, depends on the spectrum of the transmitted light. The effect of transmission of radiation through an optical fibre on the coherence of that radiation is related to the dispersion of the medium. The dispersion is either group or phase dispersion, section 2.3 and 2.4. Coherence is a correlation of amplitude and phase so it is the phase dispersion which is important. For a singlemode fibre interferometer, we have

$$\gamma_{12}(\tau) = \; < \; E_1(\; x_1, y_1, t - \frac{n_{eff}(\lambda) \, l_1}{c}) \; E_2(\; x_2, y_2, t - \frac{n_{eff}(\lambda) \, l_2}{c}) > \; , \quad (6.1)$$

where E_1 and E_2 are the complex amplitudes in each arm. The dispersion is related to absorption so the coherence of a source cannot decrease but must increase as the radiation bandwidth becomes narrower.

In a multimode fibre the primary source of dispersion is intermodal dispersion. The many modes supported by the fibre will interfere in the same manner as the waves which occur in a Fabry-Perot etalon, although the separation of the modes and their amplitudes are not as predictable. So the fibre acts as an optical filter whose characteristics depend on the modes present and the delay between them. The characteristics change over the output plane as the distribution of modes changes.

In section 4.8 it was seen that the coherence, $\gamma(\tau)$, of a laser source appeared unchanged, for small areas of the wavefront, when

149

transmitted through short lengths, of the order of tens of meters, of singlemode or 50/125 μm multimode optical fibre. This can be explained by the difference in the optical paths of the excited modes being small. It was also shown that a few metres of highly multimode fibre such as the 970μm core fibre will not change $\gamma(\tau)$ as long as a sufficiently small detector is used to overcome the spatial distortion of the fringes. After propagation through 100 m of 50/125 μm fibre it was seen that the measured value of $\gamma(\tau)$ depends on interference effects between the excited modes of the fibre and the difference in the optical paths of the modes. In two different experiments, and therefore with two different mode distributions, two different curves were obtained for $\gamma(\tau)$. One curve showed the effect of spectral filtering and the other showed the effect of large intermodal path differences.

Although we have shown that short lengths of multimode optical fibre can be used in sensors the limits to this have not been fully explored. They have been shown to be useful in that they collect many times more light than a singlemode fibre but the effect of intermodal dispersion can be a problem. If intermodal coupling was small each mode could be used as a separate channel and the dispersion could be used to obtain many optical paths. There should be interesting effects involving the modulation of multimode fibre using piezoelectric techniques. As each mode has a different wavenumber, stressing the fibre by a given amount will produce a different modulation depth for each mode. Similar effects must occur in multimode integrated optic devices although one might expect intermodal coupling to be small as the device is mounted on a solid substrate.

6.3 Discussion of fibre arrays.

The most important contributions of optical fibres to pre-detector signal processing lie in the use of fibre arrays. The arrays can vary in 1, or 2 dimensions and the number of dimensions can change from one plane to the next. by rearranging the fibres. The length of each individual fibre may be determined. As the core of each fibre is surrounded by a cladding there are regions in an array where light is not coupled into the fibres so the ratio of the core diameter to cladding diameter is important. For multimode fibre the ratio is typically 50 / 125. For singlemode the ratio is typically 8 / 125.

From the optical properties of Gaussian beams, only a beamwaist at the entrance to a singlemode optical fibre is efficiently coupled. A beamwaist corresponds to parallel light or one spatial frequency. Any light not of that spatial frequency is not coupled into the fibre. Therefore, the fibre supports only one channel and no spatial information can be transmitted. For calculating the coupling into a multimode optical fibre, geometrical optics can be used. The number of available channels in a multimode fibre corresponds to the number of guided modes. As each mode propagates with a different phase velocity, the radiation at the output does not reconstruct the image. Multimode fibres also scramble the image by cross-coupling between the modes. This removes unwanted features across the output beam.

A scene imaged onto a two-dimensional fibre array will be transmitted to the ends of the fibres but the far field diffraction pattern of the light emitted from the fibres will not reconstruct the image due to the unpredictable phases of each fibre. Rivlin and Semenov [6.1] using a hollow rectangular waveguide with reflective

151

metal walls have demonstrated that if the phase shifts between all the modes are integer values of 2π radians then the light will reconstruct the image. Yariv [6.2] has discussed using non-linear mixing to cancel the phase dispersion and retrieve the image.

If a two-dimensional array is placed in the Fourier transform plane of an object, illuminated by a coherent source, then the light coupled into a particular fibre is associated with a particular spatial frequency. As the relative phase information is lost, the fibres cannot be used to transmit the Fourier transform image (FTI) to a remote plane and reconstruct the image. However, it is possible to use arrays of fibres to encode information about a scene or FTI, for example, a geometrical transformation can be used to encode the spatial frequency information. A given spatial frequency appears on the circumference of a circle, centred on the optical axis, so the fibres could be grouped according to their distance from the optical axis. Alternatively,the light coupled into each fibre from the FTI could be modulated at a frequency dependant on position in the array. Then a spectrum analysis of the radiation would give information about the spatial frequency content of the scene.

The experiment described in section 5.1.3 to measure path differences across a scene relies on knowing the frequency spectrum of the source and hence being able to associate each value of the visibility curve with a given path difference. The source is unsuitable if the visibility goes to zero or is ambiguous over the range of the path differences. If this were the case, for example the coherence length of sunlight is only a few wavelengths, the signal processor could be based on laser enhanced imaging.

The experiment described in section 5.7.6 measured the correlation of an image with the transmission function of an array of optical fibres. Each fibre guided light to a large area photodetector. As the phase of the light emitted from each fibre is unpredictable, all the light must be collected and the correlations are in intensity and not amplitude and phase.

Further research should be carried out to investigate combinations of fibre arrays and acousto-optic devices. Bragg cells and SAW devices can be used as programmable phase reticles and for switching radiation between fibres in arrays. Optical fibres, fibre couplers and acousto-optic devices can be combined to give fully integrated heterodyne systems. Homodyne systems could be produced using optical fibres as delay lines in LIDAR. A fibre delay line could be used to store a reference beam to produce a hologram of a distant, laser enhanced, scene. In order to improve coupling into fibre arrays, arrays of holographic lenses could be introduced. Holographic elements could be used as phase reticles in place of amplitude reticles.

6.4 Wavelength demultiplexing.

In some cases it is necessary to separate out radiation into given wavebands. In section 4.6 we used a transmission grating to spatially separate three sources. A signal processor which could direct a signal into a given channel by virtue of its wavelength can be realised by spectrally sensitive couplers. These are couplers designed to have splitting ratios which are given functions of wavelength. Other wavelength sensitive devices such as surface acoustic wave devices can be used to spatially separate different

wavelengths. For a given acoustic wavelength, an optical signal is diffracted at an angle which depends on its wavelength. By altering the acoustic wavelength, the signal can be coupled into one fibre of an array of optical fibres in the output plane.

6.6 Discussion of fibre interferometers.

A fibre interferometer which is to be used for remote sensing must ideally remain singlemode over the whole spectrum of interest in order that amplitude and phase information are retained over long lengths of fibre. This can be a problem, for example, a fibre designed to be singlemode at 850 nm may support 2 modes at 600nm and more at 400 nm. If the fibre is designed to be singlemode at 400 nm then it will be singlemode at all longer wavelengths but as the wavelength increases the radiation is less strongly guided because more power is contained in the evanescent wave.

One multimode fibre contains many optical paths which can be used in an interferometer. In order to access each path, or mode, separately the fibre must be of high quality to reduce scattering, and strain free to reduce intermodal coupling. In order to obtain an interferometer with many predictable optical paths, it is easier to use an array of singlemode fibres, of different lengths, linked by access couplers. A multiple path singlemode fibre interferometer should be constructed using different lengths of singlemode fibre linked by fibre couplers. This could measure the visibility against path difference of a source at several points simultaneously. The sensor could be fully integrated, with piezoelectric phase modulation, and have pigtailed detectors spliced to the singlemode fibre.

6.7 Discussion of SIGHT-MOD.

It has been seen in section 5.4.3 that the SIGHT-MOD is most efficient for wavelengths between 500 - 550 nm. Below 500 nm the absorption is very high, and above 550 nm the Faraday rotation is low. If the SIGHT-MOD is illuminated with radiation between these values, for example, when a scene is flashed with laser light, then the SIGHT-MOD is useful as a programmable aperture plane reticle. A series of aperture plane reticles can be written onto the device, by a computer, in order to represent a rotating reticle such as a grating or chopper. The maximum speed of the device is limited to about 50 Hz by the time required to write each frame which is given as 20msec. This speed suggests that it could be very useful as a dynamic reticle, especially in processing a laser enhanced scene.

6.8 Conclusions

We have seen that optical fibres are of use in pre-detector signal processing. Optical fibre systems can be designed which can descriminate between signal radiation and background clutter in a scene.

Descrimination in favour of narrowband radiation can be achieved using phase modulated optical fibre interferometers with path differences greater than the coherence length of the background radiation. Optical fibre temporal coherence filters were described in section 4.5. A fibre interferometer has a fixed optical path difference. By linking several interferometers, each with a different optical path difference, using fibre couplers, the temporal coherence of the signal radiation can be measured with several path differences simultaneously.

Descrimination in favour of spatially coherent radiation can be achieved using arrays of optical fibres in the image plane of a sensor. The arrays, together with a modulated aperture plane reticle, can detect spatial modulation of the image of the spatially coherent source in the presence of spatially incoherent background radiation. Spatial coherence sensors have been described in section 5.3. Arrays of fibres allow spatial transforms and time delays to be employed between input and output planes, so arrays of fibres can be used to perform special tasks. For example, fibres sampling the radiation over the image plane of the sensor enables light from different points to be measured or to be correlated with one another, section 5.1.2.

Singlemode or multimode optical fibres can be used in many of the sensors. More power is coupled into multimode fibres, but when phase information is important, the intermodal dispersion introduces different optical paths and distorts the emitted phase front. This causes any interference fringes which are produced to be distorted, thus limiting detector size. Interference patterns with singlemode and multimode fibres are described in sections 4.1 to 4.3. The effect of singlemode and multimode fibres on coherence is considered in section 4.8.

A Spatial Light Modulator, such as the Semetex SIGHT-MOD, can be used as a programmable aperture plane reticle for pre-detector signal processing, section 5.4. The SIGHT-MOD, together with arrays of optical fibres in the image plane of the sensor, can descriminate between signal and background radiation using techniques such as convolution, correlation, and spatial coherence filtering.

References

[1.1] P.Sutton,A novel optical pre-detector signal processing technique,Ph.D Thesis,Southampton University (1982).

[1.2] J.W.Goodman,Introduction to Fourier Optics,McGraw-Hill(1968).

[1.3] E.G.Steward,Fourier Optics: an introduction,Ellis Horwood(1983).

[1.4] R.N.Bracewell,The Fourier transform and it applications,2nd edition,McGraw-Hill(1986)

[1.5] R.N.Bracewell,The Hartley transform, Clarendon (1986).

[1.6] N.George,S.Wang,Appl.Opt.,Vol.23,No.6,Mar.1984,pp 787-797.

[1.7] E.N.Leith,J.Upatnieks,J.O.S.A.,Vol.56,No.4,Apr.1966,pp 523.

[1.8] E.N.Leith,B.J.Chang, Opt.Comm.,Vol.17,No.3,June1976,pp350-352.

[1.9] G.A.Koepf,B.J.Markey,Appl.Opt.,Vol.23,No.20,Oct.1984,pp 3515.

[1.10] R.C.Youngquist,R.H.Wentworth,K.A.Fesler,Opt.Lett.,Vol.12, No.11,Nov.1987,pp 944-946.

[1.11] K.Wilner,A.P.Van Den Heuvel,Proc.IEEE,Vol.64,No.5,May 1976, pp 805-807.

[1.12] C.T.Chang,D.E.Altman,D.R.Wehner,D.J.Albares, IEEE Trans.Circuits and Systems, CAS-26,1979,pp 1132.

[1.13] K.P.Jackson,S.A.Newton,B.Moslehi,M.Tur,C.C.Cutler, J.W.Goodman,H.J.Shaw, IEEE Trans.Microwave Theory Tech., MTT-33,1985,pp 193.

[1.14] J.E.Bowers,S.A.Newton,W.V.Sorin,H.J.Shaw,Elect.Lett., Vol.18,No.3,Feb.1982,pp 110-111.

[2.1] Lord Rayleigh, Phil. Mag. 43, 125 (1897).

[2.2] E.Snitzer,J.Opt.Soc.Am.,Vol.51,No.5,1961, pp 491-498.

[2.3] K.C.Kao,G.A.Hockham,Proc.IEEE,Vol.113,1966,pp 1151-1158

[2.4] D.Gloge,Proc.IEEE,Vol.58,No.10,Oct.1970, pp 1513-1522.

[2.5] D.Gloge,Appl.Opt.,Vol.10,No.10,Oct.1971, pp 2252-2258.

[2.6] D.Gloge,Appl.Opt.,Vol.10,No.11,Nov.1971, pp 2442-2445.

[2.7] D.Gloge,Bell Syst.Tech.J.,Oct.1972, pp1768-83.

[2.8] D.Marcuse,Light transmission optics. Van Nostrand(1972).

[2.9] M.J.Adams,An introduction to optical waveguides. Wiley (1981).

[2.10] A.Cherin,An introduction to optical fibres. McGraw-Hill(1983).

[2.11] W.F.Love,Laser Focus,June 1982, pp 113-116.

[2.12] R.L.Ohlhaber,T.R.Ulijasz,Laser Focus,Feb.1985,pp 98-104.

[2.13] S.C.Rashleigh,R.H.Stolen,Fibre Optic Tech.,May 1983,pp 155-160.

[2.14] H.C.Lefevre,Electronics Letters,Vol.16,No.20,Sept.1980,pp 778-780.

[2.15] R.E.Epworth,Laser Focus,Sept.1981,pp109.

[2.16] K.I.White,J.Phys.E:Sci.Instrum.,Vol.18,1985,pp 813-821.

[3.1] C.M.Davis,Fibre Optic Tech.,Feb.1982,pp 112-115.

[3.2] V.Vali, R.W.Shorthill,Appl.Opt.,Vol.15,No.5,May 1976,pp 1099-1100.

[3.3] D.A.Jackson,R.Priest,A.Dandridge,A.B.Tveten,Appl.Opt.,

Vol.19,No.17, Sept.1980, pp 2926-2929.

[3.4] D.A.Jackson,A.Dandridge,S.K.Sheem,Opt.Lett.,Vol.5,No.4,

April 1980,pp 139-141.

[3.5] R.Kashyap,B.K.Nayar,J.ofLightwaveTech.,Vol.LT-1,No.4,Dec.1983,
pp619-624

[3.6] A.D.Kersey,D.A.Jackson,M.Corke,Opt.Comm.,Vol.45,No.2,

March 1983, pp 71-74.

[3.7] P.Akhavan Leilabady,J.D.C.Jones,D.A.Jackson,Opt.Comm.,

Vol.57,No.2 Feb.1986,pp 77-80.

[3.8] C.Rouchoudhuri,Appl.Opt.,Vol.19,No.12,June 1980,pp 1903-1906.

[3.9] P.Shajenko,J.Ac.Soc.Am.,Vol.69,1980,pp 1829.

[3.10] P.Shajenko,Appl.Opt.,Vol.21,No.12,June 1982,pp 2095.

[3.11] Th.Bosselman,R.Ulrich, Proc SPIE, Int. Soc.Opt.Eng.(USA),
vol.514, pp361-364.

[3.12] P.Shajenko,Appl.Opt.Vol.21,No.23,Dec.1982,pp 4185-4186.

[3.13] P.Shajenko,Appl.Opt.,Vol.22,No.13,July 1983,pp 1958-1960.

[3.14] G.A.Pavlath,H.J.Shaw,Fibre Optic Rotation Sensors,Springer
series in optical sciences,Vol32, Ed. S.Ezekiel, H.J.Arditty,

Springer-Verlag(1982). pp 111-114.

[3.15] P.M.Gray,Proc.SPIE, Int.Soc.Opt.Eng,(USA),vol.374,pp160-164.

[3.16] H.H.Hopkins,Proc.Roy.Soc.A208(1951),pp263-277.

[3.17] H.A.French,ISCNR,Tokyo 1984,pp 188-192.

[3.18] K.Youern,Optik,Vol.74,No.3,1986,pp 120-127.

[3.19] H.A.French,P.Sutton,Proc. Advanced infra-red detector systems,
       IEE,   June (1986),pp 78-92.

[3.20] L.Mertz, Transformations in optics, Wiley (1965).

[3.21] H.W.Wessely,J.O.Bolstad,J.Opt.Soc.Am.,Vol.60,No.5,May 1970,

       pp 678-682.

[3.22] J.B.Breckinridge,Appl.Opt.,Vol.11,No.12,Dec.1972,pp 2996-2998.

[3.23] J.B.Breckinridge,Appl.Opt.,Vol.13,No.12,Dec.1974,pp 2760-2762.

[3.24] P.A.Bakut,Yu.A.Zimin,A.L.Volpov,Opt.Spectrosc.(USSR),

       Vol.59,No.3, Sept.1985,pp 422-423.

[3.25] P.Sutton,ISNCR,Tokyo 1984,pp 193-198.

[4.1] S.K.Sheem, T.G.Giallorenzi,Opt.Lett.,Vol.4,No.1,Jan.1979,pp 29-31.

[4.2] R.A.Berg,G.Kotler,H.J.Shaw,Elec.Lett.,Vol.16,No.7,Mar.1980,
      pp 260-261.

[4.3] C.A.Villarruel,R.P.Moeller,Elec.Lett.,Vol.17,No.6,Mar.1981,
      pp 243-244.

[4.4] B.K.Nayar,D.R.Smith,Opt.Lett.,Vol.8,No.10,Oct.1983,pp 417-419.

[4.5] C.M.Lawson,P.M.Kopera,T.Y.Hsu,V.J.Tekippe,Elec.Lett.,Vol.16, No.7, Mar.1980,pp 260-261.

[4.6] B.Crosognani,P.Di Porto,J.Appl.Phys,Vol.44,No.10,Oct.1973,pp4616-17.

[6.1] L.A.Rivlin,A.T.Semenov,Laser Focus,Feb1981,pp 82-84.
[6.2] A.Yariv,Appl.Phys.Lett.,Vol.28,No.2,Jan.1976,pp 88-89.

Appendix A : Waveguide Theory.

The electric field of an electro-magnetic wave may be written

$$E = a_x E_x + a_y E_y + a_z E_z. \qquad \text{(A.1)}$$

Similarly, for the magnetic field of the wave, we have

$$H = a_x H_x + a_y H_y + a_z H_z. \qquad \text{(A.2)}$$

The electric and magnetic flux densities are

$$D = \varepsilon E, \qquad \text{(A.3)}$$

and

$$B = \mu H, \qquad \text{(A.4)}$$

where ε is the permittivity of the material and μ the permeability of the material. Maxwell's equations for a material with a conductivity of zero and with ε and μ independent of position and time may be written

$$\nabla \times E = -\mu \frac{dH}{dt}, \qquad \text{(A.5)}$$

$$\nabla \times H = \varepsilon \frac{dE}{dt}, \qquad \text{(A.6)}$$

$$\nabla \cdot D = 0, \qquad \text{(A.7)}$$

and

$$\nabla \cdot B = 0. \qquad \text{(A.8)}$$

The wave equation for the electric field may be written

$$\nabla^2 E = \frac{1}{c^2} \frac{d^2 E}{dt^2} , \qquad (A.9)$$

with

$$c^2 = 1/\mu\varepsilon. \qquad (A.10)$$

For a cylindrical geometry with wave propagation along the z axis we describe the fields by $e^{j\omega t - \gamma z}$, where γ is the propagation constant which gives information on the attenuation and group velocity of the wave. In free space we have

$$k^2 = \omega^2 \mu\varepsilon. \qquad (A.11)$$

So, in a medium of refractive index n_1, we have

$$(n_1 k)^2 = k_1^2 = \omega^2 \mu\varepsilon. \qquad (A.12)$$

As $\partial^2 / \partial t^2$ can be replaced by $-\omega^2$ we may write

$$\nabla^2 E = -k_1^2 E. \qquad (A.13)$$

The symbol ∇^2 can be split into two parts. The first part corresponding to directions tangential to the propagation direction and the second corresponds to the direction of propagation. We have

$$\nabla^2 E = \nabla_t^2 E + \frac{d^2 E}{dz^2} . \qquad (A.14)$$

Rearranging (A.14) and substituting from above we have

$$\nabla_t^2 E = - (\gamma^2 + k_1^2) E. \qquad (A.15)$$

The expansion of the curl E equations, (A.5), may be written

$$\frac{dE_z}{dy} + \gamma E_y = -j\,\omega\mu\,H_x, \qquad (A.16)$$

$$-\gamma E_x - \frac{dE_z}{dx} = -j\,\omega\mu\,H_y, \qquad (A.17)$$

$$\frac{dE_y}{dx} - \frac{dE_x}{dy} = -j\,\omega\mu\,H_z, \qquad (A.18)$$

and for the curl H equations, (A.6), we have

$$\frac{dH_z}{dy} + \gamma H_y = j\,\omega\varepsilon\,E_x, \qquad (A.19)$$

$$-\gamma H_x - \frac{dH_z}{dx} = j\,\omega\varepsilon\,E_y, \qquad (A.20)$$

$$\frac{dH_y}{dx} - \frac{dH_x}{dy} = j\,\omega\varepsilon\,E_z. \qquad (A.21)$$

Using equations (A.16) to (A.21) it is possible to solve for E_x, E_y, H_x and H_y in terms of E_z and H_z. If there is no attenuation in the guide then we let $\gamma = j\beta$ where β is real. We now let

$$k_c{}^2 = \gamma^2 + k_1{}^2 = k_1{}^2 - \beta^2. \qquad (A.22)$$

Then we have

$$E_x = \frac{-j}{k_c^2}\left(\beta\frac{dE_z}{dx} + \omega\mu\frac{dH_z}{dy}\right), \qquad (A.23)$$

$$E_y = \frac{j}{k_c^2}\left(-\beta\frac{dE_z}{dy} - \omega\mu\frac{dH_z}{dx}\right), \qquad (A.24)$$

$$H_x = \frac{j}{k_c^2}\left(\mu\omega\frac{dE_z}{dy} - \beta\frac{dH_z}{dx}\right), \qquad (A.25)$$

and

$$H_y = \frac{-j}{k_c^2} \left(\mu\omega\frac{dE_z}{dx} + \beta\frac{dH_z}{dy} \right). \qquad (A.26)$$

For the E_z field we also have the condition, from equations (A.15) and (A.22), given by

$$\nabla_t^2 E_z = (\beta^2 - k_1^2)E_z = -k_c^2 E_z. \qquad (A.27)$$

Using these general expressions for E and H in a waveguide we may obtain specific expressions for a step-index fibre.

Appendix B : Gaussian beam optics for a singlemode fibre.

The form of the electric field emitted by most laser devices is gaussian and for a beam propagating along the z axis the electric field may be described by the equation

$$E_x = E_{x0}(\frac{\omega_0}{\omega}) \exp[-j(kz+\phi)-(x^2+y^2)\frac{ik}{2}(\frac{1}{R(z)}-\frac{2i}{k\omega^2})], \quad (B.1)$$

where ω is the beam radius measured at the point where the electric field falls to 1/e of its maximum value and ω_0 is the minimum beam radius called the beam waist. $R(z)$ is the radius of curvature of the phase front of the beam, figure B.1. The values of ϕ, $\omega(z)$, and $R(z)$ at a point z are given by

$$\phi = Tan^{-1}\frac{2z}{k\omega_0^2}, \qquad (B.2)$$

and

$$\omega^2(z) = \omega_0^2[1+(\frac{2z}{k\omega_0^2})^2], \qquad (B.3)$$

and

$$R(z) = z[1+(\frac{k\omega_0^2}{2z})]. \qquad (B.4)$$

Equation (B.3) can also be written in terms of the divergence θ of the source. Thus we have

$$\omega^2(z) = \omega_0^2 \left[1 + (\frac{2z\theta}{\omega_0})^2 \right] . \qquad \text{(B.5)}$$

For efficient coupling of light from a source into a fibre we consider the single lens system in figure B.2. The output mirror of the laser source provides the radius of curvature of the beam at that point. The radius of the beam at the mirror must also be determined. The beam may be propagated to plane P_1 which is the input plane of the lens by equation (B.3). The beam is transformed by the lens using the equivalent lens law for gaussian beams which is

$$\frac{1}{q_1} - \frac{1}{q_2} = \frac{1}{f} . \qquad \text{(B.6)}$$

where q is the complex beam parameter defined by

$$\frac{1}{q} = \frac{1}{R(z)} - \frac{2i}{k\omega^2(z)} . \qquad \text{(B.7)}$$

For a thin lens $\omega(z)$ is the same at the output plane of the lens, P_2, and so the lens law simplifies to

$$\frac{1}{R_1} - \frac{1}{R_2} = \frac{1}{f} . \qquad \text{(B.8)}$$

Equations (B.3) and (B.4) can be solved for ω_0 and z as follows

$$\omega_0 = \frac{\omega}{\sqrt{1 + (\frac{\pi\omega^2}{\lambda R})^2}} , \qquad \text{(B.9)}$$

and

$$z = \frac{R}{1 + (\frac{\lambda R}{\pi \omega^2})^2} \quad . \qquad (B.10)$$

Thus, knowing ω and R at the output plane of the lens, we can calculate the position and size of the new beam waist $\omega_{0\,2}$.
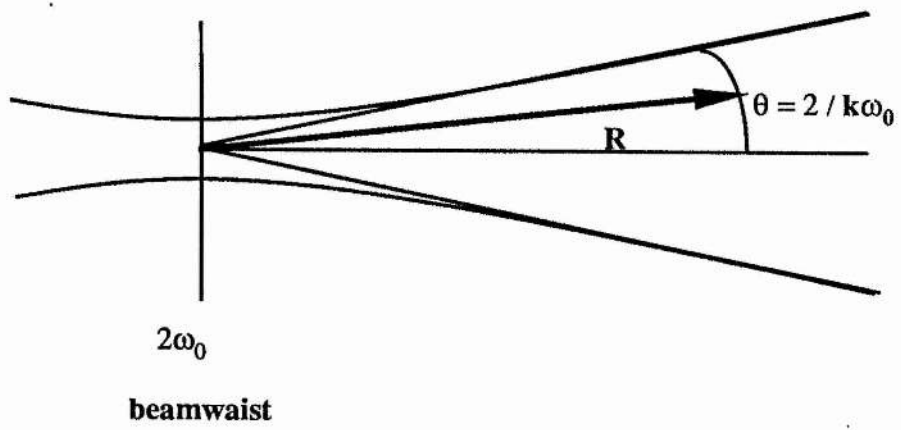
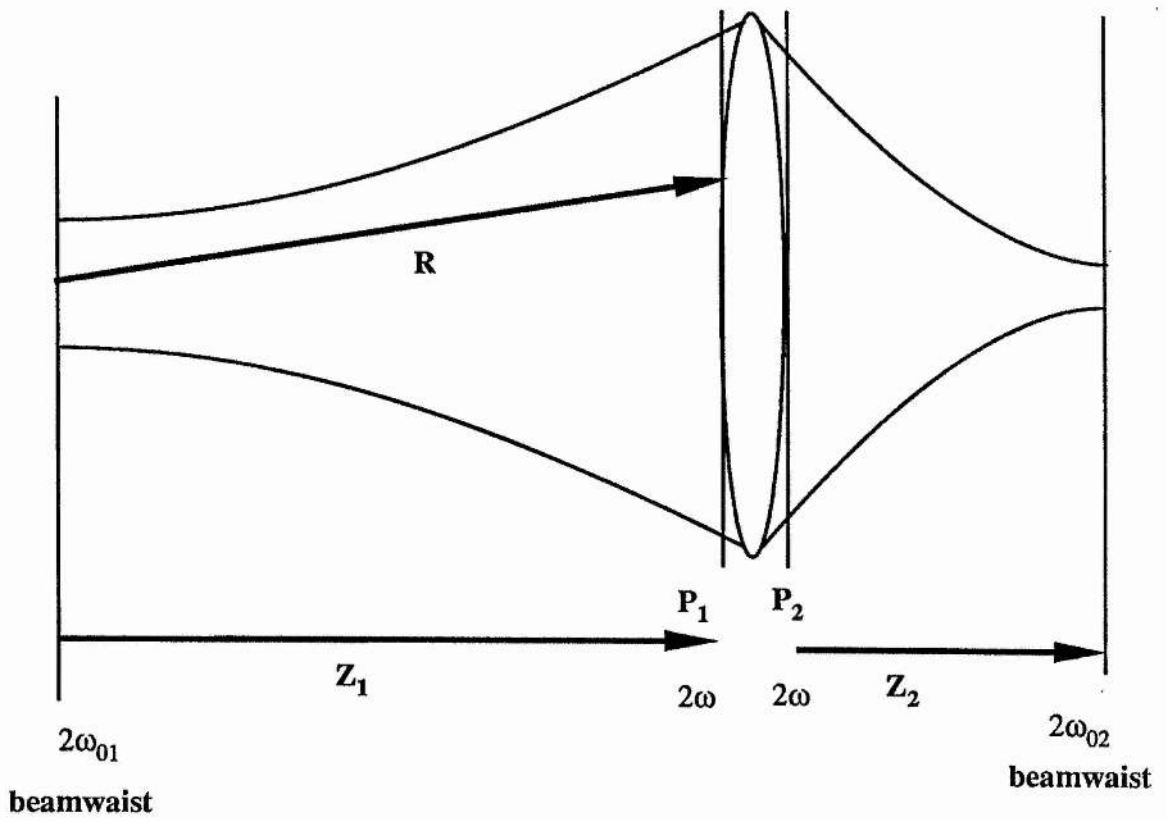**Figure B.1   Divergence of a gaussian beam**

Figure B.2   Focusing of a gaussian beam

Appendix C : Visibility curve obtained for a Lorentzian spectral profile.

A commonly occuring spectral distribution is Lorentzian in profile. The distribution may be written

$$I_S(\nu) = \frac{I_0}{1 + \dfrac{4\,(\nu - \nu_0)^2}{\partial\nu^2}} \quad . \qquad (C.1)$$

We can use the FT relationship

$$F(\nu) = \frac{1}{q^2 + \nu^2}\,, \qquad (C.2)$$

and

$$f(\tau) = \frac{\pi}{q}\,e^{-q\,|\tau|}, \qquad (C.3)$$

where $q = \partial\nu\,/\,2$, to obtain the normalised FT of (C.1). The FT may be shown to be

$$\gamma_{11}(\tau) = \exp\left(\frac{\partial\nu\,\tau}{2}\right) \exp\left(j\,2\pi\,\nu_0\tau\right). \qquad (C.4)$$

The visibility of interference fringes in an interferometer of path difference L is given by

$$v(L) = \exp\left(\frac{L}{L_C}\right). \qquad (C.5)$$

Appendix D : The Fourier transform of a 1D grating.

The grating function, $F(\omega)$, may be considered to be the convolution of a 'top hat' or a square pulse of width d with a comb function of period s. In order to calculate the FT of the grating we multiply together the FTs of the two component functions. We have

$$F(\omega) = F_T(\omega) F_C(\omega), \qquad (D.1)$$

where $F_T(\omega)$ and $F_C(\omega)$ are the FTs of the top hat and comb functions respectively. The top hat function may be expressed as

$$F_T(\omega) = 1 \text{ between } -d/2 \text{ and } +d/2$$
$$= 0 \text{ otherwise.}$$

The FT of $F_T(\omega)$ is given by

$$F_T(\omega) = \int_{-d/2}^{+d/2} e^{i\omega x} dx, \qquad (D.2)$$

which becomes

$$F_T(\omega) = [\frac{e^{i\omega x}}{i\omega}]_{-d/2}^{+d/2} = \frac{d}{2} \text{Sinc} \frac{\omega d}{2}. \qquad (D.3)$$

The comb function may be written

$$F_C(\omega) = \delta(x - nx_1). \qquad (D.4)$$

The FT of $F_C(\omega)$ is written

$$F_C(\omega) = \int_{-\infty}^{\infty} \delta(x - nx_1) e^{i\omega x} dx. \qquad (D.5)$$

169

The integral becomes

$$F_C(\omega) = \sum_{N=0}^{n} e^{i\omega n x_1} = \frac{1 - e^{i\omega n x_1}}{1 - e^{iw x_1}}. \quad (D.6)$$

The complete FT is obtained from the product of equations (D.3) and (D.6). The FT of the grating is therefore

$$F(\omega) = \frac{d}{2} \text{Sinc} \left(\frac{\omega d}{2}\right) \left(\frac{1 - e^{i\omega n x_1}}{1 - e^{i\omega x_1}}\right). \quad (D.7)$$

By taking out a factor of

$$e^{i(n-1)\frac{\omega x_1}{2}}, \quad (D.8)$$

and putting $\omega = 2\pi u$, we obtain

$$F(\omega) = \frac{d}{2} \text{Sinc}(\pi u d) \frac{\text{Sin } n\pi u x_1}{\text{Sin } \pi u x_1} \exp(i(n-1)\pi u x_1). \quad (D.9)$$

The observed intensity is the square modulus of amplitude, $F(\omega)$ so we measure $I(\omega)$ where

$$I(u) = |F(u)|^2 = \frac{d^2}{4} \text{Sinc}^2 \pi u d \left(\frac{\text{Sin } n\pi u d}{\text{Sin } \pi u d}\right)^2. \quad (D.10)$$